ALTERNATIVE APPROACHES FOR THE REGISTRATION OF TERRESTRIAL LASER SCANNERS DATA USING LINEAR/PLANAR FEATURES

A Dissertation

Submitted to the Faculty

of

Purdue University

by

Dewen Shi

In Partial Fulfillment of the

Requirements for the Degree

of

Master of Science in Civil Engineering

December 2020

Purdue University

West Lafayette, Indiana

THE PURDUE UNIVERSITY GRADUATE SCHOOL
STATEMENT OF DISSERTATION APPROVAL

Dr. Ayman Habib, Chair

Lyles School of Civil Engineering

Dr. Melba Crawford

Lyles School of Civil Engineering

Dr. Dengfeng Sun

School of Aeronautics and Astronautics

Approved by:

Dr. Dulcy Abraham

Head of the School Graduate Program

To my parents.

ACKNOWLEDGMENTS

First and foremost, I would like to express my deepest gratitude to my advisor, Dr. Ayman Habib, for his encouragement and support throughout this process. From the formation of the first draft to the revision and improvement over and over again, Dr. Habib gave me very careful guidance. He has taught me very valuable lessons about diligence and scientific rigor.

Furthermore, I wish to thank my thesis committee members, Dr. Melba Crawford and Dr. Dengfeng Sun, for providing many insightful comments and taking their precious time to participate in my defense.

I am also especially grateful to the members of Digital Photogrammetry Research Group, especially Yun-Jou Lin, Tian Zhou, Yi-Chun Lin, Radhika Ravi, Mohammed D Aldosari, Yi-Ting Cheng, Seyyed Meghdad Hasheminasab, Ankit Patel, Lisa LaForest for their great assistance throughout these years. I would also like to thank all the help from my friends, Chen Ma, Behrokh B Nazeri, Ruixin Li, Yuchi Ma, Zilong Yang, Priyankar Bhattacharjee, Xinlin Tao, Joshua Carpenter, Paul M Cleary. They helped me make a smooth transition into this new academic environment.

TABLE OF CONTENTS

Page

Page

Page

LIST OF TABLES

Table Page

Table Page

Table Page

Table Page

Table Page

LIST OF FIGURES

Figure Page

Figure Page

ABBREVIATIONS

3D	Three-dimensional
2D	Two-dimensional
ICP	Iterative Closest Point
ICPP	Iterative Closest Projected Point
LSA	Least Squares Adjustment
RANSAC	RANdom SAmple Consensus
RMSE	Root-mean-square Error
TIN	Triangulated Irregular Networks
TLS	Terrestrial Laser Scanners

ABSTRACT

Shi, Dewen MSCE, Purdue University, December 2020. Alternative Approaches for the Registration of Terrestrial Laser Scanners Data using Linear/Planar Features. Major Professor: Ayman Habib.

Static terrestrial laser scanners have been increasingly used in three-dimensional data acquisition since it can rapidly provide accurate measurements with high resolution. Several scans from multiple viewpoints are necessary to achieve complete coverage of the surveyed objects due to occlusion and large object size. Therefore, in order to reconstruct three-dimensional models of the objects, the task of registration is required to transform several individual scans into a common reference frame. This thesis introduces three alternative approaches for the coarse registration of two adjacent scans, namely, feature-based approach, pseudo-conjugate point-based method, and closed-form solution. In the feature-based approach, linear and planar features in the overlapping area of adjacent scans are selected as registration primitives. The pseudo-conjugate point-based method utilizes non-corresponding points along common linear and planar features to estimate transformation parameters. The pseudo-conjugate point-based method is simpler than the feature-based approach since the partial derivatives are easier to compute. In the closed-form solution, a rotation matrix is first estimated by using a unit quaternion, which is a concise description of the rotation. Afterward, the translation parameters are estimated with non-corresponding points along the linear or planar features by using the pseudo-conjugate point-based method. Alternative approaches for fitting a line or plane to data with errors in three-dimensional space are investigated.

Experiments are conducted using simulated and real datasets to verify the effectiveness of the introduced registration procedures and feature fitting approaches. The

proposed two approaches of line fitting are tested with simulated datasets. The results suggest that these two approaches can produce identical line parameters and variance-covariance matrix. The three registration approaches are tested with both simulated and real datasets. In the simulated datasets, all three registration approaches produced equivalent transformation parameters using linear or planar features. The comparison between the simulated linear and planar features shows that both features can produce equivalent registration results. In the real datasets, the three registration approaches using the linear or planar features also produced equivalent results. In addition, the results using real data indicates that the registration approaches using planar features produced better results than the approaches using linear features. The experiments show that the pseudo-conjugate point-based approach is easier to implement than the feature-based approach. The pseudo-conjugate point-based method and feature-based approach are nonlinear, so an initial guess of transformation parameters is required in these two approaches. Compared to the nonlinear approaches, the closed-form solution is linear and hence it can achieve the registration of two adjacent scans without the requirement of any initial guess for transformation parameters. Therefore, the pseudo-conjugate point-based method and closed-form solution are the preferred approaches for coarse registration using linear or planar features. In real practice, the planar features would have a better preference when compared to linear features since the linear features are derived indirectly by the intersection of neighboring planar features. To get enough lines with different orientations, planes that are far apart from each other have to be extrapolated to derive lines.

1. INTRODUCTION

Terrestrial laser scanners (TLS) are increasingly used to provide an accurate representation of the surface of objects. They collect the spatial coordinates of the measured object and directly generate a dense surface model. Because of high spatial resolution and fast data acquisition, TLS technology has been widely employed in many applications, such as surveying, building modeling, and cultural heritage recording.

Because of occlusions and reduced point density with an increasing object-to-scanner distance, a single scan is usually not enough to cover the whole scene. Therefore, in order to acquire a complete three-dimensional (3D) model of an object, it is necessary to collect data from multiple viewpoints. Point clouds collected from different viewpoints are referenced to their local coordinate system. A registration process is required to transform these data into a common coordinate system before the reconstruction of a 3D model.

According to Habib and Alruzouq [1], the task of registration involves four components: registration primitives, transformation function, similarity measure, and matching strategy. Registration primitives are the geometric features (e.g., points, linear and planar features) that can be identified in the overlapping region between adjacent scans. The transformation function is what mathematically describes the relationships between the coordinate systems of the involved scans. Usually, two point clouds are related to each other through a 3D similarity transformation (three rotations, three translations, and a scale factor). The similarity measure is a mathematical model that constrains the alignment of conjugate primitives after the application of a transformation function. The mathematical constraint of the similarity measure differs according to the type of the primitives used. The matching strategy is a controlling framework that uses the registration primitives, transformation function, and similarity measure to solve for transformation parameters automatically.

The task of point clouds registration consists of two main steps: a coarse registration step that is used to provide a rough initial alignment of the scans, followed by a fine registration step that achieves a more precise solution. The Iterative Closest Point (ICP) algorithm proposed by Besl and McKay [2] is one of the most popular methods used for fine registration. It is based on iteratively minimizing the point-to-point distances in the overlapping area between different TLS scans. However, the ICP algorithm needs a good initial guess of the transformation parameters to find conjugate points between two overlapping point clouds. Therefore, methods to acquire a coarse alignment of overlapping scans need to be explored.

Target-based registration is commonly used to achieve a coarse alignment. Typical markers are spheres, cylinders, or planar markers. Using retro-reflective materials, the detection of these targets can be done automatically. In order to match two point clouds, at least three targets should be placed within the overlapping area of the two scans, and these targets should not be collinear. The 3D transformation parameters can be estimated based on the position of the targets detected in the area of overlap between two point clouds. However, human interaction is required to distribute the markers in the scene. The distribution and collection of the targets need additional time, and it will increase the project cost. In addition, an optimal distribution of targets in the survey area often cannot be obtained due to scene complexities and the line-of-sight acquisition characteristic of TLS. Therefore, feature-based registration that utilizes geometric features in the scene is more desirable.

Registration approaches based on natural geometric elements in the scene can avoid the extra labor and additional time to set up the targets. Because the geometric features can provide a strong link between adjacent scans, this class of techniques is achieved through the alignment of corresponding geometric features in the overlapping area of point clouds, such as linear and planar features.

1.1 Research Objectives

This thesis introduces alternative approaches for the registration of terrestrial laser scanner data using linear and planar features. In this thesis, the following issues are investigated:

(1) The primary objective is to compare the accuracy of the registration results by three different similarity measures, namely, the feature-based approach, pseudo-conjugate point-based method, and closed-form solution, to see whether they are equivalent or not.

(2) The second objective is to compare the registration results using different primitives: linear and planar features.

1.2 Thesis Outline

The thesis is comprised of five chapters, which are briefly explained below.

In chapter 2, the term registration is defined, and a brief classification of registration approaches is given. This chapter reviews the literature relevant to registration approaches in detail.

Chapter 3 presents the methodology for three alternative registration approaches using linear and planar features. This chapter first presents the stochastic model for the least squares adjustment. Then, this chapter explains the representation schemes of linear and planar features with minimal parameters, as well as fitting models of linear and planar features. Next, this chapter describes three alternative approaches for the coarse registration of two adjacent scans, namely, feature-based approach, pseudo-conjugate point-based method, and closed-form solution. Furthermore, a quality evaluation technique of the registration results is introduced in the last section of the chapter.

Chapter 4 includes experimental results of the three alternative registration approaches with both simulated data and real data from terrestrial laser scanners. The

quality evaluation of the estimated transformation parameters is conducted and presented.

Finally, chapter 5 gives the conclusions and provides recommendations for future research.

2. BACKGROUND

This chapter reviews some of the literature relevant to laser data registration. First, the problems of working with TLS data are provided. Then, a definition of point cloud registration is introduced. Finally, some of the existing laser data registration approaches are reviewed from different aspects.

2.1 Point Cloud Registration

Full coverage of surveyed structures cannot be obtained by a single scan owing to reduced point density with an increasing object-to-scanner distance, as well as the occlusion between objects. Hence, it is necessary to acquire point clouds from two or more points of view to record complete objects. Point clouds captured from different viewpoints represent a partial region of the scene and have their local coordinate system centered at each scanners location. Before reconstructing the whole scene, we need to transform all the coordinates into the same coordinate system.

The transformation of adjacent scans into a common reference frame is denoted as registration. In the registration process, one scan is defined as a reference scan, which is stationary, and the other scan is defined as a source scan, which is transformed to match the reference scan. The objective of the registration process is to derive the 3D similarity transformation parameters which best align different scans with each other. Existing registration approaches can be classified into the following categories:

(1) Coarse registration versus fine registration;

(2) Point-based registration versus feature-based registration;

(3) Manual registration versus automated registration; and

(4) Iterative registration versus closed-form registration.

2.2 Coarse Registration Versus Fine Registration

In terms of alignment accuracy, the registration process can be divided into two groups: coarse registration and fine registration.

2.2.1 Coarse Registration

Coarse registration is usually employed to obtain a rough estimation of the transformation parameters and does not require a good initial guess. One of the most popular approaches in coarse registration is the use of targets that are recognizable in different scans. The markers are manually positioned in the scene. Typical markers are checker-board, spherical, and reflective targets. In general, two sets of measurements are related to each other through a 3D similarity transformation (three rotations, three translations, and a scale factor). Since a laser ranging device provides a true scale, only six transformation parameters (three rotations and three translations) need to be determined. In order to determine the six transformation parameters, at least three targets are necessary to align the respective point clouds. Additionally, proper target distribution within the overlap area is needed to obtain a reliable registration.

The artificial markers can be either retrieved manually or automatically. Manual detection is carried out by picking the center point of a marker. Usually, markers are designed to have high-intensity contrast compared to their surrounding area, which allows for automatic identification by the processing software. Some commercial software programs, such as the Faro Scene software, provide automated detection tools for a completely visible sphere in a scan. After detecting a target, an extraction program is employed to calculate the center of the target. The centers of targets are used as conjugate features to register point clouds [3]. However, the targets need to be physically placed in the field and require a lot of preparation in the scene in order to place them properly, which is time-consuming. As a consequence, there is a tendency to avoid the usage of targets and reduce human intervention.

Another coarse registration technique is the direct georeferencing of stationary laser scanners, whereby the scanner position and orientation can be determined directly in the field, which implies an additional reduction of field-work time. The direct georeferencing approach is based on incorporating additional sensors, such as global navigation satellite system (GNSS) and inertial navigation system (INS) [4]. During laser data collection, the position and orientation of the scanner are determined by GNSS and INS, respectively. Thus, project efficiency can be increased. The disadvantages of the direct georeferencing method are the high costs for the external sensors.

The target-based and direct georeferencing methods use external devices to help the registration process. However, the placement of additional devices needs a lot of manual work, and it will increase the cost of the project. In addition, additional instruments are not always available due to scene complexities and time constraints. Therefore, the point clouds collected by TLS itself are usually utilized to estimate the transformation parameters.

2.2.2 Fine Registration

Fine registration aims to achieve a more optimal alignment between the involved scans and demands good initial values of the registration transformation parameters. Therefore, fine registration is frequently used to improve registration accuracy based on the results of coarse registration.

One of the most important algorithms in fine registration is the iterative closest point (ICP) algorithm proposed by Besl and McKay [2]. Assuming that a good initial alignment between involved scans is available, the ICP algorithm estimates the transformation parameters by iteratively minimizing the point-to-point distances in the common area of adjacent scans.

Assuming that a scan pair is already roughly aligned, a pair of corresponding points is generated by finding the closest point in the reference scan to a given point

in the source scan. After all point correspondences are established in the overlapping area, the algorithm estimates new transformation parameters that reduce the distances of these correspondences. Then, the refined transformation parameters are used to register the involved scans and update the matching points. The process is repeated until the change of distances between the point matches become smaller than a threshold.

However, as a result of noise and irregular nature of point clouds, one cannot assume that the matched conjugate points in the overlapping area represent the same point on the surface. Consequently, many variants of ICP exist so as to improve the performance of ICP. For example, instead of a point-to-point correspondence, the Iterative Closest Patch algorithm proposed by Habib et al. [5] assumes a point-to-patch correspondence as registration primitives, namely, original points in one dataset and a Triangulated Irregular Networks (TIN) model in the other dataset. After applying the 3D similarity transformation using initial parameters, every point in the source scan will be transformed into the TIN of the reference scan. Then, a point-patch pair is established by finding the closet patch to the transformed point, and the normal distance between them should be within a certain threshold. In addition, the projection of that point onto the closet patch must be located inside the triangle. The transformed point and three vertices of the conjugate patch are assumed to be coplanar. That is to say, the volume of the pyramid formed by these four points should be zero. The transformation parameters between two scans are refined by applying the coplanarity constraint on these point-patch pairs. Then, a new set of point-patch pairs is established by applying the updated transformation parameters. The procedure will continue until a stable solution is achieved.

Inspired by the Iterative Closest Patch algorithm, Al-Durgham et al. [6] developed the Iterative Closest Projected Point (ICPP) method. Instead of using TIN, the point-to-patch correspondence in the ICPP method is established by finding the closest three points in a reference module to the transformed point. The three neighboring points are used to form a triangle. Then, one can extrude the central point

of the triangle to a user-chosen normal distance to form a tetrahedron according to Figure 2.1(a). It should be noted that two tetrahedrons can be derived by extrusion of the central point since the point can be extruded in two directions. The validity of the matched point-to-patch correspondence is examined by checking whether the transformed point falls inside the established tetrahedrons. Using the transformed point and the four vertices, the tetrahedron can be split into four new tetrahedrons, as shown in Figure 2.1(b). If the determinant of the four tetrahedrons has the same sign, then we can conclude that the transformed point falls inside the tetrahedron. Next, the transformed point will be projected to the triangular patch, and a point-to-point correspondence will be established between the transformed point and its projection on the patch. Then, all the valid point-to-projected point pairs are used to estimate transformation parameters with an appropriate mathematical model. The distance between these correspondences is reduced, and the process is performed iteratively until the convergence is obtained.

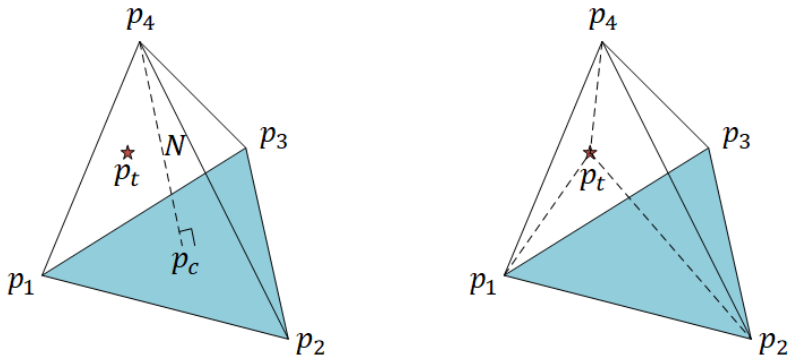

(a) The resulting tetrahedron using the points (p_1, p_2, p_3, and p_4) and the transformed point (p_t)

(b) Four tetrahedrons resulting from splitting the original tetrahedron

Fig. 2.1.: Establishing the point-to-projected point correspondence through the ICPP, adapted from [6]

2.3 Point-Based Registration Versus Feature-Based Registration

2.3.1 Point-Based Registration

Iterative closest points (ICP) method proposed by Besl and McKay [2] uses points as registration primitives, in which the transformation parameters are estimated by performing a least squares adjustment (LSA) that minimizes point-to-point distances. After applying the initial guess of transformation parameters, a search is performed for each transformed point to identify its closest point in the reference coordinate system. Then, the transformation parameters are iteratively refined by minimizing point-to-point distances and generating a new set of corresponding point pairs until distances between identified point pairs become smaller than a threshold. Nevertheless, ICP relies on a good initial alignment in order to find the right solution.

Renaudin et al. [7] presented a point-based coarse registration approach which deals with non-corresponding points along conjugate linear features. A linear feature extracted from point clouds is comprised of a set of points along the line. Since exact point-to-point correspondences cannot be assumed in laser point clouds, there is an unknown vector d resulting from using non-corresponding points, and the unknown vector d is defined along the selected linear feature in the reference coordinate system. A pseudo-conjugate point-based method is used to eliminate the displacement vector by modifying the weight matrix in the mathematical model of LSA, in other words, the elements of the weight matrix corresponding to the line direction will be assigned a zero weight, and only the weight across the line direction is considered in the LSA, so that the transformation parameters can be estimated after replacing the original weight matrix with the modified one.

2.3.2 Feature-Based Registration

Feature-based registration aims to achieve a coarse alignment of two datasets utilizing geometric features extracted from point clouds, for example, linear features

or planar features. 3D linear and planar features are common elements in man-made structures, and feature-based registration does not require a good initial guess of the transformation parameters. Thus, feature-based registration has been drawing a lot of attention in recent years.

2.3.2.1 Line-Based Registration

For linear features, Stamos and Leordeanu [8] proposed an automated line-based registration method. Following a plane segmentation process, linear features are obtained from the boundaries of the planar regions. Line correspondence is established by comparing the length of lines and the plane size on which the linear features lie. Matched line pairs are used to estimate the transformation parameters.

Habib et al. [9] used straight line segments as primitives to register photogrammetric images and Lidar data. In the images, the line segment is defined by measuring two points along the line. In the Lidar data, the linear features are extracted by the intersection of two adjacent planes, and at least two pairs of non-coplanar linear features are required to estimate the 3D similarity transformation parameters.

Alshawa [10] proposed an Iterative Closet Line method, an ICP variant that utilizes a line-to-line correspondence, to register two point clouds. The rotation parameters are determined using a closed-form solution. Afterward, the rotation matrix, together with two random points that belong to the line, is used to find the translation parameters.

2.3.2.2 Plane-Based Registration

Dold and Brenner [11] presented a registration method using planar patches. The planar patches are estimated by region growing method. The corresponding patches in the overlapping area were found by a search strategy. Implausible matches are excluded by geometric and laser scanning attributes, such as area, length of the boundary, bounding box, and mean intensity value. The rotation matrix and translation

component are determined separately using the matched planar patches. Moreover, the planar patches are textured by image data automatically given the calibration parameters of hybrid laser scanning and imaging sensors. The additional image information can be used to find corresponding patches and determine translation parameters.

Von Hansen [12] developed an automatic coarse registration method based on plane correspondences. Raw point clouds are divided into raster cells, and the RANdom SAmple Consensus (RANSAC) algorithm [13] is used to estimate planes for each raster cell. If neighboring patches are coplanar, they can be grouped into one plane. An exhaustive search algorithm is used to search for plane correspondences between adjacent scans. The normal vector of each plane is represented by inclination and azimuth. Assuming that the zenith direction is known in sensor setup, the rotation is calculated through the difference of azimuth, and the translation is computed through the difference of barycenter.

Some researchers proposed using a combination of different primitives to register point clouds. In Jaw and Chuang [14], point, linear, and planar features were used to register the TLS scans individually, and these features can also be combined to estimate the transformation parameters. It shows that combined measurements can provide more accurate transformation results than using a single type of features.

2.4 Manual Registration Versus Automated Registration

Given the various primitive extracted from point clouds, one critical step is to find correspondences between the source and reference scans. Conjugate features in adjacent scans can be identified either manually or automatically. The process of manually identifying common features in overlapping scans is efficient for low-complexity scenes. However, manual processing is heavily dependent on the users' ability to identify corresponding features. Thus, this method is time-consuming when

the number of features is large. Therefore, a wide variety of approaches have been used to automate the matching problem and reduce the matching time.

Stamos and Leordeanu [8] introduced an automated feature-based registration of point clouds. In the matching procedure, line pairs that have similar length and plane sizes will be considered in lexicographical order. The initial rotation and translation are estimated with the first pair of lines. Then, the rotation is applied to all line pairs. If the line direction and plane normal do not match after applying the rotation, the line pairs will be rejected. For the remaining line pairs, line matches that are not in agreement with the estimated translation will also be discarded. The translation is refined by including all of the remaining line pairs. The rotation and the refined translation are used to transform all lines in the source scan to the reference scan, and the estimated transformation is graded by counting the number of the valid line correspondences within a fixed threshold. The transformation and line match with the highest grades will win.

Al-Durgham et al. [15] introduced an automatic matching strategy to align corresponding linear features in overlapping scans based on conditional RANSAC approach. Candidate conjugate lines pair is selected according to spatial separation and angular deviation values between line pairs. Then, a candidate conjugate line pair is randomly chosen to estimate the transformation parameters. If the number of line correspondences is more than a predefined threshold, the ICPP procedure is utilized to refine the transformation parameters and determine the number of matched points. This process will be repeated for all hypothesized line pairs. The solution with the largest number of conjugate points would be considered as true alignment. Finally, all compatible linear features are used to estimate the transformation parameters, and the result is refined by the ICPP method.

Al-Durgham and Habib [16] introduced a matching strategy that stores hypothesized matches of linear features in an association matrix. Every row in the association matrix represents a line in the reference scan, and every column represents a line in the source scan. The association matrix is constructed by identifying candidate matches

of linear features with similar spatial separation and angular deviation values in the overlapping area. Every candidate match of linear features will increment the corresponding votes in the association matrix. Starting from the match with the highest vote in the association matrix and proceeding in descending order, conjugate linear features in adjacent scans can be identified. The association matrix approach can achieve a solution in fewer trials than the traditional RANSAC algorithm since the voting scheme has excluded improbable line pairs, and it does not need to select random samples as in the RANSAC approach.

2.5 Iterative Registration Versus Closed-Form Registration

According to the utilized approach for solving for the transformation parameters, the registration problem can be categorized into iterative and closed-form approaches. The registration approaches suggested in [2, 5–11] are nonlinear with respect to the unknowns, it is impossible to find a closed-form solution. For these situations, the unknown parameters are estimated iteratively, and initial approximate values for the unknown transformation parameters are required, which are usually acquired by roughly estimating the position and orientation of the scans. In some problems, a closed-form solution exists for the optimal translation and rotation by using a linear mathematical model, and a closed-form approach eliminates the need for having initial transformation parameters. Since the closed-form solutions are one-step procedures, they are faster than iterative approaches.

Horn [17] simplified the iterative method by using unit quaternion to parameterize rotation. Horn assumes that exact point-to-point correspondences exist in overlapping point clouds. The transformation parameters are estimated with respect to the centroids of the two point clouds. Assuming that a number of points in two different point sets are corresponding to each other, the new coordinates of points in both point sets are computed by subtracting the centroid from all measurements, respectively.

Suppose there are n corresponding points in the source and reference scans. a_i is a point in the source scan, and a'_i is a corresponding point in the reference scan. The centroid of the points in each dataset is derived by Equation (2.1). The new coordinates of points are derived by subtracting the centroid from each of the points in both datasets. The corresponding unit vector can be given as in Equation (2.2). Then, one can introduce the constraint in Equation (2.3) while considering the random errors associated with the measurements, where u_i and u'_i are unit vectors, R is the rotation matrix relating two different coordinate systems, and e_i is random noise contaminating the observations.

$$\begin{aligned} \bar{a_i} &= \frac{\sum_{i=1}^{n} a_i}{n} \\ \bar{a'_i} &= \frac{\sum_{i=1}^{n} a'_i}{n} \end{aligned} \tag{2.1}$$

$$\begin{aligned} u_i &= \frac{a_i - \bar{a_i}}{||a_i - \bar{a_i}||} \\ u'_i &= \frac{a'_i - \bar{a'_i}}{||a'_i - \bar{a'_i}||} \end{aligned} \tag{2.2}$$

$$u'_i = Ru_i + e_i \tag{2.3}$$

In order to find the optimal rotation, the least squares adjustment principle can be employed by minimizing the sum of squared residuals. It can be shown that the optimal rotation can be found by maximizing $\sum_{i=1}^{n} u_i^T R^T u'_i$. This term can be formulated as shown in Equation (2.4), where the unit quaternion $\dot{q}$ corresponds to a rotation matrix R, and $\dot{q}^*$ denotes the conjugate quaternion, which is constructed by negating the imaginary part of $\dot{q}$. The term $\dot{u}_i$ is a pure quaternion (scalar part is zero) corresponding to vector u_i. A detailed description of quaternions is shown in Chapter 3.

$$\max_{\dot{q}} \sum_{i=1}^{n} (\dot{q}\dot{u}_i\dot{q}^*) \cdot \dot{u}'_i = \max_{\dot{q}} \sum_{i=1}^{n} (\dot{q}\dot{u}_i) \cdot (\dot{u}'_i\dot{q}) \tag{2.4}$$

According to quaternion properties, quaternion multiplication can be represented in matrix form, as shown in Equation (2.5), where matrices $C(\dot{u}_i)$ and $\bar{C}(\dot{u}_i)$ can convert

a quaternion product into a matrix-vector product, for instance: $\dot{u}_1\dot{u}_2 = C(\dot{u}_1)\,\dot{u}_2 = \bar{C}(\dot{u}_2)\,\dot{u}_1$. The solution for the desired rotation $\dot{q}$ is the eigenvector that corresponds to the largest eigenvalue of the 4×4 matrix S. Then, the optimal translation is defined by the difference between the centroid of the reference coordinate system and the rotated centroid of the source coordinate system.

$$\begin{aligned}
\max_{\dot{q}} \sum_{i=1}^{n} (\dot{q}\dot{u}_i) \cdot (\dot{u}_i'\dot{q}) &= \max_{q} \sum_{i=1}^{n} \left(\bar{C}(\dot{u}_i)\,\dot{q}\right) \cdot \left(C(\dot{u}_i')\,\dot{q}\right) \\
&= \max_{\dot{q}} \sum_{i=1}^{n} \dot{q}^{\mathrm{T}} \bar{C}(\dot{u}_i)^{\mathrm{T}} C(\dot{u}_i')\,\dot{q} \\
&= \max_{\dot{q}} \dot{q}^{\mathrm{T}} \left(\sum_{i=1}^{n} \bar{C}(\dot{u}_i)^{\mathrm{T}} C(\dot{u}_i') \right) \dot{q} \\
&= \max_{\dot{q}} \dot{q}^{\mathrm{T}} S \dot{q}
\end{aligned} \tag{2.5}$$

Guan and Zhang [18] proposed a quaternion-based approach to estimate the transformation parameters using linear features. This approach uses unit quaternion to represent the rotation angles. The rotation matrix is determined first, and then the intersection of two coplanar lines are selected as conjugate points to estimate the translation parameters. This approach assumes that the direction vectors of conjugate linear features are compatible. In other words, the conjugate linear features have unified directions in space after transformation. However, conjugate linear features in adjacent scans might be partially compatible. The directional ambiguities between conjugate linear features will lead to more than one plausible estimate for the rotation angles.

He and Habib [19] proposed a closed-form solution to address the directional ambiguities between corresponding linear features. The proposed procedure started with using two noncoplanar linear features in each scan for the estimation of transformation parameters while allowing for multiple directional correspondences between these linear features. This step would lead to multiple solutions for the transformation parameters. Then, the estimated transformation parameters together with the

remaining conjugate linear features are used to identify the correct estimate for the transformation parameters. Once the correct transformation parameters have been identified, they will be used to ensure the compatibility of direction vectors for all corresponding linear features. Finally, all the corresponding linear features are used to estimate transformation parameters between adjacent scans.

2.6 Summary

In this chapter, existing literature about the registration of laser point clouds was reviewed and discussed. The literature was classified according to the registration accuracy, registration primitives, matching strategy, and similarity measure. In the coarse registration, the feature-based approach, pseudo-conjugate point-based method, and closed-form solution have been commonly employed to obtain an initial estimation of the transformation parameters using linear/planar features. However, no previous research has empirically compared the performance of these three approaches. This thesis addresses this open question by conducting experiments using simulated and real datasets. Moreover, a comparison of the usage of linear and planar features are presented in this thesis.

3. METHODOLOGY

Due to the discrete nature of point clouds data, it is difficult to obtain corresponding points from two different scans. Linear and planar features play an essential role in TLS point cloud registration since these features are common elements in urban scenes, and it is easier to establish a correspondence between conjugate linear and planar features than discrete points in coarse registration. Linear and planar features can be represented with few parameters, which will simplify the task of registering two scans. Furthermore, a good initial approximation of transformation parameters is not required in feature-based registration approaches.

In this chapter, first, the stochastic model for the least squares adjustment is presented. Then, this chapter describes the representation schemes of linear and planar features with minimal parameters, as well as the fitting models of linear and planar features. Next, three alternative registration approaches are presented for the estimation of transformation parameters between adjacent scans. Finally, a quality evaluation method of the estimated transformation parameters, which uses the point-to-surface correspondence in adjacent scans, will be described at the end of this chapter.

3.1 Stochastic Model for Least Squares Adjustment (LSA)

Least squares adjustment is used to obtain an estimate of unknown parameters using a model with a set of n_o observations. A nonlinear function can be represented by Equation (3.1), where Y is the $n_o \times 1$ vector of observations, X is the $m \times 1$ vector of unknown parameters, e is the $n_o \times 1$ vector of random errors contaminating the observations, and P is the inverse of the variance-covariance matrix of the noise vector. After Taylor series expansion and ignoring higher order terms, the nonlinear

function will be linearized as in Equation (3.2), in which X_0 is an approximate value for the unknown parameter. The mathematical expression in Equation (3.2) can be rewritten in the form given in Equation (3.3), which depicts a mathematical model with n_e observation equations. In Equation (3.3), $y = f(Y, X_0)$ is the $n_e \times 1$ vector of observation equations; $A = -\frac{\partial f}{\partial X}\big|_{Y,X_0}$ is the $n_e \times m$ design matrix composed of the partial derivatives with respect to the unknown parameters; x is the $m \times 1$ vector of unknown parameters; $B = \frac{\partial f}{\partial Y}\big|_{Y,X_0}$ is the $n_e \times n_o$ matrix composed of the partial derivatives with respect to the observations; and $\bar{e} = Be$ is the $n_e \times 1$ combined error term.

$$f(Y - e, X) = 0 \quad e \sim \left(0, \sigma_0^2 P^{-1}\right) \tag{3.1}$$

$$f(Y, X_0) + \left.\frac{\partial f}{\partial Y}\right|_{Y,X_0} (-e) + \left.\frac{\partial f}{\partial X}\right|_{Y,X_0} \mathrm{d}X = 0 \tag{3.2}$$

$$y = Ax + \bar{e} \quad \bar{e} \sim \left(0, \sigma_0^2 B P^{-1} B^{\mathrm{T}}\right) \tag{3.3}$$

The LSA procedure aims at estimating the unknown parameters which minimize the sum of squared, weighted residuals in Equation (3.4), and leads to the solution vector in Equation (3.5), the variance-covariance matrix in Equation (3.6), the predicted residuals in Equation (3.7), and the a-posteriori variance factor in Equation (3.8).

$$\bar{e}^{\mathrm{T}} (B P^{-1} B^{\mathrm{T}})^{-1} \bar{e} = min|_x \tag{3.4}$$

$$\hat{x} = (A^{\mathrm{T}} (B P^{-1} B^{\mathrm{T}})^{-1} A)^{-1} A^{\mathrm{T}} (B P^{-1} B^{\mathrm{T}})^{-1} y \tag{3.5}$$

$$\Sigma\{\hat{x}\} = \hat{\sigma}_0^2 (A^{\mathrm{T}} (B P^{-1} B^{\mathrm{T}})^{-1} A)^{-1} \tag{3.6}$$

$$\tilde{\bar{e}} = y - A\hat{x} \tag{3.7}$$

$$\hat{\sigma}_0^2 = \frac{\tilde{\tilde{e}}^{\mathrm{T}}(BP^{-1}B^{\mathrm{T}})^{-1}\tilde{\tilde{e}}}{n_e - m} \tag{3.8}$$

3.2 Alternative Approaches for Line/Plane Fitting

In this subsection, first, the representation schemes of linear and planar features with minimal parameterization are discussed. Then, alternative approaches for fitting a line or plane to data with errors in Euclidean 3D space are investigated and compared.

3.2.1 Representation Scheme of Linear Features

It is convenient to represent a straight line using two points along the line [9]. But this representation is not unique, and it is not minimal since it needs six parameters. Another popular way to represent a line is by utilizing a fixed point on the line and the direction of that line. This representation is six-dimensional and is not unique. Mulawa and Mikhail [20] added two constraints on this representation to ensure this representation is unique. Firstly, the direction vector is a unit vector. Secondly, one unique point which is closest to the origin is selected as a fixed point to represent the line.

Roberts [21] proposed a representation of a line using two orientation parameters and two positional parameters. Two direction cosines specify the orientation of the line. The positional parameters of the line are defined as follows. A 2-D coordinate system is defined on a plane passing through the origin and perpendicular to the line. The intersection of the line with the plane forms the two positional parameters, which are the coordinate values in the local frame.

Ayache and Faugeras [22] introduced a representation of lines defined by the intersection of two planes. Assuming that one plane is parallel to the y-axis, and another plane is parallel to the x-axis, then a line not perpendicular to the z-axis can be

represented in terms of the intersection of these two planes, as shown in Equation (3.9). The four parameters (a_x, a_y, b_x, b_y) can be used to define the line. The vector $(a_x, a_y, 1)$ represents the direction of the line, and the line intersects the xy-plane at the point $(b_x, b_y, 0)$. This representation scheme is shown in Figure 3.1(a). Since the third value in the direction vector is 1, this form cannot represent lines that are perpendicular to the z-axis.

$$\begin{aligned} x &= a_x z + b_x \\ y &= a_y z + b_y \end{aligned} \tag{3.9}$$

In order to avoid this singularity, the representation is extended by a second type of representation defined in terms of the intersection of two planes that are parallel to the z-axis and y-axis, respectively, as shown in Equation (3.10). Then, the direction of the line is represented by the vector $(1, a_y, a_z)$, and the line intersects the yz-plane at the point $(0, b_y, b_z)$. This representation scheme is shown in Figure 3.1(b).

$$\begin{aligned} y &= a_y x + b_y \\ z &= a_z x + b_z \end{aligned} \tag{3.10}$$

However, this representation excludes lines that are orthogonal to the x-axis. Therefore, an alternative representation can be defined as the intersection of two planes, one parallel to the z-axis and the other parallel to the x-axis, as shown in Equation (3.11). The direction of a line is given by the vector $(a_x, 1, a_z)$, and the xz-plane intersects the line at the point $(b_x, 0, b_z)$. This representation scheme is shown in Figure 3.1(c). Once again, this one cannot be used to represent lines that are perpendicular to the y-axis.

$$\begin{aligned} x &= a_x y + b_x \\ z &= a_z y + b_z \end{aligned} \tag{3.11}$$

The choice of appropriate line parameters depends on the orientation of a linear feature. Linear features that are mainly oriented along the z-axis can be represented by the first scheme, as shown in Figure 3.1(a). Similarly, linear features that are

mainly oriented along the x-axis can be represented by the second scheme, as shown in Figure 3.1(b), and linear features that are mainly oriented along the y-axis can be represented by the third scheme, as shown in Figure 3.1(c).

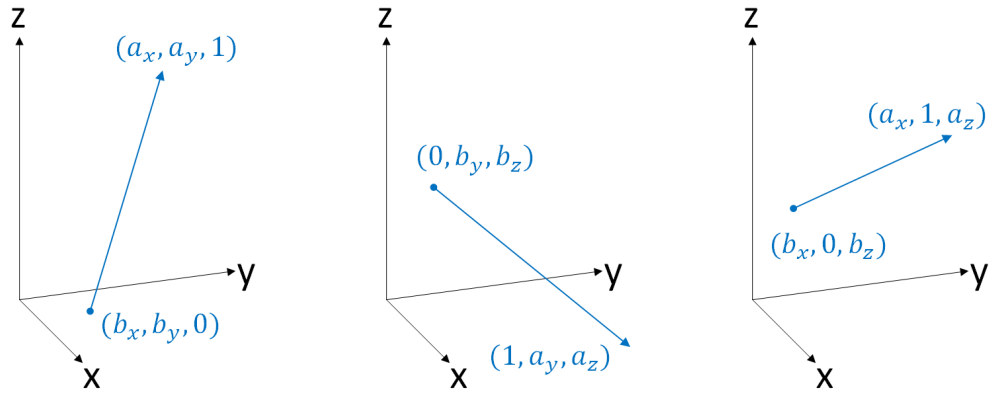

(a) Lines that are mainly oriented along the z-axis

(b) Lines that are mainly oriented along the x-axis

(c) Lines that are mainly oriented along the y-axis

Fig. 3.1.: Representation schemes for 3D linear features

3.2.2 3D Line Fitting by Minimizing 2D Distances of Points From a Line Measured Parallel to the Coordinated Planes

In this subsection, a 3D line fitting approach is generalized by minimizing the sum of squared distances of points from the line measured parallel to the xy-plane, yz-plane, or xz-plane. As shown in Figure 3.2, given a line that is mainly oriented along the z-axis, the direction vector of the line is $(a_x, a_y, 1)$, and the line intersects xy-plane at point $(b_x, b_y, 0)$, then any point (x, y, z) along the line can be represented with one fixed point $b(b_x, b_y, 0)$, one direction vector $a(a_x, a_y, 1)$, and one scale factor λ, as shown in Equation (3.12). Therefore, any observed point $p_i(x_i, y_i, z_i)$ can be

given as in Equation (3.13), where $(e_{x_i}, e_{y_i}, e_{z_i})$ is random noise contaminating the x, y, and z coordinates of the point along the line.

$$\begin{bmatrix} x \\ y \\ z \end{bmatrix} = \begin{bmatrix} b_x \\ b_y \\ 0 \end{bmatrix} + \lambda \begin{bmatrix} a_x \\ a_y \\ 1 \end{bmatrix} \tag{3.12}$$

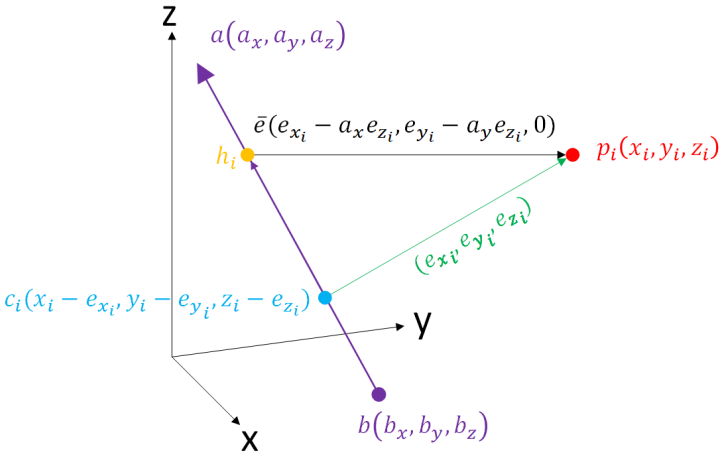

Fig. 3.2.: Schematic illustration of 3D line fitting by minimizing 2D distance of point p_i from the line measured parallel to the xy-plane

$$\begin{bmatrix} x_i \\ y_i \\ z_i \end{bmatrix} = \begin{bmatrix} b_x \\ b_y \\ 0 \end{bmatrix} + \lambda_i \begin{bmatrix} a_x \\ a_y \\ 1 \end{bmatrix} + \begin{bmatrix} e_{x_i} \\ e_{y_i} \\ e_{z_i} \end{bmatrix} \tag{3.13}$$

The above equation can be rewritten as in Equation (3.14). where the five unknown parameters are λ_i, a_x, a_y, b_x, b_y. The unknown scale factor λ_i can be eliminated through dividing the first and second equation by the third one, and then one can get Equation (3.15), where the four unknown parameters are a_x, a_y, b_x, b_y. Hence, each 3D point contributes two observation equations to the least squares model according to Equation (3.16).

$$\lambda_i \begin{bmatrix} a_x \\ a_y \\ 1 \end{bmatrix} = \begin{bmatrix} x_i \\ y_i \\ z_i \end{bmatrix} - \begin{bmatrix} e_{x_i} \\ e_{y_i} \\ e_{z_i} \end{bmatrix} - \begin{bmatrix} b_x \\ b_y \\ 0 \end{bmatrix} \tag{3.14}$$

$$\begin{aligned} a_x &= \frac{x_i - e_{x_i} - b_x}{z_i - e_{z_i}} \\ a_y &= \frac{y_i - e_{y_i} - b_y}{z_i - e_{z_i}} \end{aligned} \tag{3.15}$$

$$\begin{aligned} x_i - e_{x_i} &= a_x \left(z_i - e_{z_i}\right) + b_x \\ y_i - e_{y_i} &= a_y \left(z_i - e_{z_i}\right) + b_y \end{aligned} \tag{3.16}$$

The combined error term of Equation (3.16) is given in Equation (3.17). The combined error term $\bar{e}$ is nothing but the vector, which is parallel to the xy-plane, between the observed point and a line. As shown in Figure 3.2, assuming that a plane passing through the observed point p_i is parallel to the xy-plane, then h_i is the intersection point of this plane and the line in question. The vector between the observed point p_i and the intersection point h_i can be derived by Equation (3.18). As shown in the Figure 3.2, the vector $\overrightarrow{c_i h_i}$ is along the line direction, so $\overrightarrow{c_i h_i}$ is given by Equation (3.19). Therefore, the vector $\overrightarrow{h_i p_i}$ can be derived by Equation 3.20. The vector $\overrightarrow{h_i p_i}$ is parallel to the xy-plane, and the first two terms of $\overrightarrow{h_i p_i}$ are equivalent to the combined error terms $\bar{e}$ given in Equation (3.17). Therefore, the 3D line fitting approach searches for a minimum distances which are parallel to the xy-planes.

$$\bar{e} = Be = \begin{bmatrix} e_{x_i} - a_x e_{z_i} \\ e_{y_i} - a_y e_{z_i} \end{bmatrix} \tag{3.17}$$

$$\overrightarrow{h_i p_i} = \overrightarrow{c_i p_i} - \overrightarrow{c_i h_i}, \quad \text{where} \quad \overrightarrow{c_i p_i} = \begin{bmatrix} e_{x_i} \\ e_{y_i} \\ e_{z_i} \end{bmatrix} \tag{3.18}$$

$$\overrightarrow{c_i h_i} = e_{z_i} \begin{bmatrix} a_x \\ a_y \\ 1 \end{bmatrix} \tag{3.19}$$

$$\overrightarrow{h_i p_i} = \overrightarrow{c_i p_i} - \overrightarrow{c_i h_i} = \begin{bmatrix} e_{x_i} \\ e_{y_i} \\ e_{z_i} \end{bmatrix} - e_{z_i} \begin{bmatrix} a_x \\ a_y \\ 1 \end{bmatrix} = \begin{bmatrix} e_{x_i} - a_x e_{z_i} \\ e_{y_i} - a_y e_{z_i} \\ 0 \end{bmatrix} \tag{3.20}$$

Similarly, given a line that is mainly oriented along the x-axis, the direction vector of the line is $(1, a_y, a_z)$, and the line intersects yz-plane at point $(0, b_y, b_z)$. In Equation (3.14), the scale factor λ can be eliminated through dividing the second and third equation by the first one. Hence, each 3D point contributes two observations to the least squares model according to Equation (3.21). The combined error term is given in Equation (3.22). The combined error term $\bar{e}$ is the vector which is parallel to the yz-plane.

$$\begin{aligned} y_i - e_{y_i} &= a_y \left(x_i - e_{x_i} \right) + b_y \\ z_i - e_{z_i} &= a_z \left(x_i - e_{x_i} \right) + b_z \end{aligned} \tag{3.21}$$

$$\bar{e} = Be = \begin{bmatrix} a_y e_{x_i} - e_{y_i} \\ a_z e_{x_i} - e_{z_i} \end{bmatrix} \tag{3.22}$$

If a line is mainly oriented along the y-axis, the direction vector of the line is $(a_x, 1, a_z)$, and the line intersects xz-plane at point $(b_x, 0, b_z)$. In Equation (3.14), the scale factor λ can be eliminated through dividing the first and third equation by the second one. Hence, each 3D point contributes two observations to the least squares model according to Equation (3.23). The combined error term is given in Equation (3.24). The combined error term $\bar{e}$ is the vector which is parallel to the xz-plane.

$$\begin{aligned} x_i - e_{x_i} &= a_x \left(y_i - e_{y_i} \right) + b_x \\ z_i - e_{z_i} &= a_z \left(y_i - e_{y_i} \right) + b_z \end{aligned} \tag{3.23}$$

$$\bar{e} = Be = \begin{bmatrix} a_x e_{y_i} - e_{x_i} \\ a_z e_{y_i} - e_{z_i} \end{bmatrix} \tag{3.24}$$

3.2.3 3D Line Fitting by Minimizing the 3D Normal Distances Between Points and a Line

The second approach of line fitting in this research is to find a best-fit line to a set of points by minimizing normal distances (d_x, d_y, d_z) between points and the line.

3.2.3.1 Observation Equation of the Line Fitting Procedure

Assuming that the coordinates of an observed point is $p_i(x_i, y_i, z_i)$, and the projection of the point along a line is $p_i'\,(x_i', y_i', z_i')$, as shown in Figure 3.3, then the normal distance $\overrightarrow{p_i'p_i} = (d_x, d_y, d_z)$ between points and a line can be derived according to Equation (3.25). The vector $\overrightarrow{bp_i}$ can be derived by Equation (3.26), where $b(b_x, b_y, b_z)$ is the fixed point along a line, and $(e_{x_i}, e_{y_i}, e_{z_i})$ is the noise contaminating the x, y, and z coordinates of the point along the line. The vector $\overrightarrow{bp_i'}$, which is the projection of vector $\overrightarrow{bp_i}$ along a line, can be derived by Equation (3.27), where $a(a_x, a_y, a_z)$ is direction vector of a line. A unit vector $\left(a_x', a_y', a_z'\right)$ can be derived after normalizing the direction vector by Equation (3.28).

$$\overrightarrow{p_i'p_i} = \overrightarrow{bp_i} - \overrightarrow{bp_i'} \tag{3.25}$$

$$\overrightarrow{bp_i} = \begin{bmatrix} (x_i - e_{x_i}) - b_x \\ (y_i - e_{y_i}) - b_y \\ (z_i - e_{z_i}) - b_z \end{bmatrix} \tag{3.26}$$

$$\overrightarrow{bp_i'} = \frac{\begin{bmatrix} (x_i - e_{x_i}) - b_x \\ (y_i - e_{y_i}) - b_y \\ (z_i - e_{z_i}) - b_z \end{bmatrix} \cdot \begin{bmatrix} a_x \\ a_y \\ a_z \end{bmatrix}}{a_x^2 + a_y^2 + a_z^2} \begin{bmatrix} a_x \\ a_y \\ a_z \end{bmatrix} \tag{3.27}$$

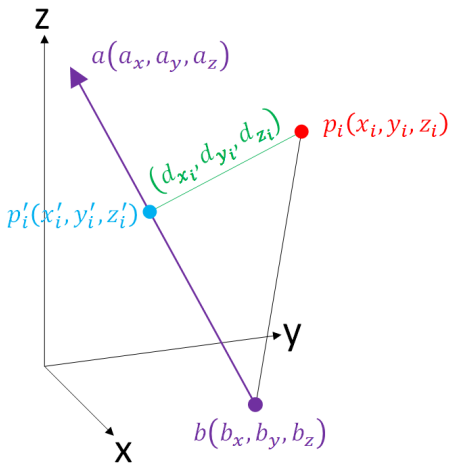

Fig. 3.3.: Schematic illustration of 3D line fitting by minimizing the normal distances between the points and the line in question

$$\begin{bmatrix} a'_x \\ a'_y \\ a'_z \end{bmatrix} = \frac{\begin{bmatrix} a_x \\ a_y \\ a_z \end{bmatrix}}{\sqrt{a_x^2 + a_y^2 + a_z^2}} \tag{3.28}$$

Using the unit direction vector a', the mathematical expression in Equation (3.27) can be rewritten in the form given in Equation (3.29). Combining Equations (3.25), (3.26), and (3.29), the error components between an observed point and its conjugate point on a line can be derived by Equation (3.30).

$$\begin{aligned} \overrightarrow{bp'_i} &= \left(\begin{bmatrix} (x_i - e_{x_i}) - b_x \\ (y_i - e_{y_i}) - b_y \\ (z_i - e_{z_i}) - b_z \end{bmatrix} \cdot \begin{bmatrix} a'_x \\ a'_y \\ a'_z \end{bmatrix} \right) \begin{bmatrix} a'_x \\ a'_y \\ a'_z \end{bmatrix} \\ &= \begin{bmatrix} ((x_i - e_{x_i}) - b_x)\, a'^2_x + ((y_i - e_{y_i}) - b_y)\, a'_x a'_y + ((z_i - e_{z_i}) - b_z)\, a'_x a'_z \\ ((x_i - e_{x_i}) - b_x)\, a'_x a'_y + ((y_i - e_{y_i}) - b_y)\, a'^2_y + ((z_i - e_{z_i}) - b_z)\, a'_y a'_z \\ ((x_i - e_{x_i}) - b_x)\, a'_x a'_z + ((y_i - e_{y_i}) - b_y)\, a'_y a'_z + ((z_i - e_{z_i}) - b_z)\, a'^2_z \end{bmatrix} \end{aligned} \tag{3.29}$$

$$\begin{bmatrix} d_x \\ d_y \\ d_z \end{bmatrix} = \begin{bmatrix} ((x_i - e_{x_i}) - b_x) - \left[((x_i - e_{x_i}) - b_x)\, a_x'^2 + ((y_i - e_{y_i}) - b_y)\, a_x' a_y' + ((z_i - e_{z_i}) - b_z)\, a_x' a_z'\right] \\ ((y_i - e_{y_i}) - b_y) - \left[((x_i - e_{x_i}) - b_x)\, a_x' a_y' + ((y_i - e_{y_i}) - b_y)\, a_y'^2 + ((z_i - e_{z_i}) - b_z)\, a_y' a_z'\right] \\ ((z_i - e_{z_i}) - b_z) - \left[((x_i - e_{x_i}) - b_x)\, a_x' a_z' + ((y_i - e_{y_i}) - b_y)\, a_y' a_z' + ((z_i - e_{z_i}) - b_z)\, a_z'^2\right] \end{bmatrix} \tag{3.30}$$

The above equations indicate that the mathematical model for 3D line fitting is nonlinear. So, the model is linearized by conducting a Taylor series expansion and ignoring second and higher-order terms, which would result in the mathematical model for LSA, as given earlier by Equation (3.3). As stated in the description of the mathematical model for LSA, matrix B is composed of the partial derivatives of the function with respect to the observations. In the case of 3D line fitting, this matrix is given by Equation (3.31), which indicates that B is rank-deficient with a rank of 2. According to the law of error propagation, the variance-covariance matrix of the combined error terms $\bar{e}$ can be derived by Equation (3.32), where P is the weight matrix for individual point and σ_{xyz} denotes the standard deviation of the 3D coordinates. Assuming that identical weights for all the 3D points (i.e., $P = I_3$), the term $\Sigma_{\bar{e}}$ can be further simplified to result in Equation (3.33).

$$B = \begin{bmatrix} \frac{\partial d_x}{\partial x} & \frac{\partial d_x}{\partial y} & \frac{\partial d_x}{\partial z} \\ \frac{\partial d_y}{\partial x} & \frac{\partial d_y}{\partial y} & \frac{\partial d_y}{\partial z} \\ \frac{\partial d_z}{\partial x} & \frac{\partial d_z}{\partial y} & \frac{\partial d_z}{\partial z} \end{bmatrix} = \begin{bmatrix} a_y'^2 + a_z'^2 & -a_x' a_y' & -a_x' a_z' \\ -a_x' a_y' & a_x'^2 + a_z'^2 & -a_y' a_z' \\ -a_x' a_z' & -a_y' a_z' & a_x'^2 + a_y' 2 \end{bmatrix} \tag{3.31}$$

$$\Sigma_{\bar{e}} = \sigma_{xyz}^2 B P^{-1} B^T \tag{3.32}$$

$$\Sigma_{\bar{e}} = \sigma_{xyz}^2 B B^T \tag{3.33}$$

The weight matrix of the combined error terms can be obtained as the inverse of the variance-covariance matrix derived above. However, one should note that the matrix $\Sigma_{\bar{e}}$ is rank-deficient with a rank of 2. This implies that the variance-covariance matrix of the combined error term, $\bar{e}$, derived above is non-invertible. In this case,

rather than using the actual inverse, we should use the pseudo inverse to derive the weight matrix of combined error terms.

3.2.3.2 Pseudo Inverse for a Positive Semi-Definite Matrix

Owing to the rank deficiency of the variance-covariance matrix, $\Sigma_{\bar{e}}$, the desired weight matrix of the combined error term is obtained by computing the Moore-Penrose pseudo-inverse of $\Sigma_{\bar{e}}$. The first step to find the Moore-Penrose pseudo-inverse is to conduct an eigenvalue decomposition of the matrix B. Taking into consideration that B is a positive semi-definite symmetric matrix, its eigenvalue decomposition can be written as shown in Equation (3.34), where V is the matrix composed of the eigenvectors of B and Λ is a diagonal matrix with the corresponding eigenvalues. The eigenvalue decomposition of the matrix B indicates that its eigenvalues would be $\lambda_1 = 0$ and $\lambda_2 = \lambda_3 = 1$. The eigenvector corresponding to λ_1 is the vector $(u_x, u_y, u_z)^T$, which lies along the direction of the line. Since the eigenvectors of a symmetric matrix form a set of orthonormal basis vectors, the remaining two eigenvectors will correspond to the two directions, v and w, that are normal to the line, as shown in Figure 2. The derived eigenvectors of the matrix B indicate that the matrix V of eigenvectors actually represents the rotation matrix from the local 3D line coordinate system to the mapping frame coordinate system, or R^{xyz}_{uvw} as shown in Figure 2.

$$B = V\Lambda V^T \tag{3.34}$$

Analyzing the combined error term $\bar{e}$, by substituting the above results for the eigenvalue decomposition of B will result in Equation (3.35). This simplification indicates that the combined error term indeed nullifies the error e_u along the line while only considering the errors e_v and e_w in the two directions normal to the 3D line for conducting the LSA for 3D line fitting. This, in turn, indicates that the effective contribution from each set of observations arising from a 3D point is only 2 equations, as indicated by the rank of the matrix B and interpreted using

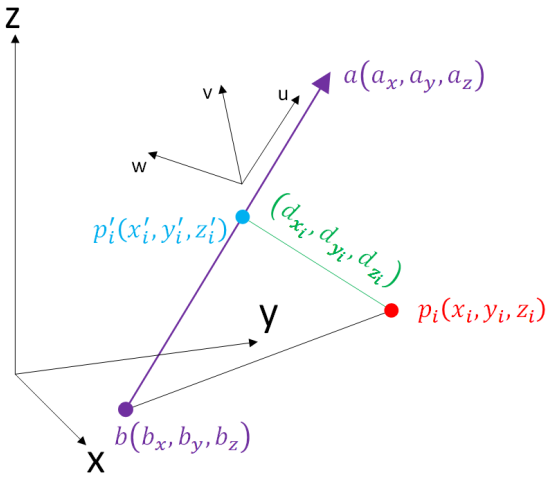

Fig. 3.4.: xyz coordinate system and local coordinate system uvw along 3D line

the eigenvector matrix of B to be considering only the errors along the two normal directions to the line.

$$\bar{e} = Be = V\Lambda \mathrm{V}^{\mathrm{T}} \begin{bmatrix} e_x \\ e_y \\ e_z \end{bmatrix} = R_{uvw}^{xyz} \Lambda R_{xyz}^{uvw} \begin{bmatrix} e_x \\ e_y \\ e_z \end{bmatrix} = R_{uvw}^{xyz} \begin{bmatrix} 0 & 0 & 0 \\ 0 & \lambda_v & 0 \\ 0 & 0 & \lambda_w \end{bmatrix} \begin{bmatrix} e_u \\ e_v \\ e_w \end{bmatrix} = R_{uvw}^{xyz} \begin{bmatrix} 0 \\ e_v \\ e_w \end{bmatrix}$$
$$= \begin{bmatrix} \bar{e}_x \\ \bar{e}_y \\ \bar{e}_z \end{bmatrix} \tag{3.35}$$

Having obtained the eigenvalue decomposition of the matrix B, the next step is to find the Moore-Penrose pseudo-inverse of the variance-covariance matrix, $\Sigma_{\bar{e}}$, as given in Equation (3.36). Finally, the expression $\bar{e}^T(BP^{-1}B^T)^+\bar{e}$ can be simplified as shown in Equation (3.37), which in turn, indicates that the objective function of the resultant LSA model in this approach for 3D line fitting works towards the minimization of normal distance between the line and the given set of 3D points. Thus, the LSA model developed in this section for 3D line fitting works towards the

estimation of line parameters by minimizing the sum of squared errors in the two directions normal to the line and this is ensured by the naturally occurring rank-deficient weight matrix of the combined error term within the LSA model. So, while it appears from initial assessment that each 3D point contributes 3 equations towards the solution, the analysis of the rank-deficient weight matrix indicates an effective contribution of only 2 equations per point.

$$\begin{aligned}\Sigma_{\bar{e}}^{+} &= \sigma_{xyz}^{-2}\left(B\mathrm{P}^{-1}B^{T}\right)^{+} = \sigma_{xyz}^{-2}V\Lambda^{2+}V^{T} \\ &= \sigma_{xyz}^{-2}V\begin{bmatrix}0 & 0 & 0\\ 0 & \frac{1}{\lambda_2^2} & 0\\ 0 & 0 & \frac{1}{\lambda_3^2}\end{bmatrix}V^{T} = \sigma_{xyz}^{-2}V\begin{bmatrix}0 & 0 & 0\\ 0 & 1 & 0\\ 0 & 0 & 1\end{bmatrix}V^{T}\end{aligned} \tag{3.36}$$

$$\begin{aligned}\bar{e}^{T}\left(BP^{-1}B^{T}\right)^{+}\bar{e} &= \bar{e}^{T}R_{uvw}^{xyz}\Lambda^{2+}\bar{e}_{uvw} \\ &= \left(R_{xyz}^{uvw}\bar{e}\right)^{T}\Lambda^{2+}\bar{e}_{uvw} \\ &= \bar{e}_{uvw}^{T}\Lambda^{2+}\bar{e}_{uvw}\end{aligned} \tag{3.37}$$

The LSA procedure aims at estimating the unknown parameters which minimize the sum of squared, weighted residuals as in Equation (3.38), and leads to the solution vector in Equation (3.39), the variance-covariance matrix in Equation (3.40), the predicted residuals in Equation (3.41), and the a-posteriori variance factor in Equation (3.42).

$$\bar{e}^{T}\left(BP^{-1}B^{T}\right)^{+}\bar{e} = \min|_{x} \tag{3.38}$$

$$\hat{x} = \left(A^{T}\left(BP^{-1}B^{T}\right)^{+}A\right)^{-1}A^{T}\left(BP^{-1}B^{T}\right)^{+}y \tag{3.39}$$

$$\Sigma\{\hat{x}\} = \hat{\sigma}_{0}^{2}\left(A^{T}\left(BP^{-1}B^{T}\right)^{+}A\right)^{-1} \tag{3.40}$$

$$\tilde{\bar{e}} = y - A\widehat{x} \tag{3.41}$$

$$\hat{\sigma}_{0}^{2} = \frac{\tilde{\bar{e}}^{T}\left(BP^{-1}B^{T}\right)^{+}\tilde{\bar{e}}}{\mathrm{rank}\left(\left(BP^{-1}B^{T}\right)^{+}\right) - m} \tag{3.42}$$

3.2.4 Representation Scheme of Planar Features

Planar features can be represented by the closest point along a plane to the origin. The vector between the closest point and origin is the normal vector of the planar feature. In a spherical coordinate system, as shown in Figure 3.5, the closest point is represented by (α, β, ρ) [23]. α is the angle between the positive x-axis and the orthogonal projection of the normal vector onto the xy-plane. β is the angle between the positive z-axis and the normal vector of the planar features. ρ is the distance from the origin to the point a. Planes that passes through the origin are represented by $(\alpha, \beta, 0)$.

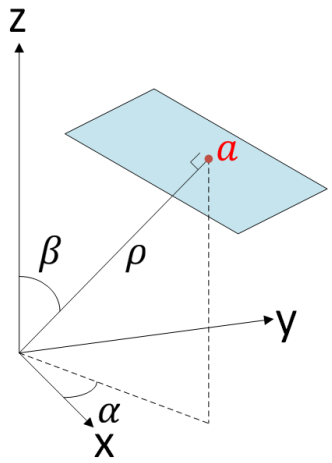

Fig. 3.5.: Representation scheme of planar features in a spherical coordinate system

In a cartesian coordinate system, as shown in Figure 3.6, planar features are represented as (a_x, a_y, a_z), which are the coordinates of the closest point along a plane to the origin, and the cartesian coordinates may be retrieved from the spherical coordinates by Equation (3.43). If there are planes passing through the origin, point clouds will be shifted to avoid the case.

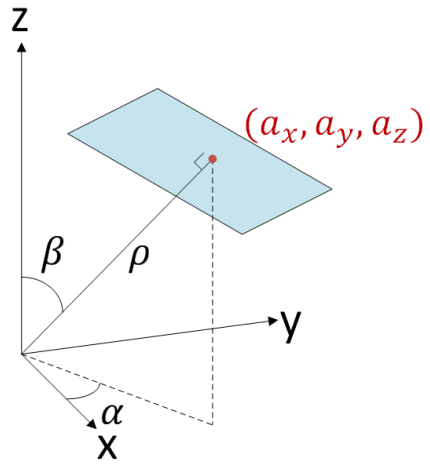

Fig. 3.6.: Representation scheme of planar features in a cartesian coordinate system

$$\begin{bmatrix} a_x \\ a_y \\ a_z \end{bmatrix} = \begin{bmatrix} \rho \sin\beta \cos\alpha \\ \rho \sin\beta \sin\alpha \\ \rho \cos\beta \end{bmatrix} \tag{3.43}$$

3.2.5 Plane Fitting

Given a set of measurements, as shown in Figure 3.7, the process of plane fitting is to find a best-fit plane so that the plane has the minimum sum of squared normal distances to the observed points [24]. Assuming that an observed point is (x_i, y_i, z_i), the normal distance e_{n_i} of the point to the plane surface can be derived by Equation (3.44). The target function of the LSA model aims at minimizing the sum of squared normal distances between the plane and the observed points (x_i, y_i, z_i). The stochastic module of LSA to estimate plane parameters was explained in section 3.1.

$$e_{n_i} = \frac{\left| a_x x_i + a_y y_i + a_z z_i - \left(a_x^2 + a_y^2 + a_z^2\right) \right|}{\sqrt{a_x^2 + a_y^2 + a_z^2}} \tag{3.44}$$

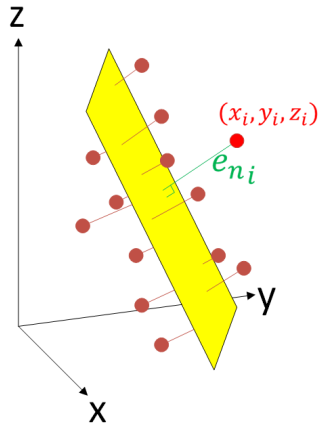

Fig. 3.7.: Schematic illustration of plane fitting by minimizing the normal distances between the observed points and plane in question

3.3 Alternative Approaches for Registration Using Linear/Planar Features

After obtaining the feature parameters in a LSA procedure, the next step is to compute the transformation parameters between two adjacent scans using the attributes of conjugate features. In this section, three alternative registration approaches are presented for the estimation of transformation parameters between adjacent scans. First, the utilized registration primitives are illustrated. Then, the mathematical models of registration approaches are described.

3.3.1 Nonlinear Approach Using Minimal Representation of Linear/Planar Features

The first approach, denoted as feature-based approach, is a nonlinear mathematical model, which makes use of linear or planar features with minimal parameters to determine the transformation parameters. The mathematical models of the feature-

based registration for the estimation of the transformation parameters will be discussed in this subsection.

3.3.1.1 Linear feature-based Registration

The representation scheme of linear features developed by Ayache and Faugeras [22] is adopted in this research because of the minimal representation of linear features using only four parameters. In the source scan, the direction vector of a line is denoted as (a_x, a_y, a_z), and the coordinates of a point along the line are denoted as (b_x, b_y, b_z). (a'_x, a'_y, a'_z) and (b'_x, b'_y, b'_z) denote the parameters of the conjugate line in the reference scan. The first constraint of linear feature-based registration is that the linear features in the source scan should be parallel to the linear features in the reference scan after applying the rotation matrix, as shown in Figure 3.8. This constraint between direction vectors of corresponding linear features is described in Equation (3.45), where λ_1 is the scale factor between the two corresponding linear features, and r_{11}, . . ., r_{33} are the elements of the rotation matrix. Given a line that is mainly oriented along the z-axis in the reference scan, dividing a'_x, a'_y by a'_z on the left-hand side of Equation (3.45) can eliminate the scale factor λ_1, as shown in Equation (3.46).

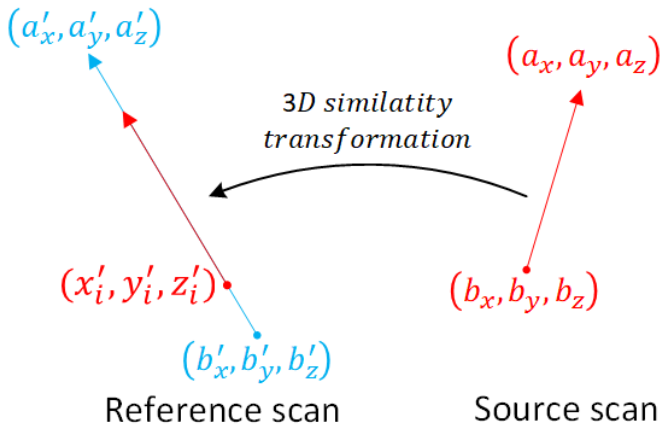

Fig. 3.8.: Transformation of a linear feature in the source scan to the reference scan

$$\begin{bmatrix} a'_x \\ a'_y \\ a'_z \end{bmatrix} = \lambda_1 \begin{bmatrix} r_{11} & r_{12} & r_{13} \\ r_{21} & r_{22} & r_{23} \\ r_{31} & r_{32} & r_{33} \end{bmatrix} \begin{bmatrix} a_x \\ a_y \\ a_z \end{bmatrix} \tag{3.45}$$

$$\begin{aligned} \frac{a'_x}{a'_z} &= \frac{r_{11}a_x + r_{12}a_y + r_{13}a_z}{r_{31}a_x + r_{32}a_y + r_{33}a_z} \\ \frac{a'_y}{a'_z} &= \frac{r_{21}a_x + r_{22}a_y + r_{23}a_z}{r_{31}a_x + r_{32}a_y + r_{33}a_z} \end{aligned} \tag{3.46}$$

Another constraint is that one point along the line segment in the source scan should lie on the conjugate linear feature in the reference scan after applying the 3D similarity transformation parameters, as shown in Figure 3.8. (b_x, b_y, b_z) denotes one point along the line in the source scan. After applying the 3D similarity transformation function, the point (b_x, b_y, b_z) will be transformed to the reference scan, as shown in Equation (3.47). This transformed point is denoted as (x'_i, y'_i, z'_i), which is a point along the line in the reference scan. According to the properties of linear features, any point along the line in the reference scan can be derived by Equation (3.48). Thus, the relationship between non-corresponding points along conjugate lines can be represented by Equation (3.49). Equation (3.50) can be derived by rearranging the different terms in Equation (3.49). Assuming that the line is mainly oriented along the z-axis in the reference scan, the scale factor λ_2 can be eliminated through dividing a'_x, a'_y by a'_z on the left-hand side of Equation (3.50), yielding Equation (3.51). Finally, Equations (3.46), (3.51) are used to estimate the transformation parameters between two overlapping scans.

$$\begin{bmatrix} x'_i \\ y'_i \\ z'_i \end{bmatrix} = \begin{bmatrix} r_{11} & r_{12} & r_{13} \\ r_{21} & r_{22} & r_{23} \\ r_{31} & r_{32} & r_{33} \end{bmatrix} \begin{bmatrix} b_x \\ b_y \\ b_z \end{bmatrix} + \begin{bmatrix} t_x \\ t_y \\ t_z \end{bmatrix} \tag{3.47}$$

$$\begin{bmatrix} x'_i \\ y'_i \\ z'_i \end{bmatrix} = \lambda_2 \begin{bmatrix} a'_x \\ a'_y \\ a'_z \end{bmatrix} + \begin{bmatrix} b'_x \\ b'_y \\ b'_z \end{bmatrix} \tag{3.48}$$

$$\lambda_2 \begin{bmatrix} a'_x \\ a'_y \\ a'_z \end{bmatrix} + \begin{bmatrix} b'_x \\ b'_y \\ b'_z \end{bmatrix} = \begin{bmatrix} t_x \\ t_y \\ t_z \end{bmatrix} + \begin{bmatrix} r_{11} & r_{12} & r_{13} \\ r_{21} & r_{22} & r_{23} \\ r_{31} & r_{32} & r_{33} \end{bmatrix} \begin{bmatrix} b_x \\ b_y \\ b_z \end{bmatrix} \tag{3.49}$$

$$\lambda_2 \begin{bmatrix} a'_x \\ a'_y \\ a'_z \end{bmatrix} = \begin{bmatrix} t_x - b'_x \\ t_y - b'_y \\ t_z - b'_z \end{bmatrix} + \begin{bmatrix} r_{11} & r_{12} & r_{13} \\ r_{21} & r_{22} & r_{23} \\ r_{31} & r_{32} & r_{33} \end{bmatrix} \begin{bmatrix} b_x \\ b_y \\ b_z \end{bmatrix} \tag{3.50}$$

$$\begin{aligned} \frac{a'_x}{a'_z} &= \frac{t_x - b'_x + (r_{11}a_x + r_{12}a_y + r_{13}a_z)}{t_z - b'_z + (r_{31}a_x + r_{32}a_y + r_{33}a_z)} \\ \frac{a'_y}{a'_z} &= \frac{t_y - b'_y + (r_{21}a_x + r_{22}a_y + r_{23}a_z)}{t_z - b'_z + (r_{31}a_x + r_{32}a_y + r_{33}a_z)} \end{aligned} \tag{3.51}$$

The mathematical model of the linear feature-based registration will differ depending on the representation schemes of the linear features. Assuming that a line is mainly oriented along the x-axis in the reference scan, the scale factors in Equations (3.45) and (3.50) could be eliminated through dividing a'_y, a'_z by a'_x, respectively, on the left-hand side of the equations. Similarly, if a line is mainly oriented along the y-axis in the reference scan, λ_1 and λ_2 can be eliminated through dividing the a'_x, a'_z by a'_y, respectively. One should note that the point (b_x, b_y, b_z) in the source scan and (b'_x, b'_y, b'_z) in the reference scan cannot be the same point. If (b_x, b_y, b_z) and (b'_x, b'_y, b'_z) are the same point, the vector in the right-hand side of Equation (3.50) will be equal to $(0, 0, 0)$ and thus Equation (3.50) cannot be transformed to Equation (3.51).

3.3.1.2 Planar feature-based Registration

A Planar feature is represented by the closest point along the plane to the origin. a and a' denote the conjugate planar features in the source and reference scans, respectively. The first constraint for plane-based transformation model is that the normal vector of a planar feature in the source scan should be parallel to the normal vector of the corresponding planar feature in the reference scan after applying the rotation matrix, as shown in Equation (3.52). Assuming that the plane is mainly parallel to the xy-plane in the reference scan, then a'_x and a'_y are divided by a'_z on the left-hand side of Equation (3.52) to eliminate the scale factor λ, yielding Equation (3.53). This mathematical model will differ depending on the orientation of the planar features in the reference scan. Assuming that the plane is mainly parallel to the yz-plane in the reference scan, the scale factor λ could be eliminated through dividing a'_y, a'_z by a'_x, respectively, on the left-hand side of Equation (3.52). Similarly, if a plane is mainly parallel to the xz-plane in the reference scan, λ can be eliminated through dividing a'_x, a'_z by a'_y, respectively.

$$\begin{bmatrix} a'_x \\ a'_y \\ a'_z \end{bmatrix} = \lambda \begin{bmatrix} r_{11} & r_{12} & r_{13} \\ r_{21} & r_{22} & r_{23} \\ r_{31} & r_{32} & r_{33} \end{bmatrix} \begin{bmatrix} a_x \\ a_y \\ a_z \end{bmatrix} \tag{3.52}$$

$$\begin{aligned} \frac{a'_x}{a'_z} &= \frac{r_{11}a_x + r_{12}a_y + r_{13}a_z}{r_{31}a_x + r_{32}a_y + r_{33}a_z} \\ \frac{a'_y}{a'_z} &= \frac{r_{21}a_x + r_{22}a_y + r_{23}a_z}{r_{31}a_x + r_{32}a_y + r_{33}a_z} \end{aligned} \tag{3.53}$$

Another constraint is that one point of a planar feature in the source scan should lie on the corresponding planar feature in the reference scan after applying the 3D similarity transformation function, as shown in Figure 3.9. After applying 3D similarity transformation function, the point a will be transformed to the reference scan, as shown in Equation (3.54). This transformed point is denoted as a_t, which is a

point along the corresponding plane in the reference scan. The vector $\overrightarrow{a'a_t}$, which lies along the plane, can be derived by Equation (3.55). According to Figure 3.9, $\overrightarrow{a'a_t}$ is orthogonal to the vector $\overrightarrow{o'a'}$, which leads to Equation (3.56). Then, Equation (3.56) can be rewritten as the form in Equation (3.57). Rearranging the terms in Equation (3.57), one can get Equation (3.58). Finally, Equations (3.53), (3.58) are used to estimate the transformation parameters between two overlapping scans.

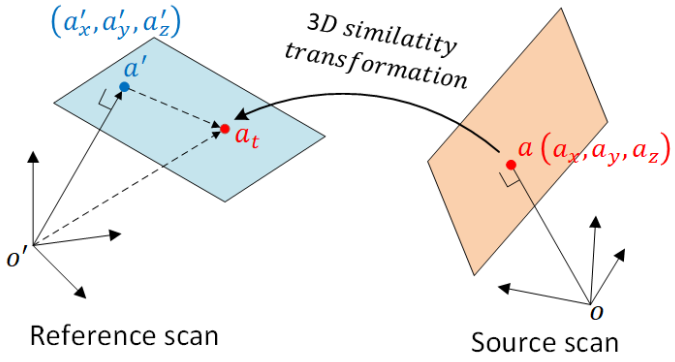

Fig. 3.9.: Transformation of a planar feature in the source scan to the reference scan

$$\overrightarrow{o'a_t} = R \begin{bmatrix} a_x \\ a_y \\ a_z \end{bmatrix} + \begin{bmatrix} t_x \\ t_y \\ t_z \end{bmatrix} \tag{3.54}$$

$$\overrightarrow{a'a_t} = \overrightarrow{o'a_t} - \overrightarrow{o'a'} = \left(R \begin{bmatrix} a_x \\ a_y \\ a_z \end{bmatrix} + \begin{bmatrix} t_x \\ t_y \\ t_z \end{bmatrix} \right) - \begin{bmatrix} a'_x \\ a'_y \\ a'_z \end{bmatrix} \tag{3.55}$$

$$\overrightarrow{a'a_t} \cdot \overrightarrow{o'a'} = 0 \tag{3.56}$$

$$\left(\left(R \begin{bmatrix} a_x \\ a_y \\ a_z \end{bmatrix} + \begin{bmatrix} t_x \\ t_y \\ t_z \end{bmatrix} \right) - \begin{bmatrix} a'_x \\ a'_y \\ a'_z \end{bmatrix} \right) \cdot \begin{bmatrix} a'_x \\ a'_y \\ a'_z \end{bmatrix} = 0 \tag{3.57}$$

$$\left(R \begin{bmatrix} a_x \\ a_y \\ a_z \end{bmatrix} + \begin{bmatrix} t_x \\ t_y \\ t_z \end{bmatrix} \right) \cdot \begin{bmatrix} a'_x \\ a'_y \\ a'_z \end{bmatrix} = {a'_x}^2 + {a'_y}^2 + {a'_z}^2 \tag{3.58}$$

3.3.2 Nonlinear Approach Using Pseudo-Conjugate Points Along Linear/Planar Features

The second approach, denoted as the pseudo-conjugate point-based method, was proposed by Renaudin et al. [7]. The pseudo-conjugate point-based method, which is a nonlinear mathematical model, deals with non-corresponding points along conjugate linear and planar features. The mathematical model of the LSA method with a modified weight matrix is introduced in this subsection, followed by the process of modifying a weight matrix.

Since linear and planar features are comprised of a set of points, the mathematical model for conjugate points in adjacent scans would get the form in Equation (3.59), which is a nonlinear function. The mathematical relationship in Equation (3.59) can be represented by the Gauss-Markov stochastic model as given in Equation (3.60). In Equation (3.60), y is the vector of observation equations with an associated weight matrix denoted by $\bar{P}$; A is the design matrix composed of the partial derivatives with respect to the unknown parameters; x is the vector of unknown parameters; and σ_0^2 is the a-priori variance factor. The combined error term, $\bar{e}$, is given in Equation (3.61), where e is random noise contaminating the x, y, and z coordinates of the point along the linear or planar features, and B is a matrix composed of the partial derivatives with respect to the observations. According to the law of error propagation, $\bar{P}$ can

be derived by Equation (3.62), where P is the weight matrix associated with the observations.

$$\begin{bmatrix} b'_x - e_{b'_x} \\ b'_y - e_{b'_y} \\ b'_z - e_{b'_z} \end{bmatrix} = \begin{bmatrix} t_x \\ t_y \\ t_z \end{bmatrix} + R \begin{bmatrix} b_x - e_{b_x} \\ b_y - e_{b_y} \\ b_z - e_{b_z} \end{bmatrix} \tag{3.59}$$

$$y = Ax + \bar{e}, \quad \bar{e} \sim (0, \sigma_0^2 \bar{P}^{-1}) \tag{3.60}$$

$$\bar{e} = Be = - \begin{bmatrix} e_{b'_x} \\ e_{b'_y} \\ e_{b'_z} \end{bmatrix} + R \begin{bmatrix} e_{b_x} \\ e_{b_y} \\ e_{b_z} \end{bmatrix} \tag{3.61}$$

$$\bar{P} = \left(B P^{-1} B^{\mathrm{T}} \right)^{-1} \tag{3.62}$$

However, the points of the corresponding extracted linear and planar features are not conjugate to each other. In this case, the traditional Gauss-Markov stochastic model cannot be used to estimate the unknown parameters. Therefore, an additional unknown vector d must be added to the mathematical model as in Equation (3.63), and this will lead to the Gauss-Markov stochastic model in Equation (3.64). For linear features, the additional unknown vector d is defined along the line direction and has no components perpendicular to the line, as shown in Figure 3.10(a). For planar features, on the other hand, the additional unknown vector d is defined along the plane surface and has no components perpendicular to the plane, as shown in Figure 3.10(b).

$$\begin{bmatrix} b'_x - e_{b'_x} \\ b'_y - e_{b'_y} \\ b'_z - e_{b'_z} \end{bmatrix} = \begin{bmatrix} t_x \\ t_y \\ t_z \end{bmatrix} + R \begin{bmatrix} b_x - e_{b_x} \\ b_y - e_{b_y} \\ b_z - e_{b_z} \end{bmatrix} + \begin{bmatrix} d_x \\ d_y \\ d_z \end{bmatrix} \tag{3.63}$$

$$y = Ax + d + \bar{e}, \quad \bar{e} \sim (0, \sigma_0^2 \bar{P}^{-1}) \tag{3.64}$$

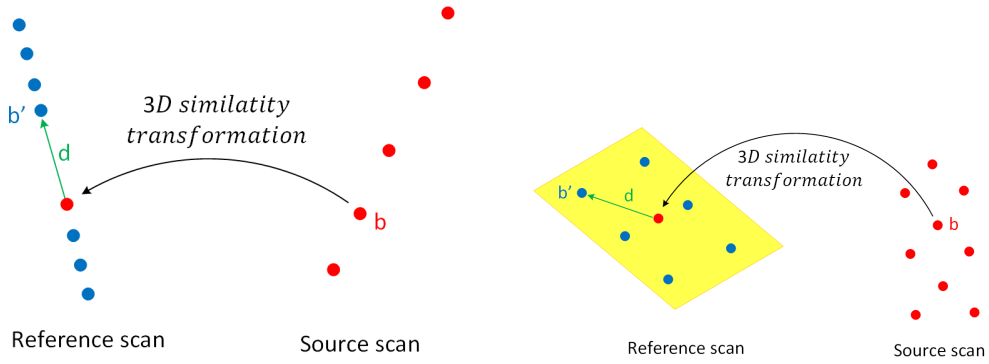

(a) The similarity measure between pseudo-conjugate points lying on conjugate linear features in the source and reference scans and unknown vector d which is defined along the linear feature.

(b) The similarity measure between pseudo-conjugate points lying on conjugate planar features in the source and reference scans and unknown vector d which is defined along the planar surface.

Fig. 3.10.: 3D similarity transformation relating pseudo-conjugate points along conjugate linear/planar features and the additional unknown vector d which is defined along conjugate linear/planar features

Renaudin et al. [7] proposed a pseudo-conjugate point-based method, which can eliminate the additional unknown vector d by modifying the weight matrix in the Gauss-Markov stochastic model. The pseudo-conjugate point-based method aims at estimating the transformation parameters while dealing with non-corresponding points along conjugate linear and planar features. In order to eliminate the additional unknown vector d in Equation (3.64), the weight matrix, $\bar{P}$, can be modified in a way that the unknown vector d belongs to the null space of the artificially modified weight matrix $\bar{P}'$. Such a condition indicates that the modified weight matrix $\bar{P}'$ is rank-deficient; that is, the inverse of $\bar{P}'$ does not exist. Based on that, the modified stochastic properties of the random noise vector is represented by Equation (3.65), where the plus sign indicates the Moore-Penrose pseudoinverse.

$$\Sigma'\{\bar{e}\} = \sigma_0^2 \bar{P}'^{+}, \quad \bar{P}'d = 0 \tag{3.65}$$

The LSA target function can be modified as in Equation (3.66), and Equation (3.67) can be obtained by eliminating the unknown vector. The solution vector $\hat{x}$ can be derived using Equation (3.68). Equation (3.69) shows the variance-covariance matrix for the solution vector. The a-posteriori variance factor can be derived according to Equation (3.70), where the redundancy is given by the difference between the rank of the modified weight matrix and the number of unknown parameters [7].

$$\bar{e}^{\mathrm{T}}\bar{P}'\bar{e} = (y - A\hat{x} - d)^{\mathrm{T}}\bar{P}'(y - A\hat{x} - d) = min|_{\hat{x},d} \tag{3.66}$$

$$\bar{e}^{\mathrm{T}}\bar{P}'\bar{e} = (y - A\hat{x})^{\mathrm{T}}\bar{P}'(y - A\hat{x}) = min|_{\hat{x}} \tag{3.67}$$

$$\hat{x} = (A^{\mathrm{T}}\bar{P}'A)^{-1}A^{\mathrm{T}}\bar{P}'y \tag{3.68}$$

$$\Sigma\{\hat{x}\} = \hat{\sigma}_0^2(A^{\mathrm{T}}\bar{P}'A)^{-1} \tag{3.69}$$

$$\hat{\sigma}_0^2 = \frac{\tilde{\bar{e}}^{\mathrm{T}}\bar{P}'\tilde{\bar{e}}}{rank(\bar{P}') - m} \tag{3.70}$$

Because the additional unknown vector d is defined along the geometric features in the reference coordinate system, in order to eliminate the unknown vector d, geometric features extracted from the reference scan are used to modify the weight matrix. The process of modifying the weight matrix is described as follows. A local coordinate system (UVW) is established first. For linear features, the U axis is defined along the line direction, and the V and W axes are arbitrarily defined in a way that they should be orthogonal to each other and to the line direction. For planar features, the W axis is parallel to the plane normal, and the U and V axes are aligned along the plane in question. An illustration of the local coordinate systems for linear and planar features is shown in Figures 3.11.

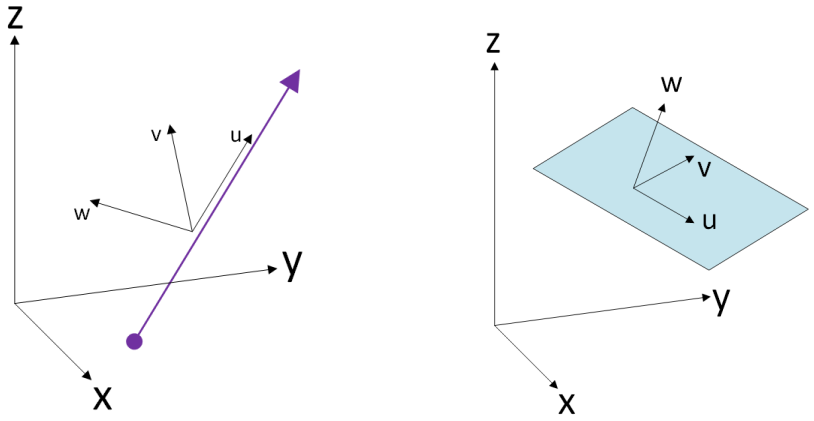

(a) (b)

Fig. 3.11.: Local coordinate systems for linear (a) and planar (b) features.

A rotation matrix M, which relates the reference coordinate system and the local coordinate system along a linear or planar feature, is derived according to the components of the unit vectors UVW relative to the reference coordinate system. The weight matrix $\bar{P}$ is derived by Equation (3.71), where P is obtained by the inverse of the variance-covariance matrix of measurements. According to Equation (3.72), the weight matrix $\bar{P}$ is transformed to a weight matrix P_{UVW} in the local coordinate system using the law of error propagation.

$$\bar{P} = \left(BP^{-1}B^{\mathrm{T}}\right)^{-1} \tag{3.71}$$

$$P_{UVW} = M\bar{P}M^{\mathrm{T}} = \begin{bmatrix} P_U & P_{UV} & P_{UW} \\ P_{VU} & P_V & P_{VW} \\ P_{WU} & P_{WV} & P_W \end{bmatrix} \tag{3.72}$$

The weight matrix P_{UVW} can be modified by setting a zero weight in the elements corresponding to the U axis for linear features, as shown in Equation (3.73). When dealing with planar features, one can assign a zero value for the elements corresponding to the U and V axes in the weight matrix according to Equation (3.74). Finally,

the modified weight matrix P_{UVW} can be transformed from the local coordinate system to the reference coordinate system using the law of error propagation according to Equation (3.75).

$$P'_{UVW} = \begin{bmatrix} 0 & 0 & 0 \\ 0 & P_V & P_{VW} \\ 0 & P_{WV} & P_W \end{bmatrix} \tag{3.73}$$

$$P'_{UVW} = \begin{bmatrix} 0 & 0 & 0 \\ 0 & 0 & 0 \\ 0 & 0 & P_W \end{bmatrix} \tag{3.74}$$

$$\bar{P}' = M^{\mathrm{T}} P'_{UVW} M \tag{3.75}$$

3.3.3 Linear Approach Using Quaternion to Represent Rotation

An initial guess for the transformation parameters is required in the feature-based and pseudo-conjugate point-based approaches since these mathematical models are nonlinear. By contrast, the third strategy is a closed-form solution and does not require an initial guess. The closed-form solution utilizes unit quaternions to represent rotation. The rotation parameters are determined in a single-step, and then the translation is determined by using the pseudo-conjugate point-based approach. The basics of the quaternion are presented as well in this subsection.

3.3.3.1 Estimation of Rotation Parameters

A linear feature in the source scan will be parallel to its conjugate linear feature in the reference scan after rotation. Similarly, the normal vector of a planar feature in the source scan will be parallel to the normal vector of the corresponding planar feature in the reference scan after rotation, as shown in Equation (3.76), where a_i and

a_i' are unit vectors of conjugate linear features or unit normal vectors of corresponding planar features in the source and reference scans, R is the rotation matrix, and e_i is random noise contaminating the observations. Assuming that there is a set of n conjugate linear or planar features and the vectors a_i and $a_i{}'$ are pointing in the same direction, the rotation matrix R can be determined on LSA basis through minimizing the sum of squared residuals, as shown in Equation (3.77).

$$a_i' = Ra_i + e_i \tag{3.76}$$

$$\begin{aligned} \min_R \sum_{i=1}^{n} e_i^{\mathrm{T}} e_i &= \min_R \sum_{i=1}^{n} \left(a_i' - Ra_i\right)^{\mathrm{T}} \left(a_i' - Ra_i\right) \\ &= \min_R \sum_{i=1}^{n} \left(a_i'^{\mathrm{T}} a_i' + a_i^{\mathrm{T}} a_i - 2a_i^{\mathrm{T}} R^{\mathrm{T}} a_i'\right) \end{aligned} \tag{3.77}$$

The first two terms $a_i'^{\mathrm{T}} a_i'$ and $a_i^{\mathrm{T}} a_i$ in Equation (3.77) are positive and do not depend on R. Only the third term depends on the rotation matrix R. The third term is always positive since Ra_i and a_i' are pointing in the same direction. Therefore, by ignoring the first two constant terms, minimizing the sum of squared residuals is equivalent to maximizing the third term. Horn [17], Guan and Zhang [18], He and Habib [19] introduced an approach to find the rotation that maximizes the term by using unit quaternions. To explain this approach, let us first introduce the related quaternion basics. A quaternion is a four-component vector consisting of a scalar part and three imaginary parts. Formally, a quaternion $\dot{q}$ can be defined as $\dot{q} = q_0 + q_1 i + q_2 j + q_3 k$. A quaternion can be normalized by dividing each of the four components by its norm to obtain a unit quaternion, which is used to represent rotation.

According to quaternion properties, the rotation of a_i to a_i' can be performed by $\dot{a}_i' = \dot{q}\dot{a}_i\dot{q}^*$, where the unit quaternion $\dot{q}$ corresponds to a rotation matrix R, and $\dot{q}^*$ denotes the conjugate quaternion, which is constructed by negating the imaginary part of $\dot{q}$. The term $\dot{a}_i$ is a pure quaternion (scalar part is zero) corresponding to vector a_i. The quaternion product can be converted into a matrix-vector product using

Matrices $C_{\dot{a}_i}$ and $\bar{C}_{\dot{a}_i}$. For instance, the quaternion product $\dot{a}_1\dot{a}_2$ can be rewritten in the forms given in Equation (3.78). Matrices $C_{\dot{a}_i}$ and $\bar{C}_{\dot{a}_i}$ are defined in Equations (3.79) and (3.80), and matrices $C_{\dot{a}_i^*}$ and $\bar{C}_{\dot{a}_i^*}$ are given in Equations (3.81) and (3.82). Thus, the term $a_i^T R^T a_i'$ can be transformed into the form as given in Equation (3.83).

$$\dot{a}_1\dot{a}_2 = C_{\dot{a}_1}\dot{a}_2 = \bar{C}_{\dot{a}_2}\dot{a}_1 \tag{3.78}$$

$$C_{\dot{a}_i} = \begin{bmatrix} \dot{a}_{i_0} & -\dot{a}_{i_x} & -\dot{a}_{i_y} & -\dot{a}_{i_z} \\ \dot{a}_{i_x} & \dot{a}_{i_0} & -\dot{a}_{i_z} & \dot{a}_{i_y} \\ \dot{a}_{i_y} & \dot{a}_{i_z} & \dot{a}_{i_0} & -\dot{a}_{i_x} \\ \dot{a}_{i_z} & -\dot{a}_{i_y} & \dot{a}_{i_x} & \dot{a}_{i_0} \end{bmatrix} \tag{3.79}$$

$$\bar{C}_{\dot{a}_i} = \begin{bmatrix} \dot{a}_{i_0} & -\dot{a}_{i_x} & -\dot{a}_{i_y} & -\dot{a}_{i_z} \\ \dot{a}_{i_x} & \dot{a}_{i_0} & \dot{a}_{i_z} & -\dot{a}_{i_y} \\ \dot{a}_{i_y} & -\dot{a}_{i_z} & \dot{a}_{i_0} & \dot{a}_{i_x} \\ \dot{a}_{i_z} & \dot{a}_{i_y} & -\dot{a}_{i_x} & \dot{a}_{i_0} \end{bmatrix} \tag{3.80}$$

$$C_{\dot{a}_i^*} = \begin{bmatrix} \dot{a}_{i_0} & \dot{a}_{i_x} & \dot{a}_{i_y} & \dot{a}_{i_z} \\ -\dot{a}_{i_x} & \dot{a}_{i_0} & \dot{a}_{i_z} & -\dot{a}_{i_y} \\ -\dot{a}_{i_y} & -\dot{a}_{i_z} & \dot{a}_{i_0} & \dot{a}_{i_x} \\ -\dot{a}_{i_z} & \dot{a}_{i_y} & -\dot{a}_{i_x} & \dot{a}_{i_0} \end{bmatrix} = C_{\dot{a}_i}^T \tag{3.81}$$

$$\bar{C}_{\dot{a}_i^*} = \begin{bmatrix} \dot{a}_{i_0} & \dot{a}_{i_x} & \dot{a}_{i_y} & \dot{a}_{i_z} \\ -\dot{a}_{i_x} & \dot{a}_{i_0} & -\dot{a}_{i_z} & \dot{a}_{i_y} \\ -\dot{a}_{i_y} & \dot{a}_{i_z} & \dot{a}_{i_0} & -\dot{a}_{i_x} \\ -\dot{a}_{i_z} & -\dot{a}_{i_y} & \dot{a}_{i_x} & \dot{a}_{i_0} \end{bmatrix} = \bar{C}_{\dot{a}_i}^T \tag{3.82}$$

$$
\begin{aligned}
\max_{R} \sum_{i=1}^{n} a_i^T R^T a_i' &= \max_{R} \sum_{i=1}^{n} (R a_i) \cdot a_i' \\
&= \max_{\dot{q}} \sum_{i=1}^{n} (\dot{q} \dot{a}_i \dot{q}^*) \cdot \dot{a}_i' \\
&= \max_{\dot{q}} \sum_{i=1}^{n} (\dot{q} \dot{a}_i C_{\dot{q}^*}) \cdot \dot{a}_i' \\
&= \max_{\dot{q}} \sum_{i=1}^{n} (\dot{q} \dot{a}_i) \cdot \left(\dot{a}_i' C_{\dot{q}^*}^T\right) \\
&= \max_{\dot{q}} \sum_{i=1}^{n} (\dot{q} \dot{a}_i) \cdot (\dot{a}_i' C_{\dot{q}}) \\
&= \max_{\dot{q}} \sum_{i=1}^{n} (\dot{q} \dot{a}_i) \cdot (\dot{a}_i' \dot{q})
\end{aligned}
\tag{3.83}
$$

Next, we use the matrix notation to express quaternion multiplication as matrix-vector multiplication, which is shown in Equation 3.84. By adjoining the unity constraint, the optimal quaternion is obtained by maximizing the target function in Equation (3.85), where λ is the Lagrange multiplier. Taking the partial derivatives of Equation (3.85) with respect to $\dot{q}$ gives Equation (3.86). Therefore, the unit quaternion $\dot{q}$ that maximizes this sum is the eigenvector that corresponds to the largest eigenvalue of the 4×4 matrix S.

$$
\begin{aligned}
\max_{\dot{q}} \sum_{i=1}^{n} (\dot{q} \dot{a}_i) \cdot (\dot{a}_i' \dot{q}) &= \max_{q} \sum_{i=1}^{n} \left(\bar{C}_{\dot{a}_i} \dot{q}\right) \cdot \left(C_{\dot{a}_i'} \dot{q}\right) \\
&= \max_{\dot{q}} \sum_{i=1}^{n} \dot{q}^{\mathrm{T}} \bar{C}_{\dot{a}_i}^{\mathrm{T}} C_{\dot{a}_i'} \dot{q} \\
&= \max_{\dot{q}} \dot{q}^{\mathrm{T}} \left(\sum_{i=1}^{n} \bar{C}_{\dot{a}_i}^{\mathrm{T}} C_{\dot{a}_i'} \right) \dot{q} \\
&= \max_{\dot{q}} \dot{q}^{\mathrm{T}} S \dot{q}
\end{aligned}
\tag{3.84}
$$

$$
\max_{\dot{q}} \varphi(\dot{q}) = \dot{q}^{\mathrm{T}} S \dot{q} - \lambda(\dot{q}^{\mathrm{T}} \dot{q} - 1) \tag{3.85}
$$

$$
\frac{\partial \varphi}{\partial \dot{q}} = 2S\dot{q} - 2\lambda\dot{q} = 0 \tag{3.86}
$$

3.3.3.2 Estimation of Translation Parameters

After the estimation of rotation by using unit quaternions, the next step is to estimate the translation parameters by using the pseudo-conjugate point-based method, in which non-corresponding points along conjugate linear or planar features are used to derive the registration parameters. Supposing that the points on corresponding linear or planar features are conjugate to each other, the 3D similarity transformation function relating the points in different scans would be the form in Equation (3.87).

$$\begin{bmatrix} b'_x - e_{b'_x} \\ b'_y - e_{b'_y} \\ b'_z - e_{b'_z} \end{bmatrix} = \begin{bmatrix} t_x \\ t_y \\ t_z \end{bmatrix} + R \begin{bmatrix} b_x - e_{b_x} \\ b_y - e_{b_y} \\ b_z - e_{b_z} \end{bmatrix} \tag{3.87}$$

Once the rotation matrix is derived, all points in the source scan will be rotated by applying the estimated rotation angles, and the new coordinates of each point in the rotated scan are given in Equation (3.88). Then, the mathematical expression in Equation (3.87) can be rewritten in the form given in Equation (3.89). The Gauss-Markov stochastic model in Equation (3.90) can be used to represent this mathematical relationship. In Equation (3.90), y is the vector of observation equations with an associated weight matrix denoted by $\bar{P}$; A is the design matrix composed of the partial derivatives with respect to the unknown parameters; x is the vector of unknown parameters; and σ_0^2 is the a-priori variance factor. The combined error term, $\bar{e}$, is given in Equation (3.91), where e is random noise contaminating the x, y, and z coordinates of the point along the linear or planar features, and B is a matrix composed of the partial derivatives with respect to the observations. According to the law of error propagation, $\bar{P}$ can be derived by Equation (3.92), where P is the weight matrix associated with the observations.

$$\begin{bmatrix} br_x - e_{br_x} \\ br_y - e_{br_y} \\ br_z - e_{br_z} \end{bmatrix} = R \begin{bmatrix} b_x - e_{b_x} \\ b_y - e_{b_y} \\ b_z - e_{b_z} \end{bmatrix} \tag{3.88}$$

$$\begin{bmatrix} b'_x - e_{b'_x} \\ b'_y - e_{b'_y} \\ b'_z - e_{b'_z} \end{bmatrix} = \begin{bmatrix} t_x \\ t_y \\ t_z \end{bmatrix} + \begin{bmatrix} br_x - e_{br_x} \\ br_y - e_{br_y} \\ br_z - e_{br_z} \end{bmatrix} \tag{3.89}$$

$$y = Ax + \bar{e}, \quad \bar{e} \sim (0, \sigma_0^2 \bar{P}^{-1}) \tag{3.90}$$

$$\bar{e} = Be = - \begin{bmatrix} e_{b'_x} \\ e_{b'_y} \\ e_{b'_z} \end{bmatrix} + \begin{bmatrix} e_{br_x} \\ e_{br_y} \\ e_{br_z} \end{bmatrix} \tag{3.91}$$

$$\bar{P} = (BP^{-1}B^T)^{-1} \tag{3.92}$$

However, the points along corresponding linear or planar features are not conjugate to each other. In this case, the traditional Gauss-Markov stochastic model cannot be used to estimate the unknown parameters. Therefore, an additional unknown vector must be added to the mathematical model as in Equation (3.93), and this will lead to the stochastic model in Equation (3.94). For linear features, the additional unknown vector d is defined along the line direction and has no components perpendicular to the line. For planar features, the additional unknown vector d is defined along the plane surface and has no components perpendicular to the plane. The additional unknown vector can be eliminated by modifying the weight matrix in the Gauss-Markov stochastic model [7, 19]. The process of modifying the weight matrix was described in subsection 3.3.2.

$$\begin{bmatrix} b'_x - e_{b'_x} \\ b'_y - e_{b'_y} \\ b'_z - e_{b'_z} \end{bmatrix} = \begin{bmatrix} t_x \\ t_y \\ t_z \end{bmatrix} + \begin{bmatrix} br_x - e_{br_x} \\ br_y - e_{br_y} \\ br_z - e_{br_z} \end{bmatrix} + \begin{bmatrix} d_x \\ d_y \\ d_z \end{bmatrix} \tag{3.93}$$

$$y = Ax + d + \bar{e}, \quad \bar{e} \sim (0, \sigma_0^2 \bar{P}^{-1}) \tag{3.94}$$

3.4 Quality Evaluation

In order to evaluate the estimated transformation parameters, average normal distances between the transformed surface and reference surface are calculated. Due to the irregular nature of point clouds describing surface models, exact point-to-point correspondence cannot be assumed. Thus, quality analysis is performed by calculating the point-to-patch normal distances between the registered surfaces, as shown in Figure 3.12.

After applying the transformation parameters to one point in the source scan, the three closest points of the transformed point are found in the reference scan. A patch, which is defined by the three closest points, and a transformed point are considered as a matching pair if the following criteria are satisfied: the projection of the transformed point onto the patch must be inside the triangle defined by its vertices; and the normal distance between the transformed point and the patch must be within a certain threshold, which is defined based on the data noise level and the average point density. Then, the quality of fit between the registered surfaces is evaluated by calculating the mean, standard deviation, root-mean-square error (RMSE) of the normal distances, as well as the number of matched point-to-patch pairs.

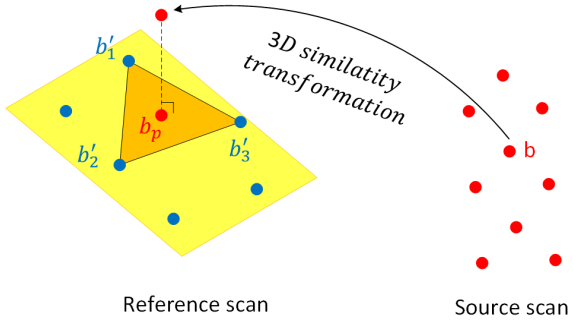

Fig. 3.12.: Conceptual basis of the point-to-patch correspondence procedure: projected point b_p is inside the patch and the normal distance between the transformed point and the patch must be within a certain threshold

3.5 Summary

Three different registration approaches are introduced in this chapter. The fitting models of linear and planar features are explained first before exploring the registration approaches. Two approaches of line fitting are proposed in this chapter. In the first approach, line fitting is performed by minimizing 2D distances of points from the line measured parallel to the coordinated planes, while the second one is conducted by minimizing the orthogonal distance between points and a line. Next, three alternative registration approaches are outlined in detail. In the feature-based approach, the registration parameters are estimated while imposing collinearity or coplanarity constraints on parameter values of corresponding linear of planar features. In the pseudo-conjugate point-based method, a point-based 3D similarity function is used to relate points of corresponding linear or planar features. Since points along the corresponding features might not be conjugate to each other, their weight matrices in LSA are modified in order to eliminate the discrepancies between the pseudo-conjugate points. The feature-based and pseudo-conjugate point-based approaches are nonlinear, so an initial guess of transformation parameters is required in these two approaches. By contrast, the closed-form solution is linear since it uses unit quaternions to represent rotation angles. Therefore, the closed-form solution does

not require an initial guess of transformation parameters. Finally, the average point-to-patch normal distance following the registration is taken as a measure to evaluate the estimated transformation parameters.

4. EXPERIMENTAL RESULTS

In this chapter, the feature-based approach, pseudo-conjugate point-based method, and closed-form solution will be tested with simulated and real datasets. The primary objective of the experiments is to assess the performance of the three registration approaches. In addition, the registration results of the registration approaches using linear and planar features are compared to find out whether the two feature primitives produce equivalent results or not. In the first experiment, the performance of the introduced registration approaches will be tested using simulated laser scans over a building model. In the second experiment, real datasets were collected over the Forney Hall of Chemical Engineering at Purdue University. In total, eight scans were collected using a FARO Focus3D terrestrial laser scanner.

4.1 Experiments with Simulated Data

The performance of the introduced registration approaches will be first tested using simulated laser scans, for which the true transformation parameters are known. The geometric parameters of the linear and planar features are simulated first, and then points along the linear and planar features are simulated using the simulated geometric parameters. After the simulation of points along the linear and planar features, the three different registration approaches were conducted using both features. The performance of the registration approaches with simulated linear and planar features are presented and evaluated in the following sections. Quality evaluation was conducted based on the point-to-point distances following the registration.

The simulated building module, as well as the relative location and orientation of the simulated scans, are illustrated in Figure 4.1. Two scans (source and reference scans) are simulated in this experiment. The 3D similarity transformation parame-

ters include three translations (t_x, t_y, t_z), three rotation angles (ω, ϕ, κ), and one scale factor λ. Since TLS scans provide true scale, the scale between the source and reference scans was fixed to one during the LSA procedure. The simulated transformation parameters between the source and reference scans are illustrated in Table 4.1.

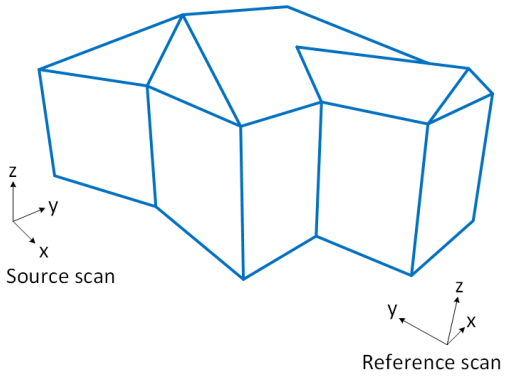

Fig. 4.1.: Simulated building module

Table 4.1.: Simulated transformation parameters

	$t_x(m)$	$t_y(m)$	$t_z(m)$	$\omega(^\circ)$	$\phi(^\circ)$	$\kappa(^\circ)$
True value	0	100	0	10	20	80

25 pairs of linear features and 10 pairs of planar features are used in this study. Point clouds along the linear and planar features in the source scan are simulated first. The process of simulating points along the linear and planar features are described as follows. In order to evaluate the parameters of the linear and planar features, the coordinates of the vertices of the building in the source scan are simulated. For linear features, line parameters are evaluated using two vertices along each line segment. Then, points are simulated along the line segments using the established line parameters. The simulated lines and their IDs are shown in Figure 4.2. The number of

points and length of each linear feature are summarized in Table 4.2. Similarly, the plane parameters are evaluated using three vertices along each planar patch. Then, points are simulated along the planar patches using the established plane parameters. The planes and their ID are shown in Figure 4.3(a). The plane 10 ($P10$) is the floor of the simulated building. Although it is impossible to scan the $P10$ using TLS, $P10$ is just used for illustration of the registration approaches based on planar features. The simulated points displayed in CloudCompare software [25] are shown in Figure 4.3(b). Points are colored according to plane ID. The number of points along each planar feature is summarized in Table 4.3.

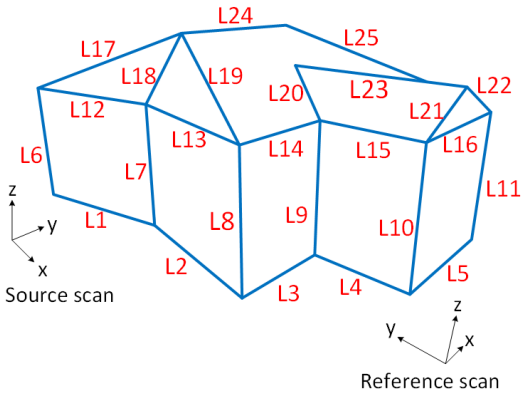

Fig. 4.2.: Simulated linear features with line IDs

Table 4.2.: Number of simulated points along each linear feature, length of each linear feature, and the total number of simulated points along 25 linear features in the source scan

Line ID	Number of points	Length (m)	Line ID	Number of points	Length (m)
1	200	25.368	14	120	14.875
2	200	25.368	15	120	14.875
3	120	14.875	16	160	19.875
4	120	14.875	17	200	29.537
5	160	19.875	18	80	12.344
6	160	19.875	19	200	29.537
7	160	19.875	20	100	16.603
8	160	19.875	21	80	11.041
9	160	19.875	22	80	11.041
10	160	19.875	23	220	27.375
11	160	19.875	24	200	24.875
12	200	25.368	25	200	29.537
13	200	25.368	Total	3,920	

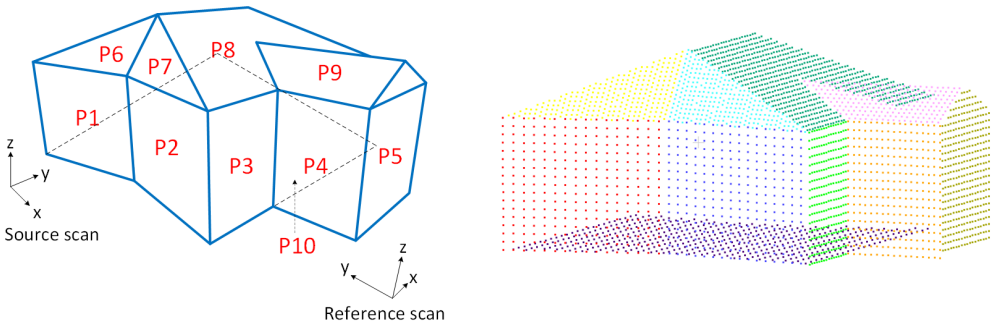

(a) Planar features and plane IDs (b) Simulated points in CloudCompare

Fig. 4.3.: Simulated points along planar features

Table 4.3.: Number of simulated points along each planar feature and the total number of simulated points along 10 planar features in the source scan

Plane ID	Number of points
1	289
2	289
3	289
4	289
5	461
6	288
7	282
8	751
9	231
10	517
Total	3,686

After the simulation of points along the linear and planar features in the source scan, then all generated points are transformed into the reference scan using the simulated transformation parameters. The simulated line parameters in the source and reference scans are presented in Table 4.4. The simulated plane parameters in the source and reference scans are shown in Table 4.5. So far, point clouds along the linear and planar features have been simulated in both scans. Next, the X, Y, and Z coordinates of the simulated points in both scans are contaminated with random noise, which is ± 3 cm at one sigma.

Table 4.4.: The simulated line parameters which are derived using two simulated vertices lying on the linear features in the source and reference scans

	Line ID	a_x	a_y	a_z	$b_x(m)$	$b_y(m)$	$b_z(m)$
Source Scan	1	1	0.2	0	0	8	10
	2	1	-0.2	0	0	22	10
	3	0	1	0	60	0	10
	4	1	0	0	0	25	10
	5	0	1	0	75	0	10
	6	0	0	1	10	10	0
	7	0	0	1	35	15	0
	8	0	0	1	60	10	0
	9	0	0	1	60	25	0
	10	0	0	1	75	25	0
	11	0	0	1	75	45	0
	12	1	0.2	0	0	8	30
	13	1	-0.2	0	0	22	30
	14	0	1	0	60	0	30
	15	1	0	0	0	25	30

continued on next page

Table 4.4.: *continued*

	Line ID	a_x	a_y	a_z	$b_x(m)$	$b_y(m)$	$b_z(m)$
	16	0	1	0	75	0	30
	17	1	0.5	0.4	0	5	26
	18	0	0.75	1	35	-7.5	0
	19	1	-0.5	-0.4	0	40	54
	20	1	-0.8	-0.4	0	73	54
	21	0	1	0.5	75	0	17.5
	22	0	1	-0.5	75	0	52.5
	23	1	0	0	0	35	35
	24	0	1	0	35	0	40
	25	1	0.5	-0.4	0	30	54
Reference Scan	1	-0.3978	1	-0.3427	50.5474	0	43.7624
	2	0.0347	1	-0.3952	19.0114	0	47.5968
	3	1	0.1148	-0.1665	0	46.8405	31.5926
	4	-0.1763	1	-0.3696	44.396	0	44.5103
	5	1	0.1148	-0.1665	0	32.6783	37.1304
	6	0.1216	0.391	1	11.2159	91.1717	0
	7	0.1216	0.391	1	19.2556	65.5745	0
	8	0.1216	0.391	1	17.2954	38.214	0
	9	0.1216	0.391	1	32.2954	40.8589	0
	10	0.1216	0.391	1	34.1192	24.9716	0
	11	0.1216	0.391	1	54.1192	28.4981	0
	12	-0.3978	1	-0.3427	55.6771	0	64.7505
	13	0.0347	1	-0.3952	21.011	0	68.9656
	14	1	0.1148	-0.1665	0	53.8194	50.4756
	15	-0.1763	1	-0.3696	47.9225	0	65.6934

continued on next page

Table 4.4.: *continued*

Line ID	a_x	a_y	a_z	$b_x(m)$	$b_y(m)$	$b_z(m)$
16	1	0.1148	-0.1665	0	39.6571	56.0134
17	-0.9639	1	-0.8705	113.8279	0	118.9745
18	1	0.5265	0.9474	0	67.6299	14.7483
19	0.3302	1	-0.0474	4.3276	0	49.3304
20	0.574	1	-0.0883	4.2947	0	49.3359
21	1	0.2831	0.289	0	32.9037	37.7403
22	1	-0.074	-0.6774	0	50.935	86.5284
23	-0.1763	1	-0.3696	58.8041	0	69.7733
24	1	0.1148	-0.1665	0	80.9125	50.6875
25	-0.5999	1	0.1082	109.2193	0	31.774

Table 4.5.: The simulated plane parameters which are derived using three simulated vertices lying on the planar features in the source and reference scans

	Plane ID	$a_x(m)$	$a_y(m)$	$a_z(m)$
	1	-1.5385	7.6923	0
	2	4.2308	21.1538	0
	3	60	0	0
	4	0	25	0
Source	5	75	0	0
Scan	6	1.8097	-9.0483	6.7863
	7	-0.0624	-0.312	0.234
	8	18.6207	0	46.5517
	9	0	-7	14

continued on next page

Table 4.5.: *continued*

	Plane ID	$a_x(m)$	$a_y(m)$	$a_z(m)$
	10	0	0	10
	1	34.4028	10.8055	-8.4082
	2	14.3581	-1.0287	-1.3436
	3	-5.31	30.1146	-11.1299
	4	35.5328	4.0791	-5.9155
Reference	5	-2.8624	16.2334	-5.9996
Scan	6	-6.3983	-0.1943	6.8616
	7	-20.2167	7.49	17.1775
	8	8.1492	-0.3807	48.6878
	9	-14.5164	11.7497	38.7172
	10	5.1969	16.7129	42.7413

4.1.1 Registration using linear features

Man-made structures commonly have linear features. A minimum of two skew linear features, which do not intersect and are not parallel to each other, in the overlapping area are required to recover the six transformation parameters [26]. In this subsection, the results of the three alternative registration approaches using linear features are presented and evaluated.

4.1.1.1 Line Fitting

Two different line fitting approaches are proposed in this study. The first approach, which was illustrated in subsection 3.2.2, minimizes 2D distances of points from the line measured parallel to the coordinated planes. The second approach minimizes 3D normal distance between points and a line, which was explained in

subsection 3.2.3. In order to evaluate these two different line fitting approaches, simulated lines 5, 6, and 23 in the source scan are used. After the evaluation of these two different line fitting approaches, this study only focuses on the first line fitting approach by minimizing 2D distances of points from the line measured parallel to the coordinated planes.

The proposed line fitting approaches are evaluated using simulated lines 5, 6, and 23 in the source scan. The estimated line parameters, standard deviations, and a-posteriori variance factors using the line fitting approach which minimizes the 2D distances of points from the line measured parallel to the coordinate planes and the line fitting approach which minimizes the 3D normal distances between the points and fitted line are presented in Table 4.6. As shown in Table 4.6, these two different line fitting procedures can produce identical line parameters and standard deviation values. Furthermore, the a-posteriori variance factor $\hat{\sigma}_0^2$ is presented in Table 4.6. Because the weight matrix P is derived by the inverse of variance-covariance matrix of the observations, the $\hat{\sigma}_0^2$ should be close to the a-priori value σ_0^2. As shown in Table 4.6, the a-posteriori variance factors $\hat{\sigma}_0^2$ are close to the a-priori value $\sigma_0^2 = 1$, which is also an indication of the reliability of the estimated line parameters. Also, the a-posteriori variance factors produced by the two different line fitting approaches are identical.

The variance-covariance matrix is presented in Table 4.7. As shown in Table 4.7, the variance-covariance matrix of the estimated line parameters by using the two different line fitting approaches are close to each other. Based on the obtained variance-covariance matrix in Table 4.7, the correlation between the estimated line parameters can be derived by normalizing the covariance value. As an example, the correlation between a_x and b_x is obtained by Equation (4.1), where $Cov(a_x, b_x)$ is the covariance between a_x and b_x, $Var(a_x)$ is the variance of the estimated parameters a_x, and $Var(b_x)$ is the variance of b_x. The variance-correlation matrix of the estimated line parameters is listed in Table 4.8. In the variance-correlation matrix, the diagonal elements are the variance of the estimated line parameters, and the off-diagonal

elements are the correlation between the estimated parameters. Since the variance-correlation matrices obtained from the two approaches are exactly the same, those are only listed once in the table. As shown in Table 4.8, the variance-correlation matrix resulting from the line fitting procedure shows that there is a high correlation between the estimated line parameters.

$$Corr(a_x, b_x) = \frac{Cov(a_x, b_x)}{\sqrt{Var(a_x)Var(b_x)}} \tag{4.1}$$

In summary, the proposed line fitting approaches can produce equivalent results. The line fitting approach, which minimizes 2D distances of points from the line measured parallel to the coordinated planes, will be used in the remaining part of the experiment.

Table 4.6.: The estimated line parameters (lines 5, 6, and 23 in the source scan), standard deviations, and a-posteriori variance factors using the line fitting approach which minimizes the 2D distances of points from the line measured parallel to the coordinate planes and the line fitting approach which minimizes the 3D normal distances between the points and fitted line

	Line	a_x (±)	a_y (±)	a_z (±)	b_x (m±m)	b_y (m±m)	b_z (m±m)	$\hat{\sigma}_0^2$
Line fitting approach which minimizes the 2D distances of points from the line measured parallel to the coordinate planes	L05	0.0002 (±0.0004)	1 (±0)	0.0003 (±0.0004)	74.9951 (±0.0151)	0 (±0)	9.9937 (±0.0151)	1.0636
	L06	0.0003 (±0.0004)	-0.0006 (±0.0004)	1 (±0)	9.9921 (±0.0083)	10.0121 (±0.0083)	0 (±0)	0.9384
	L23	1 (±0)	0.0003 (±0.0002)	0.0001 (±0.0002)	0 (±0)	34.9790 (±0.0150)	34.9970 (±0.0150)	0.9080
Line fitting approach which minimizes the 3D normal distances between the points and fitted line	L05	0.0002 (±0.0004)	1 (±0)	0.0003 (±0.0004)	74.9951 (±0.0151)	0 (±0)	9.9937 (±0.0151)	1.0636
	L06	0.0003 (±0.0004)	-0.0006 (±0.0004)	1 (±0)	9.9921 (±0.0083)	10.0121 (±0.0083)	0 (±0)	0.9384

continued on next page

Table 4.6.: *continued*

	Line	a_x (±)	a_y (±)	a_z (±)	b_x (m±m)	b_y (m±m)	b_z (m±m)	$\hat{\sigma}_0^2$
	L23	1 (±0)	0.0003 (±0.0002)	0.0001 (±0.0002)	0 (±0)	34.9790 (±0.0150)	34.9970 (±0.0150)	0.9080

Table 4.7.: The variance-covariance matrix (line 5, 6, and 23 in the source scan) by using two different line fitting approaches

	Line		a_x	a_y	a_z	b_x	b_y	b_z
Line fitting approach which minimizes the 2D distances of points from the line measured parallel to the coordinate planes	5	a_x	1.80E-07	0	1.00E-14	-6.29E-06 (m)	0 (m)	-2.80E-13 (m)
		a_y	0	0	0	0 (m)	0 (m)	0 (m)
		a_z	1.00E-14	0	1.80E-07	-2.80E-13 (m)	0 (m)	-6.29E-06 (m)
		b_x	-6.29E-06 (m)	0 (m)	-2.80E-13 (m)	2.27E-04 (m^2)	0 (m^2)	1.02E-11 (m^2)
		b_y	0 (m)	0 (m)	0 (m)	0 (m^2)	0 (m^2)	0 (m^2)
		b_z	-2.80E-13 (m)	0 (m)	-6.29E-06 (m)	1.02E-11 (m^2)	0 (m^2)	2.27E-04 (m^2)
	6	a_x	1.58E-07	-3.00E-14	0	-3.17E-06 (m)	6.40E-13 (m)	0 (m)
		a_y	-3.00E-14	1.58E-07	0	6.40E-13 (m)	-3.17E-06 (m)	0 (m)
		a_z	0	0	0	0 (m)	0 (m)	0 (m)
		b_x	-3.17E-06 (m)	6.40E-13 (m)	0 (m)	6.89E-05 (m^2)	-1.40E-11 (m^2)	0 (m^2)
		b_y	6.40E-13 (m)	-3.17E-06 (m)	0 (m)	-1.40E-11 (m^2)	6.89E-05 (m^2)	0 (m^2)
		b_z	0 (m)	0 (m)	0 (m)	0 (m^2)	0 (m^2)	0 (m^2)
	23	a_x	0	0	0	0 (m)	0 (m)	0 (m)
		a_y	0	5.89E-08	0	0 (m)	-3.61E-06 (m)	-7.00E-14 (m)
		a_z	0	0	5.89E-08	0 (m)	-7.00E-14 (m)	-3.61E-06 (m)

continued on next page

Table 4.7.: *continued*

	Line		a_x	a_y	a_z	b_x	b_y	b_z
		b_x	0 (m)	0 (m)	0 (m)	0 (m^2)	0 (m^2)	0 (m^2)
		b_y	0 (m)	-3.61E-06 (m)	-7.00E-14 (m)	0 (m^2)	2.25E-04 (m^2)	4.39E-12 (m^2)
		b_z	0 (m)	-7.00E-14 (m)	-3.61E-06 (m)	0 (m^2)	4.39E-12 (m^2)	2.25E-04 (m^2)
Line fitting approach which minimizes the 3D normal distances between the points and fitted line	5	a_x	1.80E-07	0	1.00E-14	-6.29E-06 (m)	0 (m)	-2.80E-13 (m)
		a_y	0	0	0	0 (m)	0 (m)	0 (m)
		a_z	1.00E-14	0	1.80E-07	-2.80E-13 (m)	0 (m)	-6.29E-06 (m)
		b_x	-6.29E-06 (m)	0 (m)	-2.80E-13 (m)	2.27E-04 (m^2)	0 (m^2)	1.02E-11 (m^2)
		b_y	0 (m)	0 (m)	0 (m)	0 (m^2)	0 (m^2)	0 (m^2)
		b_z	-2.80E-13 (m)	0 (m)	-6.29E-06 (m)	1.02E-11 (m^2)	0 (m^2)	2.27E-04 (m^2)
	6	a_x	1.58E-07	-3.00E-14	0	-3.17E-06 (m)	6.40E-13 (m)	0 (m)
		a_y	-3.00E-14	1.58E-07	0	6.40E-13 (m)	-3.17E-06 (m)	0 (m)
		a_z	0	0	0	0 (m)	0 (m)	0 (m)
		b_x	-3.17E-06 (m)	6.40E-13 (m)	0 (m)	6.89E-05 (m^2)	-1.40E-11 (m^2)	0 (m^2)
		b_y	6.40E-13 (m)	-3.17E-06 (m)	0 (m)	-1.40E-11 (m^2)	6.89E-05 (m^2)	0 (m^2)
		b_z	0 (m)	0 (m)	0 (m)	0 (m^2)	0 (m^2)	0 (m^2)

continued on next page

Table 4.7.: *continued*

Line		a_x	a_y	a_z	b_x	b_y	b_z
23	a_x	0	0	0	0 (m)	0 (m)	0 (m)
	a_y	0	5.89E-08	0	0 (m)	-3.61E-06 (m)	-7.00E-14 (m)
	a_z	0	0	5.89E-08	0 (m)	-7.00E-14 (m)	-3.61E-06 (m)
	b_x	0 (m)	0 (m)	0 (m)	0 (m^2)	0 (m^2)	0 (m^2)
	b_y	0 (m)	-3.61E-06 (m)	-7.00E-14 (m)	0 (m^2)	2.25E-04 (m^2)	4.39E-12 (m^2)
	b_z	0 (m)	-7.00E-14 (m)	-3.61E-06 (m)	0 (m^2)	4.39E-12 (m^2)	2.25E-04 (m^2)

Table 4.8.: The variance-correlation matrix of the estimated line parameters (lines 5, 6, and 23) in the source scan

Line		a_x	a_y	a_z	b_x	b_y	b_z
5	a_x	1.80E-07	0	0	-0.9867	0	0
	a_y	0	0	0	0	0	0
	a_z	0	0	1.80E-07	0	0	-0.9867
	b_x	-0.9867	0	0	2.27E-04 (m^2)	0	0
	b_y	0	0	0	0	0 (m^2)	0
	b_z	0	0	-0.9867	0	0	2.27E-04 (m^2)
6	a_x	1.58E-07	0	0	-0.9610	0	0
	a_y	0	1.58E-07	0	0	-0.9610	0
	a_z	0	0	0	0	0	0
	b_x	-0.9610	0	0	6.89E-05 (m^2)	0	0
	b_y	0	-0.9610	0	0	6.89E-05 (m^2)	0
	b_z	0	0	0	0	0	0 (m^2)
23	a_x	0	0	0	0	0	0
	a_y	0	5.89E-08	0	0	-0.9917	0
	a_z	0	0	5.89E-08	0	0	-0.9917

continued on next page

Table 4.8.: *continued*

Line		a_x	a_y	a_z	b_x	b_y	b_z
	b_x	0	0	0	0 (m^2)	0	0
	b_y	0	-0.9917	0	0	2.25E-04 (m^2)	0
	b_z	0	0	-0.9917	0	0	2.25E-04 (m^2)

Having compared the two different line fitting approaches, this study proceeds to discuss the elimination of the high correlation between the estimated line parameters. As shown in Table 4.8, the estimated line parameters are highly correlated. Assuming that a line segment is mainly oriented along the z-axis and is very far from the xy-plane, the (b_x, b_y, b_z) is derived by extrapolating the line segment until it intersects the xy-plane. In this case, the extrapolation of the line segment will create an artificial correlation between the line parameters. If this line is too far from the xy-plane, any small change in the orientation will affect the (b_x, b_y, b_z). However, if the line segment is close to the xy-plane, the (a_x, a_y, a_z) and (b_x, b_y, b_z) are decoupled. Therefore, one solution to the high correlation problem is to shift the origin of the coordinate system to the center of the line segment. After a line fitting procedure, the estimated point will be shifted back to the original coordinate system. The estimated point which is close to the center of the line segment is denoted as (c_x, c_y, c_z). After shifting the origin of the coordinate system to the center of the line segment, the estimated line parameters, standard deviations, and a-posteriori variance factors for lines 5, 6, and 23 in the source scan are presented in Table 4.9. The corresponding variance-correlation matrix is presented in Table 4.10. The correlation between the estimated line parameters is eliminated after shifting the origin of the coordinate system to the center of the line segment.

Table 4.9.: The estimated line parameters (lines 5, 6, and 23 in the source scan), standard deviations, and a-posteriori variance factors after shifting the origin of the coordinate system to the center of the line segment in the source scan

	Line	a_x (±)	a_y (±)	a_z (±)	c_x (m±m)	c_y (m±m)	c_z (m±m)	$\hat{\sigma}_0^2$
Source Scan	L05	0.0002 (±0.0004)	1 (±0)	0.0003 (±0.0004)	75.0007 (±0.0024)	35.0600 (±0)	10.0035 (±0.0024)	1.0636
	L06	0.0003 (±0.0004)	-0.0006 (±0.0004)	1 (±0)	9.9986 (±0.0023)	9.9996 (±0.0023)	20.0610 (±0)	0.9384
	L23	1 (±0)	0.0003 (±0.0002)	0.0001 (±0.0002)	61.3116 (±0)	35.0000 (±0.0019)	35.0005 (±0.0019)	0.9080

Table 4.10.: The variance-correlation matrix (lines 5, 6, and 23 in the source scan) after shifting the origin of the coordinate system to the center of the line segment in the source scan

Line		a_x	a_y	a_z	c_x	c_y	c_z
5	a_x	1.80E-07	0	0	0	0	0
	a_y	0	0	0	0	0	0
	a_z	0	0	1.80E-07	0	0	0
	c_x	0	0	0	5.98E-06 (m^2)	0	0
	c_y	0	0	0	0	0 (m^2)	0
	c_z	0	0	0	0	0	5.98E-06 (m^2)
6	a_x	1.58E-07	0	0	0	0	0
	a_y	0	1.58E-07	0	0	0	0
	a_z	0	0	0	0	0	0
	c_x	0	0	0	5.28E-06 (m^2)	0	0
	c_y	0	0	0	0	5.28E-06 (m^2)	0
	c_z	0	0	0	0	0	0 (m^2)
23	a_x	0	0	0	0	0	0
	a_y	0	5.89E-08	0	0	0	0

continued on next page

Table 4.10.: *continued*

Line	a_x	a_y	a_z	c_x	c_y	c_z
a_z	0	0	5.89E-08	0	0	0
c_x	0	0	0	0 (m^2)	0	0
c_y	0	0	0	0	3.71E-06 (m^2)	0
c_z	0	0	0	0	0	3.71E-06 (m^2)

According to Equation (3.50), the estimated point (b_x, b_y, b_z) in the source scan and (b'_x, b'_y, b'_z) in the reference scan cannot be the same point. To ensure (c_x, c_y, c_z) and (c'_x, c'_y, c'_z) are not the same point, the estimated point is extrapolated 50 m away along the line direction in the source scan. In the reference scan, the point is extrapolated in the opposite direction and by the same measure. The extrapolation of the point is mathematically illustrated by Equation (4.2), where λ is given by Equation (4.3). The choice of the plus or minus sign depends on the orientation of (a_x, a_y, a_z) and the direction of the extrapolation. The variance-covariance matrix $\Sigma_{(a_x,a_y,a_z,b_x,b_y,b_z)}$ is derived based on the law of error propagation according to Equation (4.4), where B is given by Equation (4.5). After the extrapolation of the points, the estimated line parameters, standard deviations, and a-posteriori variance factors for lines 5, 6, and 23 in the source scan are presented in Table 4.11. Furthermore, the a-posteriori variance factor $\hat{\sigma}_0^2$ is used to evaluate the estimated line parameters. Because the weight matrix P is derived by the inverse of variance-covariance matrix of the observations, the $\hat{\sigma}_0^2$ should be close to the a-priori value σ_0^2. As shown in Table 4.11, the a-posteriori variance factors $\hat{\sigma}_0^2$ are close to the a-priori value $\sigma_0^2 = 1$, which is also an indication of the reliability of the estimated line parameters. The corresponding variance-correlation matrix is presented in Table 4.12. As shown in Table 4.12, there are high correlation between the estimated line parameters.

$$\begin{bmatrix} b_x \\ b_y \\ b_z \end{bmatrix} = \begin{bmatrix} c_x \\ c_y \\ c_z \end{bmatrix} + \lambda \begin{bmatrix} a_x \\ a_y \\ a_z \end{bmatrix} \tag{4.2}$$

$$\lambda = \pm \frac{50}{\sqrt{a_x^2 + a_y^2 + a_z^2}} \tag{4.3}$$

$$\Sigma_{(a_x,a_y,a_z,b_x,b_y,b_z)} = B \Sigma_{(a_x,a_y,a_z,c_x,c_y,c_z)} B^T \tag{4.4}$$

$$B = \begin{bmatrix} 1 & 0 & 0 & 0 & 0 & 0 \\ 0 & 1 & 0 & 0 & 0 & 0 \\ 0 & 0 & 1 & 0 & 0 & 0 \\ \lambda & 0 & 0 & 1 & 0 & 0 \\ 0 & \lambda & 0 & 0 & 1 & 0 \\ 0 & 0 & \lambda & 0 & 0 & 1 \end{bmatrix} \tag{4.5}$$

Having discussed the elimination of the high correlation between the estimated line parameters, the next step is to estimate the line parameters for 25 pairs of lines in the source and reference scans using the line fitting approach by minimizing 2D distances of points from the line measured parallel to the coordinated planes. The estimated line parameters, standard deviations, and a-posteriori variance factors for 25 pairs of lines without the shift of origin in the source and reference scans are presented in Table 4.13. Comparing the estimated line parameters in Table 4.13 with the simulated line parameters in Table 4.4, one can see that the estimated parameters seem to be close to the true ones. The standard deviation overall was below 0.002 and 6 cm for the direction vector (a_x, a_y, a_z) and position parameter (b_x, b_y, b_z), respectively. As highlighted in red in the table, line 22 in the reference scan has a large standard deviation in position parameter (b_x, b_y, b_z). The line 22 is short and oblique, so the accuracy of the estimated line parameters is low. The numerical values and the standard deviations indicate the line fitting procedure is reliable. Furthermore, the a-posteriori variance factor $\hat{\sigma}_0^2$ is used to evaluate the estimated line parameters. Because the weight matrix P is derived by the inverse of variance-covariance matrix of the observations, the $\hat{\sigma}_0^2$ should be close to the a-priori value σ_0^2. As shown in Table 4.13, the a-posteriori variance factors $\hat{\sigma}_0^2$ are close to the a-priori value $\sigma_0^2 = 1$, which is also an indication of the reliability of the estimated line parameters.

Table 4.11.: The estimated line parameters (lines 5, 6, and 23 in the source scan), standard deviations, and a-posteriori variance factors after extrapolating the estimated points 50 m away along the line direction in the source scan

	Line	a_x (±)	a_y (±)	a_z (±)	b_x (m±m)	b_y (m±m)	b_z (m±m)	$\hat{\sigma}_0^2$
Source Scan	L05	0.0002 (±0.0004)	1 (±0)	0.0003 (±0.0004)	74.9927 (±0.0213)	-14.9400 (±0)	9.9895 (±0.0213)	1.0636
	L06	0.0003 (±0.0004)	-0.0006 (±0.0004)	1 (±0)	9.9823 (±0.0200)	10.0308 (±0.0200)	-29.9389 (±0)	0.9384
	L23	1 (±0)	0.0003 (±0.0002)	0.0001 (±0.0002)	11.3116 (±0)	34.9829 (±0.0123)	34.9976 (±0.0123)	0.9080

Table 4.12.: The variance-correlation matrix (lines 5, 6, and 23 in the source scan) after extrapolating the estimated points 50 m away along the line direction

Line		a_x	a_y	a_z	b_x	b_y	b_z
5	a_x	1.80E-07	0	0	-0.9934	0	0
	a_y	0	0	0	0	0	0
	a_z	0	0	1.80E-07	0	0	-0.9934
	b_x	-0.9934	0	0	0.0005 (m^2)	0	0
	b_y	0	0	0	0	0 (m^2)	0
	b_z	0	0	-0.9934	0	0	0.0005 (m^2)
6	a_x	1.58E-07	0	0	-0.9934	0	0
	a_y	0	1.58E-07	0	0	-0.9934	0
	a_z	0	0	0	0	0	0
	b_x	-0.9934	0	0	0.0004 (m^2)	0	0
	b_y	0	-0.9934	0	0	0.0004 (m^2)	0
	b_z	0	0	0	0	0	0 (m^2)
23	a_x	0	0	0	0	0	0
	a_y	0	5.89E-08	0	0	-0.9876	0

continued on next page

Table 4.12.: *continued*

Line		a_x	a_y	a_z	b_x	b_y	b_z
	a_z	0	0	5.89E-08	0	0	-0.9876
	b_x	0	0	0	0 (m^2)	0	0
	b_y	0	-0.9876	0	0	0.0002 (m^2)	0
	b_z	0	0	-0.9876	0	0	0.0002 (m^2)

Table 4.13.: The estimated line parameters, standard deviations, and a-posteriori variance factors for 25 pairs of lines without the shift of origin in the source and reference scans

	Line	a_x (±)	a_y (±)	a_z (±)	b_x (m±m)	b_y (m±m)	b_z (m±m)	$\hat{\sigma}_0^2$
Source Scan	L01	1 (±0)	0.2003 (±0.0003)	-0.0001 (±0.0003)	0 (±0)	7.9927 (±0.0068)	9.9987 (±0.0067)	0.9183
	L02	1 (±0)	-0.2001 (±0.0003)	-0.0004 (±0.0003)	0 (±0)	22.0056 (±0.0144)	10.0160 (±0.0141)	0.997
	L03	-0.0004 (±0.0006)	1 (±0)	0.0004 (±0.0006)	60.0045 (±0.0104)	0 (±0)	9.9928 (±0.0104)	0.8342
	L04	1 (±0)	-0.0008 (±0.0007)	0.0006 (±0.0007)	0 (±0)	25.0526 (±0.0472)	9.9589 (±0.0472)	1.2123
	L05	0.0002 (±0.0004)	1 (±0)	0.0003 (±0.0004)	74.9951 (±0.0151)	0 (±0)	9.9937 (±0.0151)	1.0636
	L06	0.0003 (±0.0004)	-0.0006 (±0.0004)	1 (±0)	9.9921 (±0.0083)	10.0121 (±0.0083)	0 (±0)	0.9384

continued on next page

Table 4.13.: *continued*

Line	a_x (±)	a_y (±)	a_z (±)	b_x (m±m)	b_y (m±m)	b_z (m±m)	$\hat{\sigma}_0^2$
L07	0.0006 (±0.0004)	0.0000 (±0.0004)	1 (±0)	34.9882 (±0.0085)	15.0016 (±0.0085)	0 (±0)	0.9939
L08	-0.0004 (±0.0004)	0.0004 (±0.0004)	1 (±0)	60.0088 (±0.0082)	9.9920 (±0.0082)	0 (±0)	0.9113
L09	-0.0001 (±0.0004)	-0.0009 (±0.0004)	1 (±0)	59.9981 (±0.0086)	25.0163 (±0.0086)	0 (±0)	0.9976
L10	0.0000 (±0.0004)	0.0004 (±0.0004)	1 (±0)	74.9918 (±0.0084)	24.9951 (±0.0084)	0 (±0)	0.9664
L11	0.0003 (±0.0004)	0.0002 (±0.0004)	1 (±0)	74.9904 (±0.0091)	44.9973 (±0.0091)	0 (±0)	1.1173
L12	1 (±0)	0.1997 (±0.0003)	0.0001 (±0.0003)	0 (±0)	8.0064 (±0.0067)	29.9980 (±0.0066)	0.8884

continued on next page

Table 4.13.: *continued*

Line	a_x (±)	a_y (±)	a_z (±)	b_x (m±m)	b_y (m±m)	b_z (m±m)	$\hat{\sigma}_0^2$
L13	1 (±0)	-0.2003 (±0.0003)	-0.0001 (±0.0003)	0 (±0)	22.0171 (±0.0137)	30.0064 (±0.0135)	0.9084
L14	-0.0014 (±0.0006)	1 (±0)	-0.0015 (±0.0006)	60.0267 (±0.0107)	0 (±0)	30.0254 (±0.0107)	0.8695
L15	1 (±0)	-0.0005 (±0.0007)	-0.0001 (±0.0007)	0 (±0)	25.0318 (±0.0455)	30.0034 (±0.0455)	1.1315
L16	-0.0001 (±0.0004)	1 (±0)	0.0001 (±0.0004)	75.0029 (±0.0153)	0 (±0)	29.9951 (±0.0153)	1.0923
L17	1 (±0)	0.4998 (±0.0003)	0.3996 (±0.0003)	0 (±0)	5.0058 (±0.0078)	26.0069 (±0.0075)	1.0006
L18	0.0028 (±0.0011)	0.7503 (±0.0014)	1 (±0)	34.8981 (±0.0397)	-7.5119 (±0.0496)	0 (±0)	0.9427

continued on next page

Table 4.13.: *continued*

Line	a_x (±)	a_y (±)	a_z (±)	b_x (m±m)	b_y (m±m)	b_z (m±m)	$\hat{\sigma}_0^2$
L19	1 (±0)	-0.4995 (±0.0003)	-0.3997 (±0.0003)	0 (±0)	39.9760 (±0.0164)	53.9797 (±0.0158)	1.0821
L20	1 (±0)	-0.7997 (±0.0010)	-0.4005 (±0.0009)	0 (±0)	72.9863 (±0.0556)	54.0311 (±0.0468)	0.9375
L21	-0.0002 (±0.0012)	1 (±0)	0.4985 (±0.0014)	75.0096 (±0.0376)	0 (±0)	17.5457 (±0.0420)	1.15
L22	0.0003 (±0.0012)	1 (±0)	-0.5001 (±0.0014)	74.9887 (±0.0494)	0 (±0)	52.5013 (±0.0552)	1.1178
L23	1 (±0)	0.0003 (±0.0002)	0.0001 (±0.0002)	0 (±0)	34.9790 (±0.0150)	34.9970 (±0.0150)	0.908
L24	0.0005 (±0.0003)	1 (±0)	-0.0002 (±0.0003)	34.9803 (±0.0108)	0 (±0)	40.0114 (±0.0108)	1.0506

continued on next page

Table 4.13.: *continued*

	Line	a_x (±)	a_y (±)	a_z (±)	b_x (m±m)	b_y (m±m)	b_z (m±m)	$\hat{\sigma}_0^2$
	L25	1 (±0)	0.4997 (±0.0003)	-0.4002 (±0.0003)	0 (±0)	30.0147 (±0.0163)	54.0084 (±0.0157)	1.0639
Reference Scan	L01	-0.3976 (±0.0004)	1 (±0)	-0.3428 (±0.0003)	50.5306 (±0.0300)	0 (±0)	43.7673 (±0.0295)	1.0294
	L02	0.0349 (±0.0003)	1 (±0)	-0.3955 (±0.0003)	18.9979 (±0.0186)	0 (±0)	47.6160 (±0.0200)	0.9583
	L03	1 (±0)	0.1152 (±0.0006)	-0.1656 (±0.0006)	0 (±0)	46.8301 (±0.0177)	31.5667 (±0.0178)	0.9189
	L04	-0.1768 (±0.0007)	1 (±0)	-0.3702 (±0.0007)	44.4170 (±0.0313)	0 (±0)	44.5390 (±0.0328)	1.042
	L05	1 (±0)	0.1151 (±0.0004)	-0.1666 (±0.0004)	0 (±0)	32.6603 (±0.0205)	37.1358 (±0.0207)	1.0222

continued on next page

Table 4.13.: *continued*

Line	a_x (±)	a_y (±)	a_z (±)	b_x (m±m)	b_y (m±m)	b_z (m±m)	$\hat{\sigma}_0^2$
L06	0.1223 (±0.0004)	0.3912 (±0.0005)	1 (±0)	11.2016 (±0.0092)	91.1658 (±0.0098)	0 (±0)	0.9508
L07	0.1224 (±0.0004)	0.3909 (±0.0005)	1 (±0)	19.2355 (±0.0123)	65.5803 (±0.0131)	0 (±0)	0.9231
L08	0.1215 (±0.0004)	0.3905 (±0.0005)	1 (±0)	17.2980 (±0.0162)	38.2328 (±0.0172)	0 (±0)	0.9158
L09	0.1212 (±0.0005)	0.3901 (±0.0005)	1 (±0)	32.3108 (±0.0162)	40.8879 (±0.0173)	0 (±0)	1.0462
L10	0.1222 (±0.0004)	0.3903 (±0.0005)	1 (±0)	34.0951 (±0.0172)	25.0037 (±0.0183)	0 (±0)	0.9047
L11	0.1213 (±0.0004)	0.3910 (±0.0005)	1 (±0)	54.1305 (±0.0162)	28.5007 (±0.0172)	0 (±0)	0.9407

continued on next page

Table 4.13.: *continued*

Line	a_x (±)	a_y (±)	a_z (±)	b_x (m±m)	b_y (m±m)	b_z (m±m)	$\hat{\sigma}_0^2$
L12	-0.3976 (±0.0003)	1 (±0)	-0.3421 (±0.0003)	55.6475 (±0.0300)	0 (±0)	64.6955 (±0.0294)	0.871
L13	0.0346 (±0.0003)	1 (±0)	-0.3948 (±0.0003)	21.0146 (±0.0201)	0 (±0)	68.9388 (±0.0216)	0.8883
L14	1 (±0)	0.1149 (±0.0006)	-0.1662 (±0.0006)	0 (±0)	53.8177 (±0.0197)	50.4622 (±0.0198)	0.9786
L15	-0.1757 (±0.0007)	1 (±0)	-0.3702 (±0.0007)	47.8904 (±0.0360)	0 (±0)	65.7234 (±0.0378)	1.0206
L16	1 (±0)	0.1151 (±0.0004)	-0.1668 (±0.0004)	0 (±0)	39.6379 (±0.0219)	56.0303 (±0.0221)	1.0636
L17	-0.9640 (±0.0005)	1 (±0)	-0.8702 (±0.0005)	113.8349 (±0.0513)	0 (±0)	118.9515 (±0.0490)	0.9433

continued on next page

Table 4.13.: *continued*

Line	a_x (±)	a_y (±)	a_z (±)	b_x (m±m)	b_y (m±m)	b_z (m±m)	$\hat{\sigma}_0^2$
L18	1 (±0)	0.5263 (±0.0016)	0.9477 (±0.0019)	0 (±0)	67.6323 (±0.0448)	14.7373 (±0.0546)	1.0531
L19	0.3307 (±0.0003)	1 (±0)	-0.0472 (±0.0003)	4.2879 (±0.0198)	0 (±0)	49.3213 (±0.0188)	1.0328
L20	0.5727 (±0.0008)	1 (±0)	-0.0890 (±0.0007)	4.3906 (±0.0527)	0 (±0)	49.3807 (±0.0459)	0.9524
L21	1 (±0)	0.2838 (±0.0011)	0.2880 (±0.0011)	0 (±0)	32.8731 (±0.0494)	37.7792 (±0.0495)	0.8695
L22	1 (±0)	-0.0756 (±0.0012)	-0.6766 (±0.0015)	0 (±0)	51.0196 (±0.0687)	86.4784 (±0.0827)	0.9741
L23	-0.1762 (±0.0003)	1 (±0)	-0.3695 (±0.0003)	58.7960 (±0.0174)	0 (±0)	69.7721 (±0.0183)	1.0644

continued on next page

Table 4.13.: *continued*

	Line	a_x (±)	a_y (±)	a_z (±)	b_x (m±m)	b_y (m±m)	b_z (m±m)	$\hat{\sigma}_0^2$
	L24	1 (±0)	0.1145 (±0.0003)	-0.1667 (±0.0003)	0 (±0)	80.9282 (±0.0143)	50.6969 (±0.0144)	1.0982
	L25	-0.5999 (±0.0004)	1 (±0)	0.1080 (±0.0003)	109.2171 (±0.0266)	0 (±0)	31.7893 (±0.0229)	1.0983

The estimated line parameters, standard deviations, and a-posteriori variance factors for 25 pairs of lines after shifting the origin and extrapolating the estimated points 50 m away along the line direction in the source and reference scans are shown in Table 4.14. The estimated parameters (a_x, a_y, a_z) and the corresponding standard deviations in Table 4.14 are identical to those values in Table 4.13. The estimated parameters (a_x, a_y, a_z) in Table 4.14 are found to be in accordance with the true values of the line parameters used for simulated data in Table 4.4, and the standard deviation values corresponding to (a_x, a_y, a_z) overall were below 0.002. The parameters (b_x, b_y, b_z) in Table 4.14 are derived by extrapolating the estimated points 50 m away along the line direction. The standard deviation values corresponding to (b_x, b_y, b_z) are close to 3 cm, which is coherent with the simulated noise level in the 3D points along the features, thus indicating the validity of the estimated 3D line parameters. As shown in Table 4.14, the a-posteriori variance factors $\hat{\sigma}_0^2$ are close to the a-priori value $\sigma_0^2 = 1$, which is also an indication of the reliability of the estimated line parameters.

Table 4.14.: The estimated line parameters, standard deviations, and a-posteriori variance factors for 25 pairs of lines after shifting the origin and extrapolating the estimated points 50 m away along the line direction in the source and reference scans

	Line	a_x (±)	a_y (±)	a_z (±)	b_x (m±m)	b_y (m±m)	b_z (m±m)	$\hat{\sigma}_0^2$
Source Scan	L01	1 (±0)	0.2003 (±0.0003)	-0.0001 (±0.0003)	-26.4651 (±0)	2.6925 (±0.0142)	10.0005 (±0.0140)	0.9183
	L02	1 (±0)	-0.2001 (±0.0003)	-0.0004 (±0.0003)	-1.4619 (±0)	22.2981 (±0.0148)	10.0166 (±0.0145)	0.9970
	L03	-0.0004 (±0.0006)	1 (±0)	0.0004 (±0.0006)	60.0167 (±0.0290)	-32.4353 (±0)	9.9799 (±0.0290)	0.8342
	L04	1 (±0)	-0.0008 (±0.0007)	0.0006 (±0.0007)	17.5648 (±0)	25.0388 (±0.0350)	9.9691 (±0.0350)	1.2123
	L05	0.0002 (±0.0004)	1 (±0)	0.0003 (±0.0004)	74.9927 (±0.0213)	-14.9400 (±0)	9.9895 (±0.0213)	1.0636

continued on next page

Table 4.14.: *continued*

Line	a_x (±)	a_y (±)	a_z (±)	b_x (m±m)	b_y (m±m)	b_z (m±m)	$\hat{\sigma}_0^2$
L06	0.0003 (±0.0004)	-0.0006 (±0.0004)	1 (±0)	9.9823 (±0.0200)	10.0308 (±0.0200)	-29.9389 (±0)	0.9384
L07	0.0006 (±0.0004)	0.0000 (±0.0004)	1 (±0)	34.9705 (±0.0206)	15.0005 (±0.0206)	-29.9381 (±0)	0.9939
L08	-0.0004 (±0.0004)	0.0004 (±0.0004)	1 (±0)	60.0196 (±0.0197)	9.9788 (±0.0197)	-29.9337 (±0)	0.9113
L09	-0.0001 (±0.0004)	-0.0009 (±0.0004)	1 (±0)	60.0001 (±0.0206)	25.0429 (±0.0206)	-29.9336 (±0)	0.9976
L10	0.0000 (±0.0004)	0.0004 (±0.0004)	1 (±0)	74.9906 (±0.0203)	24.9843 (±0.0203)	-29.9375 (±0)	0.9664
L11	0.0003 (±0.0004)	0.0002 (±0.0004)	1 (±0)	74.9802 (±0.0219)	44.9909 (±0.0219)	-29.9381 (±0)	1.1173

continued on next page

Table 4.14.: *continued*

Line	a_x (±)	a_y (±)	a_z (±)	b_x (m±m)	b_y (m±m)	b_z (m±m)	$\hat{\sigma}_0^2$
L12	1 (±0)	0.1997 (±0.0003)	0.0001 (±0.0003)	-26.4675 (±0)	2.7203 (±0.0140)	29.9957 (±0.0137)	0.8884
L13	1 (±0)	-0.2003 (±0.0003)	-0.0001 (±0.0003)	-1.4606 (±0)	22.3097 (±0.0142)	30.0065 (±0.0139)	0.9084
L14	-0.0014 (±0.0006)	1 (±0)	-0.0015 (±0.0006)	60.0721 (±0.0296)	-32.4395 (±0)	30.0732 (±0.0296)	0.8695
L15	1 (±0)	-0.0005 (±0.0007)	-0.0001 (±0.0007)	17.5562 (±0)	25.0238 (±0.0338)	30.0024 (±0.0338)	1.1315
L16	-0.0001 (±0.0004)	1 (±0)	0.0001 (±0.0004)	75.0044 (±0.0216)	-14.9387 (±0)	29.9930 (±0.0216)	1.0923
L17	1 (±0)	0.4998 (±0.0003)	0.3996 (±0.0003)	-19.5552 (±0)	-4.7673 (±0.0140)	18.1927 (±0.0135)	1.0006

continued on next page

Table 4.14.: *continued*

Line	a_x (±)	a_y (±)	a_z (±)	b_x (m±m)	b_y (m±m)	b_z (m±m)	$\hat{\sigma}_0^2$
L18	0.0028 (±0.0011)	0.7503 (±0.0014)	1 (±0)	34.8841 (±0.0452)	-11.2111 (±0.0565)	-4.9300 (±0)	0.9427
L19	1 (±0)	-0.4995 (±0.0003)	-0.3997 (±0.0003)	5.4407 (±0)	37.2584 (±0.0146)	51.8051 (±0.0141)	1.0821
L20	1 (±0)	-0.7997 (±0.0010)	-0.4005 (±0.0009)	16.5459 (±0)	59.7541 (±0.0386)	47.4045 (±0.0325)	0.9375
L21	-0.0002 (±0.0012)	1 (±0)	0.4985 (±0.0014)	75.0127 (±0.0558)	-14.6866 (±0)	10.2238 (±0.0624)	1.1500
L22	0.0003 (±0.0012)	1 (±0)	-0.5001 (±0.0014)	74.9871 (±0.0551)	-4.6555 (±0)	54.8296 (±0.0616)	1.1178
L23	1 (±0)	0.0003 (±0.0002)	0.0001 (±0.0002)	11.3116 (±0)	34.9829 (±0.0123)	34.9976 (±0.0123)	0.9080

continued on next page

Table 4.14.: *continued*

	Line	a_x (±)	a_y (±)	a_z (±)	b_x (m±m)	b_y (m±m)	b_z (m±m)	$\hat{\sigma}_0^2$
	L24	0.0005 (±0.0003)	1 (±0)	-0.0002 (±0.0003)	34.9735 (±0.0152)	-14.9400 (±0)	40.0144 (±0.0152)	1.0506
	L25	1 (±0)	0.4997 (±0.0003)	-0.4002 (±0.0003)	5.4534 (±0)	32.7397 (±0.0145)	51.8262 (±0.0140)	1.0639
Reference Scan	L01	-0.3976 (±0.0004)	1 (±0)	-0.3428 (±0.0003)	34.6760 (±0.0159)	39.8745 (±0)	30.0994 (±0.0156)	1.0294
	L02	0.0349 (±0.0003)	1 (±0)	-0.3955 (±0.0003)	19.5055 (±0.0143)	14.5407 (±0)	41.8645 (±0.0153)	0.9583
	L03	1 (±0)	0.1152 (±0.0006)	-0.1656 (±0.0006)	77.1391 (±0)	55.7183 (±0.0306)	18.7920 (±0.0309)	0.9189
	L04	-0.1768 (±0.0007)	1 (±0)	-0.3702 (±0.0007)	44.8322 (±0.0329)	-2.3484 (±0)	45.4085 (±0.0346)	1.0420

continued on next page

Table 4.14.: *continued*

	Line	a_x (±)	a_y (±)	a_z (±)	b_x (m±m)	b_y (m±m)	b_z (m±m)	$\hat{\sigma}_0^2$
	L05	1 (±0)	0.1151 (±0.0004)	-0.1666 (±0.0004)	96.7363 (±0)	43.7945 (±0.0211)	21.0159 (±0.0212)	1.0222
	L06	0.1223 (±0.0004)	0.3912 (±0.0005)	1 (±0)	19.3492 (±0.0203)	117.2314 (±0.0216)	66.6248 (±0)	0.9508
	L07	0.1224 (±0.0004)	0.3909 (±0.0005)	1 (±0)	28.3333 (±0.0200)	94.6481 (±0.0213)	74.3577 (±0)	0.9231
	L08	0.1215 (±0.0004)	0.3905 (±0.0005)	1 (±0)	27.4754 (±0.0199)	70.9315 (±0.0212)	83.7345 (±0)	0.9158
	L09	0.1212 (±0.0005)	0.3901 (±0.0005)	1 (±0)	42.1633 (±0.0213)	72.6057 (±0.0227)	81.2999 (±0)	1.0462
	L10	0.1222 (±0.0004)	0.3903 (±0.0005)	1 (±0)	44.6563 (±0.0198)	58.7294 (±0.0211)	86.4165 (±0)	0.9047

continued on next page

Table 4.14.: *continued*

Line	a_x (±)	a_y (±)	a_z (±)	b_x (m±m)	b_y (m±m)	b_z (m±m)	$\hat{\sigma}_0^2$
L11	0.1213 (±0.0004)	0.3910 (±0.0005)	1 (±0)	64.2194 (±0.0202)	61.0137 (±0.0215)	83.1462 (±0)	0.9407
L12	-0.3976 (±0.0003)	1 (±0)	-0.3421 (±0.0003)	36.9208 (±0.0146)	47.1016 (±0)	48.5844 (±0.0144)	0.8710
L13	0.0346 (±0.0003)	1 (±0)	-0.3948 (±0.0003)	21.7672 (±0.0137)	21.7632 (±0)	60.3469 (±0.0148)	0.8883
L14	1 (±0)	0.1149 (±0.0006)	-0.1662 (±0.0006)	79.3900 (±0)	62.9408 (±0.0316)	37.2679 (±0.0318)	0.9786
L15	-0.1757 (±0.0007)	1 (±0)	-0.3702 (±0.0007)	47.0329 (±0.0326)	4.8811 (±0)	63.9166 (±0.0342)	1.0206
L16	1 (±0)	0.1151 (±0.0004)	-0.1668 (±0.0004)	98.9843 (±0)	51.0314 (±0.0215)	39.5160 (±0.0216)	1.0636

continued on next page

Table 4.14.: *continued*

Line	a_x (±)	a_y (±)	a_z (±)	b_x (m±m)	b_y (m±m)	b_z (m±m)	$\hat{\sigma}_0^2$
L17	-0.9640 (±0.0005)	1 (±0)	-0.8702 (±0.0005)	52.9855 (±0.0169)	63.1240 (±0)	64.0181 (±0.0162)	0.9433
L18	1 (±0)	0.5263 (±0.0016)	0.9477 (±0.0019)	61.9815 (±0)	100.2544 (±0.0540)	73.4790 (±0.0659)	1.0531
L19	0.3307 (±0.0003)	1 (±0)	-0.0472 (±0.0003)	11.9090 (±0.0134)	23.0422 (±0)	48.2326 (±0.0128)	1.0328
L20	0.5727 (±0.0008)	1 (±0)	-0.0890 (±0.0007)	17.0226 (±0.0350)	22.0576 (±0)	47.4184 (±0.0305)	0.9524
L21	1 (±0)	0.2838 (±0.0011)	0.2880 (±0.0011)	91.7205 (±0)	58.9003 (±0.0505)	64.1980 (±0.0506)	0.8695
L22	1 (±0)	-0.0756 (±0.0012)	-0.6766 (±0.0015)	96.4892 (±0)	43.7233 (±0.0515)	21.1940 (±0.0620)	0.9741

continued on next page

Table 4.14.: *continued*

	Line	a_x (±)	a_y (±)	a_z (±)	b_x (m±m)	b_y (m±m)	b_z (m±m)	$\hat{\sigma}_0^2$
	L23	-0.1762 (±0.0003)	1 (±0)	-0.3695 (±0.0003)	56.4009 (±0.0135)	13.5913 (±0)	64.7498 (±0.0142)	1.0644
	L24	1 (±0)	0.1145 (±0.0003)	-0.1667 (±0.0003)	93.5842 (±0)	91.6433 (±0.0157)	35.0939 (±0.0158)	1.0982
	L25	-0.5999 (±0.0004)	1 (±0)	0.1080 (±0.0003)	90.0217 (±0.0153)	31.9974 (±0)	35.2449 (±0.0132)	1.0983

4.1.1.2 Estimation of Transformation Parameters

After the estimation of line parameters, the next step is to estimate transformation parameters using the three alternative registration approaches. The registration process aims to estimate the 3D similarity transformation parameters, which include three translations (t_x, t_y, t_z) and three rotation parameters (ω, ϕ, κ).

The observations for performing the three registration approaches are specified as follows. In the linear feature-based approach, two tests were conducted using the simulated points along linear features. In the first test, the observations are estimated line parameters from a line fitting procedure, and the weight matrix P is defined by the inverse of the variance-covariance matrix of the estimated line parameters. However, the estimated line parameters in the first test are highly correlated. In the second test, a local coordinate system is established by shifting the origin of the original coordinate system to the center of the line segment. Then, a line fitting procedure is performed in the local coordinate system to derive the line parameters. The results show that the correlation between the estimated line parameters is eliminated. Next, the estimated line parameters are shifted back to the original coordinate system. After that, the estimated point is extrapolated 50 m away along the line direction to ensure that the estimated points are not the same point in conjugate lines. In the second test, the observations are the estimated line parameters after the extrapolation. The weight matrix P is defined by the inverse of the variance-covariance matrix Σ, which is derived based on the law of error propagation.

In the pseudo-conjugate point-based method, the observations are coordinates of simulated points along lines in the source and reference scans. The weight matrix depends on the noise added to the point clouds. The estimated line parameters in the reference scan are used to modify the weight matrix to eliminate the additional vector resulting from using non-corresponding points along linear features. In the 3D similarity transformation function, each point pair contributes three equations towards the transformation parameter estimation. There are 3,920 points along linear

features in each scan, so the total number of observation equations is $3,920 \times 3 = 11,760$. However, the discussion in the subsection 3.3.2 indicates that the effective contribution is only two equations from each point pair. According to Equation (3.73) in the subsection 3.3.2, all the elements in the weight matrix pertaining to the U-axis along the linear features are assigned a zero weight. The modified weight matrix in the LSA procedure nullifies the error along the line direction while minimizing the errors in the two directions normal to the line. Therefore, the effective contribution of a 3D point pair towards redundancy is 2 equations instead of 3. In this case, the redundancy is given by the difference between the rank of the weight matrix and the number of the unknowns, thus resulting in a redundancy of $3,920 \times 2 - 6 = 7,834$.

In the closed-form solution, the rotation parameters and the translation parameters are estimated separately. The rotation matrix is derived first using a quaternion-based approach, which is a single-step solution. The observations are the direction vectors of linear features. A weight matrix is not used in this procedure, and there is no standard deviation to evaluate the estimated rotation parameters. Once the rotation matrix is derived, the next step is to estimate translation parameters using the pseudo-conjugate point-based method. In this step, the observations are coordinates of points along linear features, and the weight matrix is obtained as the inverse of the variance-covariance matrix of the observations.

The estimated transformation parameters, standard deviations, a-posteriori variance factors, and execution times from the linear feature-based approach, pseudo-conjugate point-based method, and closed-form solution using the simulated linear features are presented in Table 4.15. All approaches based on the linear features produced similar parameters to the true values. As an example, Table 4.15 shows that the errors in translation and rotation are in the order of 1 millimeters and 0.001° respectively by using the linear feature-based approach after using the line fitting approach with the shift of origin, pseudo-conjugate point-based method, and closed-form solution when compared to true values, and it is in the order of 0.1 millimeters and 0.001° by using the linear feature-based approach after using the line fitting ap-

proach without the shift of origin. In the linear feature-based approach after using the line fitting approach without the shift of origin, linear feature-based approach after using the line fitting approach with the shift of origin, and pseudo-conjugate point-based method registration results, the standard deviations are close to each other. In the closed-form solution, the standard deviations are in the order of 0.1 mm for the translation parameters. Since the rotation parameters are estimated by quaternions, there is no standard deviation to evaluate the rotation parameters. As we can see, there is no significant difference between the estimated transformation parameters and standard deviations for all approaches based on the linear features, so the registration results estimated using different approaches based on the linear features could be considered equivalent.

Furthermore, the a-posteriori variance factors are also presented in Table 4.15. Because the weight matrix P in LSA is derived by the inverse of variance-covariance matrix of the measurements, the $\hat{\sigma}_0^2$ should be close to the a-priori value $\sigma_0^2 = 1$. As shown in Table 4.15, $\hat{\sigma}_0^2$ is close to the a-priori value $\sigma_0^2 = 1$ when using the pseudo-conjugate point-based method and closed-form solution, which indicates the validity of the estimated 3D line parameters. In the linear feature-based approach after using the line fitting approach without the shift of origin, the $\hat{\sigma}_0^2 = 1.4002$. After shifting the origin of the coordinate system to the center of the line, the $\hat{\sigma}_0^2$ decreases to 1.0706, which is coherent with the a-priori value $\sigma_0^2 = 1$. Regarding the execution time, the two linear feature-based approach had the shortest execution time, as listed in Table 4.15. The linear feature-based approach after using the line fitting approach without the shift of origin and linear feature-based approach after using the line fitting approach with the shift of origin led to identical execution time. The pseudo-conjugate point-based and closed-form approaches based on linear features led to longer execution times due to a large number of point cloud data.

Table 4.15.: The estimated transformation parameters, standard deviations, a-posteriori variance factors, and execution times from the linear feature-based approach, pseudo-conjugate point-based method, and closed-form solution using the simulated linear features

	$t_x(m \pm m)$	$t_y(m \pm m)$	$t_z(m \pm m)$	$\omega(^\circ \pm ^\circ)$	$\phi(^\circ \pm ^\circ)$	$\kappa(^\circ \pm ^\circ)$	$\hat{\sigma}_0^2$	Execution time (seconds)
True value	0	100	0	10	20	80		
Linear feature-based approach after using the line fitting approach without the shift of origin	-0.0006 (±0.0019)	99.9996 (±0.0022)	0.0007 (±0.0022)	10.0000 (±0.0033)	19.9987 (±0.0026)	80.0001 (±0.0020)	1.4002	0.4
Linear feature-based approach after using the line fitting approach with the shift of origin	-0.0013 (±0.0020)	99.9997 (±0.0021)	0.0022 (±0.0021)	10.0028 (±0.0033)	19.9987 (±0.0024)	80.0000 (±0.0021)	1.0706	0.4
Pseudo-conjugate point-based method	-0.0014 (±0.0019)	99.9996 (±0.0020)	0.0024 (±0.0020)	10.0033 (±0.0031)	19.9989 (±0.0023)	80.0000 (±0.0021)	0.9895	3.5
Closed-form solution	-0.0019 (±0.0008)	99.9909 (±0.0009)	-0.0058 (±0.0008)	9.9995 (N/A)	20.0079 (N/A)	79.9953 (N/A)	0.9928	7.4

After applying the estimated transformation parameters, the points along the lines in the source scan were transformed to the reference scan. These results of the registration are quantified in terms of the root-mean-square error (RMSE) values of distances between 3,920 conjugate points in reference and transformed scans, as shown in Table 4.16. Comparing the distances between conjugate points, the difference of RMSE values between the different approaches is below 0.3 mm, which indicates the equivalency of the registration results between the three registration approaches using linear features. More specifically, a one by one comparison for the RMSE values along the x, y, and z axes shows that the three approaches have similar RMSE values along the x, y, and z axes. In summary, the introduced alternative registration approaches using linear features can achieve equivalent registration results.

Table 4.16.: Quantitative comparison between linear feature-based approach, pseudo-conjugate point-based method, and closed-form solution through RMSE analysis of the point-to-point distances between 3,920 pairs of points along linear features in the source and reference scans

	RMSE			
	X(cm)	Y(cm)	Z(cm)	Total(cm)
Linear feature-based approach after using the line fitting approach without the shift of origin	4.23	4.18	4.25	7.30
Linear feature-based approach after using the line fitting approach with the shift of origin	4.23	4.18	4.24	7.30
Pseudo-conjugate point-based method	4.23	4.18	4.24	7.31
Closed-form solution	4.23	4.19	4.26	7.32

4.1.2 Registration using planar features

After the linear features were used for the introduced registration approaches, the planar features were also used as the registration primitives to investigate the quality of the registration results with a different type of feature. A minimum of three planar features, which are not parallel to each other in the common area of adjacent scans, are required for the estimation of the transformation parameters [11]. In this subsection, estimated plane parameters using simulated points along planar features are presented first. Then, the results of the three alternative registration approaches using planar features are presented and evaluated.

4.1.2.1 Plane Fitting

A plane fitting procedure was performed to estimate plane parameters using the mathematical model as stated in the subsection 3.2.5. The estimated plane parameters, standard deviations, and a-posteriori variance factors for 10 pairs of simulated planar features in the source and reference scans are presented in Table 4.17. Comparing the estimated plane parameters in Table 4.17 with the simulated plane parameters in Table 4.5, one can see that the estimated parameters seem to be close to the true ones. The standard deviations overall were below 6 cm for plane parameters in the source and reference scans. The numerical values and the standard deviations indicate that the plane fitting procedure is reliable. Furthermore, the a-posteriori variance factor is also presented in Table 4.17. Because the weight matrix P in LSA is derived by the inverse of variance-covariance matrix of the measurements, the $\hat{\sigma}_0^2$ should be close to the a-priori value $\sigma_0^2 = 1$. As shown in Table 4.17, the a-posteriori variance factor $\hat{\sigma}_0^2$ is close to the a-priori value $\sigma_0^2 = 1$, which is also an indication of the reliability of the estimated plane parameters.

Table 4.17.: The estimated plane parameters, standard deviations, and a-posteriori variance factors for 10 pairs of simulated planar features in the source and reference scans

	Plane ID	$a_x(m \pm m)$	$a_y(m \pm m)$	$a_z(m \pm m)$	$\hat{\sigma}_0^2$
Source Scan	1	-1.5385 ($\pm$0.0013)	7.6913 ($\pm$0.0081)	-0.0003 ($\pm$0.0022)	0.9632
	2	4.2125 ($\pm$0.0070)	21.1253 ($\pm$0.0110)	-0.0025 ($\pm$0.0064)	1.0648
	3	60.0063 ($\pm$0.0092)	0.0443 ($\pm$0.0235)	-0.0092 ($\pm$0.0176)	1.0385
	4	0.0068 ($\pm$0.0098)	25.0202 ($\pm$0.0271)	0.0014 ($\pm$0.0073)	1.0386
	5	75.0203 ($\pm$0.0096)	0.0323 ($\pm$0.0182)	0.0134 ($\pm$0.0150)	0.9874
	6	1.8152 ($\pm$0.0040)	-9.0623 ($\pm$0.0105)	6.8050 ($\pm$0.0162)	0.8924
	7	-0.0618 ($\pm$0.0052)	-0.3084 ($\pm$0.0264)	0.2314 ($\pm$0.0201)	0.8439
	8	18.6317 ($\pm$0.0088)	0.0012 ($\pm$0.0046)	46.5529 ($\pm$0.0035)	1.043
	9	-0.0061 ($\pm$0.0050)	-6.9920 ($\pm$0.0106)	13.9956 ($\pm$0.0402)	1.0451
	10	0.0004 ($\pm$0.0010)	-0.0005 ($\pm$0.0011)	9.9982 ($\pm$0.0053)	1.1309
Reference Scan	1	34.4562 ($\pm$0.0206)	10.8534 ($\pm$0.0154)	-8.4175 ($\pm$0.0091)	1.133
	2	14.3533 ($\pm$0.0189)	-1.0306 ($\pm$0.0022)	-1.3397 ($\pm$0.0031)	0.8942
	3	-5.3219 ($\pm$0.0105)	30.0928 ($\pm$0.0217)	-11.1248 ($\pm$0.0066)	0.9908
	4	35.5513 ($\pm$0.0181)	4.0934 ($\pm$0.0147)	-5.9124 ($\pm$0.0092)	0.9465

continued on next page

Table 4.17.: *continued*

Plane ID	$a_x(m \pm m)$	$a_y(m \pm m)$	$a_z(m \pm m)$	$\hat{\sigma}_0^2$
5	-2.8641 ($\pm$0.0027)	16.2429 ($\pm$0.0158)	-5.9997 ($\pm$0.0045)	0.9394
6	-6.4273 ($\pm$0.0419)	-0.1918 ($\pm$0.0037)	6.8959 ($\pm$0.0515)	1.0081
7	-20.2167 ($\pm$0.0158)	7.4892 ($\pm$0.0136)	17.1809 ($\pm$0.0347)	0.8611
8	8.1494 ($\pm$0.0051)	-0.3812 ($\pm$0.0071)	48.6879 ($\pm$0.0105)	0.9823
9	-14.5237 ($\pm$0.0140)	11.7397 ($\pm$0.0224)	38.6868 ($\pm$0.0498)	1.023
10	5.1945 ($\pm$0.0050)	16.7210 ($\pm$0.0060)	42.7450 ($\pm$0.0049)	0.947

4.1.2.2 Estimation of Transformation Parameters

After the estimation of the plane parameters, the next step is to estimate transformation parameters using the three alternative registration approaches. The registration parameters in the 3D similarity function consist of three translations (t_x, t_y, t_z), three rotation parameters (ω, ϕ, κ). The observations and weight matrix in the three alternative registration approaches are specified as follows. In the planar feature-based approach, the observations are the plane parameters estimated in a plane fitting procedure, and the weight matrix P is defined by the inverse of the variance-covariance matrix of measurements.

In the pseudo-conjugate point-based method, the observations are the coordinates of simulated points along planes in the source and reference scans. The weight matrix P depends on the noise added to the point clouds. The estimated plane parameters in the reference scan are used to modify the weight matrix to eliminate the additional vector resulting from using non-corresponding points along planar features. In the 3D similarity transformation function, each 3D point pair contributes three equations towards the transformation parameter estimation. There are 3,686 points along planar features in each scan, so the total number of observation equations is $3,686 \times 3 = 11,058$. However, the discussion in the subsection 3.3.2 indicates that the effective contribution is only one equation from each point pair. According to Equation (3.74) in the subsection 3.3.2, all the elements in the weight matrix pertaining to the U- and V-axes along the planar features are assigned a zero weight. The modified weight matrix in the LSA procedure nullifies the errors along a planar feature while minimizing the errors in the direction normal to the planar feature. Therefore, the effective contribution of a 3D point pair towards redundancy is 1 equation instead of 3. In this case, the redundancy is given by the difference between the rank of the weight matrix and the number of the unknowns, thus resulting in a redundancy of $3,686 \times 1 - 6 = 3,680$.

In the closed-form solution, the rotation parameters and the translation parameters are estimated separately. The rotation matrix is derived first using a quaternion-based approach, which is a single-step solution. The observations are the estimated plane parameters, which also represent the normal vectors of planar features. A weight matrix is not used in this procedure, and there is no standard deviation to evaluate the estimated rotation parameters. Once the rotation matrix is derived, the next step is to estimate translation parameters using the pseudo-conjugate point-based method. In this step, the observations are the coordinates of points along planar features, and the weight matrix is obtained as the inverse of the variance-covariance matrix of the observations.

The estimated transformation parameters, standard deviations, a-posteriori variance factors, and execution times from the planar feature-based approach, pseudo-conjugate point-based method, and closed-form solution using the simulated planar features are presented in Table 4.18. Since the rotation parameters are estimated by quaternions in the closed-form solution, there is no standard deviation for the rotation parameters. All approaches based on the planar features produced similar parameters to the true values. As an example, Table 4.18 shows that the errors in translation and rotation parameters are in the order of 1 centimeter and 0.001° respectively by using the three registration approaches based on planar features. The small standard deviation values of the registration parameters indicate that reliable results were estimated using the three alternative registration approaches. According to Table 4.18, the difference between estimated registration parameters using the three approaches are not significant, so the three approaches based on planar features can produce equivalent registration results.

Table 4.18.: The estimated transformation parameters, standard deviations, a-posteriori variance factors, and execution times from the planar feature-based approach, pseudo-conjugate point-based method, and closed-form solution using the simulated planar features

	$X_T(m \pm m)$	$Y_T(m \pm m)$	$Z_T(m \pm m)$	$\omega(^\circ \pm ^\circ)$	$\varphi(^\circ \pm ^\circ)$	$\kappa(^\circ \pm ^\circ)$	$\hat{\sigma}_0^2$	Execution time (seconds)
True value	0	100	0	10	20	80		
Planar feature-based approach	-0.0021 (±0.0033)	99.9987 (±0.0046)	0.0011 (±0.0048)	9.9963 (±0.0063)	19.9968 (±0.0049)	79.9973 (±0.0045)	1.4499	0.5
Pseudo-conjugate point-based method	-0.0022 (±0.0027)	99.9985 (±0.0037)	0.0011 (±0.0039)	9.9964 (±0.0051)	19.9970 (±0.0039)	79.9972 (±0.0036)	0.9581	2.0
Closed-form solution	0.0035 (±0.0012)	99.9973 (±0.0015)	-0.0081 (±0.0010)	9.9846 (N/A)	20.0001 (N/A)	80.0012 (N/A)	0.9594	3.7

Furthermore, the a-posteriori variance factors are also presented in Table 4.18. Because the weight matrix P is obtained as the inverse of variance-covariance matrix of the estimated plane parameters, the $\hat{\sigma}_0^2$ should be close to the a-priori value $\sigma_0^2 = 1$. As shown in Table 4.18, $\hat{\sigma}_0^2$ is close to the a-priori value $\sigma_0^2 = 1$ for all three approaches, which indicates the validity of the estimated plane parameters. Regarding the execution time, the planar feature-based approach had the shortest execution time, as listed in Table 4.18. The pseudo-conjugate point-based and closed-form approaches based on planar features led to longer execution times due to a large number of point cloud data.

After applying the estimated transformation parameters, the points along the planes in the source scan were transformed into the reference scan. The quality of the registration results was analyzed by calculating the RMSE values of distances between 3,686 conjugate points in the reference and transformed scans, as shown in Table 4.19. The RMSE values of distances shown in Table 4.19 are similar to each other, which indicates that the registration results using the three registration approaches based on planar features can be considered equivalent.

The comparison between linear and planar features is conducted based on the RMSE values of distances between conjugate points in the reference and transformed scans after applying the estimated transformation parameters. The RMSE values of distances are close to 7.3 cm for both features. Therefore, linear and planar features can produce equivalent registration results.

Table 4.19.: Quantitative comparison between planar feature-based approach, pseudo-conjugate point-based method, and closed-form solution through RMSE analysis of the point-to-point distances between 3,686 pairs of points along planar features in the source and reference scans

	RMSE			
	X(cm)	Y(cm)	Z(cm)	Total(cm)
Planar feature-based approach	4.16	4.25	4.22	7.3
Pseudo-conjugate point-based method	4.16	4.25	4.22	7.3
Closed-form solution	4.17	4.26	4.24	7.31

4.2 Experiment with Real Data

In the second experiment, the performance of the introduced registration approaches will be tested using real datasets collected over the Forney Hall of Chemical Engineering at Purdue University. The registration approaches using planar and linear features were performed and the registration results are presented in the following subsections. The introduced three alternative registration approaches are compared to find out whether they can produce equivalent results or not. Quality evaluation was conducted based on the point-to-patch normal distances following the registration. Furthermore, comparisons between the registration approaches using planar and linear features were conducted to see whether the two feature primitives produce equivalent registration results or not.

4.2.1 Data Description

Eight TLS scans were collected around the Forney Hall using a FARO Focus3D terrestrial laser scanner. Figure 4.4 illustrates the positions of TLS scans covering

the Forney Hall on Google Maps. FARO Focus3D terrestrial laser scanner is shown in Figure 4.5. The scanning range of the instrument allows distance measurements between 0.6 m and 330 m, and the ranging error is ±2 mm at 25 m, one sigma [27]. The Focus3D scanner deploys an integrated color camera, and the point clouds are color-coded automatically. The eight TLS scans and the number of points in each scan are shown in Figure 4.6. In order to make sure there are enough conjugate features with various orientation and separation, large overlapping areas between each scan pair are required to register them. Therefore, the distance between two adjacent scans is around 40 m-45 m. The approximate percentages of the overlapping areas between neighboring scans are listed in Table 4.20.

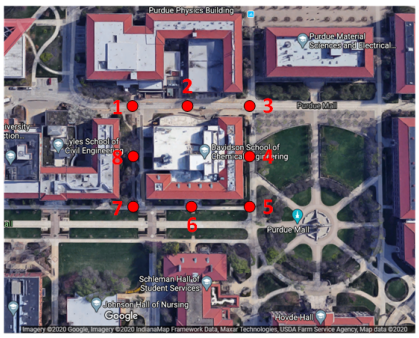

Fig. 4.4.: Position of TLS scans covering the Forney Hall

Fig. 4.5.: FARO Focus3D X 330

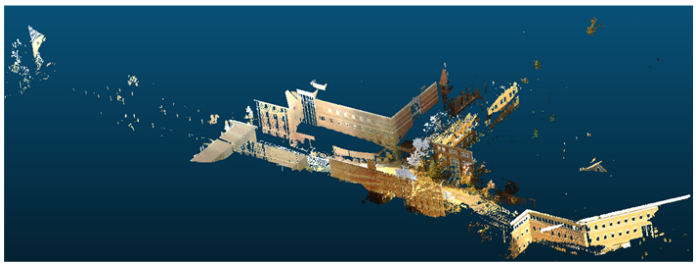

(a) Scan 1 (15,266,683 points)

Fig. 4.6.: True color display of the eight scans and the number of points in each scan

(continued on next page)

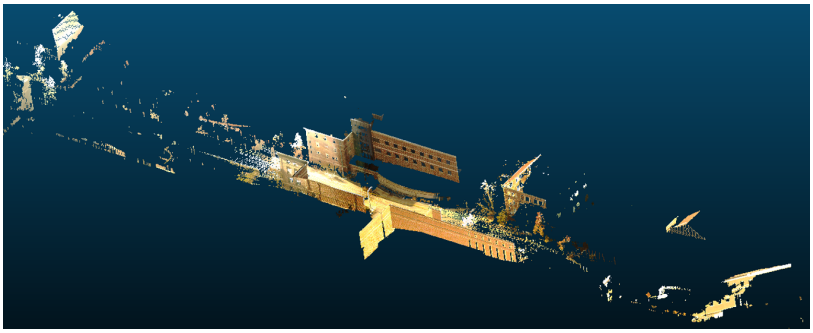

(b) Scan 2 (16,047,213 points)

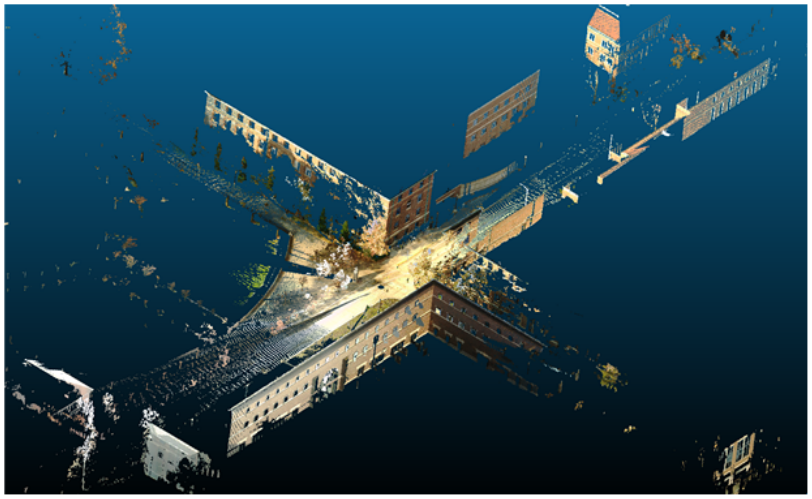

(c) Scan 3 (13,721,108 points)

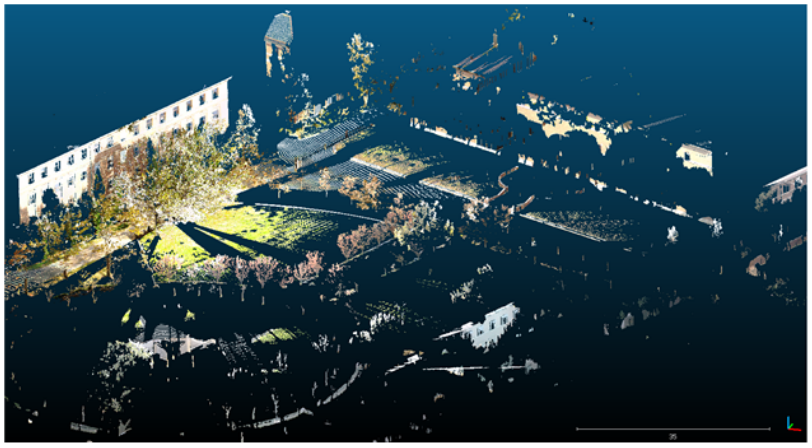

(d) Scan 4 (20,074,031 points)

Fig. 4.6.: True color display of the eight scans and the number of points in each scan (continued from the previous page)

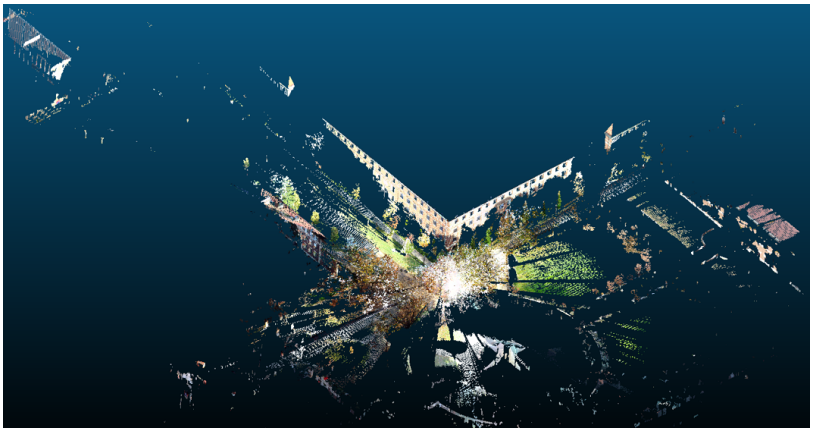

(e) Scan 5 (18,882,433 points)

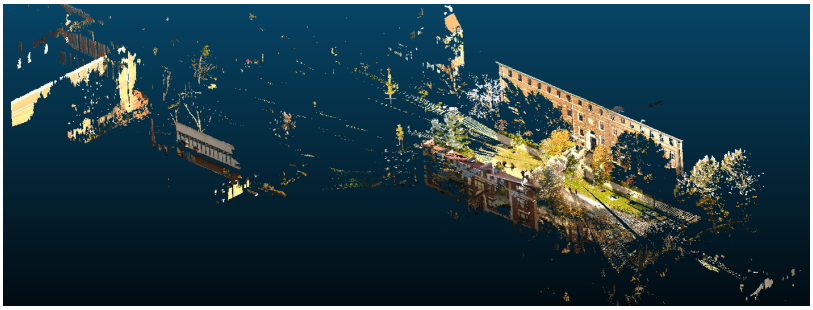

(f) Scan 6 (15,739,754 points)

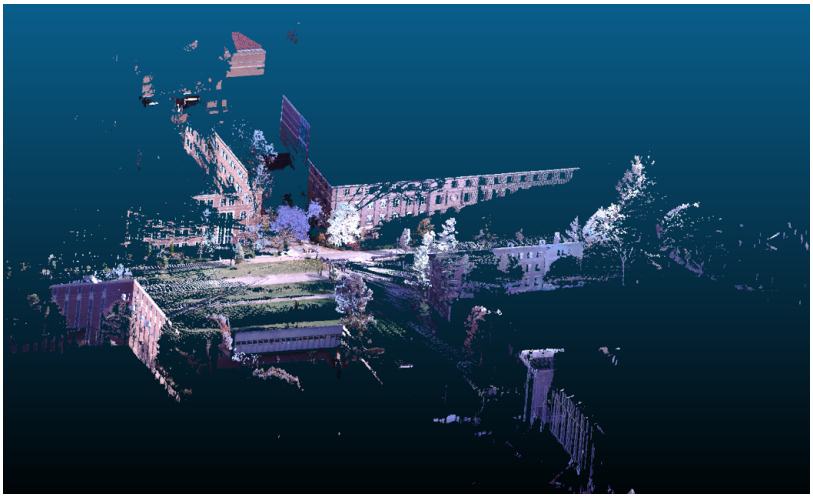

(g) Scan 7 (13,882,749 points)

Fig. 4.6.: True color display of the eight scans and the number of points in each scan (continued from the previous page)

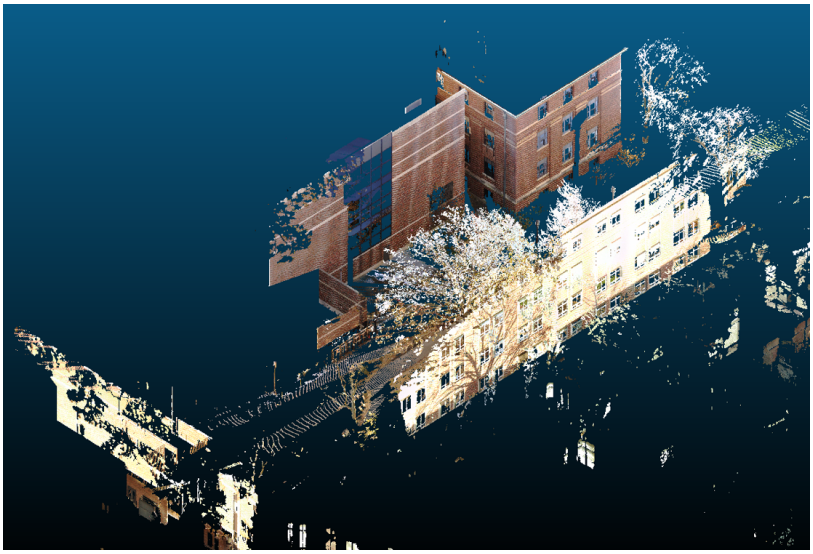

(h) Scan 8 (16,629,929 points)

Fig. 4.6.: True color display of the eight scans and the number of points in each scan (continued from the previous page)

Table 4.20.: The approximate percentages of the overlapping areas between neighboring scans

	Scan 1	Scan 2	Scan 3	Scan 4	Scan 5	Scan 6	Scan 7	Scan 8
Scan 1	N/A	60%	0%	0%	0%	0%	0%	45%
Scan 2	60%	N/A	50%	0%	0%	0%	0%	0%
Scan 3	0%	50%	N/A	45%	20%	0%	0%	0%
Scan 4	0%	0%	45%	N/A	50%	0%	0%	0%
Scan 5	0%	0%	20%	50%	N/A	50%	15%	0%
Scan 6	0%	0%	0%	0%	50%	N/A	45%	0%
Scan 7	0%	0%	0%	0%	15%	45%	N/A	45%
Scan 8	45%	0%	0%	0%	0%	0%	45%	N/A

The planar feature extraction from a point cloud is performed using a feature extraction tool in Image-LiDAR Interactive Visualization Environment (I-LIVE) software developed by Ravi and Habib [28]. I-LIVE is a software aimed for end-users to conduct a qualitative and quantitative evaluation of 2D and 3D data. Starting from a single seed-point, points that belong to the same plane will be grouped through a segmentation process, as shown in Figure 4.7. Linear features are extracted indirectly by the intersection of the segmented planar features from TLS scans. The planar features do not need to be physically connected. Then, twenty points are simulated along the derived linear features in each scan. The simulated points along linear features do not need to correspond to the physical linear features.

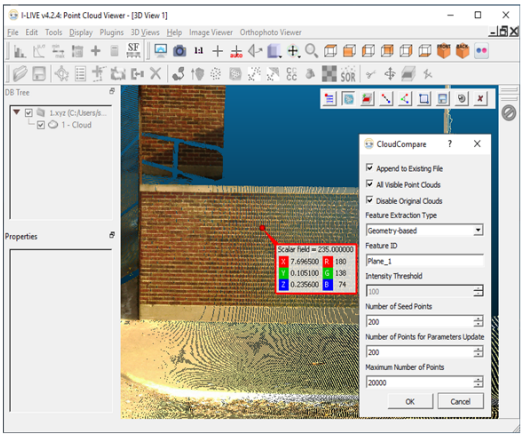

Fig. 4.7.: Extraction of planar features in I-LIVE

4.2.2 Registration Between Scans 1 and 2

Figure 4.8 illustrates the positions of TLS scans 1 and 2 on Google Maps. The blue arrow represents the direction of the registration process. In this pairwise registration, scan 1 is the reference scan, and scan 2 is the source scan.

Fig. 4.8.: Position of TLS scans 1 and 2

4.2.2.1 Registration Between Scans 1 and 2 Using Planar Features

Figure 4.9 illustrates the planar features in the overlapping area between scans 1 and 2. A plane fitting procedure, as stated in subsection 3.2.5, was performed to estimate plane parameters. The estimated plane parameters, standard deviations, and square roots of the a-posteriori variance factors for 19 pairs of planar features in scans 1 and 2 are presented in Table 4.21. The standard deviation overall was below 1 cm for plane parameters in the source and reference scans except plane 12, as highlighted in the table. The small standard deviation values indicate the estimated plane parameters are reliable. Plane 12 is 200 m away from TLS, so the range error is large. Furthermore, the a-posteriori variance factor $\hat{\sigma}_0^2$ is used to check the quality of the estimated plane parameters. Since the weight matrix P is an identity matrix, the $\hat{\sigma}_0^2$ is the variance of the measurements. The square roots of the a-posteriori variance factors ($\hat{\sigma}_0$) after plane fitting are close to the expected accuracy of around 2 mm according to the accuracy of the TLS, thus indicating the validity of the estimated plane parameters.

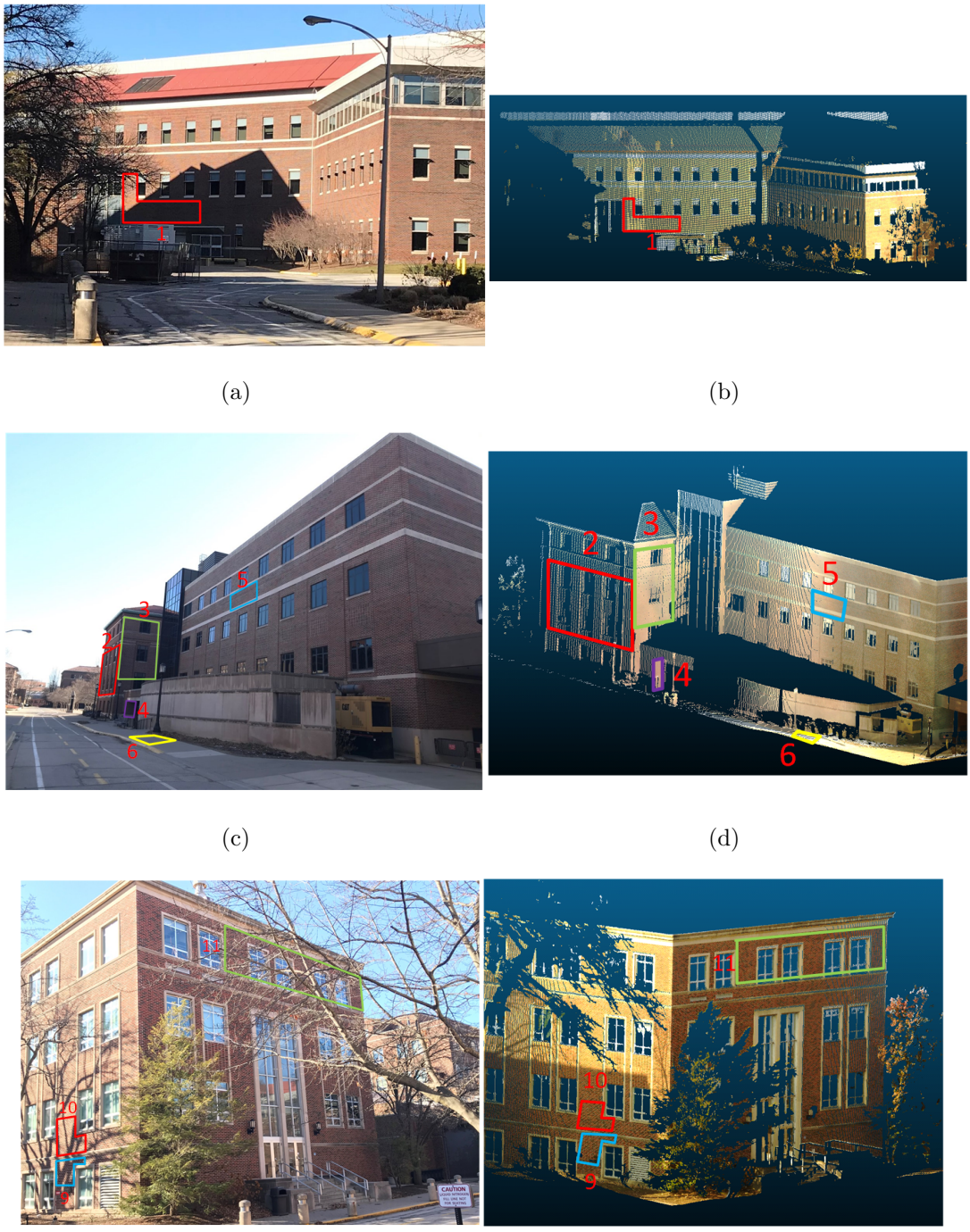

(a) (b)

(c) (d)

(e) (f)

Fig. 4.9.: Planar features in the overlapping area between scans 1 and 2 displayed in images (a, c, e, g, i, k), which are captured by an external camera, and point clouds (b, d, f, h, j, l) (continued on next page)

(g) (h)

(i) (j)

(k) (l)

Fig. 4.9.: Planar features in the overlapping area between scans 1 and 2 displayed in images (a, c, e, g, i, k), which are captured by an external camera, and point clouds (b, d, f, h, j, l) (continued from the previous page)

Table 4.21.: The estimated plane parameters, standard deviations, and square roots of the a-posteriori variance factors of 19 pairs of planar features in scans 1 and 2

	Plane ID	$a_x(m \pm m)$	$a_y(m \pm m)$	$a_z(m \pm m)$	$\hat{\sigma}_0(mm)$
Scan 2	1	-104.7102 ($\pm$0.0053)	69.0432 ($\pm$0.0019)	0.0417 ($\pm$0.0152)	4.7
	2	1.1999 ($\pm$0.0000)	-9.2369 ($\pm$0.0001)	0.0065 ($\pm$0.0001)	3.3
	3	14.5270 ($\pm$0.0000)	1.9243 ($\pm$0.0000)	-0.0035 ($\pm$0.0000)	1.9
	4	12.1413 ($\pm$0.0005)	1.5888 ($\pm$0.0004)	-0.0168 ($\pm$0.0002)	1.3
	5	2.0357 ($\pm$0.0001)	-15.5477 ($\pm$0.0002)	0.0252 ($\pm$0.0003)	1.7
	6	-0.0054 ($\pm$0.0000)	-0.0184 ($\pm$0.0001)	-1.4753 ($\pm$0.0006)	0.8
	7	-0.0179 ($\pm$0.0001)	0.0313 ($\pm$0.0002)	-1.5280 ($\pm$0.0010)	1.6
	8	-0.0118 ($\pm$0.0001)	0.0040 ($\pm$0.0002)	-1.5536 ($\pm$0.0012)	1.0
	9	-54.8445 ($\pm$0.0007)	-7.2352 ($\pm$0.0038)	-0.0453 ($\pm$0.0070)	1.7
	10	-54.8368 ($\pm$0.0004)	-7.1517 ($\pm$0.0023)	0.0015 ($\pm$0.0043)	1.1
	11	1.3906 ($\pm$0.0002)	-10.6929 ($\pm$0.0019)	0.0113 ($\pm$0.0012)	2.3
	12	139.8450 ($\pm$0.0095)	18.3089 ($\pm$0.0407)	-0.0936 ($\pm$0.0525)	3.4
	13	-2.1538 ($\pm$0.0004)	16.4659 ($\pm$0.0006)	0.0288 ($\pm$0.0005)	1.7
	14	-2.1640 ($\pm$0.0006)	16.4478 ($\pm$0.0016)	-0.0283 ($\pm$0.0022)	1.2

continued on next page

Table 4.21.: *continued*

	Plane ID	$a_x(m \pm m)$	$a_y(m \pm m)$	$a_z(m \pm m)$	$\hat{\sigma}_0$(mm)
	15	-2.1855 ($\pm$0.0005)	16.5142 ($\pm$0.0008)	0.0491 ($\pm$0.0006)	1.3
	16	-0.5799 ($\pm$0.0004)	4.2171 ($\pm$0.0016)	0.0328 ($\pm$0.0004)	1.8
	17	-0.7937 ($\pm$0.0001)	5.9658 ($\pm$0.0002)	0.0012 ($\pm$0.0001)	1.2
	18	-1.1391 ($\pm$0.0000)	8.6986 ($\pm$0.0000)	0.0274 ($\pm$0.0001)	1.8
	19	18.6360 ($\pm$0.0001)	2.4453 ($\pm$0.0002)	0.0035 ($\pm$0.0001)	1.7
Scan 1	1	-37.4554 ($\pm$0.0024)	81.9178 ($\pm$0.0006)	0.0158 ($\pm$0.0053)	3.2
	2	-4.1545 ($\pm$0.0003)	-9.0669 ($\pm$0.0011)	0.0056 ($\pm$0.0004)	4.2
	3	55.3082 ($\pm$0.0002)	-25.1826 ($\pm$0.0007)	-0.0101 ($\pm$0.0004)	1.9
	4	53.0839 ($\pm$0.0016)	-24.2461 ($\pm$0.0069)	0.0044 ($\pm$0.0032)	1.6
	5	-6.8075 ($\pm$0.0002)	-14.8940 ($\pm$0.0008)	0.0213 ($\pm$0.0008)	1.6
	6	-0.0150 ($\pm$0.0001)	-0.0130 ($\pm$0.0001)	-1.4859 ($\pm$0.0013)	0.9
	7	0.0011 ($\pm$0.0001)	0.0310 ($\pm$0.0001)	-1.3519 ($\pm$0.0008)	1.8
	8	-0.0070 ($\pm$0.0000)	0.0099 ($\pm$0.0001)	-1.4699 ($\pm$0.0004)	1.2
	9	-8.3941 ($\pm$0.0009)	3.8155 ($\pm$0.0001)	-0.0138 ($\pm$0.0009)	1.5
	10	-8.3610 ($\pm$0.0004)	3.8199 ($\pm$0.0000)	-0.0040 ($\pm$0.0002)	1.1

continued on next page

Table 4.21.: *continued*

Plane ID	$a_x(m \pm m)$	$a_y(m \pm m)$	$a_z(m \pm m)$	$\hat{\sigma}_0$(mm)
11	-4.7672 (±0.0001)	-10.4033 (±0.0002)	0.0077 (±0.0002)	2.1
12	170.1970 (±0.0304)	-77.8360 (±0.0770)	-0.2380 (±0.1027)	4.3
13	6.5983 (±0.0004)	14.4648 (±0.0002)	0.0398 (±0.0002)	1.7
14	6.5931 (±0.0008)	14.4435 (±0.0011)	-0.0025 (±0.0017)	1.3
15	6.5671 (±0.0004)	14.4525 (±0.0004)	0.0476 (±0.0005)	1.2
16	1.3352 (±0.0000)	2.9688 (±0.0000)	0.0290 (±0.0000)	2.0
17	2.1581 (±0.0003)	4.7499 (±0.0005)	0.0023 (±0.0002)	1.1
18	3.3513 (±0.0010)	7.3353 (±0.0016)	0.0224 (±0.0004)	2.0
19	59.0558 (±0.0009)	-26.9502 (±0.0015)	0.0046 (±0.0012)	1.7

The estimated transformation parameters, standard deviations, and a-posteriori variance factors, and execution times from the planar feature-based approach, pseudo-conjugate point-based method, and closed-form solution using the planar features in scans 1 and 2 are presented in Table 4.22. Since the rotation parameters are estimated by quaternions in the closed-form solution, there is no standard deviation for the rotation parameters. As shown in Table 4.22, the estimated transformation parameters produced by different registration approaches are close to each other. Also, the standard deviation values of the registration parameters indicate that reliable results were estimated using the three alternative registration approaches. As an example, Table 4.22 shows that the standard deviations of the estimated parameters were below 2 mm for the translation parameters and below 0.004 degrees for the rotation angels using the three different approaches. In the closed-form solution, since the rotation parameters are estimated by quaternions, there is no standard deviation to evaluate the rotation parameters. As can be seen in Table 4.22, there is no significant difference between the estimated transformation parameters for all approaches, so the registration results estimated using different approaches based on planar features could be considered equivalent.

Furthermore, the a-posteriori variance factor $\hat{\sigma}_0^2$ is presented in Table 4.22. In the planar feature-based approach, the weight matrix P is derived by the inverse of the variance-covariance matrix, so the $\hat{\sigma}_0^2$ should be close to 1. As shown in Table 4.22, the a-posteriori variance factor $\hat{\sigma}_0^2$ was 348.1317, which indicates that the noise level in the observation is larger than previously assumed. In the pseudo-conjugate point-based method and closed-form solution, the $\hat{\sigma}_0^2$ is the variance of the measurements since the weight matrix P is an identity matrix. The square roots of the a-posteriori variance factors ($\hat{\sigma}_0$) in Table 4.22 are not significantly different from the expected accuracy of around 2 mm according to the accuracy of the TLS, thus indicating the validity of the estimated transformation parameters using the pseudo-conjugate point-based method and closed-form solution based on planar features. Regarding the execution time, the planar feature-based approach had the shortest execution time, as listed in

Table 4.22. The pseudo-conjugate point-based and closed-form approaches based on planar features led to longer execution times due to a large number of point cloud data.

The quality evaluation of the registration results was analyzed by calculating the point-to-patch normal distances between TLS scans. After applying the estimated registration parameters, the point clouds in the source scan were transformed into the reference scan. A point-patch pair is established by using the approach discussed in section 3.4. The normal distance between the transformed point and the patch must be within a certain threshold, which is 10 cm in this test. The mean, standard deviation, and RMSE of the point-to-patch normal distances between the TLS scans are presented in Table 4.23.

The mean, standard deviation, and RMSE of the calculated point-to-patch normal distances of each approach were all below 5 mm, which substantiates the quality of the registration results. In the planar feature-based approach and pseudo-conjugate point-based method, the average of the calculated point-to-patch normal distances were around 2 mm, and the value of standard deviation and RMSE is close between the two approaches, which indicates the equivalency between the two approaches. The average point-to-patch normal distances was 3.6 mm for the closed-form solution. The standard deviation and RMSE values were also larger than those values produced by using the planar-feature based approach and pseudo-conjugate point-based method, which indicates that the registration results produced by the closed-form solution were worse than the registration results by using the other two approaches.

Table 4.22.: The estimated transformation parameters, standard deviations, and a-posteriori variance factors, and execution times from the planar feature-based approach, pseudo-conjugate point-based method, and closed-form solution using the planar features in scans 1 and 2

	$t_x(m \pm m)$	$t_y(m \pm m)$	$t_z(m \pm m)$	$\omega(^\circ \pm ^\circ)$	$\phi(^\circ \pm ^\circ)$	$\kappa(^\circ \pm ^\circ)$	$\hat{\sigma}_0^2$	$\hat{\sigma}_0$	Execution time (seconds)
Planar feature-based approach	41.6531 (±0.0005)	-19.8073 (±0.0005)	-0.2491 (±0.0015)	-0.0033 (±0.0026)	0.0017 (±0.0032)	32.0189 (±0.0008)	348.1317	18.6583	0.3
Pseudo-conjugate point-based method	41.6524 (±0.0000)	-19.8083 (±0.0000)	-0.2490 (±0.0001)	0.0055 (±0.0001)	0.0027 (±0.0001)	32.0191 (±0.0000)	6.34E-06 (m^2)	2.5 (mm)	91.5
Closed-form solution	41.6541 (±0.0000)	-19.8049 (±0.0000)	-0.2439 (±0.0001)	-0.0200 (N/A)	0.0103 (N/A)	32.0103 (N/A)	1.32E-05 (m^2)	3.6 (mm)	92.3

Table 4.23.: Quantitative comparison between planar feature-based approach, pseudo-conjugate point-based method, and closed-form solution based on planar features through the mean, standard deviation, and RMSE of the point-to-patch normal distances between the TLS scans 1 and 2

	Mean (m)	Standard deviation (m)	RMSE (m)	Number of used points	Total number of points
Planar feature-based approach	0.0021	0.0028	0.0035	488,745	3,654,034
Pseudo-conjugate point-based method	0.0020	0.0028	0.0034	489,362	3,654,034
Closed-form solution	0.0036	0.0033	0.0049	488,968	3,654,034

4.2.2.2 Registration Between Scans 1 and 2 Using Linear Features

After the planar features were used for the introduced registration approaches, the linear features were used as the registration primitives for the same experiment data to investigate the quality of the registration results with a different type of feature. Linear features are extracted indirectly using the segmented planar features from the TLS scans. The estimated line parameters and standard deviations of linear features which are derived by the intersection of neighboring planar features in scans 1 and 2 are presented in Table 4.24. Then, twenty points are simulated along the derived linear features in each scan. The simulated points along linear features are presented in Figure 4.10. The standard deviation overall was below 0.0003 and 6 mm for the direction vector (a_x, a_y, a_z) and position parameter (b_x, b_y, b_z), respectively, which indicates the estimated line parameters are reliable.

Table 4.24.: The estimated line parameters and standard deviations of linear features which are derived by the intersection of neighboring planar features in scans 1 and 2

	Plane Intersection	a_x (±)	a_y (±)	a_z (±)	b_x (m±m)	b_y (m±m)	b_z (m±m)
Scan 2	6&13	1 (±0)	0.1308 (±0.0000)	-0.0053 (±0.0000)	0 (±0)	16.7506 (±0.0007)	-1.6841 (±0.0013)
	7&13	1 (±0)	0.1308 (±0.0000)	-0.0090 (±0.0000)	0 (±0)	16.7497 (±0.0007)	-1.1862 (±0.0018)
	8&13	1 (±0)	0.1308 (±0.0000)	-0.0073 (±0.0000)	0 (±0)	16.7503 (±0.0007)	-1.5105 (±0.0023)
	6&16	1 (±0)	0.1376 (±0.0000)	-0.0054 (±0.0000)	0 (±0)	4.3090 (±0.0016)	-1.5292 (±0.0008)
	7&16	1 (±0)	0.1376 (±0.0000)	-0.0089 (±0.0000)	0 (±0)	4.3083 (±0.0016)	-1.4407 (±0.0009)
	8&16	1 (±0)	0.1376 (±0.0000)	-0.0072 (±0.0000)	0 (±0)	4.3091 (±0.0016)	-1.5426 (±0.0014)
	6&17	1 (±0)	0.1330 (±0.0000)	-0.0053 (±0.0000)	0 (±0)	6.0717 (±0.0002)	-1.5511 (±0.0009)
	7&17	1 (±0)	0.1330 (±0.0000)	-0.0090 (±0.0000)	0 (±0)	6.0717 (±0.0002)	-1.4046 (±0.0010)
	8&17	1 (±0)	0.1330 (±0.0000)	-0.0073 (±0.0000)	0 (±0)	6.0717 (±0.0002)	-1.5380 (±0.0014)
	6&18	1 (±0)	0.1310 (±0.0000)	-0.0053 (±0.0000)	0 (±0)	8.8529 (±0.0000)	-1.5858 (±0.0010)

continued on next page

Table 4.24.: *continued*

Plane Intersection	a_x (±)	a_y (±)	a_z (±)	b_x (m±m)	b_y (m±m)	b_z (m±m)
7&18	1 (±0)	0.1310 (±0.0000)	-0.0090 (±0.0000)	0 (±0)	8.8522 (±0.0000)	-1.3477 (±0.0011)
8&18	1 (±0)	0.1310 (±0.0000)	-0.0073 (±0.0000)	0 (±0)	8.8527 (±0.0000)	-1.5309 (±0.0016)
6&19	-0.1312 (±0.0000)	1 (±0)	-0.0120 (±0.0001)	18.9571 (±0.0001)	0 (±0)	-1.5447 (±0.0011)
7&19	-0.1312 (±0.0000)	1 (±0)	0.0220 (±0.0001)	18.9572 (±0.0001)	0 (±0)	-1.7507 (±0.0018)
8&19	-0.1312 (±0.0000)	1 (±0)	0.0036 (±0.0001)	18.9571 (±0.0001)	0 (±0)	-1.6978 (±0.0020)
6&9	-0.1319 (±0.0001)	1 (±0)	-0.0120 (±0.0001)	-55.7980 (±0.0017)	0 (±0)	-1.2721 (±0.0011)
7&9	-0.1319 (±0.0001)	1 (±0)	0.0220 (±0.0001)	-55.7983 (±0.0017)	0 (±0)	-0.8756 (±0.0013)
8&9	-0.1319 (±0.0001)	1 (±0)	0.0036 (±0.0001)	-55.7981 (±0.0017)	0 (±0)	-1.1295 (±0.0014)
6&10	-0.1304 (±0.0000)	1 (±0)	-0.0120 (±0.0001)	-55.7696 (±0.0009)	0 (±0)	-1.2722 (±0.0011)
7&10	-0.1304 (±0.0000)	1 (±0)	0.0220 (±0.0001)	-55.7696 (±0.0009)	0 (±0)	-0.8760 (±0.0013)
8&10	-0.1304 (±0.0000)	1 (±0)	0.0036 (±0.0001)	-55.7696 (±0.0009)	0 (±0)	-1.1297 (±0.0014)

continued on next page

Table 4.24.: *continued*

Plane Intersection	a_x (±)	a_y (±)	a_z (±)	b_x (m±m)	b_y (m±m)	b_z (m±m)
6&4	-0.1309 (±0.0000)	1 (±0)	-0.0120 (±0.0001)	12.3471 (±0.0004)	0 (±0)	-1.5206 (±0.0009)
7&4	-0.1308 (±0.0000)	1 (±0)	0.0220 (±0.0001)	12.3469 (±0.0004)	0 (±0)	-1.6733 (±0.0015)
8&4	-0.1309 (±0.0000)	1 (±0)	0.0036 (±0.0001)	12.3469 (±0.0004)	0 (±0)	-1.6476 (±0.0018)
6&3	-0.1325 (±0.0000)	1 (±0)	-0.0120 (±0.0001)	14.7816 (±0.0000)	0 (±0)	-1.5294 (±0.0010)
7&3	-0.1325 (±0.0000)	1 (±0)	0.0220 (±0.0001)	14.7815 (±0.0000)	0 (±0)	-1.7018 (±0.0016)
8&3	-0.1325 (±0.0000)	1 (±0)	0.0036 (±0.0001)	14.7815 (±0.0000)	0 (±0)	-1.6661 (±0.0019)
6&2	1 (±0)	0.1299 (±0.0000)	-0.0053 (±0.0000)	0 (±0)	-9.3938 (±0.0001)	-1.3586 (±0.0005)
7&2	1 (±0)	0.1299 (±0.0000)	-0.0090 (±0.0000)	0 (±0)	-9.3940 (±0.0001)	-1.7210 (±0.0017)
8&2	1 (±0)	0.1299 (±0.0000)	-0.0073 (±0.0000)	0 (±0)	-9.3939 (±0.0001)	-1.5779 (±0.0015)
6&5	1 (±0)	0.1309 (±0.0000)	-0.0053 (±0.0000)	0 (±0)	-15.8163 (±0.0002)	-1.2786 (±0.0007)
7&5	1 (±0)	0.1309 (±0.0000)	-0.0090 (±0.0000)	0 (±0)	-15.8173 (±0.0002)	-1.8524 (±0.0024)

continued on next page

Table 4.24.: *continued*

Plane Intersection	a_x (±)	a_y (±)	a_z (±)	b_x (m±m)	b_y (m±m)	b_z (m±m)
8&5	1 (±0)	0.1309 (±0.0000)	-0.0073 (±0.0000)	0 (±0)	-15.8168 (±0.0002)	-1.5944 (±0.0020)
1&2	0.0009 (±0.0002)	0.0008 (±0.0000)	1 (±0)	-171.0829 (±0.0015)	-31.6168 (±0.0006)	0 (±0)
2&3	0.0001 (±0.0000)	0.0007 (±0.0000)	1 (±0)	15.7550 (±0.0000)	-7.3462 (±0.0000)	0 (±0)
2&4	0.0013 (±0.0000)	0.0009 (±0.0000)	1 (±0)	13.3514 (±0.0001)	-7.6584 (±0.0000)	0 (±0)
2&19	-0.0003 (±0.0000)	0.0007 (±0.0000)	1 (±0)	19.8509 (±0.0002)	-6.8141 (±0.0000)	0 (±0)
3&5	0.0000 (±0.0000)	0.0016 (±0.0000)	1 (±0)	16.5890 (±0.0000)	-13.6422 (±0.0002)	0 (±0)
3&18	0.0006 (±0.0000)	-0.0031 (±0.0000)	1 (±0)	13.3778 (±0.0001)	10.5998 (±0.0000)	0 (±0)
4&5	0.0011 (±0.0000)	0.0018 (±0.0000)	1 (±0)	14.1757 (±0.0002)	-13.9582 (±0.0002)	0 (±0)
4&18	0.0018 (±0.0000)	-0.0029 (±0.0000)	1 (±0)	11.0028 (±0.0008)	10.2887 (±0.0001)	0 (±0)
5&9	-0.0010 (±0.0001)	0.0015 (±0.0000)	1 (±0)	-52.8008 (±0.0002)	-22.7277 (±0.0003)	0 (±0)
5&10	-0.0002 (±0.0001)	0.0016 (±0.0000)	1 (±0)	-52.8054 (±0.0002)	-22.7283 (±0.0003)	0 (±0)

continued on next page

Table 4.24.: *continued*

	Plane Intersection	a_x (±)	a_y (±)	a_z (±)	b_x (m±m)	b_y (m±m)	b_z (m±m)
	9&11	-0.0009 (±0.0001)	0.0009 (±0.0001)	1 (±0)	-53.4476 (±0.0005)	-17.8244 (±0.0014)	0 (±0)
	10&11	-0.0001 (±0.0001)	0.0010 (±0.0001)	1 (±0)	-53.4450 (±0.0003)	-17.8240 (±0.0014)	0 (±0)
	18&19	0.0002 (±0.0000)	-0.0031 (±0.0000)	1 (±0)	17.4953 (±0.0001)	11.1389 (±0.0000)	0 (±0)
Scan 1	6&13	1 (±0)	-0.4561 (±0.0000)	-0.0061 (±0.0000)	0 (±0)	17.4793 (±0.0006)	-1.6389 (±0.0025)
	7&13	1 (±0)	-0.4561 (±0.0000)	-0.0096 (±0.0000)	0 (±0)	17.4774 (±0.0006)	-0.9520 (±0.0016)
	8&13	1 (±0)	-0.4561 (±0.0000)	-0.0078 (±0.0000)	0 (±0)	17.4785 (±0.0006)	-1.3519 (±0.0010)
	6&16	1 (±0)	-0.4497 (±0.0000)	-0.0062 (±0.0000)	0 (±0)	3.5843 (±0.0000)	-1.5175 (±0.0015)
	7&16	1 (±0)	-0.4496 (±0.0000)	-0.0095 (±0.0000)	0 (±0)	3.5819 (±0.0000)	-1.2705 (±0.0007)
	8&16	1 (±0)	-0.4497 (±0.0000)	-0.0078 (±0.0000)	0 (±0)	3.5836 (±0.0000)	-1.4458 (±0.0004)
	6&17	1 (±0)	-0.4543 (±0.0000)	-0.0061 (±0.0000)	0 (±0)	5.7312 (±0.0007)	-1.5362 (±0.0016)
	7&17	1 (±0)	-0.4543 (±0.0000)	-0.0096 (±0.0000)	0 (±0)	5.7310 (±0.0007)	-1.2212 (±0.0008)

continued on next page

Table 4.24.: *continued*

Plane Intersection	a_x (±)	a_y (±)	a_z (±)	b_x (m±m)	b_y (m±m)	b_z (m±m)
8&17	1 (±0)	-0.4543 (±0.0000)	-0.0078 (±0.0000)	0 (±0)	5.7311 (±0.0007)	-1.4313 (±0.0005)
6&18	1 (±0)	-0.4569 (±0.0000)	-0.0061 (±0.0000)	0 (±0)	8.8712 (±0.0022)	-1.5637 (±0.0018)
7&18	1 (±0)	-0.4568 (±0.0000)	-0.0096 (±0.0000)	0 (±0)	8.8700 (±0.0022)	-1.1493 (±0.0009)
8&18	1 (±0)	-0.4568 (±0.0000)	-0.0078 (±0.0000)	0 (±0)	8.8708 (±0.0022)	-1.4101 (±0.0006)
6&19	0.4564 (±0.0000)	1 (±0)	-0.0133 (±0.0001)	71.3547 (±0.0007)	0 (±0)	-2.2067 (±0.0035)
7&19	0.4563 (±0.0000)	1 (±0)	0.0233 (±0.0001)	71.3546 (±0.0007)	0 (±0)	-1.2936 (±0.0036)
8&19	0.4564 (±0.0000)	1 (±0)	0.0046 (±0.0001)	71.3547 (±0.0007)	0 (±0)	-1.8084 (±0.0022)
6&9	0.4546 (±0.0001)	1 (±0)	-0.0133 (±0.0001)	-10.1262 (±0.0008)	0 (±0)	-1.3839 (±0.0015)
7&9	0.4545 (±0.0001)	1 (±0)	0.0233 (±0.0001)	-10.1262 (±0.0008)	0 (±0)	-1.3610 (±0.0013)
8&9	0.4545 (±0.0001)	1 (±0)	0.0046 (±0.0001)	-10.1261 (±0.0008)	0 (±0)	-1.4220 (±0.0007)
6&10	0.4569 (±0.0000)	1 (±0)	-0.0133 (±0.0001)	-10.1056 (±0.0003)	0 (±0)	-1.3841 (±0.0015)

continued on next page

Table 4.24.: *continued*

Plane Intersection	a_x (±)	a_y (±)	a_z (±)	b_x (m±m)	b_y (m±m)	b_z (m±m)
7&10	0.4569 (±0.0000)	1 (±0)	0.0233 (±0.0001)	-10.1056 (±0.0003)	0 (±0)	-1.3610 (±0.0013)
8&10	0.4569 (±0.0000)	1 (±0)	0.0046 (±0.0001)	-10.1056 (±0.0003)	0 (±0)	-1.4221 (±0.0007)
6&4	0.4568 (±0.0001)	1 (±0)	-0.0133 (±0.0001)	64.1585 (±0.0051)	0 (±0)	-2.1341 (±0.0031)
7&4	0.4567 (±0.0001)	1 (±0)	0.0233 (±0.0001)	64.1584 (±0.0051)	0 (±0)	-1.2996 (±0.0032)
8&4	0.4567 (±0.0001)	1 (±0)	0.0046 (±0.0001)	64.1584 (±0.0051)	0 (±0)	-1.7743 (±0.0019)
6&3	0.4553 (±0.0000)	1 (±0)	-0.0133 (±0.0001)	66.7738 (±0.0005)	0 (±0)	-2.1605 (±0.0033)
7&3	0.4553 (±0.0000)	1 (±0)	0.0233 (±0.0001)	66.7739 (±0.0005)	0 (±0)	-1.2974 (±0.0033)
8&3	0.4553 (±0.0000)	1 (±0)	0.0046 (±0.0001)	66.7739 (±0.0005)	0 (±0)	-1.7867 (±0.0020)
6&2	1 (±0)	-0.4582 (±0.0000)	-0.0061 (±0.0000)	0 (±0)	-10.9714 (±0.0012)	-1.3903 (±0.0010)
7&2	1 (±0)	-0.4582 (±0.0000)	-0.0097 (±0.0000)	0 (±0)	-10.9715 (±0.0012)	-1.6041 (±0.0015)
8&2	1 (±0)	-0.4582 (±0.0000)	-0.0078 (±0.0000)	0 (±0)	-10.9715 (±0.0012)	-1.5442 (±0.0007)

continued on next page

Table 4.24.: *continued*

Plane Intersection	a_x (±)	a_y (±)	a_z (±)	b_x (m±m)	b_y (m±m)	b_z (m±m)
6&5	1 (±0)	-0.4571 (±0.0000)	-0.0061 (±0.0000)	0 (±0)	-18.0074 (±0.0008)	-1.3288 (±0.0012)
7&5	1 (±0)	-0.4571 (±0.0000)	-0.0097 (±0.0000)	0 (±0)	-18.0081 (±0.0008)	-1.7654 (±0.0021)
8&5	1 (±0)	-0.4571 (±0.0000)	-0.0078 (±0.0000)	0 (±0)	-18.0078 (±0.0008)	-1.5917 (±0.0010)
1&2	0.0009 (±0.0001)	0.0002 (±0.0000)	1 (±0)	-120.1766 (±0.0040)	44.0950 (±0.0018)	0 (±0)
2&3	0.0004 (±0.0000)	0.0004 (±0.0000)	1 (±0)	51.1152 (±0.0001)	-34.3917 (±0.0003)	0 (±0)
2&4	0.0002 (±0.0001)	0.0005 (±0.0000)	1 (±0)	48.9111 (±0.0002)	-33.3819 (±0.0003)	0 (±0)
2&19	0.0002 (±0.0000)	0.0005 (±0.0000)	1 (±0)	54.8739 (±0.0005)	-36.1140 (±0.0003)	0 (±0)
3&5	0.0007 (±0.0000)	0.0011 (±0.0000)	1 (±0)	48.4858 (±0.0003)	-40.1666 (±0.0006)	0 (±0)
3&18	-0.0010 (±0.0000)	-0.0026 (±0.0000)	1 (±0)	58.6176 (±0.0002)	-17.9142 (±0.0003)	0 (±0)
4&5	0.0005 (±0.0001)	0.0012 (±0.0000)	1 (±0)	46.2739 (±0.0006)	-39.1557 (±0.0006)	0 (±0)
4&18	-0.0012 (±0.0001)	-0.0025 (±0.0000)	1 (±0)	56.4321 (±0.0022)	-16.9156 (±0.0010)	0 (±0)

continued on next page

Table 4.24.: *continued*

Plane Intersection	a_x (±)	a_y (±)	a_z (±)	b_x (m±m)	b_y (m±m)	b_z (m±m)
5&9	-0.0008 (±0.0001)	0.0018 (±0.0001)	1 (±0)	-15.1626 (±0.0004)	-11.0752 (±0.0008)	0 (±0)
5&10	0.0001 (±0.0000)	0.0014 (±0.0000)	1 (±0)	-15.1656 (±0.0004)	-11.0739 (±0.0008)	0 (±0)
9&11	-0.0011 (±0.0001)	0.0012 (±0.0000)	1 (±0)	-13.1179 (±0.0003)	-6.5767 (±0.0003)	0 (±0)
10&11	-0.0001 (±0.0000)	0.0008 (±0.0000)	1 (±0)	-13.1122 (±0.0001)	-6.5793 (±0.0002)	0 (±0)
18&19	-0.0012 (±0.0000)	-0.0025 (±0.0000)	1 (±0)	62.3924 (±0.0003)	-19.6387 (±0.0004)	0 (±0)

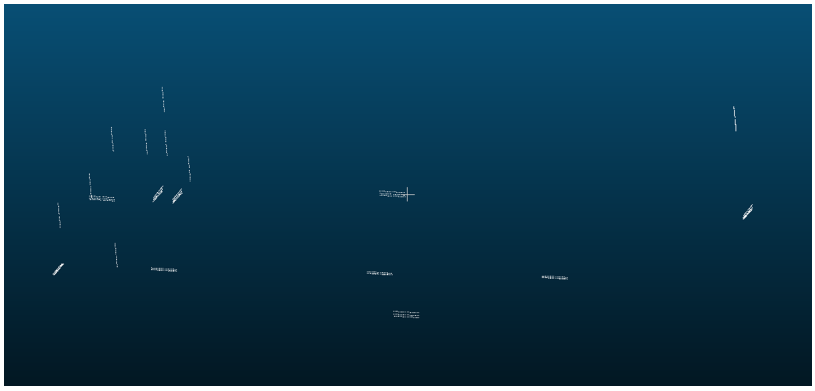

Fig. 4.10.: Simulated points along linear features in the overlapping area between scans 1 and 2

After the estimation of line parameters, the next step is to estimate transformation parameters using the three alternative registration approaches. The registration

process aims to estimate the 3D similarity transformation parameters, which include three translations (t_x, t_y, t_z) and three rotation parameters (ω, ϕ, κ).

The observations and weight matrix P in the three alternative registration approaches are specified as follows. In the linear feature-based approach, the observations are is estimated line parameters from a line fitting procedure, and the weight matrix P is defined by the inverse of the variance-covariance matrix of extracted line parameters, which is derived by using the law of error propagation.

In the pseudo-conjugate point-based method, the observations are coordinates of simulated points along lines in the source and reference scans. The weight matrix P depends on the noise added to the point clouds. The estimated line parameters in the reference scan are used to modify the weight matrix to eliminate the additional vector resulting from using non-corresponding points along linear features. In the 3D similarity transformation function, each 3D point pair contributes three equations towards the transformation parameters estimation. There are 920 points along linear features in each scan, so the total number of observation equations is $920 \times 3 = 2,760$. However, the discussion in the subsection 3.3.2 indicates that the effective contribution is only two equations from each point pair. According to Equation (3.73) in the subsection 3.3.2, all the elements in the weight matrix pertaining to the U-axis along the linear features are assigned a zero weight. The modified weight matrix in the LSA procedure nullifies the error along the line direction while minimizing the errors in the two directions normal to the line. Therefore, the effective contribution of a 3D point pair towards redundancy is 2 equations instead of 3. In this case, the redundancy is given by the difference between the rank of the weight matrix and the number of the unknowns, thus resulting in a redundancy of $920 \times 2 - 6 = 1,834$.

In the closed-form solution, the rotation parameters and the translation parameters are estimated separately. The rotation matrix is derived first using a quaternion-based approach, which is a single-step solution. The observations are the direction vectors of linear features. A weight matrix is not used in this procedure, and there is no standard deviation to evaluate the estimated the rotation parameters. Once

the rotation matrix is derived, the next step is to estimate translation parameters using the pseudo-conjugate point-based method. In this step, the observations are coordinates of points along linear features, and the weight matrix P is obtained as the inverse of the variance-covariance matrix of the observations.

The estimated transformation parameters, standard deviations, a-posteriori variance factors, and execution times from the linear feature-based approach, pseudo-conjugate point-based method, and closed-form solution using the linear features in scans 1 and 2 are presented in Table 4.25. In the linear feature-based approach, the standard deviation overall was below 0.2 cm and 0.004 degrees for the translation and the rotation parameters, respectively, while it is below 1.3 cm and 0.06 degrees in the registration results by using the pseudo-conjugate point-based method. In the closed-form registration results, the standard deviation overall was below 1.3 cm for the translation parameters. Since the rotation parameters were estimated by quaternions, there is no standard deviation for the rotation parameters. In summary, according to the standard deviation, reliable transformation parameters were estimated using the introduced three registration approaches with linear features. The linear feature-based approach produced better results than the other two approaches.

Furthermore, the a-posteriori variance factor $\hat{\sigma}_0^2$ in Table 4.25 is used to evaluate the estimated transformation parameters. In the linear feature-based approach, the weight matrix P is derived by the inverse of variance-covariance matrix, so the $\hat{\sigma}_0^2$ should be close to 1. The a-posteriori variance factor $\hat{\sigma}_0^2$ was 81.0749, which indicates that the noise level in the observation is larger than previously assumed. In the pseudo-conjugate point-based method and closed-form solution, the $\hat{\sigma}_0^2$ is the variance of the observations since the weight matrix P is an identity matrix. The square roots of the a-posteriori variance factors ($\hat{\sigma}_0$) in Table 4.25 are larger than the expected accuracy of around 2 mm according to the accuracy of the TLS. In the experiment with real data, linear features are extracted indirectly by the intersection of neighboring planar features. To get enough lines, planes that are far apart from each other have to be extrapolated to derive lines, which will result in large $\hat{\sigma}_0$ values. Regarding the

execution time, the linear feature-based approach had the shortest execution time, as listed in Table 4.25. The pseudo-conjugate point-based and closed-form approaches based on linear features led to longer execution times due to a large number of point cloud data.

The quality evaluation of the registration results was analyzed by calculating the point-to-patch normal distances between TLS scans. After applying the estimated registration parameters, the point clouds in the source scan were transformed to the reference scan. A point-patch pair is established by using the approach discussed in section 3.4. The normal distance between the transformed point and the patch must be within a certain threshold, which is 10 cm in this test. The mean, standard deviation, and RMSE of the point-to-patch normal distances between the TLS scans are presented in Table 4.26. The mean, standard deviation, and RMSE of the calculated point-to-patch normal distances of the linear feature-based approach were all below 4 mm, while it was all below 4 cm for the pseudo-conjugate point-based method and closed-form solution, which indicates that the linear feature-based approach can produce better results than the pseudo-conjugate point-based method and closed-form solution using linear features.

Moreover, the comparison between registration approaches using linear and planar features is conducted based on point-to-patch normal distances between TLS scans. The quality evaluation of the registration results shows that these two features can produce equivalent registration results by using the feature-based approach since the normal distances calculated were all below 4 mm. However, the pseudo-conjugate point-based method and closed-form solution can produce better registration results when the planar features were the registration primitives. For example, when linear features are the registration primitives, the normal distances calculated using the registration results of the two approaches were below 4 cm, while it is only 4 mm when planar features are the registration primitives.

Table 4.25.: The estimated transformation parameters, standard deviations, a-posteriori variance factors, and execution times from the linear feature-based approach, pseudo-conjugate point-based method, and closed-form solution using the linear features in scans 1 and 2

	$t_x(m \pm m)$	$t_y(m \pm m)$	$t_z(m \pm m)$	$\omega(^\circ \pm ^\circ)$	$\phi(^\circ \pm ^\circ)$	$\kappa(^\circ \pm ^\circ)$	$\hat{\sigma}_0^2$	$\hat{\sigma}_0$	Execution time (seconds)
Linear feature-based approach	41.6533 (±0.0002)	-19.8084 (±0.0003)	-0.2483 (±0.0014)	-0.0096 (±0.0034)	0.0040 (±0.0014)	32.0212 (±0.0006)	81.0749	9.0042	0.2
Pseudo-conjugate point-based method	41.5879 (±0.0121)	-19.8072 (±0.0124)	-0.1847 (±0.0125)	0.0443 (±0.0545)	0.0122 (±0.0189)	32.0378 (±0.0158)	0.0418 (m^2)	0.2045 (m)	5.5
Closed-form solution	41.5891 (±0.0121)	-19.7979 (±0.0117)	-0.1794 (±0.0113)	-0.0021 (N/A)	0.0119 (N/A)	32.0059 (N/A)	0.0419 (m^2)	0.2046 (m)	9.9

Table 4.26.: Quantitative comparison between linear feature-based approach, pseudo-conjugate point-based method, and closed-form solution based on linear features through the mean, standard deviation, and RMSE of the point-to-patch normal distances between the TLS scans 1 and 2

	Mean (m)	Standard deviation (m)	RMSE (m)	Number of used points	Total number of points
Linear feature-based approach	0.0027	0.0030	0.0040	489,533	3,654,034
Pseudo-conjugate point-based method	0.0298	0.0221	0.0371	481,393	3,654,034
Closed-form solution	0.0339	0.0192	0.0390	479,091	3,654,034

4.2.3 Registration Between Scans 2 and 3

The positions of TLS scans 2 and 3 are presented in Figure 4.11. Scan 3 is the source scan, and scan 2 is the reference scan.

Fig. 4.11.: Position of TLS scans 2 and 3

4.2.3.1 Registration Between Scans 2 and 3 Using Planar Features

The extracted planar features in scans 2 and 3 are presented in Figure 4.12. The planar feature extraction is performed by using I-LIVE. After a plane fitting procedure as stated in subsection 3.2.5, the estimated plane parameters, standard deviations, and square roots of the a-posteriori variance factors of 10 pairs of planar features in scans 2 and 3 are presented in Table 4.27. The standard deviation overall was below 1.3 cm for plane parameters in the source and reference scans, which indicates the estimated plane parameters are reliable. Furthermore, the a-posteriori variance factor $\hat{\sigma}_0^2$ is used to check the quality of the estimated plane parameters. Since the weight matrix P is an identity matrix, the $\hat{\sigma}_0^2$ is the variance of the measurements. The square roots of the a-posteriori variance factors ($\hat{\sigma}_0$) after plane fitting are close to the expected accuracy of around 2 mm according to the accuracy of the TLS, thus indicating the validity of the estimated plane parameters.

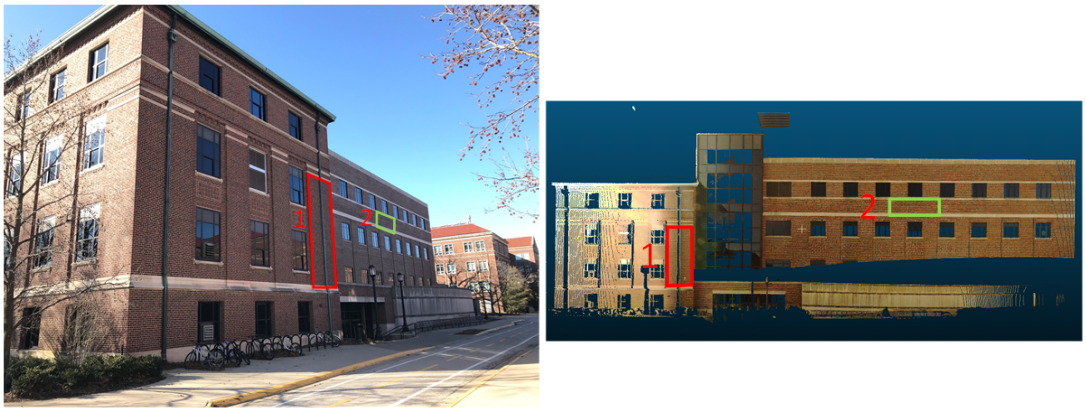

(a) (b)

Fig. 4.12.: Planar features in the overlapping area between scans 2 and 3 displayed in images (a, c, e), which are captured by an external camera, and point clouds (b, d, f) (continued on next page)

(c) (d)

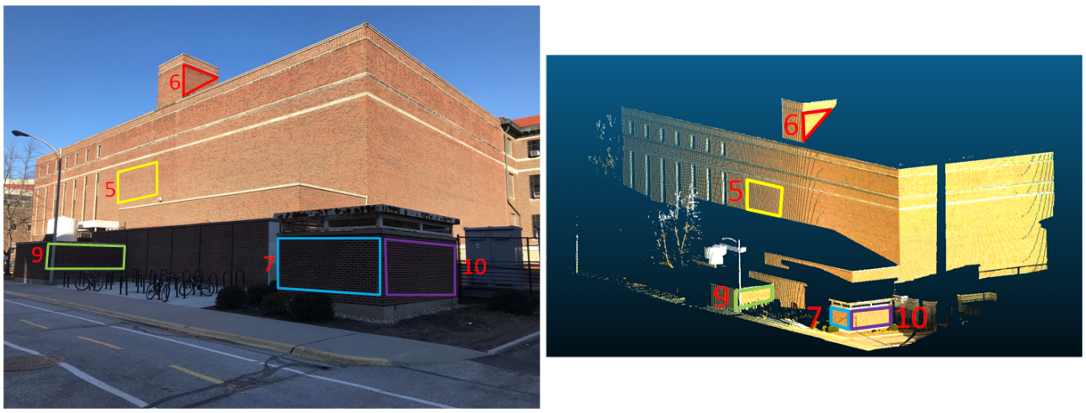

(e) (f)

Fig. 4.12.: Planar features in the overlapping area between scans 2 and 3 displayed in images (a, c, e), which are captured by an external camera, and point clouds (b, d, f) (continued from the previous page)

Table 4.27.: The estimated plane parameters, standard deviations, and square roots of the a-posteriori variance factors of 10 pairs of planar features in scans 2 and 3

	Plane ID	$a_x(m \pm m)$	$a_y(m \pm m)$	$a_z(m \pm m)$	$\hat{\sigma}_0(mm)$
Scan 3	1	-7.5163 ($\pm$0.0004)	-4.9959 ($\pm$0.0001)	0.0076 ($\pm$0.0001)	1.5
	2	-12.7123 ($\pm$0.0017)	-8.5034 ($\pm$0.0007)	0.0218 ($\pm$0.0013)	1.7
	3	0.0287 ($\pm$0.0002)	0.0187 ($\pm$0.0003)	-1.7232 ($\pm$0.0034)	1.6
	4	0.0002 ($\pm$0.0001)	0.0063 ($\pm$0.0001)	-1.8663 ($\pm$0.0004)	1.2
	5	14.1665 ($\pm$0.0036)	9.4926 ($\pm$0.0035)	0.0087 ($\pm$0.0016)	2.5
	6	-47.6620 ($\pm$0.0054)	70.7728 ($\pm$0.0045)	-0.0198 ($\pm$0.0079)	1.6
	7	5.3404 ($\pm$0.0062)	3.5805 ($\pm$0.0052)	0.0012 ($\pm$0.0013)	1.5
	8	7.6096 ($\pm$0.0004)	5.0887 ($\pm$0.0005)	0.0318 ($\pm$0.0003)	1.7
	9	-43.7661 ($\pm$0.0040)	65.4798 ($\pm$0.0032)	-0.0483 ($\pm$0.0124)	1.6
	10	-32.8993 ($\pm$0.0009)	49.0242 ($\pm$0.0008)	0.0018 ($\pm$0.0039)	1.4
Scan 2	1	1.1783 ($\pm$0.0001)	-9.2102 ($\pm$0.0001)	0.0107 ($\pm$0.0000)	1.4
	2	2.0357 ($\pm$0.0001)	-15.5477 ($\pm$0.0002)	0.0252 ($\pm$0.0003)	1.7
	3	-0.0008 ($\pm$0.0001)	0.0330 ($\pm$0.0001)	-1.5565 ($\pm$0.0015)	1.6
	4	-0.0029 ($\pm$0.0001)	-0.0016 ($\pm$0.0002)	-1.5599 ($\pm$0.0016)	1.2

continued on next page

Table 4.27.: *continued*

Plane ID	$a_x(m \pm m)$	$a_y(m \pm m)$	$a_z(m \pm m)$	$\hat{\sigma}_0(mm)$
5	-2.1685 ($\pm$0.0005)	16.4834 ($\pm$0.0012)	0.0099 ($\pm$0.0006)	1.5
6	-42.5661 ($\pm$0.0009)	-5.6939 ($\pm$0.0017)	-0.0035 ($\pm$0.0019)	1.5
7	-0.7937 ($\pm$0.0001)	5.9658 ($\pm$0.0002)	0.0012 ($\pm$0.0001)	1.2
8	-1.1391 ($\pm$0.0000)	8.6986 ($\pm$0.0000)	0.0274 ($\pm$0.0001)	1.8
9	-36.0577 ($\pm$0.0002)	-4.7354 ($\pm$0.0006)	-0.0078 ($\pm$0.0025)	1.7
10	-16.5076 ($\pm$0.0001)	-2.1878 ($\pm$0.0001)	-0.0030 ($\pm$0.0002)	1.3

The estimated transformation parameters, standard deviations, a-posteriori variance factors, and execution times from the planar feature-based approach, pseudo-conjugate point-based method, and closed-form solution using the planar features in scans 2 and 3 are presented in Table 4.28. Since the rotation parameters were estimated by quaternions in the closed-form solution, there is no standard deviation for the rotation parameters. The standard deviation values of the registration parameters indicate that reliable results were estimated using the three alternative registration approaches. The standard deviations of the estimated parameters were below 0.1 mm for the translation parameters and below 0.0002 degrees for the rotation angels by using the pseudo-conjugate point-based method, while it is below 1.5 mm and 0.0045 degrees for the translation and the rotation parameters, respectively, by using the planar feature-based approach, which indicates that the pseudo-conjugate point-based method can produce better registration results than the planar feature-based approach. In the closed-form solution, the standard deviations of the estimated parameters were below 0.1 mm for the translation parameters, which indicates the estimated translation parameters are reliable.

Furthermore, as shown in Table 4.28, the a-posteriori variance factor $\hat{\sigma}_0^2$ is used to evaluate the estimated transformation parameters. In the planar feature-based approach, the weight matrix P is derived by the inverse of the variance-covariance matrix, so the $\hat{\sigma}_0^2$ should be close to 1. The a-posteriori variance factor $\hat{\sigma}_0^2$ was 210.3468, which indicates that the noise level in the observation is larger than previously assumed. In the pseudo-conjugate point-based method and closed-form solution, the $\hat{\sigma}_0^2$ is the variance of the observations since the weight matrix P is an identity matrix. The square roots of the a-posteriori variance factors ($\hat{\sigma}_0$) in Table 4.28 are not significantly different from the expected accuracy of around 2 mm according to the accuracy of the TLS, thus indicating the validity of the estimated transformation parameters using the pseudo-conjugate point-based method and closed-form solution based on planar features. Regarding the execution time, the planar feature-based approach had the shortest execution time, as listed in Table 4.28. The pseudo-conjugate point-

based and closed-form approaches based on planar features led to longer execution times due to a large number of point cloud data.

The quality evaluation of the registration results was analyzed by calculating the point-to-patch normal distances between TLS scans. After applying the estimated registration parameters, the point clouds in the source scan were transformed to the reference scan. A point-patch pair is established by using the approach discussed in section 3.4. The normal distance between the transformed point and the patch must be within a certain threshold, which is 10 cm in this test. The mean, standard deviation, and RMSE of the point-to-patch normal distances between the TLS scans are presented in Table 4.29. The mean, standard deviation, and RMSE of the calculated point-to-patch normal distances of each approach were all below 6.5 mm, which substantiates the quality of the registration results. In the planar feature-based approach and pseudo-conjugate point-based method, the average of the calculated point-to-patch normal distances were around 2.1 mm, and the value of standard deviation and RMSE is close between the two approaches, which indicates the equivalency between the two approaches. The average point-to-patch normal distances is 3.2 mm for the closed-form solution. The standard deviation and RMSE values are also larger than the other two approaches, which indicates that the registration results produced by the closed-form solution are worse than the registration results by using the other two approaches.

Table 4.28.: The estimated transformation parameters, standard deviations, a-posteriori variance factors, and execution times from the planar feature-based approach, pseudo-conjugate point-based method, and closed-form solution using the planar features in scans 2 and 3

	$t_x(m \pm m)$	$t_y(m \pm m)$	$t_z(m \pm m)$	$\omega(^\circ \pm ^\circ)$	$\phi(^\circ \pm ^\circ)$	$\kappa(^\circ \pm ^\circ)$	$\hat{\sigma}_0^2$	$\hat{\sigma}_0$	Execution time (seconds)
Planar feature-based approach	42.0797 (±0.0004)	5.1231 (±0.0006)	0.2057 (±0.0013)	0.0029 (±0.0034)	-0.0185 (±0.0042)	-63.6839 (±0.0009)	210.3468	14.5033	0.2
Pseudo-conjugate point-based method	42.0795 (±0.0000)	5.1218 (±0.0000)	0.2064 (±0.0001)	0.0015 (±0.0001)	-0.0138 (±0.0001)	-63.6821 (±0.0000)	2.94E-06 (m^2)	1.7 (mm)	55.6
Closed-form solution	42.0810 (±0.0000)	5.1271 (±0.0000)	0.2184 (±0.0000)	0.0342 (N/A)	-0.0001 (N/A)	-63.6907 (N/A)	4.84E-06 (m^2)	2.2 (mm)	50.9

Table 4.29.: Quantitative comparison between planar feature-based approach, pseudo-conjugate point-based method, and closed-form solution based on planar features through the mean, standard deviation, and RMSE of the point-to-patch normal distances between the TLS scans 2 and 3

	Mean (m)	Standard deviation (m)	RMSE (m)	Number of used points	Total number of points
Planar feature-based approach	0.0021	0.0049	0.0054	109,010	746,894
Pseudo-conjugate point-based method	0.0021	0.0049	0.0053	109,297	746,894
Closed-form solution	0.0032	0.0052	0.0061	108,359	746,894

4.2.3.2 Registration Between Scans 2 and 3 Using Linear Features

After the planar features were used for the introduced registration approaches, the linear features were used as the registration primitives for the same experiment data to investigate the quality of the registration results with a different type of feature. Linear features are extracted indirectly using the segmented planar features from the TLS scans. The estimated line parameters and standard deviations of linear features which are derived by the intersection of neighboring planar features in scans 2 and 3 are presented in Table 4.30. Then, twenty points are simulated along the derived linear features in each scan. The simulated points along linear features are presented in Figure 4.13. The standard deviation overall was below 0.003 and 1.1 cm for the direction vector (a_x, a_y, a_z) and position parameter (b_x, b_y, b_z), respectively, which indicates the estimated line parameters are reliable.

Table 4.30.: The estimated line parameters and standard deviations of linear features which are derived by the intersection of neighboring planar features in scans 2 and 3

	Plane Intersection	a_x (±)	a_y (±)	a_z (±)	b_x (m±m)	b_y (m±m)	b_z (m±m)
Scan 3	1&3	-0.6647 (±0.0000)	1 (±0)	-0.0002 (±0.0002)	-10.8388 (±0.0004)	0 (±0)	-1.9045 (±0.0030)
	1&4	-0.6647 (±0.0000)	1 (±0)	0.0033 (±0.0000)	-10.8388 (±0.0004)	0 (±0)	-1.8676 (±0.0009)
	1&6	0.0006 (±0.0001)	0.0007 (±0.0001)	1 (±0)	-54.7187 (±0.0013)	66.0205 (±0.0016)	0 (±0)
	1&9	0.0004 (±0.0001)	0.0010 (±0.0001)	1 (±0)	-51.1008 (±0.0009)	60.5774 (±0.0009)	0 (±0)
	1&10	0.0007 (±0.0000)	0.0004 (±0.0001)	1 (±0)	-40.1760 (±0.0005)	44.1409 (±0.0004)	0 (±0)
	2&3	-0.6689 (±0.0000)	1 (±0)	-0.0003 (±0.0002)	-18.4039 (±0.0020)	0 (±0)	-2.0306 (±0.0031)
	2&4	-0.6689 (±0.0000)	1 (±0)	0.0033 (±0.0000)	-18.4036 (±0.0020)	0 (±0)	-1.8685 (±0.0014)
	2&6	0.0011 (±0.0001)	0.0010 (±0.0001)	1 (±0)	-60.1264 (±0.0016)	62.3786 (±0.0020)	0 (±0)
	2&9	0.0008 (±0.0001)	0.0013 (±0.0001)	1 (±0)	-56.5052 (±0.0012)	56.9651 (±0.0013)	0 (±0)
	2&10	0.0012 (±0.0001)	0.0008 (±0.0001)	1 (±0)	-45.5255 (±0.0008)	40.5509 (±0.0007)	0 (±0)

continued on next page

Table 4.30.: *continued*

Plane Intersection	a_x (±)	a_y (±)	a_z (±)	b_x (m±m)	b_y (m±m)	b_z (m±m)
3&5	-0.6701 (±0.0001)	1 (±0)	-0.0003 (±0.0002)	20.5281 (±0.0067)	0 (±0)	-1.3818 (±0.0049)
3&6	1 (±0)	0.6735 (±0.0001)	0.0240 (±0.0001)	0 (±0)	102.8707 (±0.0051)	-0.6062 (±0.0104)
3&7	-0.6704 (±0.0002)	1 (±0)	-0.0003 (±0.0002)	7.7413 (±0.0104)	0 (±0)	-1.5949 (±0.0039)
3&8	-0.6687 (±0.0000)	1 (±0)	-0.0003 (±0.0002)	11.0191 (±0.0008)	0 (±0)	-1.5402 (±0.0041)
3&9	1 (±0)	0.6684 (±0.0001)	0.0239 (±0.0001)	0 (±0)	94.7322 (±0.0037)	-0.6947 (±0.0093)
3&10	1 (±0)	0.6711 (±0.0000)	0.0240 (±0.0001)	0 (±0)	71.1024 (±0.0008)	-0.9514 (±0.0063)
4&5	-0.6701 (±0.0001)	1 (±0)	0.0033 (±0.0000)	20.5284 (±0.0067)	0 (±0)	-1.8638 (±0.0016)
4&6	1 (±0)	0.6735 (±0.0001)	0.0024 (±0.0001)	0 (±0)	102.8704 (±0.0052)	-1.5182 (±0.0052)
4&7	-0.6704 (±0.0002)	1 (±0)	0.0033 (±0.0000)	7.7414 (±0.0104)	0 (±0)	-1.8654 (±0.0007)
4&8	-0.6687 (±0.0000)	1 (±0)	0.0033 (±0.0000)	11.0205 (±0.0009)	0 (±0)	-1.8650 (±0.0009)
4&9	1 (±0)	0.6684 (±0.0001)	0.0024 (±0.0001)	0 (±0)	94.7316 (±0.0037)	-1.5457 (±0.0047)

continued on next page

Table 4.30.: *continued*

	Plane Intersection	a_x (±)	a_y (±)	a_z (±)	b_x (m±m)	b_y (m±m)	b_z (m±m)
	4&10	1 (±0)	0.6711 (±0.0000)	0.0024 (±0.0001)	0 (±0)	71.1024 (±0.0008)	-1.6257 (±0.0035)
	5&6	-0.0006 (±0.0001)	-0.0001 (±0.0001)	1 (±0)	-33.3528 (±0.0011)	80.4093 (±0.0013)	0 (±0)
	5&9	-0.0008 (±0.0001)	0.0002 (±0.0001)	1 (±0)	-29.6646 (±0.0009)	74.9052 (±0.0008)	0 (±0)
	5&10	-0.0004 (±0.0001)	-0.0003 (±0.0001)	1 (±0)	-18.7052 (±0.0016)	58.5496 (±0.0011)	0 (±0)
	6&7	-0.0003 (±0.0002)	0.0001 (±0.0001)	1 (±0)	-42.1825 (±0.0029)	74.4630 (±0.0022)	0 (±0)
	6&8	-0.0030 (±0.0001)	-0.0017 (±0.0001)	1 (±0)	-39.8380 (±0.0010)	76.0419 (±0.0012)	0 (±0)
	7&9	-0.0005 (±0.0002)	0.0004 (±0.0002)	1 (±0)	-38.5135 (±0.0020)	68.9906 (±0.0014)	0 (±0)
	7&10	-0.0001 (±0.0002)	-0.0001 (±0.0001)	1 (±0)	-27.5389 (±0.0002)	52.6215 (±0.0001)	0 (±0)
	8&9	-0.0032 (±0.0001)	-0.0014 (±0.0001)	1 (±0)	-36.1701 (±0.0006)	70.5570 (±0.0004)	0 (±0)
	8&10	-0.0029 (±0.0000)	-0.0020 (±0.0001)	1 (±0)	-25.2179 (±0.0004)	54.1791 (±0.0002)	0 (±0)
Scan 2	1&3	1 (±0)	0.1279 (±0.0000)	0.0022 (±0.0001)	0 (±0)	-9.3630 (±0.0001)	-1.7554 (±0.0018)

continued on next page

Table 4.30.: *continued*

Plane Intersection	a_x (±)	a_y (±)	a_z (±)	b_x (m±m)	b_y (m±m)	b_z (m±m)
1&4	1 (±0)	0.1279 (±0.0000)	-0.0020 (±0.0001)	0 (±0)	-9.3628 (±0.0001)	-1.5504 (±0.0022)
1&6	-0.0002 (±0.0000)	0.0011 (±0.0000)	1 (±0)	-41.3676 (±0.0010)	-14.6535 (±0.0005)	0 (±0)
1&9	-0.0004 (±0.0001)	0.0011 (±0.0000)	1 (±0)	-34.8644 (±0.0003)	-13.8215 (±0.0004)	0 (±0)
1&10	-0.0003 (±0.0000)	0.0011 (±0.0000)	1 (±0)	-15.2975 (±0.0001)	-11.3181 (±0.0002)	0 (±0)
2&3	1 (±0)	0.1309 (±0.0000)	0.0023 (±0.0001)	0 (±0)	-15.8173 (±0.0002)	-1.8920 (±0.0021)
2&4	1 (±0)	0.1309 (±0.0000)	-0.0020 (±0.0001)	0 (±0)	-15.8168 (±0.0002)	-1.5438 (±0.0029)
2&6	-0.0003 (±0.0000)	0.0016 (±0.0000)	1 (±0)	-40.5030 (±0.0012)	-21.1175 (±0.0003)	0 (±0)
2&9	-0.0004 (±0.0001)	0.0016 (±0.0000)	1 (±0)	-34.0178 (±0.0004)	-20.2683 (±0.0002)	0 (±0)
2&10	-0.0004 (±0.0000)	0.0016 (±0.0000)	1 (±0)	-14.4509 (±0.0001)	-17.7064 (±0.0002)	0 (±0)
3&5	1 (±0)	0.1316 (±0.0000)	0.0023 (±0.0001)	0 (±0)	16.7695 (±0.0013)	-1.2021 (±0.0015)
3&6	-0.1338 (±0.0000)	1 (±0)	0.0212 (±0.0001)	-43.3277 (±0.0007)	0 (±0)	-1.5359 (±0.0050)

continued on next page

Table 4.30.: *continued*

Plane Intersection	a_x (±)	a_y (±)	a_z (±)	b_x (m±m)	b_y (m±m)	b_z (m±m)
3&7	1 (±0)	0.1330 (±0.0000)	0.0023 (±0.0001)	0 (±0)	6.0717 (±0.0002)	-1.4286 (±0.0014)
3&8	1 (±0)	0.1309 (±0.0000)	0.0023 (±0.0001)	0 (±0)	8.8522 (±0.0000)	-1.3697 (±0.0014)
3&9	-0.1313 (±0.0000)	1 (±0)	0.0212 (±0.0001)	-36.6793 (±0.0001)	0 (±0)	-1.5391 (±0.0044)
3&10	-0.1325 (±0.0000)	1 (±0)	0.0212 (±0.0001)	-16.7973 (±0.0000)	0 (±0)	-1.5489 (±0.0028)
4&5	1 (±0)	0.1316 (±0.0000)	-0.0020 (±0.0001)	0 (±0)	16.7697 (±0.0013)	-1.5771 (±0.0026)
4&6	-0.1338 (±0.0000)	1 (±0)	-0.0008 (±0.0001)	-43.3277 (±0.0007)	0 (±0)	-1.4802 (±0.0041)
4&7	1 (±0)	0.1330 (±0.0000)	-0.0020 (±0.0001)	0 (±0)	6.0717 (±0.0002)	-1.5661 (±0.0016)
4&8	1 (±0)	0.1310 (±0.0000)	-0.0020 (±0.0001)	0 (±0)	8.8528 (±0.0000)	-1.5690 (±0.0018)
4&9	-0.1313 (±0.0000)	1 (±0)	-0.0008 (±0.0001)	-36.6793 (±0.0001)	0 (±0)	-1.4924 (±0.0037)
4&10	-0.1325 (±0.0000)	1 (±0)	-0.0008 (±0.0001)	-16.7973 (±0.0000)	0 (±0)	-1.5290 (±0.0025)
5&6	-0.0000 (±0.0000)	-0.0006 (±0.0000)	1 (±0)	-44.7828 (±0.0007)	10.8771 (±0.0004)	0 (±0)

continued on next page

Table 4.30.: *continued*

Plane Intersection	a_x (±)	a_y (±)	a_z (±)	b_x (m±m)	b_y (m±m)	b_z (m±m)
5&9	-0.0001 (±0.0001)	-0.0006 (±0.0000)	1 (±0)	-38.2214 (±0.0002)	11.7404 (±0.0004)	0 (±0)
5&10	-0.0001 (±0.0000)	-0.0006 (±0.0000)	1 (±0)	-18.6940 (±0.0001)	14.3094 (±0.0008)	0 (±0)
6&7	-0.0001 (±0.0000)	-0.0002 (±0.0000)	1 (±0)	-43.3681 (±0.0007)	0.3015 (±0.0003)	0 (±0)
6&8	0.0003 (±0.0000)	-0.0031 (±0.0000)	1 (±0)	-43.7451 (±0.0006)	3.1194 (±0.0002)	0 (±0)
7&9	-0.0002 (±0.0001)	-0.0002 (±0.0000)	1 (±0)	-36.8334 (±0.0000)	1.1709 (±0.0002)	0 (±0)
7&10	-0.0002 (±0.0000)	-0.0002 (±0.0000)	1 (±0)	-17.2972 (±0.0000)	3.7701 (±0.0000)	0 (±0)
8&9	0.0002 (±0.0001)	-0.0031 (±0.0000)	1 (±0)	-37.2018 (±0.0001)	3.9763 (±0.0002)	0 (±0)
8&10	0.0002 (±0.0000)	-0.0031 (±0.0000)	1 (±0)	-17.6636 (±0.0000)	6.5348 (±0.0001)	0 (±0)

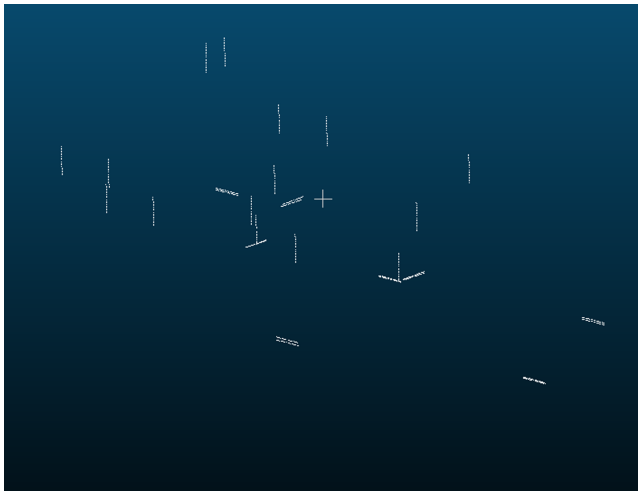

Fig. 4.13.: Simulated points along linear features in the overlapping area between scans 2 and 3

After the estimation of line parameters, the next step is to estimate transformation parameters using the three alternative registration approaches. The aim of the registration process is to estimate the 3D similarity transformation parameters, which include three translations (t_x, t_y, t_z) and three rotation parameters (ω, ϕ, κ). The observations and weight matrix P in the three alternative registration approaches are specified as follows. In the linear feature-based approach, the observations are estimated line parameters from a line fitting procedure, and the weight matrix P is defined by the inverse of the variance-covariance matrix of extracted line parameters, which is derived by using the law of error propagation.

In the pseudo-conjugate point-based method, the observations are coordinates of simulated points along lines in the source and reference scans. The weight matrix P depends on the noise added to the point clouds. The estimated line parameters in the reference scan are used to modify the weight matrix to eliminate the additional vector resulting from using non-corresponding points along linear features. In the 3D similarity transformation function, each 3D point pair contributes three equations towards the transformation parameters estimation. There are 620 points along linear features in each scan, so the total number of observation equations is $620 \times 3 =$

1,860. However, the discussion in the subsection 3.3.2 indicates that the effective contribution is only two equations from each point pair. According to Equation (3.73) in the subsection 3.3.2, all the elements in the weight matrix pertaining to the U-axis along the linear features are assigned a zero weight. The modified weight matrix in the LSA procedure nullifies the error along the line direction while minimizing the errors in the two directions normal to the line. Therefore, the effective contribution of a 3D point pair towards redundancy is 2 equations instead of 3. In this case, the redundancy is given by the difference between the rank of the weight matrix and the number of the unknowns, thus resulting in a redundancy of $620 \times 2 - 6 = 1,234$.

In the closed-form solution, the rotation parameters and the translation parameters are estimated separately. The rotation matrix is derived first using a quaternion-based approach, which is a single-step solution. The observations are the direction vectors of linear features. A weight matrix is not used in this procedure, and there is no standard deviation to evaluate the estimated rotation parameters. Once the rotation matrix is derived, the next step is to estimate translation parameters using the pseudo-conjugate point-based method. In this step, the observations are coordinates of points along linear features, and the weight matrix P is obtained as the inverse of the variance-covariance matrix of the observations.

The estimated transformation parameters, standard deviations, a-posteriori variance factors, and execution times from the linear feature-based approach, pseudo-conjugate point-based method, and closed-form solution using the linear features in scans 2 and 3 are presented in Table 4.31. In the linear feature-based approach and pseudo-conjugate point-based method, the standard deviation overall was below 3.2 mm and 0.004 degrees for the translation and the rotation parameters, respectively, which indicates the estimated transformation parameters are reliable. In the closed-form registration results, the standard deviation overall was below 1.1 mm for the translation parameters, which indicates the estimated translation parameters are reliable.

Furthermore, the a-posteriori variance factor $\hat{\sigma}_0^2$ in Table 4.31 is used to evaluate the estimated transformation parameters. In the linear feature-based approach, the weight matrix P is derived by the inverse of variance-covariance matrix, so the $\hat{\sigma}_0^2$ should be close to 1. The a-posteriori variance factor $\hat{\sigma}_0^2$ was 73.4982, which indicates that the noise level in the observation is larger than previously assumed. In the pseudo-conjugate point-based method and closed-form solution, the $\hat{\sigma}_0^2$ is the variance of the observations since the weight matrix P is an identity matrix. The square roots of the a-posteriori variance factors ($\hat{\sigma}_0$) in Table 4.31 are not significantly different from the expected accuracy of around 2 mm according to the accuracy of the TLS, thus indicating the validity of the estimated transformation parameters using the pseudo-conjugate point-based method and closed-form solution based on linear features. Regarding the execution time, the linear feature-based approach had the shortest execution time, as listed in Table 4.31. The pseudo-conjugate point-based and closed-form approaches based on linear features led to longer execution times due to a large number of point cloud data.

Table 4.31.: The estimated transformation parameters, standard deviations, a-posteriori variance factors, and execution times from the linear feature-based approach, pseudo-conjugate point-based method, and closed-form solution using the linear features in scans 2 and 3

	$t_x(m \pm m)$	$t_y(m \pm m)$	$t_z(m \pm m)$	$\omega(^\circ \pm ^\circ)$	$\phi(^\circ \pm ^\circ)$	$\kappa(^\circ \pm ^\circ)$	$\hat{\sigma}_0^2$	$\hat{\sigma}_0$	Execution time (seconds)
Linear feature-based approach	42.0795 (±0.0002)	5.1228 (±0.0006)	0.2087 (±0.0031)	0.0097 (±0.0031)	-0.0134 (±0.0026)	-63.6828 (±0.0010)	210.3468	14.5033	0.1
Pseudo-conjugate point-based method	42.0858 (±0.0007)	5.1305 (±0.0018)	0.2346 (±0.0022)	0.0833 (±0.0019)	0.0146 (±0.0038)	-63.6917 (±0.0015)	8.42E-05 (m^2)	0.0092 (m)	4.7
Closed-form solution	42.0816 (±0.0008)	5.1299 (±0.0008)	0.1807 (±0.0010)	0.0342 (N/A)	-0.0001 (N/A)	-63.6907 (N/A)	1.45E-04 (m^2)	0.0120 (m)	7.2

The quality evaluation of the registration results was analyzed by calculating the point-to-patch normal distances between TLS scans. After applying the estimated registration parameters, the point clouds in the source scan were transformed to the reference scan. A point-patch pair is established by using the approach discussed in section 3.4. The normal distance between the transformed point and the patch must be within a certain threshold, which is 10 cm in this test. The mean, standard deviation, and RMSE of the point-to-patch normal distances between the TLS scans are presented in Table 4.32. The mean of the calculated point-to-patch normal distances of the linear feature-based approach was below 2.3 mm, while it was all below 8 mm for the pseudo-conjugate point-based method and closed-form solution, which indicates that the linear feature-based approach can produce better results than the pseudo-conjugate point-based method and closed-form solution using linear features. The mean, standard deviation, and RMSE of the calculated point-to-patch normal distances of the closed-form solution were all larger than the values of the pseudo-conjugate point-based method, which indicates that the registration results using the closed-form solution were worse than the pseudo-conjugate point-based method.

Moreover, the comparison between registration approaches using linear and planar features is conducted based on point-to-patch normal distances between TLS scans. The quality evaluation of the registration results shows that these two features can produce equivalent registration results by using the feature-based approach since the normal distances calculated were all below 2.3 mm. However, the pseudo-conjugate point-based method and closed-form solution can produce better registration results when the planar features were the registration primitives. For example, when linear features are the registration primitives, the normal distances calculated using the registration results of the two approaches were below 8 mm, while it is only 4 mm when planar features are the registration primitives.

Table 4.32.: Quantitative comparison between linear feature-based approach, pseudo-conjugate point-based method, and closed-form solution based on linear features through the mean, standard deviation, and RMSE of the point-to-patch normal distances between the TLS scans 2 and 3

	Mean (m)	Standard deviation (m)	RMSE (m)	Number of used points	Total number of points
Linear feature-based approach	0.0022	0.0048	0.0053	109,163	746,894
Pseudo-conjugate point-based method	0.0065	0.0063	0.0091	107,322	746,894
Closed-form solution	0.0078	0.0107	0.0133	107,935	746,894

4.2.4 Registration Between Scans 3 and 4

In this pairwise registration, scan 3 is the reference scan, and scan 4 is the source scan. Figure 4.14 illustrates the positions of TLS scans 3 and 4 on Google Maps.

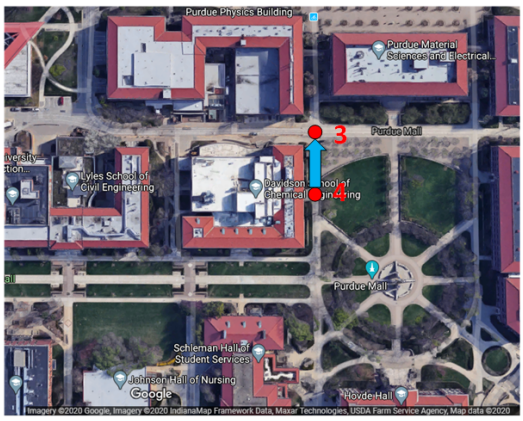

Fig. 4.14.: Position of TLS scans 3 and 4

4.2.4.1 Registration Between Scans 3 and 4 Using Planar Features

Figure 4.15 illustrates the planar features in the overlapping area between scans 3 and 4. The planar feature extraction is performed by using I-LIVE. A plane fitting procedure, as stated in subsection 3.2.5, was performed to estimate plane parameters. The estimated plane parameters, standard deviations, and square roots of the a-posteriori variance factors of 12 pairs of planar features in scans 3 and 4 are presented in Table 4.33. The standard deviation overall was below 7 mm for plane parameters in the source and reference scans. The small standard deviation values indicate the estimated plane parameters are reliable. Furthermore, the a-posteriori variance factor $\hat{\sigma}_0^2$ is used to check the quality of the estimated plane parameters. Since the weight matrix P is an identity matrix, the $\hat{\sigma}_0^2$ is the variance of the measurements. The square roots of the a-posteriori variance factors ($\hat{\sigma}_0$) after plane fitting are close to the expected accuracy of around 2 mm according to the accuracy of the TLS, thus indicating the validity of the estimated plane parameters.

(a) (b)

(c) (d)

(e) (f)

Fig. 4.15.: Planar features in the overlapping area between scans 3 and 4 displayed in images (a, c, e), which are captured by an external camera, and point clouds (b, d, f)

Table 4.33.: The estimated plane parameters, standard deviations, and square roots of the a-posteriori variance factors of 12 pairs of planar features in scans 3 and 4

	Plane ID	$a_x(m \pm m)$	$a_y(m \pm m)$	$a_z(m \pm m)$	$\hat{\sigma}_0(mm)$
Scan 4	1	-9.7112 ($\pm$0.0003)	4.3347 ($\pm$0.0002)	0.0128 ($\pm$0.0002)	1.4
	2	-9.7014 ($\pm$0.0002)	4.3301 ($\pm$0.0001)	0.0043 ($\pm$0.0002)	1.0
	3	-9.6929 ($\pm$0.0002)	4.3313 ($\pm$0.0002)	-0.0024 ($\pm$0.0002)	1.2
	4	-9.7011 ($\pm$0.0002)	4.3423 ($\pm$0.0002)	0.0051 ($\pm$0.0002)	1.0
	5	-9.6760 ($\pm$0.0001)	4.3492 ($\pm$0.0003)	0.0020 ($\pm$0.0001)	1.4
	6	-9.7607 ($\pm$0.0002)	4.3544 ($\pm$0.0002)	-0.0266 ($\pm$0.0003)	1.5
	7	-9.6791 ($\pm$0.0001)	4.3304 ($\pm$0.0004)	-0.0023 ($\pm$0.0001)	1.2
	8	0.0220 ($\pm$0.0000)	0.0166 ($\pm$0.0000)	-1.6651 ($\pm$0.0002)	1.2
	9	23.4332 ($\pm$0.0022)	52.3732 ($\pm$0.0010)	0.0912 ($\pm$0.0052)	1.5
	10	23.4753 ($\pm$0.0025)	52.3650 ($\pm$0.0004)	-0.0436 ($\pm$0.0043)	1.8
	11	23.4373 ($\pm$0.0064)	52.3587 ($\pm$0.0026)	-0.0225 ($\pm$0.0046)	1.5
	12	23.2972 ($\pm$0.0036)	52.2843 ($\pm$0.0022)	-0.0438 ($\pm$0.0048)	2.0
Scan 3	1	-6.2946 ($\pm$0.0052)	9.3888 ($\pm$0.0048)	0.0184 ($\pm$0.0016)	1.7
	2	-6.2935 ($\pm$0.0038)	9.3820 ($\pm$0.0033)	0.0040 ($\pm$0.0013)	1.3

continued on next page

Table 4.33.: *continued*

Plane ID	$a_x(m \pm m)$	$a_y(m \pm m)$	$a_z(m \pm m)$	$\hat{\sigma}_0(mm)$
3	-6.2725 ($\pm$0.0035)	9.3635 ($\pm$0.0029)	-0.0003 ($\pm$0.0013)	1.3
4	-6.2737 ($\pm$0.0023)	9.3721 ($\pm$0.0019)	0.0157 ($\pm$0.0010)	1.2
5	-6.2142 ($\pm$0.0055)	9.3136 ($\pm$0.0045)	0.0091 ($\pm$0.0008)	1.6
6	-6.3362 ($\pm$0.0034)	9.4438 ($\pm$0.0028)	-0.0224 ($\pm$0.0019)	1.6
7	-6.2476 ($\pm$0.0042)	9.3415 ($\pm$0.0032)	0.0074 ($\pm$0.0011)	1.3
8	0.0232 ($\pm$0.0001)	0.0008 ($\pm$0.0002)	-1.3290 ($\pm$0.0017)	1.6
9	16.6484 ($\pm$0.0008)	11.1416 ($\pm$0.0003)	0.0382 ($\pm$0.0011)	1.3
10	16.6345 ($\pm$0.0008)	11.1318 ($\pm$0.0003)	-0.0024 ($\pm$0.0009)	1.9
11	16.6057 ($\pm$0.0054)	11.1250 ($\pm$0.0014)	-0.0051 ($\pm$0.0014)	1.3
12	16.4977 ($\pm$0.0041)	11.0860 ($\pm$0.0016)	-0.0180 ($\pm$0.0022)	2.1

The estimated transformation parameters, standard deviations, a-posteriori variance factors, and execution times from the planar feature-based approach, pseudo-conjugate point-based method, and closed-form solution using the planar features in scans 3 and 4 are presented in Table 4.34. Since the rotation parameters were estimated by quaternions in the closed-form solution, there is no standard deviation for the rotation parameters. The standard deviation values of the registration parameters indicate that reliable results were estimated using the three alternative registration approaches. The standard deviations of the estimated parameters were below 0.3 mm for the translation parameters and below 0.0009 degrees for the rotation angels by using the pseudo-conjugate point-based method, while it is below 2 mm and 0.008 degrees for the translation and the rotation parameters, respectively, by using the planar feature-based approach, which indicates that the pseudo-conjugate point-based method can produce better registration results than the planar feature-based approach. In the closed-form solution, the standard deviations of the estimated parameters were below 0.1 mm for the translation parameters, which indicates the estimated translation parameters are reliable.

Furthermore, as shown in Table 4.34, the a-posteriori variance factor $\hat{\sigma}_0^2$ is used to evaluate the estimated transformation parameters. In the planar feature-based approach, the weight matrix P is derived by the inverse of the variance-covariance matrix, so the $\hat{\sigma}_0^2$ should be close to 1. The a-posteriori variance factor $\hat{\sigma}_0^2$ was 29.2663, which indicates that the noise level in the observation is larger than previously assumed. In the pseudo-conjugate point-based method and closed-form solution, the $\hat{\sigma}_0^2$ is the variance of the observations since the weight matrix P is an identity matrix. The square roots of the a-posteriori variance factors ($\hat{\sigma}_0$) in Table 4.34 are below the expected accuracy of 2 mm according to the accuracy of the TLS, thus indicating the validity of the estimated transformation parameters using the pseudo-conjugate point-based method and closed-form solution based on planar features. Regarding the execution time, the planar feature-based approach had the shortest execution time, as listed in Table 4.34. The pseudo-conjugate point-based and closed-form approaches

based on planar features led to longer execution times due to a large number of point cloud data.

The quality evaluation of the registration results was analyzed by calculating the point-to-patch normal distances between TLS scans. After applying the estimated registration parameters, the point clouds in the source scan were transformed to the reference scan. A point-patch pair is established by using the approach discussed in section 3.4. The normal distance between the transformed point and the patch must be within a certain threshold, which is 10 cm in this test. The mean, standard deviation, and RMSE of the point-to-patch normal distances between the TLS scans are presented in Table 4.35. The mean of the calculated point-to-patch normal distances of the three registration approaches overall were below 9 mm, which substantiates the quality of the registration results. The mean, standard deviation, and RMSE of the calculated point-to-patch normal distances of the three registration approaches were close to each other, which indicates that the three registration approaches can produce equivalent registration results.

Table 4.34.: The estimated transformation parameters, standard deviations, a-posteriori variance factors, and execution times from the planar feature-based approach, pseudo-conjugate point-based method, and closed-form solution using the planar features in scans 3 and 4

	$t_x(m \pm m)$	$t_y(m \pm m)$	$t_z(m \pm m)$	$\omega(^\circ \pm ^\circ)$	$\phi(^\circ \pm ^\circ)$	$\kappa(^\circ \pm ^\circ)$	$\hat{\sigma}_0^2$	$\hat{\sigma}_0$	Execution time (seconds)
Planar feature-based approach	-31.4025 (±0.0011)	-20.2471 (±0.0008)	-0.2187 (±0.0017)	0.0017 (±0.0076)	-0.0246 (±0.0041)	32.0885 (±0.0008)	29.2663	5.4098	0.2
Pseudo-conjugate point-based method	-31.4014 (±0.0001)	-20.2467 (±0.0001)	-0.2196 (±0.0002)	-0.0016 (±0.0008)	-0.0216 (±0.0004)	32.0891 (±0.0001)	2.03E-06 (m^2)	1.4 (mm)	24.9
Closed-form solution	-31.3958 (±0.0000)	-20.2437 (±0.0000)	-0.2239 (±0.0000)	-0.0205 (N/A)	-0.0085 (N/A)	32.0921 (N/A)	2.12E-06 (m^2)	1.5 (mm)	26.7

Table 4.35.: Quantitative comparison between planar feature-based approach, pseudo-conjugate point-based method, and closed-form solution based on planar features through the mean, standard deviation, and RMSE of the point-to-patch normal distances between the TLS scans 3 and 4

	Mean (m)	Standard deviation (m)	RMSE (m)	Number of used points	Total number of points
Planar feature-based approach	0.0085	0.0128	0.0154	218,484	1,557,259
Pseudo-conjugate point-based method	0.0083	0.0128	0.0153	218,464	1,557,259
Closed-form solution	0.0081	0.0126	0.0150	218,167	1,557,259

4.2.4.2 Registration Between Scans 3 and 4 Using Linear Features

After the planar features were used for the introduced registration approaches, the linear features were used as the registration primitives for the same experiment data to investigate the quality of the registration results with a different type of feature. Linear features are extracted indirectly using the segmented planar features from the TLS scans. The estimated line parameters and standard deviations of linear features which are derived by the intersection of neighboring planar features in scans 3 and 4 are presented in Table 4.36. Then, twenty points are simulated along the derived linear features in each scan. The simulated points along linear features are presented in Figure 4.16. The standard deviation overall was below 0.0004 and 1 cm for the direction vector (a_x, a_y, a_z) and position parameter (b_x, b_y, b_z), respectively, which indicates the estimated line parameters are reliable.

Table 4.36.: The estimated line parameters and standard deviations of linear features which are derived by the intersection of neighboring planar features in scans 3 and 4

	Plane Intersection	a_x (±)	a_y (±)	a_z (±)	b_x (m±m)	b_y (m±m)	b_z (m±m)
Scan 4	1&8	0.4464 (±0.0000)	1 (±0)	0.0159 (±0.0000)	-11.6484 (±0.0003)	0 (±0)	-1.8191 (±0.0004)
	2&8	0.4463 (±0.0000)	1 (±0)	0.0159 (±0.0000)	-11.6349 (±0.0002)	0 (±0)	-1.8189 (±0.0004)
	3&8	0.4468 (±0.0000)	1 (±0)	0.0159 (±0.0000)	-11.6280 (±0.0003)	0 (±0)	-1.8188 (±0.0004)
	4&8	0.4476 (±0.0000)	1 (±0)	0.0159 (±0.0000)	-11.6457 (±0.0003)	0 (±0)	-1.8191 (±0.0004)
	5&8	0.4495 (±0.0000)	1 (±0)	0.0159 (±0.0000)	-11.6313 (±0.0002)	0 (±0)	-1.8189 (±0.0004)
	6&8	0.4461 (±0.0000)	1 (±0)	0.0159 (±0.0000)	-11.6984 (±0.0003)	0 (±0)	-1.8198 (±0.0004)
	7&8	0.4474 (±0.0000)	1 (±0)	0.0159 (±0.0000)	-11.6160 (±0.0004)	0 (±0)	-1.8187 (±0.0004)
	9&8	1 (±0)	-0.4474 (±0.0000)	0.0087 (±0.0000)	0 (±0)	62.8598 (±0.0027)	-1.0382 (±0.0012)
	10&8	1 (±0)	-0.4483 (±0.0000)	0.0087 (±0.0000)	0 (±0)	62.8882 (±0.0024)	-1.0379 (±0.0012)
	11&8	1 (±0)	-0.4476 (±0.0001)	0.0087 (±0.0000)	0 (±0)	62.8495 (±0.0079)	-1.0383 (±0.0012)

continued on next page

Table 4.36.: *continued*

	Plane Intersection	a_x (±)	a_y (±)	a_z (±)	b_x (m±m)	b_y (m±m)	b_z (m±m)
	12&8	1 (±0)	-0.4456 (±0.0001)	0.0087 (±0.0000)	0 (±0)	62.6644 (±0.0049)	-1.0402 (±0.0012)
	9&1	0.0004 (±0.0000)	-0.0019 (±0.0001)	1 (±0)	13.6793 (±0.0015)	56.7375 (±0.0019)	0 (±0)
	10&1	0.0014 (±0.0000)	0.0002 (±0.0001)	1 (±0)	13.6864 (±0.0014)	56.7534 (±0.0016)	0 (±0)
	11&1	0.0013 (±0.0000)	-0.0001 (±0.0001)	1 (±0)	13.6752 (±0.0027)	56.7285 (±0.0054)	0 (±0)
	12&1	0.0014 (±0.0000)	0.0002 (±0.0001)	1 (±0)	13.6169 (±0.0020)	56.5977 (±0.0036)	0 (±0)
	9&7	-0.0008 (±0.0000)	-0.0014 (±0.0001)	1 (±0)	13.7529 (±0.0016)	56.7046 (±0.0019)	0 (±0)
	10&7	0.0001 (±0.0000)	0.0008 (±0.0001)	1 (±0)	13.7600 (±0.0015)	56.7204 (±0.0016)	0 (±0)
	11&7	-0.0000 (±0.0000)	0.0004 (±0.0001)	1 (±0)	13.7489 (±0.0028)	56.6956 (±0.0054)	0 (±0)
	12&7	0.0001 (±0.0000)	0.0008 (±0.0001)	1 (±0)	13.6904 (±0.0021)	56.5650 (±0.0036)	0 (±0)
Scan 3	1&8	1 (±0)	0.6704 (±0.0002)	0.0179 (±0.0001)	0 (±0)	13.6115 (±0.0097)	-1.3210 (±0.0029)
	2&8	1 (±0)	0.6708 (±0.0002)	0.0179 (±0.0001)	0 (±0)	13.6043 (±0.0069)	-1.3210 (±0.0029)

continued on next page

Table 4.36.: *continued*

Plane Intersection	a_x (±)	a_y (±)	a_z (±)	b_x (m±m)	b_y (m±m)	b_z (m±m)
3&8	1 (±0)	0.6699 (±0.0002)	0.0179 (±0.0001)	0 (±0)	13.5653 (±0.0062)	-1.3210 (±0.0029)
4&8	1 (±0)	0.6694 (±0.0001)	0.0179 (±0.0001)	0 (±0)	13.5739 (±0.0042)	-1.3210 (±0.0029)
5&8	1 (±0)	0.6672 (±0.0003)	0.0179 (±0.0001)	0 (±0)	13.4611 (±0.0098)	-1.3211 (±0.0029)
6&8	1 (±0)	0.6710 (±0.0002)	0.0179 (±0.0001)	0 (±0)	13.6920 (±0.0062)	-1.3209 (±0.0029)
7&8	1 (±0)	0.6688 (±0.0002)	0.0179 (±0.0001)	0 (±0)	13.5209 (±0.0074)	-1.3210 (±0.0029)
9&8	-0.6692 (±0.0000)	1 (±0)	-0.0111 (±0.0002)	24.1069 (±0.0008)	0 (±0)	-0.9079 (±0.0038)
10&8	-0.6692 (±0.0000)	1 (±0)	-0.0111 (±0.0002)	24.0838 (±0.0008)	0 (±0)	-0.9084 (±0.0038)
11&8	-0.6700 (±0.0001)	1 (±0)	-0.0111 (±0.0002)	24.0586 (±0.0050)	0 (±0)	-0.9088 (±0.0038)
12&8	-0.6720 (±0.0001)	1 (±0)	-0.0111 (±0.0002)	23.9462 (±0.0044)	0 (±0)	-0.9108 (±0.0038)
9&1	-0.0007 (±0.0001)	-0.0024 (±0.0001)	1 (±0)	10.3524 (±0.0055)	20.5496 (±0.0082)	0 (±0)
10&1	0.0010 (±0.0001)	-0.0013 (±0.0001)	1 (±0)	10.3384 (±0.0055)	20.5402 (±0.0082)	0 (±0)

continued on next page

Table 4.36.: *continued*

Plane Intersection	a_x (±)	a_y (±)	a_z (±)	b_x (m±m)	b_y (m±m)	b_z (m±m)
11&1	0.0011 (±0.0001)	-0.0012 (±0.0001)	1 (±0)	10.3105 (±0.0076)	20.5215 (±0.0089)	0 (±0)
12&1	0.0017 (±0.0001)	-0.0008 (±0.0001)	1 (±0)	10.2049 (±0.0068)	20.4507 (±0.0086)	0 (±0)
9&7	-0.0012 (±0.0001)	-0.0016 (±0.0001)	1 (±0)	10.4014 (±0.0046)	20.4764 (±0.0067)	0 (±0)
10&7	0.0005 (±0.0001)	-0.0005 (±0.0001)	1 (±0)	10.3874 (±0.0046)	20.4670 (±0.0067)	0 (±0)
11&7	0.0006 (±0.0001)	-0.0004 (±0.0001)	1 (±0)	10.3595 (±0.0069)	20.4484 (±0.0076)	0 (±0)
12&7	0.0011 (±0.0001)	-0.0000 (±0.0001)	1 (±0)	10.2539 (±0.0060)	20.3778 (±0.0072)	0 (±0)

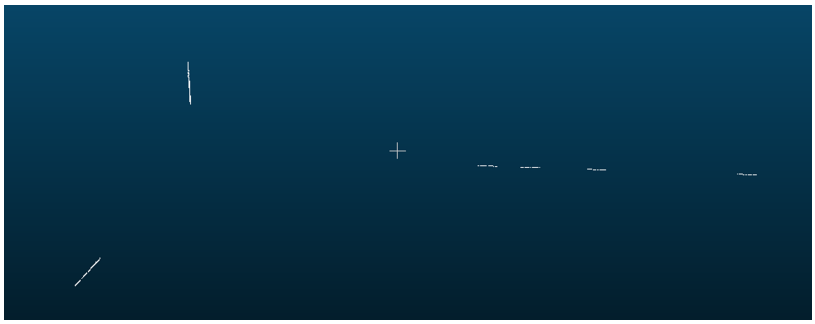

Fig. 4.16.: Simulated points along linear features in the overlapping area between scans 3 and 4

After the estimation of line parameters, the next step is to estimate transformation parameters using the three alternative registration approaches. The aim of the

registration process is to estimate the 3D similarity transformation parameters, which include three translations (t_x, t_y, t_z) and three rotation parameters (ω, ϕ, κ). The observations and weight matrix P in the three alternative registration approaches are specified as follows. In the linear feature-based approach, the observations are estimated line parameters from a line fitting procedure, and the weight matrix P is defined by the inverse of the variance-covariance matrix of extracted line parameters, which is derived by using the law of error propagation.

In the pseudo-conjugate point-based method, the observations are coordinates of simulated points along lines in the source and reference scans. The weight matrix P depends on the noise added to the point clouds. The estimated line parameters in the reference scan are used to modify the weight matrix to eliminate the additional vector resulting from using non-corresponding points along linear features. In the 3D similarity transformation function, each 3D point pair contributes three equations towards the transformation parameters estimation. There are 380 points along linear features in each scan, so the total number of observation equations is $380 \times 3 = 1,140$. However, the discussion in the subsection 3.3.2 indicates that the effective contribution is only two equations from each point pair. According to Equation (3.73) in the subsection 3.3.2, all the elements in the weight matrix pertaining to the U-axis along the linear features are assigned a zero weight. The modified weight matrix in the LSA procedure nullifies the error along the line direction while minimizing the errors in the two directions normal to the line. Therefore, the effective contribution of a 3D point pair towards redundancy is 2 equations instead of 3. In this case, the redundancy is given by the difference between the rank of the weight matrix and the number of the unknowns, thus resulting in a redundancy of $380 \times 2 - 6 = 754$.

In the closed-form solution, the rotation parameters and the translation parameters are estimated separately. The rotation matrix is derived first using a quaternion-based approach, which is a single-step solution. The observations are the direction vectors of linear features. A weight matrix is not used in this procedure, and there is no standard deviation to evaluate the estimated rotation parameters. Once the rota-

tion matrix is derived, the next step is to estimate translation parameters using the pseudo-conjugate point-based method. In this step, the observations are coordinates of points along linear features, and the weight matrix P is obtained as the inverse of the variance-covariance matrix of the observations.

The estimated transformation parameters, standard deviations, a-posteriori variance factors, and execution times from the linear feature-based approach, pseudo-conjugate point-based method, and closed-form solution using the linear features in scans 3 and 4 are presented in Table 4.37. In the linear feature-based approach, the standard deviation overall was below 0.4 cm and 0.01 degrees for the translation and the rotation parameters, respectively, while it is below 5.3 cm and 0.12 degrees in the registration results by using the pseudo-conjugate point-based method. In the closed-form registration results, the standard deviation overall was below 3.7 cm for the translation parameters. Since the rotation parameters were estimated by quaternions, there is no standard deviation for the rotation parameters. In summary, according to the standard deviation, reliable transformation parameters were estimated using the introduced three registration approaches. The linear feature-based approach produced better results than the other two approaches.

Furthermore, the a-posteriori variance factor $\hat{\sigma}_0^2$ in Table 4.37 is used to evaluate the estimated transformation parameters. In the linear feature-based approach, the weight matrix P is derived by the inverse of variance-covariance matrix, so the $\hat{\sigma}_0^2$ should be close to 1. The a-posteriori variance factor $\hat{\sigma}_0^2$ was 25.4428, which indicates that the noise level in the observation is larger than previously assumed. In the pseudo-conjugate point-based method and closed-form solution using linear features, the $\hat{\sigma}_0^2$ is the variance of the observations since the weight matrix P is an identity matrix. The square roots of the a-posteriori variance factors ($\hat{\sigma}_0$) in Table 4.37 are larger than the expected accuracy of around 2 mm according to the accuracy of the TLS. Since there are a limited number of planar features with various orientation in the overlapping area between scans 3 and 4, linear features are extracted indirectly using the segmented planar features which are not physically connected, and most of

the extracted linear features are coplanar. Also, planes 9-12 in the source scan are 50 m away from the laser scanner, so the range error is also large. Regarding the execution time, the linear feature-based approach had the shortest execution time, as listed in Table 4.37. The pseudo-conjugate point-based and closed-form approaches based on linear features led to longer execution times due to a large number of point cloud data.

The quality evaluation of the registration results was analyzed by calculating the point-to-patch normal distances between TLS scans. After applying the estimated registration parameters, the point clouds in the source scan were transformed to the reference scan. A point-patch pair is established by using the approach discussed in section 3.4. The normal distance between the transformed point and the patch must be within a certain threshold, which is 10 cm in this test. The mean, standard deviation, and RMSE of the point-to-patch normal distances between the TLS scans are presented in Table 4.38. The mean, standard deviation, and RMSE of the calculated point-to-patch normal distances of the linear feature-based method and pseudo-conjugate point-based method overall were below 2 cm, while it was below 4 cm by using the closed-form solution, which indicates that registration results by using the closed-form solution was worse than the other two approaches. The mean of the calculated point-to-patch normal distances of the linear feature-based approach was 0.92 mm, while it was 1.41 mm by using the pseudo-conjugate point-based method, which indicates that the linear feature-based approach can produce better registration results than the pseudo-conjugate point-based method.

Table 4.37.: The estimated transformation parameters, standard deviations, a-posteriori variance factors, and execution times from the linear feature-based approach, pseudo-conjugate point-based method, and closed-form solution using the linear features in scans 3 and 4

	$t_x(m \pm m)$	$t_y(m \pm m)$	$t_z(m \pm m)$	$\omega(^\circ \pm ^\circ)$	$\phi(^\circ \pm ^\circ)$	$\kappa(^\circ \pm ^\circ)$	$\hat{\sigma}_0^2$	$\hat{\sigma}_0$	Execution time (seconds)
Linear feature-based approach	-31.4007 (±0.0023)	-20.2439 (±0.0023)	-0.2395 (±0.0039)	-0.0249 (±0.0065)	-0.0082 (±0.0092)	32.0879 (±0.0028)	25.4428	5.0441	0.1
Pseudo-conjugate point-based method	-31.3804 (±0.0347)	-20.2624 (±0.0416)	-0.2279 (±0.0522)	-0.0052 (±0.1060)	0.0943 (±0.1132)	32.1410 (±0.0457)	0.1431 (m^2)	0.3783 (m)	2.3
Closed-form solution	-31.3779 (±0.0334)	-20.2877 (±0.0320)	-0.2266 (±0.0360)	-0.0162 (N/A)	0.0062 (N/A)	32.0922 (N/A)	0.1431 (m^2)	0.3779 (m)	4.7

Table 4.38.: Quantitative comparison between linear feature-based approach, pseudo-conjugate point-based method, and closed-form solution based on linear features through the mean, standard deviation, and RMSE of the point-to-patch normal distances between the TLS scans 3 and 4

	Mean (m)	Standard deviation (m)	RMSE (m)	Number of used points	Total number of points
Linear feature-based approach	0.0092	0.0121	0.0152	217,862	1,557,259
Pseudo-conjugate point-based method	0.0141	0.0120	0.0186	213,111	1,557,259
Closed-form solution	0.0356	0.0155	0.0389	200,141	1,557,259

Moreover, the comparison between registration approaches using linear and planar features is conducted based on point-to-patch normal distances between TLS scans. The quality evaluation of the registration results shows that these two features can produce equivalent registration results by using the feature-based approach since the normal distances calculated were all below 3.6 cm. However, the pseudo-conjugate point-based method and closed-form solution can produce better registration results when the planar features were the registration primitives. For example, when linear features are the registration primitives, the normal distances calculated using the registration results of the two approaches were below 4 cm, while it is only 9 mm when planar features are the registration primitives.

4.2.5 Registration Between Scans 5 and 6

The positions of TLS scans 5 and 6 are shown in Figure 4.17. In this pairwise registration, scan 5 is the source scan, and scan 6 is the reference scan. The blue arrow represents the direction of the registration process.

Fig. 4.17.: Position of TLS scans 5 and 6

4.2.5.1 Registration Between Scans 5 and 6 Using Planar Features

The planar features, as shown in Figure 4.18, in the overlapping area between scans 5 and 6 are extracted by using I-LIVE. The plane parameters are estimated through a plane fitting procedure, as stated in subsection 3.2.5. The estimated plane parameters, standard deviations, and square roots of the a-posteriori variance factors for 23 pairs of planar features in scans 5 and 6 are presented in Table 4.39. As highlighted in the table, the standard deviation of planes 9, 10, 11 in the reference scan was large, which was resulted from the large range error, since these planes are 75 m away from the laser scanner. The standard deviation of plane 14 was large in the reference and source scans since this plane is blocked by a tree, which causes large noise in the data. The planes 16, 17, 18, 21 are narrow, which causes the large standard deviation. Plane 22 is on the roof of the building, and the surface is not flat, so the standard deviation of the plane 22 in the source scan is large. The

standard deviation of the plane 23 in both scans are large, which is resulting from the range error, since plane 7 is 100 m away from the laser scanner. Furthermore, the a-posteriori variance factor $\hat{\sigma}_0^2$ is used to check the quality of the estimated plane parameters. Since the weight matrix P is an identity matrix, the $\hat{\sigma}_0^2$ is the variance of the measurements. The square roots of the a-posteriori variance factors ($\hat{\sigma}_0$) after plane fitting are close to the expected accuracy of around 2 mm according to the accuracy of the TLS, thus indicating the validity of the estimated plane parameters.

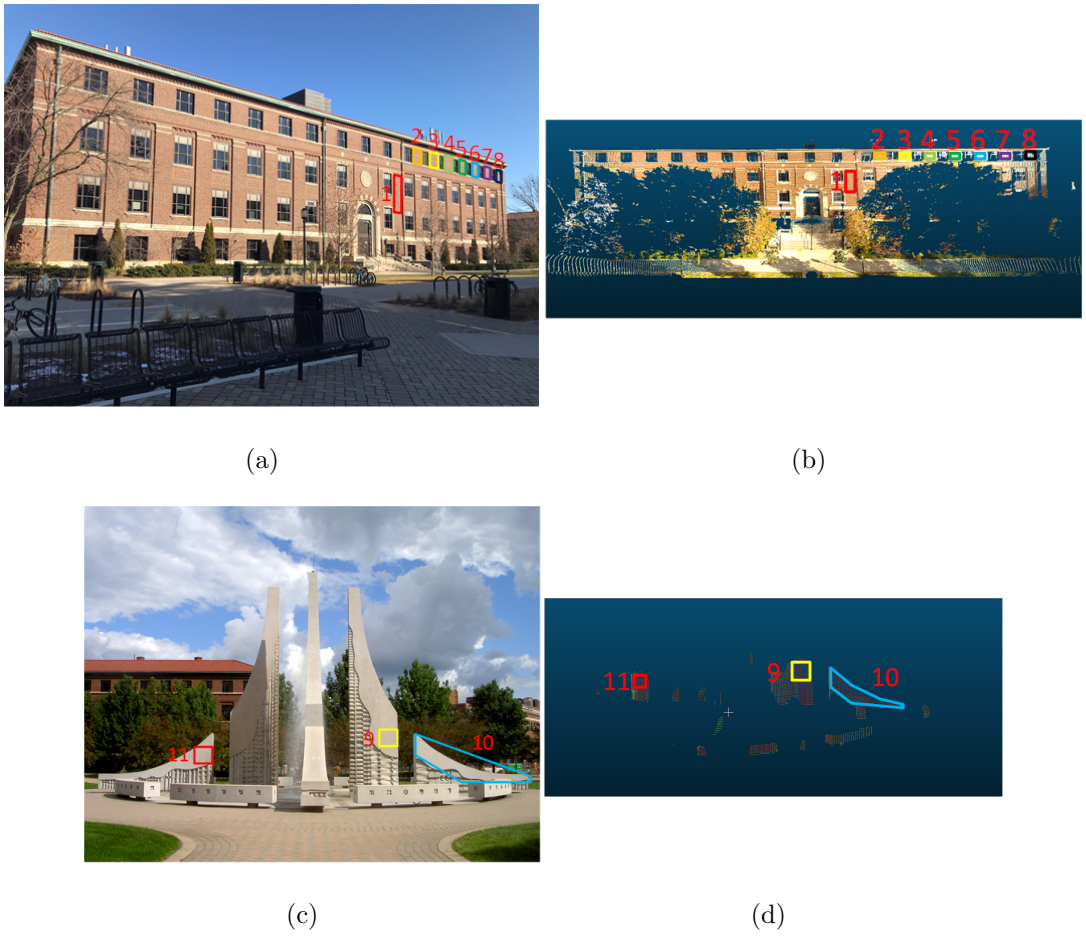

(a) (b)

(c) (d)

Fig. 4.18.: Planar features in the overlapping area between scans 5 and 6 displayed in images (a, c, e, g, i, k), which are captured by an external camera, and point clouds (b, d, f, h, j, l) (continued on next page)

(e) (f)

(g) (h)

(i) (j)

Fig. 4.18.: Planar features in the overlapping area between scans 5 and 6 displayed in images (a, c, e, g, i, k), which are captured by an external camera, and point clouds (b, d, f, h, j, l) (continued from the previous page)

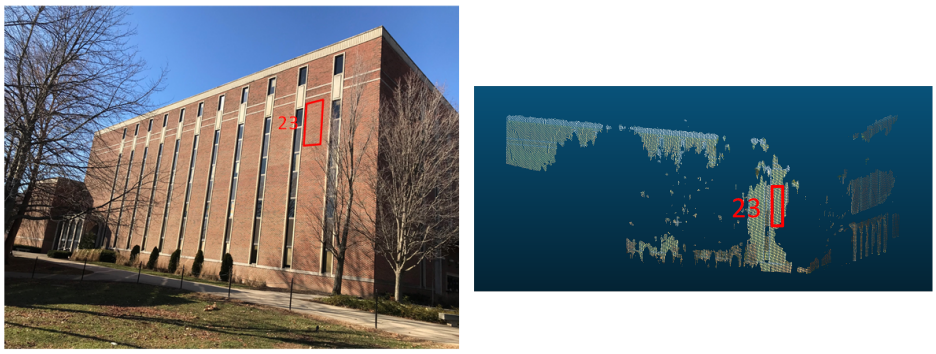

(k) (l)

Fig. 4.18.: Planar features in the overlapping area between scans 5 and 6 displayed in images (a, c, e, g, i, k), which are captured by an external camera, and point clouds (b, d, f, h, j, l) (continued from the previous page)

The estimated transformation parameters, standard deviations, a-posteriori variance factors, and execution times from the planar feature-based approach, pseudo-conjugate point-based method, and closed-form solution using the planar features in scans 5 and 6 are presented in Table 4.40. Since the rotation parameters were estimated by quaternions in the closed-form solution, there is no standard deviation for the rotation parameters. The standard deviation values of the registration parameters indicate that reliable results were estimated using the three alternative registration approaches. The standard deviations of the estimated parameters were below 0.2 mm for the translation parameters and below 0.0003 degrees for the rotation angels by using the pseudo-conjugate point-based method, while it is below 2.6 mm and 0.006 degrees for the translation and the rotation parameters, respectively, by using the planar feature-based approach, which indicates that the pseudo-conjugate point-based method can produce better registration results than the planar feature-based approach. In the closed-form solution, the standard deviation of the estimated parameters were below 0.2 mm for the translation parameters, which indicates the estimated translation parameters are reliable.

Table 4.39.: The estimated plane parameters, standard deviations, and square roots of the a-posteriori variance factors of 23 pairs of planar features in scans 5 and 6

	Plane ID	$a_x(m \pm m)$	$a_y(m \pm m)$	$a_z(m \pm m)$	$\hat{\sigma}_0(mm)$
Scan 5	1	1.0336 (±0.0007)	9.6007 (±0.0046)	-0.0015 (±0.0003)	1.9
	2	1.0234 (±0.0007)	9.8434 (±0.0041)	-0.0045 (±0.0011)	1.7
	3	1.0240 (±0.0006)	9.8162 (±0.0028)	-0.0184 (±0.0008)	1.5
	4	1.0225 (±0.0005)	9.8519 (±0.0019)	-0.0032 (±0.0006)	1.4
	5	1.0181 (±0.0004)	9.8371 (±0.0015)	-0.0191 (±0.0005)	1.5
	6	1.0302 (±0.0004)	9.8139 (±0.0012)	-0.0107 (±0.0005)	1.6
	7	1.0041 (±0.0003)	9.8983 (±0.0008)	0.0053 (±0.0004)	1.4
	8	1.0207 (±0.0004)	9.8497 (±0.0007)	-0.0054 (±0.0003)	1.2
	9	43.6957 (±0.0011)	-4.3694 (±0.0049)	-1.1018 (±0.0026)	1.0
	10	43.7129 (±0.0015)	-4.5655 (±0.0039)	-1.3731 (±0.0082)	1.3
	11	43.7249 (±0.0002)	-4.5645 (±0.0036)	-1.1443 (±0.0030)	0.5
	12	0.0086 (±0.0000)	0.0189 (±0.0001)	-1.4782 (±0.0002)	2.1
	13	-0.0084 (±0.0000)	0.0103 (±0.0000)	-1.5699 (±0.0004)	1.8
	14	-96.5233 (±0.0033)	9.5267 (±0.0223)	0.6095 (±0.0278)	2.5

continued on next page

Table 4.39.: *continued*

	Plane ID	$a_x(m \pm m)$	$a_y(m \pm m)$	$a_z(m \pm m)$	$\hat{\sigma}_0(mm)$
	15	-3.0902 (±0.0020)	-29.6163 (±0.0013)	-0.0905 (±0.0027)	1.2
	16	-3.2780 (±0.0115)	-29.8482 (±0.0119)	0.1026 (±0.0038)	1.1
	17	-3.2705 (±0.0121)	-29.8086 (±0.0134)	-0.0343 (±0.0042)	1.4
	18	-3.1654 (±0.0116)	-29.7086 (±0.0145)	-0.0262 (±0.0045)	1.2
	19	-3.1247 (±0.0081)	-29.6651 (±0.0091)	0.0603 (±0.0024)	1.7
	20	-3.1207 (±0.0029)	-29.6850 (±0.0033)	0.2562 (±0.0071)	1.1
	21	-3.1048 (±0.0033)	-29.6385 (±0.0035)	0.1380 (±0.0107)	1.0
	22	-53.9992 (±0.0083)	5.7450 (±0.0074)	0.1049 (±0.0197)	1.9
	23	-151.0886 (±0.0202)	15.7338 (±0.0454)	0.0845 (±0.0365)	2.8
Scan 6	1	-4.1548 (±0.0002)	8.9207 (±0.0002)	-0.0071 (±0.0001)	1.8
	2	-4.2166 (±0.0003)	8.9875 (±0.0006)	-0.0090 (±0.0003)	1.7
	3	-4.2110 (±0.0002)	8.9731 (±0.0007)	-0.0216 (±0.0004)	1.5
	4	-4.2196 (±0.0002)	8.9833 (±0.0009)	-0.0075 (±0.0004)	1.3
	5	-4.2119 (±0.0003)	8.9543 (±0.0013)	-0.0206 (±0.0005)	1.5
	6	-4.2160 (±0.0004)	8.9988 (±0.0020)	-0.0131 (±0.0006)	1.5

continued on next page

Table 4.39.: *continued*

Plane ID	$a_x(m \pm m)$	$a_y(m \pm m)$	$a_z(m \pm m)$	$\hat{\sigma}_0(mm)$
7	-4.2162 (±0.0004)	8.9132 (±0.0023)	0.0041 (±0.0007)	1.5
8	-4.2181 (±0.0006)	8.9757 (±0.0034)	-0.0069 (±0.0008)	1.3
9	79.1675 (±0.0152)	37.8679 (±0.0209)	-2.2439 (±0.0270)	1.5
10	79.5004 (±0.0124)	37.3108 (±0.0132)	-2.8078 (±0.0391)	1.4
11	79.5079 (±0.0138)	37.3576 (±0.0263)	-2.3686 (±0.0309)	0.9
12	-0.0030 (±0.0001)	0.0205 (±0.0001)	-1.5780 (±0.0007)	2.0
13	-0.0092 (±0.0000)	0.0035 (±0.0000)	-1.2395 (±0.0002)	2.0
14	-48.1664 (±0.0365)	-22.5577 (±0.0382)	0.5163 (±0.0225)	2.0
15	12.6477 (±0.0014)	-26.9172 (±0.0002)	-0.1527 (±0.0020)	0.9
16	12.5108 (±0.0033)	-26.9943 (±0.0010)	0.1069 (±0.0013)	1.0
17	12.4506 (±0.0030)	-26.9787 (±0.0011)	-0.0214 (±0.0013)	1.1
18	12.5579 (±0.0036)	-26.9570 (±0.0021)	-0.0295 (±0.0015)	1.2
19	12.6197 (±0.0026)	-26.9369 (±0.0010)	0.0591 (±0.0008)	1.7
20	12.6237 (±0.0008)	-26.9660 (±0.0004)	0.2564 (±0.0024)	0.7
21	12.6245 (±0.0006)	-26.9323 (±0.0002)	0.1447 (±0.0033)	0.8
22	-9.3735 (±0.0068)	-4.3701 (±0.0040)	0.0068 (±0.0049)	1.8

continued on next page

Table 4.39.: *continued*

Plane ID	$a_x(m \pm m)$	$a_y(m \pm m)$	$a_z(m \pm m)$	$\hat{\sigma}_0(mm)$
23	-97.7186 ($\pm$0.0013)	-45.7281 ($\pm$0.0306)	-0.2013 ($\pm$0.0125)	2.6

Furthermore, the a-posteriori variance factor $\hat{\sigma}_0^2$ is presented in Table 4.40. In the planar feature-based approach, the weight matrix P is derived by the inverse of the variance-covariance matrix, so the $\hat{\sigma}_0^2$ should be close to 1. The a-posteriori variance factor $\hat{\sigma}_0^2$ was 499.9185, which indicates that the noise level in the observation is larger than previously assumed. In the pseudo-conjugate point-based method and closed-form solution, the $\hat{\sigma}_0^2$ is the variance of the observations since the weight matrix P is an identity matrix. The square roots of the a-posteriori variance factors ($\hat{\sigma}_0$) in Table 4.40 are not significantly different from the expected accuracy of around 2 mm according to the accuracy of the TLS, thus indicating the validity of the estimated transformation parameters using the pseudo-conjugate point-based method and closed-form solution based on planar features. Regarding the execution time, the planar feature-based approach had the shortest execution time, as listed in Table 4.40. The pseudo-conjugate point-based and closed-form approaches based on planar features led to longer execution times due to a large number of point cloud data.

The quality evaluation of the registration results was analyzed by calculating the point-to-patch normal distances between TLS scans. After applying the estimated registration parameters, the point clouds in the source scan were transformed to the reference scan. A point-patch pair is established by using the approach discussed in section 3.4. The normal distance between the transformed point and the patch must be within a certain threshold, which is 10 cm in this test. The mean, standard deviation, and RMSE of the point-to-patch normal distances between the TLS scans are presented in Table 4.41.

Table 4.40.: The estimated transformation parameters, standard deviations, a-posteriori variance factors, and execution times from the planar feature-based approach, pseudo-conjugate point-based method, and closed-form solution using the planar features in scans 5 and 6

	$t_x(m \pm m)$	$t_y(m \pm m)$	$t_z(m \pm m)$	$\omega(^\circ \pm ^\circ)$	$\phi(^\circ \pm ^\circ)$	$\kappa(^\circ \pm ^\circ)$	$\hat{\sigma}_0^2$	$\hat{\sigma}_0$	Execution time (seconds)
Planar feature-based approach	39.7448 (±0.0014)	18.6968 (±0.0010)	0.0788 (±0.0025)	0.0208 (±0.0038)	0.0074 (±0.0058)	-31.0966 (±0.0017)	499.9185	22.3589	0.2
Pseudo-conjugate point-based method	39.7470 (±0.0001)	18.6952 (±0.0000)	0.0779 (±0.0001)	0.0247 (±0.0002)	0.0063 (±0.0002)	-31.0911 (±0.0001)	5.06E-06 (m^2)	2.2 (mm)	29.7
Closed-form solution	39.7477 (±0.0001)	18.6931 (±0.0000)	0.0704 (±0.0000)	0.0051 (N/A)	-0.0154 (N/A)	-31.0828 (N/A)	6.93E-06 (m^2)	2.6 (mm)	33.7

Table 4.41.: Quantitative comparison between planar feature-based approach, pseudo-conjugate point-based method, and closed-form solution based on planar features through the mean, standard deviation, and RMSE of the point-to-patch normal distances between the TLS scans 5 and 6

	Mean (m)	Standard deviation (m)	RMSE (m)	Number of used points	Total number of points
Planar feature-based approach	0.0040	0.0087	0.0096	20,486	132,379
Pseudo-conjugate point-based method	0.0038	0.0087	0.0095	20,416	132,379
Closed-form solution	0.0047	0.0084	0.0096	20,276	132,379

The mean, standard deviation, and RMSE of the calculated point-to-patch normal distances of each approach were all below 5 mm, which substantiates the quality of the registration results. The pseudo-conjugate point-based method produced the best registration result since the mean of the calculated point-to-patch normal distance is the smallest by using this approach. The mean of the calculated point-to-patch normal distances is 4 mm for the planar feature-based approach, while it is 4.7 mm by using the closed-form solution, which indicates that the planar feature-based approach can produce better registration results than the closed-form solution.

4.2.5.2 Registration Between Scans 5 and 6 Using Linear Features

After the planar features were used for the introduced registration approaches, the linear features were used as the registration primitives for the same experiment data to investigate the quality of the registration results with a different type of feature.

Linear features are extracted indirectly using the segmented planar features from the TLS scans. The estimated line parameters and standard deviations of linear features which are derived by the intersection of neighboring planar features in scans 5 and 6 are presented in Table 4.42. Then, twenty points are simulated along the derived linear features in each scan. The simulated points along linear features are presented in Figure 4.19. The standard deviation highlighted in red were larger than 1 cm. This results from using planes 10, 16, 17, 18, 19, 23, which has bad geometry or large range errors. The standard deviation of other lines was below 0.0012 and 1 cm for the direction vector (a_x, a_y, a_z) and position parameter (b_x, b_y, b_z), respectively, which indicates the estimated line parameters are reliable.

Table 4.42.: The estimated line parameters and standard deviations of linear features which are derived by the intersection of neighboring planar features in scans 5 and 6

	Plane Intersection	a_x (±)	a_y (±)	a_z (±)	b_x (m±m)	b_y (m±m)	b_z (m±m)
Scan 5	1&12	1 (±0)	-0.1077 (±0.0001)	0.0044 (±0.0000)	0 (±0)	9.7118 (±0.0045)	-1.3544 (±0.0004)
	2&12	1 (±0)	-0.1040 (±0.0001)	0.0045 (±0.0000)	0 (±0)	9.9492 (±0.0040)	-1.3514 (±0.0004)
	3&12	1 (±0)	-0.1043 (±0.0001)	0.0045 (±0.0000)	0 (±0)	9.9205 (±0.0027)	-1.3517 (±0.0004)
	4&12	1 (±0)	-0.1038 (±0.0001)	0.0045 (±0.0000)	0 (±0)	9.9576 (±0.0018)	-1.3513 (±0.0004)
	5&12	1 (±0)	-0.1035 (±0.0001)	0.0045 (±0.0000)	0 (±0)	9.9399 (±0.0015)	-1.3515 (±0.0004)
	6&12	1 (±0)	-0.1050 (±0.0001)	0.0045 (±0.0000)	0 (±0)	9.9206 (±0.0012)	-1.3517 (±0.0004)

continued on next page

Table 4.42.: *continued*

Plane Intersection	a_x (±)	a_y (±)	a_z (±)	b_x (m±m)	b_y (m±m)	b_z (m±m)
7&12	1 (±0)	-0.1014 (±0.0000)	0.0045 (±0.0000)	0 (±0)	10.0009 (±0.0008)	-1.3507 (±0.0004)
8&12	1 (±0)	-0.1036 (±0.0000)	0.0045 (±0.0000)	0 (±0)	9.9548 (±0.0007)	-1.3513 (±0.0004)
9&12	0.1003 (±0.0001)	1 (±0)	0.0134 (±0.0000)	44.1296 (±0.0020)	0 (±0)	-1.2215 (±0.0006)
10&12	0.1049 (±0.0001)	1 (±0)	0.0134 (±0.0000)	44.1946 (±0.0020)	0 (±0)	-1.2211 (±0.0006)
11&12	0.1047 (±0.0001)	1 (±0)	0.0134 (±0.0000)	44.1994 (±0.0007)	0 (±0)	-1.2210 (±0.0006)
14&12	0.0988 (±0.0002)	1 (±0)	0.0134 (±0.0000)	-97.4804 (±0.0044)	0 (±0)	-2.0464 (±0.0010)
15&12	1 (±0)	-0.1044 (±0.0001)	0.0045 (±0.0000)	0 (±0)	-29.9333 (±0.0017)	-1.8611 (±0.0014)
16&12	1 (±0)	-0.1098 (±0.0003)	0.0044 (±0.0000)	0 (±0)	-30.2150 (±0.0142)	-1.8647 (±0.0014)
17&12	1 (±0)	-0.1097 (±0.0004)	0.0044 (±0.0000)	0 (±0)	-30.1653 (±0.0159)	-1.8641 (±0.0014)
18&12	1 (±0)	-0.1066 (±0.0003)	0.0045 (±0.0000)	0 (±0)	-30.0442 (±0.0169)	-1.8625 (±0.0014)
19&12	1 (±0)	-0.1053 (±0.0002)	0.0045 (±0.0000)	0 (±0)	-29.9981 (±0.0107)	-1.8619 (±0.0014)

continued on next page

Table 4.42.: *continued*

	Plane Intersection	a_x (±)	a_y (±)	a_z (±)	b_x (m±m)	b_y (m±m)	b_z (m±m)
	20&12	1 (±0)	-0.1051 (±0.0001)	0.0045 (±0.0000)	0 (±0)	-30.0314 (±0.0040)	-1.8623 (±0.0014)
	21&12	1 (±0)	-0.1047 (±0.0001)	0.0045 (±0.0000)	0 (±0)	-29.9731 (±0.0043)	-1.8616 (±0.0014)
	22&12	0.1064 (±0.0001)	1 (±0)	0.0134 (±0.0000)	-54.6141 (±0.0080)	0 (±0)	-1.7967 (±0.0005)
	23&12	0.1041 (±0.0003)	1 (±0)	0.0134 (±0.0000)	-152.7284 (±0.0109)	0 (±0)	-2.3683 (±0.0017)
	18&22	0.0018 (±0.0004)	-0.0011 (±0.0002)	1 (±0)	-57.1593 (±0.0063)	-23.9556 (±0.0031)	0 (±0)
	15&22	0.0016 (±0.0004)	-0.0032 (±0.0001)	1 (±0)	-57.1613 (±0.0063)	-23.9747 (±0.0019)	0 (±0)
Scan 6	1&12	1 (±0)	0.4657 (±0.0000)	0.0041 (±0.0000)	0 (±0)	10.8547 (±0.0001)	-1.4370 (±0.0008)
	2&12	1 (±0)	0.4692 (±0.0000)	0.0042 (±0.0000)	0 (±0)	10.9644 (±0.0006)	-1.4356 (±0.0008)
	3&12	1 (±0)	0.4693 (±0.0000)	0.0042 (±0.0000)	0 (±0)	10.9458 (±0.0007)	-1.4358 (±0.0008)
	4&12	1 (±0)	0.4697 (±0.0000)	0.0042 (±0.0000)	0 (±0)	10.9642 (±0.0008)	-1.4356 (±0.0008)
	5&12	1 (±0)	0.4704 (±0.0001)	0.0042 (±0.0000)	0 (±0)	10.9322 (±0.0012)	-1.4360 (±0.0008)

continued on next page

Table 4.42.: *continued*

Plane Intersection	a_x (±)	a_y (±)	a_z (±)	b_x (m±m)	b_y (m±m)	b_z (m±m)
6&12	1 (±0)	0.4685 (±0.0001)	0.0042 (±0.0000)	0 (±0)	10.9719 (±0.0018)	-1.4355 (±0.0008)
7&12	1 (±0)	0.4730 (±0.0001)	0.0042 (±0.0000)	0 (±0)	10.9082 (±0.0022)	-1.4363 (±0.0008)
8&12	1 (±0)	0.4699 (±0.0001)	0.0042 (±0.0000)	0 (±0)	10.9568 (±0.0032)	-1.4357 (±0.0008)
9&12	-0.4779 (±0.0004)	1 (±0)	0.0139 (±0.0001)	97.2943 (±0.0086)	0 (±0)	-1.7653 (±0.0037)
10&12	-0.4688 (±0.0002)	1 (±0)	0.0139 (±0.0001)	97.0478 (±0.0045)	0 (±0)	-1.7649 (±0.0037)
11&12	-0.4694 (±0.0004)	1 (±0)	0.0139 (±0.0001)	97.0787 (±0.0140)	0 (±0)	-1.7649 (±0.0037)
14&12	-0.4682 (±0.0011)	1 (±0)	0.0139 (±0.0001)	-58.7521 (±0.0094)	0 (±0)	-1.4653 (±0.0026)
15&12	1 (±0)	0.4698 (±0.0000)	0.0042 (±0.0000)	0 (±0)	-32.8495 (±0.0015)	-2.0059 (±0.0027)
16&12	1 (±0)	0.4635 (±0.0001)	0.0041 (±0.0000)	0 (±0)	-32.8009 (±0.0024)	-2.0052 (±0.0027)
17&12	1 (±0)	0.4615 (±0.0001)	0.0041 (±0.0000)	0 (±0)	-32.7230 (±0.0020)	-2.0042 (±0.0027)
18&12	1 (±0)	0.4658 (±0.0002)	0.0041 (±0.0000)	0 (±0)	-32.8049 (±0.0019)	-2.0053 (±0.0027)

continued on next page

Table 4.42.: *continued*

Plane Intersection	a_x (±)	a_y (±)	a_z (±)	b_x (m±m)	b_y (m±m)	b_z (m±m)
19&12	1 (±0)	0.4685 (±0.0001)	0.0042 (±0.0000)	0 (±0)	-32.8536 (±0.0017)	-2.0059 (±0.0027)
20&12	1 (±0)	0.4682 (±0.0000)	0.0042 (±0.0000)	0 (±0)	-32.8971 (±0.0008)	-2.0065 (±0.0027)
21&12	1 (±0)	0.4688 (±0.0000)	0.0042 (±0.0000)	0 (±0)	-32.8616 (±0.0005)	-2.0060 (±0.0027)
22&12	-0.4662 (±0.0002)	1 (±0)	0.0139 (±0.0001)	-11.4121 (±0.0094)	0 (±0)	-1.5563 (±0.0009)
23&12	-0.4680 (±0.0003)	1 (±0)	0.0139 (±0.0001)	-119.1150 (±0.0285)	0 (±0)	-1.3492 (±0.0050)
18&22	0.0010 (±0.0004)	-0.0006 (±0.0002)	1 (±0)	3.1914 (±0.0071)	-31.3204 (±0.0035)	0 (±0)
15&22	0.0028 (±0.0004)	-0.0044 (±0.0002)	1 (±0)	3.2070 (±0.0071)	-31.3540 (±0.0035)	0 (±0)

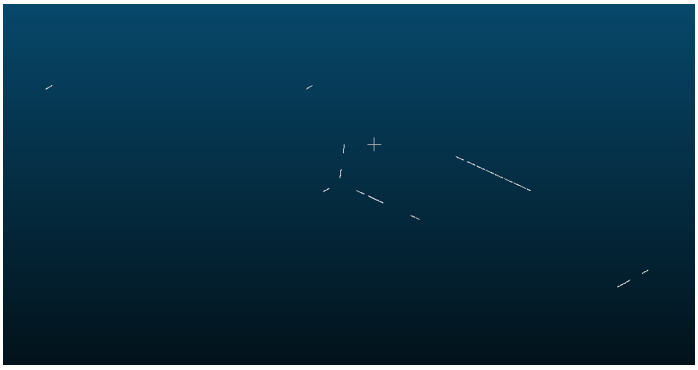

Fig. 4.19.: Simulated points along linear features in the overlapping area between scans 5 and 6

After the estimation of line parameters, the next step is to estimate transformation parameters using the three alternative registration approaches. The aim of the registration process is to estimate the 3D similarity transformation parameters, which include three translations (t_x, t_y, t_z) and three rotation parameters (ω, ϕ, κ). The observations and weight matrix P in the three alternative registration approaches are specified as follows. In the linear feature-based approach, the observations are estimated line parameters from a line fitting procedure, and the weight matrix P is defined by the inverse of the variance-covariance matrix of extracted line parameters, which is derived by using the law of error propagation.

In the pseudo-conjugate point-based method, the observations are coordinates of simulated points along lines in the source and reference scans. The weight matrix P depends on the noise added to the point clouds. The estimated line parameters in the reference scan are used to modify the weight matrix to eliminate the additional vector resulting from using non-corresponding points along linear features. In the 3D similarity transformation function, each 3D point pair contributes three equations towards the transformation parameters estimation. There are 460 points along linear features in each scan, so the total number of observation equations is $460 \times 3 = 1,380$. However, the discussion in the subsection 3.3.2 indicates that the effective contribution is only two equations from each point pair. According to Equation (3.73) in the subsection 3.3.2, all the elements in the weight matrix pertaining to the U-axis along the linear features are assigned a zero weight. The modified weight matrix in the LSA procedure nullifies the error along the line direction while minimizing the errors in the two directions normal to the line. Therefore, the effective contribution of a 3D point pair towards redundancy is 2 equations instead of 3. In this case, the redundancy is given by the difference between the rank of the weight matrix and the number of the unknowns, thus resulting in a redundancy of $460 \times 2 - 6 = 914$.

In the closed-form solution, the rotation parameters and the translation parameters are estimated separately. The rotation matrix is derived first using a quaternion-based approach, which is a single-step solution. The observations are the direction

vectors of linear features. A weight matrix is not used in this procedure, and there is no standard deviation to evaluate the estimated rotation parameters. Once the rotation matrix is derived, the next step is to estimate translation parameters using the pseudo-conjugate point-based method. In this step, the observations are coordinates of points along linear features, and the weight matrix P is obtained as the inverse of the variance-covariance matrix of the observations.

The estimated transformation parameters, standard deviations, a-posteriori variance factors, and execution times from the linear feature-based approach, pseudo-conjugate point-based method, and closed-form solution using the linear features in scans 5 and 6 are presented in Table 4.43. In the linear feature-based approach, the standard deviation overall was below 2.2 mm and 0.0051 degrees for the translation and the rotation parameters, respectively, while it is below 5.9 mm and 0.01 degrees in the registration results by using the pseudo-conjugate point-based method. In the closed-form registration results, the standard deviation overall was below 4.6 mm for the translation parameters. Since the rotation parameters were estimated by quaternions, there is no standard deviation for the rotation parameters. In summary, according to the standard deviation, reliable transformation parameters were estimated using the introduced three registration approaches. The linear feature-based approach produced better results than the other two approaches.

Furthermore, the a-posteriori variance factor $\hat{\sigma}_0^2$ in Table 4.43 is used to evaluate the estimated transformation parameters. In the linear feature-based approach, the weight matrix P is derived by the inverse of variance-covariance matrix, so the $\hat{\sigma}_0^2$ should be close to 1. The a-posteriori variance factor $\hat{\sigma}_0^2$ was 17.1509, which indicates that the noise level in the observation is larger than previously assumed. In the pseudo-conjugate point-based method and closed-form solution, the $\hat{\sigma}_0^2$ is the variance of the observations since the weight matrix P is an identity matrix. The square roots of the a-posteriori variance factors ($\hat{\sigma}_0$) in Table 4.43 are larger than the expected accuracy of around 2 mm according to the accuracy of the TLS. In the experiment with real data, linear features are extracted indirectly by the intersection of neighboring

planar features. To get enough lines, planes that are far apart from each other have to be extrapolated to derive lines, which will result in large ($\hat{\sigma}_0$) values. Regarding the execution time, the linear feature-based approach had the shortest execution time, as listed in Table 4.43. The pseudo-conjugate point-based and closed-form approaches based on linear features led to longer execution times due to a large number of point cloud data.

The quality evaluation of the registration results was analyzed by calculating the point-to-patch normal distances between TLS scans. After applying the estimated registration parameters, the point clouds in the source scan were transformed to the reference scan. A point-patch pair is established by using the approach discussed in section 3.4. The normal distance between the transformed point and the patch must be within a certain threshold, which is 10 cm in this test. The mean, standard deviation, and RMSE of the point-to-patch normal distances between the TLS scans are presented in Table 4.44. The mean of the calculated point-to-patch normal distances of the linear feature-based approach was 7 mm, while it was all over 1 cm for the pseudo-conjugate point-based method and closed-form solution, which indicates that the linear feature-based approach can produce better results than the pseudo-conjugate point-based method and closed-form solution using linear features. The mean, standard deviation, and RMSE of the calculated point-to-patch normal distances of the pseudo-conjugate point-based method and closed-form solution were all close to each other, which indicates the equivalency between the registration results by using the two approaches.

Table 4.43.: The estimated transformation parameters, standard deviations, a-posteriori variance factors, and execution times from the linear feature-based approach, pseudo-conjugate point-based method, and closed-form solution using the linear features in scans 5 and 6

	$t_x(m \pm m)$	$t_y(m \pm m)$	$t_z(m \pm m)$	$\omega(^\circ \pm ^\circ)$	$\phi(^\circ \pm ^\circ)$	$\kappa(^\circ \pm ^\circ)$	$\hat{\sigma}_0^2$	$\hat{\sigma}_0$	Execution time (seconds)
Linear feature-based approach	39.7368 (±0.0021)	18.7026 (±0.0016)	0.0663 (±0.0012)	0.0285 (±0.0050)	-0.0416 (±0.0014)	-31.1055 (±0.0035)	17.1509	4.1414	0.1
Pseudo-conjugate point-based method	39.6972 (±0.0058)	18.6888 (±0.0045)	0.0688 (±0.0039)	0.0028 (±0.0090)	-0.0246 (±0.0050)	-31.1014 (±0.0057)	0.0018 (m^2)	0.0422 (m)	2.6
Closed-form solution	39.7091 (±0.0045)	18.6796 (±0.0036)	0.0663 (±0.0029)	0.0121 (N/A)	-0.0272 (N/A)	-31.0829 (N/A)	0.0018 (m^2)	0.0424 (m)	5.2

Table 4.44.: Quantitative comparison between linear feature-based approach, pseudo-conjugate point-based method, and closed-form solution based on linear features through the mean, standard deviation, and RMSE of the point-to-patch normal distances between the TLS scans 5 and 6

	Mean (m)	Standard deviation (m)	RMSE (m)	Number of used points	Total number of points
Linear feature-based approach	0.0070	0.0092	0.0115	20,468	132,379
Pseudo-conjugate point-based method	0.0109	0.0131	0.0170	20,567	132,379
Closed-form solution	0.0101	0.0145	0.0177	20,615	132,379

Moreover, the comparison between registration approaches using linear and planar features is conducted based on point-to-patch normal distances between TLS scans. The quality evaluation of the registration results shows that the mean of the normal distance were all smaller when planar features were the registration primitives in the three approaches, which indicates that planar features produced better registration results than the linear features.

4.2.6 Registration Between Scans 6 and 7

In this pairwise registration, scan 7 is the reference scan, and scan 6 is the source scan. The positions of TLS scans 6 and 7 are presented in Figure 4.20.

Fig. 4.20.: Position of TLS scans 6 and 7

4.2.6.1 Registration Between Scans 6 and 7 Using Planar Features

The extracted planar features in scans 6 and 7 are shown in Figure 4.21. The planar feature extraction is conducted by using I-LIVE. A plane fitting procedure, as stated in subsection 3.2.5, was performed to estimate plane parameters. The estimated plane parameters, standard deviations, and square roots of the a-posteriori variance factors for 19 pairs of planar features in scans 6 and 7 are presented in Table 4.45. As highlighted in the table, the standard deviation of the plane 7 in the source scan is large, which is resulting from the range error, since the plane 7 is 50 m away from the laser scanner. The plane 7 is narrow, which will also cause a large standard deviation. Plane 8, 10, 11 in the reference scan were narrow, which cause the large standard deviation. Plane 13 is on the roof of the building, and the surface is not flat, so the standard deviation of the plane 13 in the reference scan is also large. The standard deviation overall was below 1 cm for plane parameters in the source and reference scans. The small standard deviation values indicate the estimated plane parameters are reliable. Furthermore, the a-posteriori variance factor $\hat{\sigma}_0^2$ is used to check the quality of the estimated plane parameters. Since the weight matrix P is an identity matrix, the $\hat{\sigma}_0^2$ is the variance of the measurements. The square roots of the a-posteriori variance factors ($\hat{\sigma}_0$) after plane fitting are close to the expected accuracy

of around 2 mm according to the accuracy of the TLS, thus indicating the validity of the estimated plane parameters.

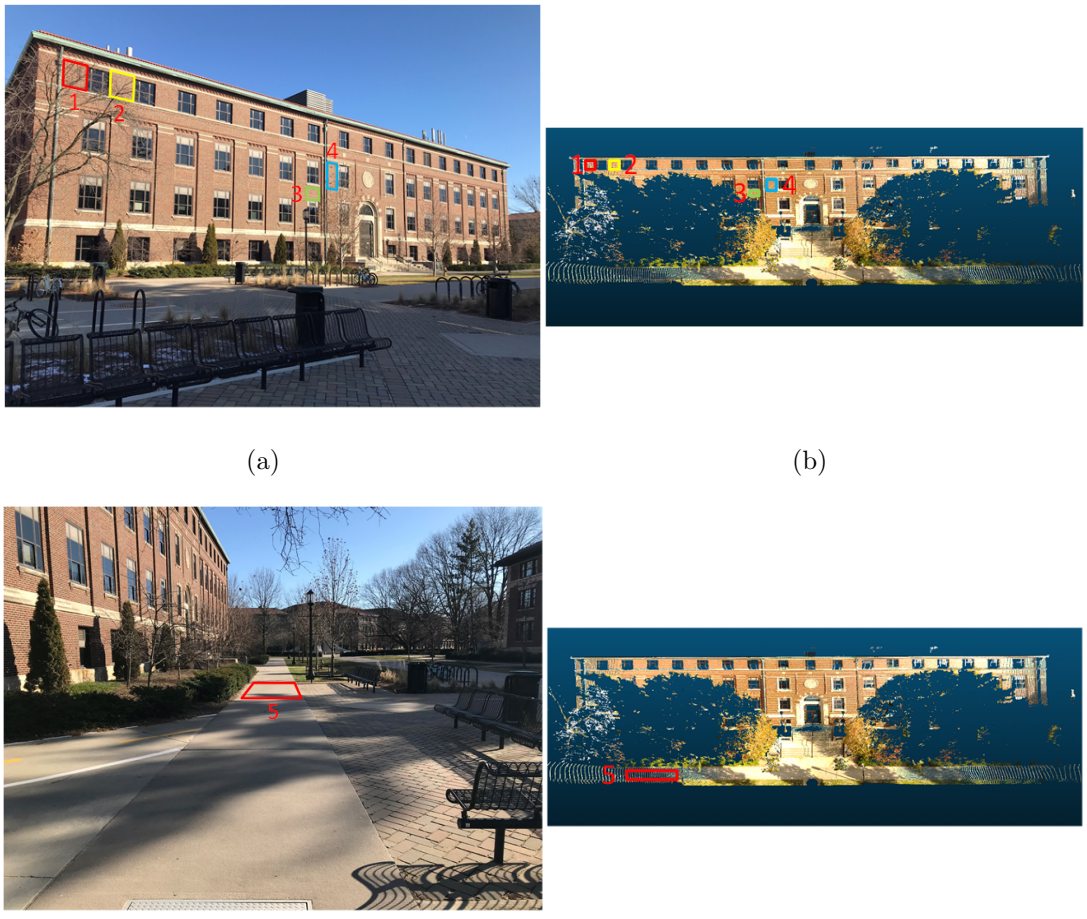

(a) (b)

(c) (d)

Fig. 4.21.: Planar features in the overlapping area between scans 6 and 7 displayed in images (a, c, e, g, i), which are captured by an external camera, and point clouds (b, d, f, h, j) (continued on next page)

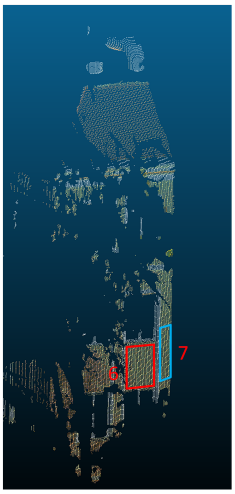

(e) (f)

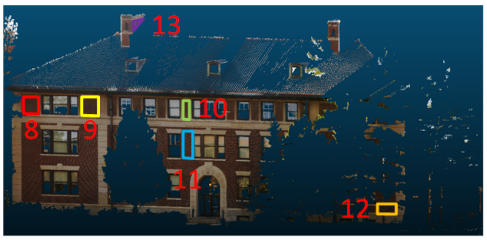

(g) (h)

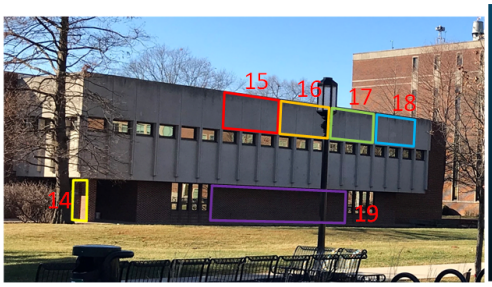

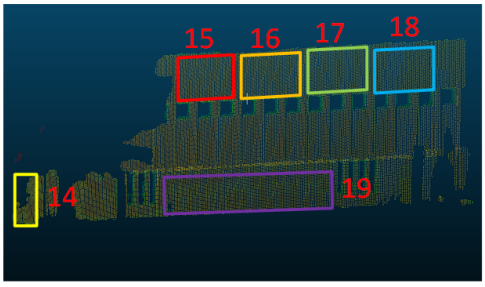

(i) (j)

Fig. 4.21.: Planar features in the overlapping area between scans 6 and 7 displayed in images (a, c, e, g, i), which are captured by an external camera, and point clouds (b, d, f, h, j) (continued from the previous page)

Table 4.45.: The estimated plane parameters, standard deviations, and square roots of the a-posteriori variance factors of 19 pairs of planar features in scans 6 and 7

	Plane ID	$a_x(m \pm m)$	$a_y(m \pm m)$	$a_z(m \pm m)$	$\hat{\sigma}_0(mm)$
	1	-4.2109 ($\pm$0.0028)	8.9952 ($\pm$0.0032)	0.0152 ($\pm$0.0010)	1.5
	2	-4.2047 ($\pm$0.0015)	8.9981 ($\pm$0.0017)	0.0229 ($\pm$0.0007)	1.4
	3	-4.2510 ($\pm$0.0003)	9.0846 ($\pm$0.0002)	-0.0146 ($\pm$0.0004)	1.2
	4	-4.1869 ($\pm$0.0003)	8.8995 ($\pm$0.0001)	0.0034 ($\pm$0.0001)	1.5
	5	-0.0084 ($\pm$0.0001)	-0.0049 ($\pm$0.0001)	-1.5320 ($\pm$0.0004)	2.7
	6	-48.0009 ($\pm$0.0036)	-22.5221 ($\pm$0.0042)	-0.1992 ($\pm$0.0036)	0.9
	7	-48.1363 ($\pm$0.0123)	-22.3809 ($\pm$0.0142)	-0.1279 ($\pm$0.0041)	1.3
	8	12.6399 ($\pm$0.0030)	-26.9305 ($\pm$0.0008)	0.0030 ($\pm$0.0022)	1.6
	9	12.6525 ($\pm$0.0014)	-26.9622 ($\pm$0.0004)	0.0875 ($\pm$0.0012)	1.2
Scan 6	10	12.5129 ($\pm$0.0032)	-26.9926 ($\pm$0.0010)	0.1036 ($\pm$0.0012)	1.0
	11	12.6204 ($\pm$0.0022)	-26.9370 ($\pm$0.0007)	0.0486 ($\pm$0.0009)	1.2
	12	12.5959 ($\pm$0.0012)	-26.9662 ($\pm$0.0018)	0.1056 ($\pm$0.0047)	0.9
	13	9.3673 ($\pm$0.0045)	4.3883 ($\pm$0.0020)	-0.0023 ($\pm$0.0031)	1.3
	14	-53.6285 ($\pm$0.0026)	-24.9887 ($\pm$0.0069)	0.0907 ($\pm$0.0100)	1.6

continued on next page

Table 4.45.: *continued*

	Plane ID	$a_x(m \pm m)$	$a_y(m \pm m)$	$a_z(m \pm m)$	$\hat{\sigma}_0(mm)$
	15	24.0171 (±0.0011)	-51.3153 (±0.0040)	-0.1045 (±0.0062)	1.8
	16	23.9849 (±0.0012)	-51.4508 (±0.0049)	-0.0971 (±0.0074)	2.1
	17	23.9823 (±0.0015)	-51.4611 (±0.0066)	-0.0778 (±0.0094)	2.5
	18	23.9766 (±0.0011)	-51.5041 (±0.0056)	0.0147 (±0.0074)	1.9
	19	24.8135 (±0.0003)	-52.9065 (±0.0010)	-0.0623 (±0.0042)	2.1
Scan 7	1	7.3733 (±0.0008)	4.6548 (±0.0003)	0.0089 (±0.0004)	1.3
	2	7.3939 (±0.0007)	4.6654 (±0.0003)	0.0167 (±0.0004)	1.3
	3	7.4759 (±0.0040)	4.7139 (±0.0013)	-0.0142 (±0.0015)	1.4
	4	7.1994 (±0.0042)	4.5690 (±0.0015)	0.0039 (±0.0004)	1.7
	5	-0.0058 (±0.0001)	0.0070 (±0.0000)	-1.4647 (±0.0003)	2.1
	6	-5.7942 (±0.0001)	9.1047 (±0.0016)	-0.0435 (±0.0005)	1.0
	7	-5.7862 (±0.0001)	9.1994 (±0.0011)	-0.0397 (±0.0003)	0.9
	8	-26.1451 (±0.0072)	-16.4811 (±0.0117)	-0.0064 (±0.0077)	2.0
	9	-26.2152 (±0.0043)	-16.5539 (±0.0078)	0.1157 (±0.0049)	1.5
	10	-26.1343 (±0.0079)	-16.3889 (±0.0170)	0.1149 (±0.0041)	1.3

continued on next page

Table 4.45.: *continued*

Plane ID	$a_x(m \pm m)$	$a_y(m \pm m)$	$a_z(m \pm m)$	$\hat{\sigma}_0(mm)$
11	-26.1671 ($\pm$0.0070)	-16.4953 ($\pm$0.0149)	0.0542 ($\pm$0.0041)	1.6
12	-26.1732 ($\pm$0.0002)	-16.4809 ($\pm$0.0026)	0.0477 ($\pm$0.0050)	0.8
13	28.0091 ($\pm$0.0031)	-44.4718 ($\pm$0.0064)	-0.0860 ($\pm$0.0130)	1.5
14	-9.0534 ($\pm$0.0028)	14.3831 ($\pm$0.0025)	0.0312 ($\pm$0.0014)	1.4
15	-48.9124 ($\pm$0.0012)	-30.8983 ($\pm$0.0008)	-0.1128 ($\pm$0.0027)	1.6
16	-49.0093 ($\pm$0.0010)	-30.8385 ($\pm$0.0006)	-0.1029 ($\pm$0.0024)	1.2
17	-49.0254 ($\pm$0.0017)	-30.8310 ($\pm$0.0009)	-0.0640 ($\pm$0.0037)	1.7
18	-49.0871 ($\pm$0.0014)	-30.8058 ($\pm$0.0007)	0.0301 ($\pm$0.0030)	1.3
19	-50.4322 ($\pm$0.0003)	-31.8969 ($\pm$0.0002)	-0.0630 ($\pm$0.0019)	1.3

The estimated transformation parameters, standard deviations, a-posteriori variance factors, and execution times from the planar feature-based approach, pseudo-conjugate point-based method, and closed-form solution using the planar features in scans 6 and 7 are presented in Table 4.46. Since the rotation parameters were estimated by quaternions in the closed-form solution, there is no standard deviation for the rotation parameters. The standard deviation values of the registration parameters indicate that reliable results were estimated using the three alternative registration approaches. The standard deviations of the estimated parameters were below 0.3 mm for the translation parameters and below 0.0006 degrees for the rotation angels by using the pseudo-conjugate point-based method, while it is below 5 mm and 0.011 degrees for the translation and the rotation parameters, respectively, by using the planar feature-based approach, which indicates that the pseudo-conjugate point-based method can produce better registration results than the planar feature-based approach. In the closed-form solution, the standard deviations of the estimated parameters were below 0.2 mm for the translation parameters, which indicates the estimated translation parameters are reliable.

Furthermore, the a-posteriori variance factor $\hat{\sigma}_0^2$ in Table 4.46 is used to evaluate the estimated transformation parameters. In the planar feature-based approach, the weight matrix P is derived by the inverse of the variance-covariance matrix, so the $\hat{\sigma}_0^2$ should be close to 1. The a-posteriori variance factor $\hat{\sigma}_0^2$ was 718.7692, which indicates that the noise level in the observation is larger than previously assumed. In the pseudo-conjugate point-based method and closed-form solution, the $\hat{\sigma}_0^2$ is the variance of the observations since the weight matrix P is an identity matrix. The square roots of the a-posteriori variance factors ($\hat{\sigma}_0$) in Table 4.46 are not significantly different from the expected accuracy of around 2 mm according to the accuracy of the TLS, thus indicating the validity of the estimated transformation parameters using the pseudo-conjugate point-based method and closed-form solution based on planar features. Regarding the execution time, the planar feature-based approach had the shortest execution time, as listed in Table 4.46. The pseudo-conjugate point-based

and closed-form approaches based on planar features led to longer execution times due to a large number of point cloud data.

The quality evaluation of the registration results was analyzed by calculating the point-to-patch normal distances between TLS scans. After applying the estimated registration parameters, the point clouds in the source scan were transformed to the reference scan. A point-patch pair is established by using the approach discussed in section 3.4. The normal distance between the transformed point and the patch must be within a certain threshold, which is 10 cm in this test. The mean, standard deviation, and RMSE of the point-to-patch normal distances between the TLS scans are presented in Table 4.47. The mean, standard deviation, and RMSE of the calculated point-to-patch normal distances of each approach were all below 7 mm, which substantiates the quality of the registration results. In the planar feature-based approach and pseudo-conjugate point-based method, the mean of the calculated point-to-patch normal distances were around 6.2 mm, and the value of standard deviation and RMSE is identical to each other between the two approaches, which indicates the equivalency between the two approaches. The average point-to-patch normal distances is 6.9 mm for the closed-form solution. The RMSE value is also larger than the value produced by using the planar-feature based approach and pseudo-conjugate point-based method, which indicates that the registration results produced by the closed-form solution are worse than the registration results by using the other two approaches.

Table 4.46.: The estimated transformation parameters, standard deviations, a-posteriori variance factors, and execution times from the planar feature-based approach, pseudo-conjugate point-based method, and closed-form solution using the planar features in scans 6 and 7

	$t_x(m \pm m)$	$t_y(m \pm m)$	$t_z(m \pm m)$	$\omega(^\circ \pm ^\circ)$	$\phi(^\circ \pm ^\circ)$	$\kappa(^\circ \pm ^\circ)$	$\hat{\sigma}_0^2$	$\hat{\sigma}_0$	Execution time (seconds)
Planar feature-based approach	21.4982 (±0.0012)	-36.3299 (±0.0014)	-0.1851 (±0.0047)	0.0029 (±0.0070)	0.0316 (±0.0108)	82.8261 (±0.0008)	718.7692	26.8099	0.1
Pseudo-conjugate point-based method	21.4971 (±0.0001)	-36.3298 (±0.0001)	-0.1854 (±0.0002)	0.0079 (±0.0003)	0.0327 (±0.0005)	82.8265 (±0.0000)	5.43E-06 (m^2)	2.3 (mm)	16.5
Closed-form solution	21.4999 (±0.0000)	-36.3250 (±0.0000)	-0.1962 (±0.0001)	0.0016 (N/A)	0.0002 (N/A)	82.8201 (N/A)	9.21E-06 (m^2)	3.0 (mm)	25.9

Table 4.47.: Quantitative comparison between planar feature-based approach, pseudo-conjugate point-based method, and closed-form solution based on planar features through the mean, standard deviation, and RMSE of the point-to-patch normal distances between the TLS scans 6 and 7

	Mean (m)	Standard deviation (m)	RMSE (m)	Number of used points	Total number of points
Planar feature-based approach	0.0062	0.0107	0.0124	82,725	787,901
Pseudo-conjugate point-based method	0.0062	0.0107	0.0124	82,527	787,901
Closed-form solution	0.0069	0.0107	0.0127	83,026	787,901

4.2.6.2 Registration Between Scans 6 and 7 Using Linear Features

After the planar features were used for the introduced registration approaches, the linear features were used as the registration primitives for the same experiment data to investigate the quality of the registration results with a different type of feature. Linear features are extracted indirectly using the segmented planar features from the TLS scans. The estimated line parameters and standard deviations of linear features which are derived by the intersection of neighboring planar features in scans 6 and 7 are presented in Table 4.48. Then, twenty points are simulated along the derived linear features in each scan. The simulated points along linear features are presented in Figure 4.22. The standard deviation highlighted in red were larger than 1.2 cm. This results from using planes 8, 9, 10, 11, which has large range errors. The standard deviation of other lines was below 0.0006 and 8.6 mm for the direction

vector (a_x, a_y, a_z) and position parameter (b_x, b_y, b_z), respectively, which indicates the estimated line parameters are reliable.

Table 4.48.: The estimated line parameters and standard deviations of linear features which are derived by the intersection of neighboring planar features in scans 6 and 7

	Plane Intersection	a_x (±)	a_y (±)	a_z (±)	b_x (m±m)	b_y (m±m)	b_z (m±m)
Scan 6	1&5	1 (±0)	0.4681 (±0.0002)	-0.0070 (±0.0000)	0 (±0)	10.9691 (±0.0052)	-1.5671 (±0.0007)
	2&5	1 (±0)	0.4673 (±0.0001)	-0.0070 (±0.0000)	0 (±0)	10.9669 (±0.0028)	-1.5671 (±0.0007)
	3&5	1 (±0)	0.4679 (±0.0000)	-0.0070 (±0.0000)	0 (±0)	11.0713 (±0.0004)	-1.5674 (±0.0007)
	4&5	1 (±0)	0.4705 (±0.0000)	-0.0070 (±0.0000)	0 (±0)	10.8699 (±0.0003)	-1.5668 (±0.0007)
	6&5	-0.4692 (±0.0001)	1 (±0)	-0.0006 (±0.0001)	-58.5640 (±0.0013)	0 (±0)	-1.2105 (±0.0016)
	7&5	-0.4649 (±0.0004)	1 (±0)	-0.0006 (±0.0001)	-58.5394 (±0.0036)	0 (±0)	-1.2106 (±0.0016)
	8&5	1 (±0)	0.4694 (±0.0001)	-0.0070 (±0.0000)	0 (±0)	-32.8632 (±0.0032)	-1.4271 (±0.0020)
	9&5	1 (±0)	0.4692 (±0.0001)	-0.0070 (±0.0000)	0 (±0)	-32.9046 (±0.0014)	-1.4269 (±0.0020)
	10&5	1 (±0)	0.4635 (±0.0001)	-0.0070 (±0.0000)	0 (±0)	-32.7991 (±0.0024)	-1.4273 (±0.0020)

continued on next page

Table 4.48.: *continued*

Plane Intersection	a_x (±)	a_y (±)	a_z (±)	b_x (m±m)	b_y (m±m)	b_z (m±m)
11&5	1 (±0)	0.4685 (±0.0001)	-0.0070 (±0.0000)	0 (±0)	-32.8525 (±0.0016)	-1.4271 (±0.0020)
12&5	1 (±0)	0.4671 (±0.0001)	-0.0070 (±0.0000)	0 (±0)	-32.8558 (±0.0005)	-1.4271 (±0.0020)
13&5	-0.4685 (±0.0001)	1 (±0)	-0.0006 (±0.0001)	11.4227 (±0.0056)	0 (±0)	-1.5948 (±0.0007)
14&5	-0.4660 (±0.0001)	1 (±0)	-0.0006 (±0.0001)	-65.2744 (±0.0085)	0 (±0)	-1.1736 (±0.0018)
15&5	1 (±0)	0.4680 (±0.0001)	-0.0070 (±0.0000)	0 (±0)	-62.5535 (±0.0022)	-1.3322 (±0.0036)
16&5	1 (±0)	0.4662 (±0.0001)	-0.0070 (±0.0000)	0 (±0)	-62.6295 (±0.0029)	-1.3320 (±0.0036)
17&5	1 (±0)	0.4660 (±0.0001)	-0.0070 (±0.0000)	0 (±0)	-62.6356 (±0.0040)	-1.3320 (±0.0036)
18&5	1 (±0)	0.4655 (±0.0001)	-0.0070 (±0.0000)	0 (±0)	-62.6663 (±0.0035)	-1.3319 (±0.0036)
19&5	1 (±0)	0.4690 (±0.0000)	-0.0070 (±0.0000)	0 (±0)	-64.5427 (±0.0006)	-1.3259 (±0.0037)
9&13	-0.0010 (±0.0003)	0.0028 (±0.0001)	1 (±0)	21.9994 (±0.0045)	-22.5763 (±0.0021)	0 (±0)
1&14	0.0020 (±0.0002)	-0.0007 (±0.0001)	1 (±0)	-57.7792 (±0.0058)	-16.0812 (±0.0042)	0 (±0)

continued on next page

Table 4.48.: *continued*

	Plane Intersection	a_x (±)	a_y (±)	a_z (±)	b_x (m±m)	b_y (m±m)	b_z (m±m)
	2&14	0.0024 (±0.0002)	-0.0014 (±0.0001)	1 (±0)	-57.7963 (±0.0056)	-16.0445 (±0.0034)	0 (±0)
	3&14	0.0008 (±0.0002)	0.0020 (±0.0001)	1 (±0)	-57.8243 (±0.0056)	-15.9844 (±0.0029)	0 (±0)
	4&14	0.0015 (±0.0002)	0.0003 (±0.0001)	1 (±0)	-57.6903 (±0.0056)	-16.2720 (±0.0029)	0 (±0)
	15&14	0.0022 (±0.0002)	-0.0010 (±0.0001)	1 (±0)	-29.6562 (±0.0004)	-76.4361 (±0.0007)	0 (±0)
Scan 7	1&5	-0.6313 (±0.0001)	1 (±0)	0.0073 (±0.0000)	10.3138 (±0.0007)	0 (±0)	-1.5057 (±0.0004)
	2&5	-0.6310 (±0.0001)	1 (±0)	0.0073 (±0.0000)	10.3411 (±0.0007)	0 (±0)	-1.5058 (±0.0004)
	3&5	-0.6305 (±0.0002)	1 (±0)	0.0073 (±0.0000)	10.4454 (±0.0042)	0 (±0)	-1.5062 (±0.0004)
	4&5	-0.6346 (±0.0002)	1 (±0)	0.0073 (±0.0000)	10.0999 (±0.0044)	0 (±0)	-1.5048 (±0.0004)
	6&5	1 (±0)	0.6364 (±0.0001)	-0.0009 (±0.0001)	0 (±0)	12.7856 (±0.0010)	-1.4034 (±0.0005)
	7&5	1 (±0)	0.6290 (±0.0001)	-0.0009 (±0.0001)	0 (±0)	12.8329 (±0.0006)	-1.4032 (±0.0005)
	8&5	-0.6304 (±0.0003)	1 (±0)	0.0073 (±0.0000)	-36.5340 (±0.0191)	0 (±0)	-1.3200 (±0.0016)

continued on next page

Table 4.48.: *continued*

Plane Intersection	a_x (±)	a_y (±)	a_z (±)	b_x (m±m)	b_y (m±m)	b_z (m±m)
9&5	-0.6314 (±0.0002)	1 (±0)	0.0073 (±0.0000)	-36.6747 (±0.0124)	0 (±0)	-1.3194 (±0.0016)
10&5	-0.6271 (±0.0005)	1 (±0)	0.0073 (±0.0000)	-36.4181 (±0.0261)	0 (±0)	-1.3205 (±0.0016)
11&5	-0.6304 (±0.0004)	1 (±0)	0.0073 (±0.0000)	-36.5683 (±0.0230)	0 (±0)	-1.3199 (±0.0016)
12&5	-0.6297 (±0.0001)	1 (±0)	0.0073 (±0.0000)	-36.5535 (±0.0035)	0 (±0)	-1.3199 (±0.0016)
13&5	1 (±0)	0.6298 (±0.0001)	-0.0009 (±0.0001)	0 (±0)	-62.1092 (±0.0056)	-1.7630 (±0.0017)
14&5	1 (±0)	0.6294 (±0.0001)	-0.0009 (±0.0001)	0 (±0)	20.0847 (±0.0050)	-1.3684 (±0.0007)
15&5	-0.6317 (±0.0000)	1 (±0)	0.0073 (±0.0000)	-68.4286 (±0.0005)	0 (±0)	-1.1936 (±0.0029)
16&5	-0.6293 (±0.0000)	1 (±0)	0.0073 (±0.0000)	-68.4118 (±0.0004)	0 (±0)	-1.1936 (±0.0029)
17&5	-0.6289 (±0.0000)	1 (±0)	0.0073 (±0.0000)	-68.4129 (±0.0005)	0 (±0)	-1.1936 (±0.0029)
18&5	-0.6276 (±0.0000)	1 (±0)	0.0073 (±0.0000)	-68.4207 (±0.0004)	0 (±0)	-1.1936 (±0.0029)
19&5	-0.6325 (±0.0000)	1 (±0)	0.0073 (±0.0000)	-70.6047 (±0.0001)	0 (±0)	-1.1850 (±0.0029)

continued on next page

Table 4.48.: *continued*

Plane Intersection	a_x (±)	a_y (±)	a_z (±)	b_x (m±m)	b_y (m±m)	b_z (m±m)
9&13	0.0040 (±0.0002)	0.0006 (±0.0002)	1 (±0)	1.8265 (±0.0027)	-60.9622 (±0.0038)	0 (±0)
1&14	0.0001 (±0.0001)	-0.0021 (±0.0001)	1 (±0)	-1.6930 (±0.0025)	19.0161 (±0.0036)	0 (±0)
2&14	-0.0006 (±0.0001)	-0.0026 (±0.0001)	1 (±0)	-1.6701 (±0.0025)	19.0305 (±0.0036)	0 (±0)
3&14	0.0023 (±0.0002)	-0.0007 (±0.0001)	1 (±0)	-1.5851 (±0.0056)	19.0840 (±0.0048)	0 (±0)
4&14	0.0006 (±0.0001)	-0.0018 (±0.0001)	1 (±0)	-1.8904 (±0.0059)	18.8918 (±0.0049)	0 (±0)
15&14	-0.0007 (±0.0001)	-0.0026 (±0.0001)	1 (±0)	-58.0393 (±0.0003)	-16.4508 (±0.0002)	0 (±0)

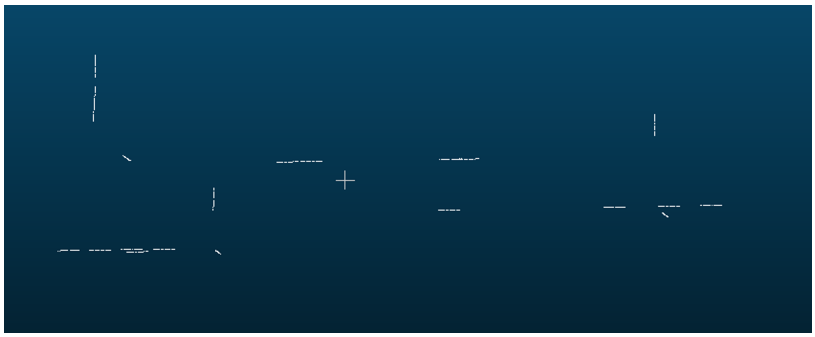

Fig. 4.22.: Simulated points along linear features in the overlapping area between scans 6 and 7

After the estimation of line parameters, the next step is to estimate transformation parameters using the three alternative registration approaches. The aim of the

registration process is to estimate the 3D similarity transformation parameters, which include three translations (t_x, t_y, t_z) and three rotation parameters (ω, ϕ, κ). The observations and weight matrix P in the three alternative registration approaches are specified as follows. In the linear feature-based approach, the observations are estimated line parameters from a line fitting procedure, and the weight matrix P is defined by the inverse of the variance-covariance matrix of extracted line parameters, which is derived by using the law of error propagation.

In the pseudo-conjugate point-based method, the observations are coordinates of simulated points along lines in the source and reference scans. The weight matrix P depends on the noise added to the point clouds. The estimated line parameters in the reference scan are used to modify the weight matrix to eliminate the additional vector resulting from using non-corresponding points along linear features. In the 3D similarity transformation function, each 3D point pair contributes three equations towards the transformation parameters estimation. There are 480 points along linear features in each scan, so the total number of observation equations is $480 \times 3 = 1,440$. However, the discussion in the subsection 3.3.2 indicates that the effective contribution is only two equations from each point pair. According to Equation (3.73) in the subsection 3.3.2, all the elements in the weight matrix pertaining to the U-axis along the linear features are assigned a zero weight. The modified weight matrix in the LSA procedure nullifies the error along the line direction while minimizing the errors in the two directions normal to the line. Therefore, the effective contribution of a 3D point pair towards redundancy is 2 equations instead of 3. In this case, the redundancy is given by the difference between the rank of the weight matrix and the number of the unknowns, thus resulting in a redundancy of $480 \times 2 - 6 = 954$.

In the closed-form solution, the rotation parameters and the translation parameters are estimated separately. The rotation matrix is derived first using a quaternion-based approach, which is a single-step solution. The observations are the direction vectors of linear features. A weight matrix is not used in this procedure, and there is no standard deviation to evaluate the estimated rotation parameters. Once the rota-

tion matrix is derived, the next step is to estimate translation parameters using the pseudo-conjugate point-based method. In this step, the observations are coordinates of points along linear features, and the weight matrix P is obtained as the inverse of the variance-covariance matrix of the observations.

The estimated transformation parameters, standard deviations, a-posteriori variance factors, and execution times from the linear feature-based approach, pseudo-conjugate point-based method, and closed-form solution using the linear features in scans 6 and 7 are presented in Table 4.49. In the linear feature-based approach, the standard deviation overall was below 0.2 cm and 0.005 degrees for the translation and the rotation parameters, respectively, while it is below 7.2 cm and 0.12 degrees in the registration results by using the pseudo-conjugate point-based method. In the closed-form registration results, the standard deviation overall was below 4.7 cm for the translation parameters. Since the rotation parameters were estimated by quaternions, there is no standard deviation for the rotation parameters. In summary, according to the standard deviation, reliable transformation parameters were estimated using the introduced three registration approaches. The linear feature-based approach produced better results than the other two approaches.

Furthermore, the a-posteriori variance factor $\hat{\sigma}_0^2$ in Table 4.49 is used to evaluate the estimated transformation parameters. In the linear feature-based approach, the weight matrix P is derived by the inverse of variance-covariance matrix, so the $\hat{\sigma}_0^2$ should be close to 1. The a-posteriori variance factor $\hat{\sigma}_0^2$ was 42.662, which indicates that the noise level in the observation is larger than previously assumed. In the pseudo-conjugate point-based method and closed-form solution using linear features, the $\hat{\sigma}_0^2$ is the variance of the observations since the weight matrix P is an identity matrix. The square roots of the a-posteriori variance factors ($\hat{\sigma}_0$) in Table 4.49 are larger than the expected accuracy of around 2 mm according to the accuracy of the TLS. Since there are a limited number of planar features with various orientation in the overlapping area between scans 6 and 7, linear features are extracted indirectly using the segmented planar features which are not physically connected, and most

of the extracted linear features are coplanar. Also, planes 14-19 in the source scan are 50 m away from the laser scanner, so the range error is also large. Regarding the execution time, the linear feature-based approach had the shortest execution time, as listed in Table 4.49. The pseudo-conjugate point-based and closed-form approaches based on linear features led to longer execution times due to a large number of point cloud data.

The quality evaluation of the registration results was analyzed by calculating the point-to-patch normal distances between TLS scans. After applying the estimated registration parameters, the point clouds in the source scan were transformed to the reference scan. A point-patch pair is established by using the approach discussed in section 3.4. The normal distance between the transformed point and the patch must be within a certain threshold, which is 10 cm in this test. The mean, standard deviation, and RMSE of the point-to-patch normal distances between the TLS scans are presented in Table 4.50. The mean of the calculated point-to-patch normal distances of the pseudo-conjugate point-based method was 3.58 cm, while it was below 1.7 cm for the linear feature-based approach and closed-form solution, which indicates that the pseudo-conjugate point-based method produced worse registration results than the feature-based approach and closed-form solution using linear features. The mean, standard deviation, and RMSE of the calculated point-to-patch normal distances of the closed-form solution were all larger than the values of the linear feature-based approach, which indicates that the registration results using the closed-form solution were worse than the pseudo-conjugate point-based method.

Table 4.49.: The estimated transformation parameters, standard deviations, a-posteriori variance factors, and execution times from the linear feature-based approach, pseudo-conjugate point-based method, and closed-form solution using the linear features in scans 6 and 7

	$t_x(m \pm m)$	$t_y(m \pm m)$	$t_z(m \pm m)$	$\omega(^\circ \pm ^\circ)$	$\phi(^\circ \pm ^\circ)$	$\kappa(^\circ \pm ^\circ)$	$\hat{\sigma}_0^2$	$\hat{\sigma}_0$	Execution time (seconds)
Linear feature-based approach	21.5008 (±0.0007)	-36.3280 (±0.0013)	-0.1936 (±0.0019)	-0.0016 (±0.0048)	0.0082 (±0.0029)	82.8236 (±0.0008)	42.6620	6.5316	0.1
Pseudo-conjugate point-based method	21.4551 (±0.0429)	-36.3345 (±0.0712)	-0.1948 (±0.0596)	0.0010 (±0.1167)	0.0226 (±0.0662)	82.8794 (±0.0568)	0.2573 (m^2)	0.5073 (m)	2.8
Closed-form solution	21.4691 (±0.0406)	-36.2783 (±0.0469)	-0.2047 (±0.0378)	0.0141 (N/A)	0.0040 (N/A)	82.8200 (N/A)	0.2568 (m^2)	0.5068 (m)	5.4

Table 4.50.: Quantitative comparison between linear feature-based approach, pseudo-conjugate point-based method, and closed-form solution based on linear features through the mean, standard deviation, and RMSE of the point-to-patch normal distances between the TLS scans 6 and 7

	Mean (m)	Standard deviation (m)	RMSE (m)	Number of used points	Total number of points
Linear feature-based approach	0.0061	0.0107	0.0123	82,972	787,901
Pseudo-conjugate point-based method	0.0358	0.0179	0.0401	79,060	787,901
Closed-form solution	0.0170	0.0200	0.0262	84,962	787,901

Moreover, the comparison between registration approaches using linear and planar features is conducted based on point-to-patch normal distances between TLS scans. The quality evaluation of the registration results shows that these two features can produce equivalent registration results by using the feature-based approach since the normal distances calculated were all below 6.3 mm. However, the pseudo-conjugate point-based method and closed-form solution can produce better registration results when the planar features were the registration primitives. For example, when linear features are the registration primitives, the normal distances calculated using the registration results of the two approaches were larger than 1.6 cm, while it was below 7 mm when planar features are the registration primitives.

4.2.7 Registration Between Scans 7 and 8

The positions of TLS scans 7 and 8 are presented in Figure 4.23. In this pairwise registration, scan 8 is the reference scan, and scan 7 is the source scan.

Fig. 4.23.: Position of TLS scans 7 and 8

4.2.7.1 Registration Between Scans 7 and 8 Using Planar Features

The planar features, as shown in Figure 4.24, in scans 7 and 8 are extracted through I-LIVE. Then, a plane fitting procedure, as stated in subsection 3.2.5, was conducted to estimate plane parameters. The estimated plane parameters, standard deviations, and square roots of the a-posteriori variance factors of 16 pairs of planar features in scans 7 and 8 are presented in Table 4.51. The standard deviation overall was below 1 cm for plane parameters in the source and reference scans, except planes 13, 14, 15, and 16 in the source scan, as highlighted in the table. The small standard deviation values indicate the estimated plane parameters are reliable. In the source scan, plane 13, 14, 15 and 16 were 80 m away from TLS, and the large standard deviation didn't happen in the reference scan, so the large standard deviation of plane 13, 14, 15 and 16 in the source scan resulted from range error. Furthermore, the a-posteriori variance factor $\hat{\sigma}_0^2$ is used to check the quality of the estimated plane parameters. Since the weight matrix P is an identity matrix, the $\hat{\sigma}_0^2$ is the variance

of the measurements. The square roots of the a-posteriori variance factors ($\hat{\sigma}_0$) after plane fitting are close to the expected accuracy of around 2 mm according to the accuracy of the TLS, thus indicating the validity of the estimated plane parameters.

(a) (b)

(c) (d)

Fig. 4.24.: Planar features in the overlapping area between scans 7 and 8 displayed in images (a, c, e), which are captured by an external camera, and point clouds (b, d, f) (continued on next page)

(e) (f)

Fig. 4.24.: Planar features in the overlapping area between scans 7 and 8 displayed in images (a, c, e), which are captured by an external camera, and point clouds (b, d, f) (continued from the previous page)

The estimated transformation parameters, standard deviations, a-posteriori variance factors, and execution times from the planar feature-based approach, pseudo-conjugate point-based method, and closed-form solution using the planar features in scans 7 and 8 are presented in Table 4.52. Since the rotation parameters were estimated by quaternions in the closed-form solution, there is no standard deviation for the rotation parameters. The standard deviation values of the registration parameters indicate that reliable results were estimated using the three alternative registration approaches. The standard deviations of the estimated parameters were below 0.3 mm for the translation parameters and below 0.0005 degrees for the rotation angels by using the pseudo-conjugate point-based method, while it is below 6 mm and 0.02 degrees for the translation and the rotation parameters, respectively, by using the planar feature-based approach, which indicates that the pseudo-conjugate point-based method can produce better registration results than the planar feature-based approach. In the closed-form solution, the standard deviations of the estimated parameters were below 0.2 mm for the translation parameters, which indicates the estimated translation parameters are reliable.

Table 4.51.: The estimated plane parameters, standard deviations, and square roots of the a-posteriori variance factors of 16 pairs of planar features in scans 7 and 8

	Plane ID	$a_x(m \pm m)$	$a_y(m \pm m)$	$a_z(m \pm m)$	$\hat{\sigma}_0(mm)$
Scan 7	1	43.3392 (±0.0004)	27.2809 (±0.0004)	-0.0113 (±0.0011)	2.2
	2	7.0846 (±0.0027)	-11.2005 (±0.0028)	0.0022 (±0.0015)	1.2
	3	4.6496 (±0.0004)	-7.2971 (±0.0003)	0.0035 (±0.0001)	1.5
	4	4.5975 (±0.0007)	-7.2557 (±0.0005)	-0.0065 (±0.0001)	1.6
	5	4.5597 (±0.0001)	-7.2416 (±0.0000)	0.0007 (±0.0000)	1.3
	6	0.0067 (±0.0001)	0.0480 (±0.0001)	-1.5263 (±0.0007)	2.0
	7	-5.8005 (±0.0001)	9.1913 (±0.0005)	-0.0020 (±0.0001)	1.9
	8	-5.8082 (±0.0001)	9.2191 (±0.0006)	0.0130 (±0.0001)	1.0
	9	-5.8234 (±0.0003)	9.2501 (±0.0013)	0.0243 (±0.0004)	0.9
	10	-5.8103 (±0.0007)	9.2048 (±0.0025)	0.0132 (±0.0006)	1.1
	11	-5.8092 (±0.0005)	9.2162 (±0.0025)	0.0109 (±0.0007)	2.2
	12	-5.8165 (±0.0008)	9.2238 (±0.0028)	0.0241 (±0.0007)	1.5
	13	69.8697 (±0.0076)	45.0881 (±0.0135)	-0.7011 (±0.0204)	1.9
	14	77.1011 (±0.0054)	48.9657 (±0.0082)	-0.0116 (±0.0122)	1.5

continued on next page

Table 4.51.: *continued*

	Plane ID	$a_x(m \pm m)$	$a_y(m \pm m)$	$a_z(m \pm m)$	$\hat{\sigma}_0(mm)$
	15	72.2349 (±0.0046)	45.6446 (±0.0063)	0.1810 (±0.0160)	1.3
	16	72.1911 (±0.0145)	45.6905 (±0.0189)	-0.0578 (±0.0175)	1.6
Scan 8	1	7.3667 (±0.0001)	14.9560 (±0.0000)	0.0009 (±0.0001)	2.3
	2	12.3124 (±0.0005)	-6.0341 (±0.0002)	0.0042 (±0.0004)	1.0
	3	8.0864 (±0.0001)	-3.9294 (±0.0001)	-0.0019 (±0.0001)	1.4
	4	8.1016 (±0.0003)	-3.9637 (±0.0004)	-0.0101 (±0.0001)	1.6
	5	8.1452 (±0.0003)	-4.0115 (±0.0003)	-0.0035 (±0.0001)	1.3
	6	-0.0175 (±0.0001)	0.0352 (±0.0001)	-1.2354 (±0.0008)	1.8
	7	-9.3187 (±0.0015)	4.5775 (±0.0001)	0.0053 (±0.0002)	1.8
	8	-9.3016 (±0.0004)	4.5827 (±0.0001)	0.0060 (±0.0002)	1.0
	9	-9.3308 (±0.0002)	4.5993 (±0.0001)	0.0280 (±0.0001)	0.9
	10	-9.3388 (±0.0001)	4.5833 (±0.0001)	0.0197 (±0.0001)	1.0
	11	-9.3173 (±0.0004)	4.5847 (±0.0002)	0.0121 (±0.0002)	2.2
	12	-9.3349 (±0.0001)	4.5935 (±0.0001)	0.0289 (±0.0001)	1.5
	13	21.0115 (±0.0022)	43.8408 (±0.0013)	-0.4447 (±0.0040)	1.9

continued on next page

Table 4.51.: *continued*

Plane ID	$a_x(m \pm m)$	$a_y(m \pm m)$	$a_z(m \pm m)$	$\hat{\sigma}_0(mm)$
14	24.8748 ($\pm$0.0031)	51.0594 ($\pm$0.0014)	0.0578 ($\pm$0.0021)	1.2
15	22.4239 ($\pm$0.0018)	45.7040 ($\pm$0.0007)	0.1365 ($\pm$0.0037)	1.0
16	22.4377 ($\pm$0.0093)	45.6925 ($\pm$0.0024)	-0.0813 ($\pm$0.0073)	1.6

Table 4.52.: The estimated transformation parameters, standard deviations, a-posteriori variance factors, and execution times from the planar feature-based approach, pseudo-conjugate point-based method, and closed-form solution using the planar features in scans 7 and 8

	$t_x(m \pm m)$	$t_y(m \pm m)$	$t_z(m \pm m)$	$\omega(^\circ \pm ^\circ)$	$\phi(^\circ \pm ^\circ)$	$\kappa(^\circ \pm ^\circ)$	$\hat{\sigma}_0^2$	$\hat{\sigma}_0$	Execution time (seconds)
Planar feature-based approach	-14.7908 (±0.0005)	-31.2148 (±0.0007)	-0.4120 (±0.0059)	-0.0165 (±0.0102)	-0.0021 (±0.0156)	-31.5782 (±0.0010)	251.2683	15.8514	0.3
Pseudo-conjugate point-based method	-14.7907 (±0.0000)	-31.2144 (±0.0000)	-0.4149 (±0.0002)	-0.0250 (±0.0003)	0.0062 (±0.0004)	-31.5789 (±0.0000)	3.16E-06 (m^2)	1.8 (mm)	80.2
Closed-form solution	-14.7932 (±0.0000)	-31.2135 (±0.0000)	-0.4067 (±0.0001)	-0.0147 (N/A)	-0.0185 (N/A)	-31.5738 (N/A)	3.58E-06 (m^2)	1.9 (mm)	81.7

Furthermore, the a-posteriori variance factor $\hat{\sigma}_0^2$ in Table 4.52 is used to evaluate the estimated transformation parameters. In the planar feature-based approach, the weight matrix P is derived by the inverse of the variance-covariance matrix, so the $\hat{\sigma}_0^2$ should be close to 1. The a-posteriori variance factor $\hat{\sigma}_0^2$ was 251.2683, which indicates that the noise level in the observation is larger than previously assumed. In the pseudo-conjugate point-based method and closed-form solution, the $\hat{\sigma}_0^2$ is the variance of the observations since the weight matrix P is an identity matrix. The square roots of the a-posteriori variance factors ($\hat{\sigma}_0$) in Table 4.52 are below the expected accuracy of around 2 mm according to the accuracy of the TLS, thus indicating the validity of the estimated transformation parameters using the pseudo-conjugate point-based method and closed-form solution based on planar features. Regarding the execution time, the planar feature-based approach had the shortest execution time, as listed in Table 4.52. The pseudo-conjugate point-based and closed-form approaches based on planar features led to longer execution times due to a large number of point cloud data.

The quality evaluation of the registration results was analyzed by calculating the point-to-patch normal distances between TLS scans. After applying the estimated registration parameters, the point clouds in the source scan were transformed to the reference scan. A point-patch pair is established by using the approach discussed in section 3.4. The normal distance between the transformed point and the patch must be within a certain threshold, which is 10 cm in this test. The mean, standard deviation, and RMSE of the point-to-patch normal distances between the TLS scans are presented in Table 4.53. The mean, standard deviation, and RMSE of the calculated point-to-patch normal distances of each approach were all below 6 mm, which substantiates the quality of the registration results and indicates the equivalency of the registration results between the three registration approaches using planar features.

Table 4.53.: Quantitative comparison between planar feature-based approach, pseudo-conjugate point-based method, and closed-form solution based on planar features through the mean, standard deviation, and RMSE of the point-to-patch normal distances between the TLS scans 7 and 8

	Mean (m)	Standard deviation (m)	RMSE (m)	Number of used points	Total number of points
Planar feature-based approach	0.0020	0.0052	0.0055	116,608	588,604
Pseudo-conjugate point-based method	0.0021	0.0053	0.0057	116,254	588,604
Closed-form solution	0.0021	0.0051	0.0055	116,524	588,604

4.2.7.2 Registration Between Scans 7 and 8 Using Linear Features

After the planar features were used for the introduced registration approaches, the linear features were used as the registration primitives for the same experiment data to investigate the quality of the registration results with a different type of feature. Linear features are extracted indirectly using the segmented planar features from the TLS scans. The estimated line parameters and standard deviations of linear features which are derived by the intersection of neighboring planar features in scans 7 and 8 are presented in Table 4.54. Then, twenty points are simulated along the derived linear features in each scan. The simulated points along linear features are presented in Figure 4.25. The standard deviation highlighted in red were larger than 1.2 cm. This results from using the plane 13 and 16, which has large range errors. The standard deviation of other lines was below 0.0003 and 7.5 mm for the direction

vector (a_x, a_y, a_z) and position parameter (b_x, b_y, b_z), respectively, which indicates the estimated line parameters are reliable.

Table 4.54.: The estimated line parameters and standard deviations of linear features which are derived by the intersection of neighboring planar features in scans 7 and 8

	Plane Intersection	a_x (±)	a_y (±)	a_z (±)	b_x (m±m)	b_y (m±m)	b_z (m±m)
Scan 7	1&2	0.0001 (±0.0001)	0.0003 (±0.0001)	1 (±0)	50.3398 (±0.0008)	16.1595 (±0.0012)	0 (±0)
	1&3	-0.0000 (±0.0000)	0.0005 (±0.0000)	1 (±0)	47.7985 (±0.0003)	20.1967 (±0.0005)	0 (±0)
	1&4	0.0006 (±0.0000)	-0.0005 (±0.0000)	1 (±0)	47.8337 (±0.0007)	20.1407 (±0.0011)	0 (±0)
	1&5	0.0001 (±0.0000)	0.0002 (±0.0000)	1 (±0)	47.8943 (±0.0001)	20.0445 (±0.0002)	0 (±0)
	1&6	-0.6295 (±0.0000)	1 (±0)	0.0287 (±0.0001)	60.5115 (±0.0003)	0 (±0)	-1.2630 (±0.0031)
	1&7	0.0001 (±0.0000)	0.0003 (±0.0000)	1 (±0)	37.5177 (±0.0006)	36.5290 (±0.0009)	0 (±0)
	1&8	0.0008 (±0.0000)	-0.0009 (±0.0000)	1 (±0)	37.5240 (±0.0004)	36.5190 (±0.0006)	0 (±0)
	1&9	0.0014 (±0.0000)	-0.0018 (±0.0000)	1 (±0)	37.5148 (±0.0006)	36.5337 (±0.0010)	0 (±0)
	1&10	0.0008 (±0.0000)	-0.0009 (±0.0000)	1 (±0)	37.5063 (±0.0008)	36.5472 (±0.0012)	0 (±0)

continued on next page

Table 4.54.: *continued*

Plane Intersection	a_x (±)	a_y (±)	a_z (±)	b_x (m±m)	b_y (m±m)	b_z (m±m)
1&11	0.0007 (±0.0000)	-0.0007 (±0.0001)	1 (±0)	37.5190 (±0.0012)	36.5270 (±0.0018)	0 (±0)
1&12	0.0014 (±0.0000)	-0.0018 (±0.0001)	1 (±0)	37.5082 (±0.0008)	36.5441 (±0.0012)	0 (±0)
2&6	1 (±0)	0.6325 (±0.0001)	0.0243 (±0.0000)	0 (±0)	-15.6821 (±0.0052)	-2.0212 (±0.0015)
2&13	0.0070 (±0.0002)	0.0046 (±0.0002)	1 (±0)	77.4706 (±0.0031)	33.3204 (±0.0028)	0 (±0)
2&14	0.0000 (±0.0001)	0.0002 (±0.0001)	1 (±0)	84.2956 (±0.0020)	37.6373 (±0.0026)	0 (±0)
2&15	-0.0019 (±0.0002)	-0.0010 (±0.0001)	1 (±0)	79.2941 (±0.0016)	34.4738 (±0.0023)	0 (±0)
2&16	0.0005 (±0.0002)	0.0005 (±0.0001)	1 (±0)	79.2914 (±0.0020)	34.4721 (±0.0024)	0 (±0)
3&6	1 (±0)	0.6372 (±0.0000)	0.0244 (±0.0000)	0 (±0)	-10.2606 (±0.0007)	-1.8506 (±0.0012)
3&13	0.0069 (±0.0002)	0.0049 (±0.0001)	1 (±0)	74.8262 (±0.0021)	37.4183 (±0.0017)	0 (±0)
3&14	-0.0001 (±0.0001)	0.0004 (±0.0001)	1 (±0)	81.6666 (±0.0010)	41.7769 (±0.0012)	0 (±0)
3&15	-0.0020 (±0.0002)	-0.0008 (±0.0001)	1 (±0)	76.6850 (±0.0008)	38.6027 (±0.0011)	0 (±0)

continued on next page

Table 4.54.: *continued*

Plane Intersection	a_x (±)	a_y (±)	a_z (±)	b_x (m±m)	b_y (m±m)	b_z (m±m)
3&16	0.0004 (±0.0002)	0.0007 (±0.0001)	1 (±0)	76.6794 (±0.0009)	38.5991 (±0.0011)	0 (±0)
4&6	1 (±0)	0.6336 (±0.0001)	0.0243 (±0.0000)	0 (±0)	-10.1672 (±0.0012)	-1.8477 (±0.0012)
4&13	0.0075 (±0.0002)	0.0039 (±0.0001)	1 (±0)	74.9058 (±0.0025)	37.2948 (±0.0025)	0 (±0)
4&14	0.0005 (±0.0001)	-0.0006 (±0.0001)	1 (±0)	81.7563 (±0.0017)	41.6356 (±0.0025)	0 (±0)
4&15	-0.0014 (±0.0002)	-0.0018 (±0.0001)	1 (±0)	76.7665 (±0.0015)	38.4738 (±0.0023)	0 (±0)
4&16	0.0010 (±0.0002)	-0.0003 (±0.0001)	1 (±0)	76.7609 (±0.0015)	38.4703 (±0.0023)	0 (±0)
5&6	1 (±0)	0.6297 (±0.0000)	0.0242 (±0.0000)	0 (±0)	-10.1128 (±0.0001)	-1.8460 (±0.0011)
5&13	0.0071 (±0.0002)	0.0046 (±0.0001)	1 (±0)	75.0170 (±0.0021)	37.1226 (±0.0014)	0 (±0)
5&14	0.0001 (±0.0001)	0.0001 (±0.0001)	1 (±0)	81.8786 (±0.0008)	41.4431 (±0.0006)	0 (±0)
5&15	-0.0018 (±0.0002)	-0.0011 (±0.0001)	1 (±0)	76.8793 (±0.0006)	38.2952 (±0.0005)	0 (±0)
5&16	0.0005 (±0.0002)	0.0004 (±0.0001)	1 (±0)	76.8739 (±0.0006)	38.2918 (±0.0005)	0 (±0)

continued on next page

Table 4.54.: *continued*

Plane Intersection	a_x (±)	a_y (±)	a_z (±)	b_x (m±m)	b_y (m±m)	b_z (m±m)
6&7	1 (±0)	0.6311 (±0.0000)	0.0242 (±0.0000)	0 (±0)	12.8517 (±0.0003)	-1.1236 (±0.0010)
6&8	1 (±0)	0.6300 (±0.0000)	0.0242 (±0.0000)	0 (±0)	12.8799 (±0.0004)	-1.1227 (±0.0010)
6&9	1 (±0)	0.6295 (±0.0001)	0.0242 (±0.0000)	0 (±0)	12.9192 (±0.0012)	-1.1214 (±0.0010)
6&10	1 (±0)	0.6312 (±0.0001)	0.0242 (±0.0000)	0 (±0)	12.8740 (±0.0024)	-1.1229 (±0.0010)
6&11	1 (±0)	0.6303 (±0.0001)	0.0242 (±0.0000)	0 (±0)	12.8792 (±0.0022)	-1.1227 (±0.0010)
6&12	1 (±0)	0.6305 (±0.0001)	0.0242 (±0.0000)	0 (±0)	12.8946 (±0.0027)	-1.1222 (±0.0010)
6&13	-0.6450 (±0.0003)	1 (±0)	0.0286 (±0.0001)	98.9618 (±0.0129)	0 (±0)	-1.0948 (±0.0053)
6&14	-0.6351 (±0.0002)	1 (±0)	0.0287 (±0.0001)	108.1983 (±0.0073)	0 (±0)	-1.0544 (±0.0058)
6&15	-0.6320 (±0.0001)	1 (±0)	0.0287 (±0.0001)	101.0804 (±0.0052)	0 (±0)	-1.0855 (±0.0054)
6&16	-0.6329 (±0.0004)	1 (±0)	0.0287 (±0.0001)	101.1083 (±0.0153)	0 (±0)	-1.0854 (±0.0054)
7&13	0.0070 (±0.0002)	0.0047 (±0.0001)	1 (±0)	64.4371 (±0.0015)	53.5175 (±0.0018)	0 (±0)

continued on next page

Table 4.54.: *continued*

Plane Intersection	a_x (±)	a_y (±)	a_z (±)	b_x (m±m)	b_y (m±m)	b_z (m±m)
7&14	0.0000 (±0.0001)	0.0002 (±0.0001)	1 (±0)	71.4140 (±0.0016)	57.9206 (±0.0020)	0 (±0)
7&15	-0.0019 (±0.0002)	-0.0010 (±0.0001)	1 (±0)	66.4556 (±0.0017)	54.7914 (±0.0019)	0 (±0)
7&16	0.0005 (±0.0002)	0.0005 (±0.0001)	1 (±0)	66.4381 (±0.0045)	54.7803 (±0.0033)	0 (±0)
8&13	0.0078 (±0.0002)	0.0035 (±0.0001)	1 (±0)	64.4567 (±0.0013)	53.4870 (±0.0014)	0 (±0)
8&14	0.0007 (±0.0001)	-0.0009 (±0.0001)	1 (±0)	71.4369 (±0.0014)	57.8846 (±0.0016)	0 (±0)
8&15	-0.0012 (±0.0002)	-0.0021 (±0.0001)	1 (±0)	66.4759 (±0.0016)	54.7592 (±0.0016)	0 (±0)
8&16	0.0012 (±0.0002)	-0.0006 (±0.0001)	1 (±0)	66.4585 (±0.0044)	54.7481 (±0.0031)	0 (±0)
9&13	0.0083 (±0.0002)	0.0026 (±0.0001)	1 (±0)	64.4531 (±0.0017)	53.4927 (±0.0022)	0 (±0)
9&14	0.0013 (±0.0001)	-0.0018 (±0.0001)	1 (±0)	71.4347 (±0.0019)	57.8880 (±0.0025)	0 (±0)
9&15	-0.0006 (±0.0002)	-0.0030 (±0.0001)	1 (±0)	66.4727 (±0.0019)	54.7642 (±0.0024)	0 (±0)
9&16	0.0018 (±0.0002)	-0.0015 (±0.0001)	1 (±0)	66.4552 (±0.0046)	54.7532 (±0.0035)	0 (±0)

continued on next page

Table 4.54.: *continued*

Plane Intersection	a_x (±)	a_y (±)	a_z (±)	b_x (m±m)	b_y (m±m)	b_z (m±m)
10&13	0.0078 (±0.0002)	0.0035 (±0.0001)	1 (±0)	64.4238 (±0.0022)	53.5381 (±0.0031)	0 (±0)
10&14	0.0008 (±0.0001)	-0.0010 (±0.0001)	1 (±0)	71.4005 (±0.0025)	57.9419 (±0.0036)	0 (±0)
10&15	-0.0011 (±0.0002)	-0.0022 (±0.0001)	1 (±0)	66.4424 (±0.0024)	54.8122 (±0.0033)	0 (±0)
10&16	0.0012 (±0.0002)	-0.0007 (±0.0001)	1 (±0)	66.4249 (±0.0048)	54.8012 (±0.0042)	0 (±0)
11&13	0.0077 (±0.0002)	0.0037 (±0.0001)	1 (±0)	64.4478 (±0.0028)	53.5008 (±0.0042)	0 (±0)
11&14	0.0006 (±0.0001)	-0.0008 (±0.0001)	1 (±0)	71.4271 (±0.0032)	57.9000 (±0.0048)	0 (±0)
11&15	-0.0013 (±0.0002)	-0.0020 (±0.0001)	1 (±0)	66.4669 (±0.0030)	54.7735 (±0.0044)	0 (±0)
11&16	0.0011 (±0.0002)	-0.0005 (±0.0001)	1 (±0)	66.4494 (±0.0051)	54.7624 (±0.0051)	0 (±0)
12&13	0.0083 (±0.0002)	0.0026 (±0.0001)	1 (±0)	64.4335 (±0.0023)	53.5230 (±0.0033)	0 (±0)
12&14	0.0013 (±0.0001)	-0.0018 (±0.0001)	1 (±0)	71.4121 (±0.0027)	57.9236 (±0.0039)	0 (±0)
12&15	-0.0006 (±0.0002)	-0.0030 (±0.0001)	1 (±0)	66.4525 (±0.0025)	54.7962 (±0.0035)	0 (±0)

continued on next page

Table 4.54.: *continued*

	Plane Intersection	a_x (±)	a_y (±)	a_z (±)	b_x (m±m)	b_y (m±m)	b_z (m±m)
	12&16	0.0018 (±0.0002)	-0.0015 (±0.0001)	1 (±0)	66.4350 (±0.0049)	54.7852 (±0.0044)	0 (±0)
Scan 8	1&2	-0.0003 (±0.0000)	0.0001 (±0.0000)	1 (±0)	19.6372 (±0.0003)	8.9120 (±0.0002)	0 (±0)
	1&3	0.0002 (±0.0000)	-0.0001 (±0.0000)	1 (±0)	15.3520 (±0.0002)	11.0227 (±0.0001)	0 (±0)
	1&4	0.0010 (±0.0000)	-0.0005 (±0.0000)	1 (±0)	15.4178 (±0.0008)	10.9903 (±0.0004)	0 (±0)
	1&5	0.0003 (±0.0000)	-0.0002 (±0.0000)	1 (±0)	15.5109 (±0.0006)	10.9445 (±0.0003)	0 (±0)
	1&6	1 (±0)	-0.4926 (±0.0000)	-0.0282 (±0.0001)	0 (±0)	18.5845 (±0.0001)	-0.7069 (±0.0017)
	1&7	0.0004 (±0.0000)	-0.0003 (±0.0000)	1 (±0)	-1.9633 (±0.0021)	19.5515 (±0.0011)	0 (±0)
	1&8	0.0005 (±0.0000)	-0.0003 (±0.0000)	1 (±0)	-1.9340 (±0.0006)	19.5371 (±0.0003)	0 (±0)
	1&9	0.0024 (±0.0000)	-0.0012 (±0.0000)	1 (±0)	-1.9613 (±0.0003)	19.5505 (±0.0002)	0 (±0)
	1&10	0.0017 (±0.0000)	-0.0009 (±0.0000)	1 (±0)	-1.9870 (±0.0002)	19.5632 (±0.0001)	0 (±0)
	1&11	0.0010 (±0.0000)	-0.0006 (±0.0000)	1 (±0)	-1.9547 (±0.0007)	19.5473 (±0.0004)	0 (±0)

continued on next page

Table 4.54.: *continued*

Plane Intersection	a_x (±)	a_y (±)	a_z (±)	b_x (m±m)	b_y (m±m)	b_z (m±m)
1&12	0.0025 (±0.0000)	-0.0013 (±0.0000)	1 (±0)	-1.9722 (±0.0003)	19.5559 (±0.0002)	0 (±0)
2&6	0.4901 (±0.0000)	1 (±0)	0.0216 (±0.0001)	15.2701 (±0.0005)	0 (±0)	-1.4531 (±0.0016)
2&13	0.0038 (±0.0000)	0.0083 (±0.0001)	1 (±0)	33.7625 (±0.0007)	37.7342 (±0.0009)	0 (±0)
2&14	-0.0007 (±0.0000)	-0.0008 (±0.0000)	1 (±0)	37.3214 (±0.0007)	44.9959 (±0.0007)	0 (±0)
2&15	-0.0015 (±0.0000)	-0.0023 (±0.0001)	1 (±0)	34.7135 (±0.0006)	39.6747 (±0.0004)	0 (±0)
2&16	0.0004 (±0.0001)	0.0016 (±0.0001)	1 (±0)	34.7095 (±0.0006)	39.6665 (±0.0006)	0 (±0)
3&6	0.4859 (±0.0000)	1 (±0)	0.0216 (±0.0001)	9.9955 (±0.0002)	0 (±0)	-1.3783 (±0.0013)
3&13	0.0042 (±0.0000)	0.0081 (±0.0001)	1 (±0)	29.3577 (±0.0005)	39.8453 (±0.0007)	0 (±0)
3&14	-0.0003 (±0.0000)	-0.0010 (±0.0000)	1 (±0)	32.9058 (±0.0005)	47.1470 (±0.0005)	0 (±0)
3&15	-0.0010 (±0.0000)	-0.0025 (±0.0001)	1 (±0)	30.3219 (±0.0005)	41.8294 (±0.0003)	0 (±0)
3&16	0.0009 (±0.0001)	0.0013 (±0.0001)	1 (±0)	30.3186 (±0.0005)	41.8226 (±0.0005)	0 (±0)

continued on next page

Table 4.54.: *continued*

Plane Intersection	a_x (±)	a_y (±)	a_z (±)	b_x (m±m)	b_y (m±m)	b_z (m±m)
4&6	0.4893 (±0.0000)	1 (±0)	0.0216 (±0.0001)	10.0392 (±0.0006)	0 (±0)	-1.3790 (±0.0013)
4&13	0.0050 (±0.0000)	0.0077 (±0.0001)	1 (±0)	29.5014 (±0.0016)	39.7764 (±0.0010)	0 (±0)
4&14	0.0006 (±0.0000)	-0.0014 (±0.0000)	1 (±0)	33.0686 (±0.0018)	47.0677 (±0.0009)	0 (±0)
4&15	-0.0002 (±0.0000)	-0.0029 (±0.0001)	1 (±0)	30.4702 (±0.0016)	41.7567 (±0.0008)	0 (±0)
4&16	0.0017 (±0.0001)	0.0009 (±0.0001)	1 (±0)	30.4669 (±0.0016)	41.7498 (±0.0009)	0 (±0)
5&6	0.4925 (±0.0000)	1 (±0)	0.0215 (±0.0001)	10.1202 (±0.0005)	0 (±0)	-1.3801 (±0.0013)
5&13	0.0044 (±0.0000)	0.0080 (±0.0001)	1 (±0)	29.6705 (±0.0011)	39.6954 (±0.0008)	0 (±0)
5&14	-0.0001 (±0.0000)	-0.0011 (±0.0000)	1 (±0)	33.2563 (±0.0011)	46.9762 (±0.0007)	0 (±0)
5&15	-0.0008 (±0.0000)	-0.0026 (±0.0001)	1 (±0)	30.6438 (±0.0010)	41.6715 (±0.0005)	0 (±0)
5&16	0.0011 (±0.0001)	0.0013 (±0.0001)	1 (±0)	30.6404 (±0.0011)	41.6646 (±0.0007)	0 (±0)
6&7	0.4912 (±0.0001)	1 (±0)	0.0215 (±0.0001)	-11.5679 (±0.0011)	0 (±0)	-1.0727 (±0.0010)

continued on next page

Table 4.54.: *continued*

Plane Intersection	a_x (±)	a_y (±)	a_z (±)	b_x (m±m)	b_y (m±m)	b_z (m±m)
6&8	0.4927 (±0.0000)	1 (±0)	0.0215 (±0.0001)	-11.5601 (±0.0003)	0 (±0)	-1.0728 (±0.0010)
6&9	0.4930 (±0.0000)	1 (±0)	0.0215 (±0.0001)	-11.6012 (±0.0002)	0 (±0)	-1.0722 (±0.0010)
6&10	0.4908 (±0.0000)	1 (±0)	0.0215 (±0.0001)	-11.5905 (±0.0002)	0 (±0)	-1.0723 (±0.0010)
6&11	0.4921 (±0.0000)	1 (±0)	0.0215 (±0.0001)	-11.5746 (±0.0002)	0 (±0)	-1.0726 (±0.0010)
6&12	0.4921 (±0.0000)	1 (±0)	0.0215 (±0.0001)	-11.5986 (±0.0001)	0 (±0)	-1.0722 (±0.0010)
6&13	1 (±0)	-0.4795 (±0.0001)	-0.0278 (±0.0001)	0 (±0)	53.9185 (±0.0011)	0.3003 (±0.0037)
6&14	1 (±0)	-0.4871 (±0.0001)	-0.0281 (±0.0001)	0 (±0)	63.1772 (±0.0020)	0.5643 (±0.0042)
6&15	1 (±0)	-0.4905 (±0.0000)	-0.0282 (±0.0001)	0 (±0)	56.7052 (±0.0012)	0.3798 (±0.0038)
6&16	1 (±0)	-0.4911 (±0.0002)	-0.0282 (±0.0001)	0 (±0)	56.7115 (±0.0074)	0.3800 (±0.0038)
7&13	0.0045 (±0.0000)	0.0080 (±0.0001)	1 (±0)	12.0744 (±0.0040)	48.1286 (±0.0020)	0 (±0)
7&14	0.0000 (±0.0000)	-0.0011 (±0.0000)	1 (±0)	15.7079 (±0.0045)	55.5254 (±0.0023)	0 (±0)

continued on next page

Table 4.54.: *continued*

Plane Intersection	a_x (±)	a_y (±)	a_z (±)	b_x (m±m)	b_y (m±m)	b_z (m±m)
7&15	-0.0007 (±0.0000)	-0.0026 (±0.0001)	1 (±0)	13.1248 (±0.0042)	50.2669 (±0.0021)	0 (±0)
7&16	0.0012 (±0.0001)	0.0012 (±0.0001)	1 (±0)	13.1243 (±0.0045)	50.2660 (±0.0041)	0 (±0)
8&13	0.0046 (±0.0000)	0.0080 (±0.0001)	1 (±0)	12.1374 (±0.0012)	48.0984 (±0.0006)	0 (±0)
8&14	0.0001 (±0.0000)	-0.0012 (±0.0000)	1 (±0)	15.7794 (±0.0014)	55.4906 (±0.0009)	0 (±0)
8&15	-0.0007 (±0.0000)	-0.0027 (±0.0001)	1 (±0)	13.1900 (±0.0012)	50.2349 (±0.0008)	0 (±0)
8&16	0.0012 (±0.0001)	0.0012 (±0.0001)	1 (±0)	13.1896 (±0.0021)	50.2340 (±0.0036)	0 (±0)
9&13	0.0065 (±0.0000)	0.0070 (±0.0001)	1 (±0)	12.1155 (±0.0008)	48.1089 (±0.0005)	0 (±0)
9&14	0.0020 (±0.0000)	-0.0021 (±0.0000)	1 (±0)	15.7589 (±0.0009)	55.5006 (±0.0008)	0 (±0)
9&15	0.0012 (±0.0000)	-0.0036 (±0.0001)	1 (±0)	13.1686 (±0.0008)	50.2454 (±0.0007)	0 (±0)
9&16	0.0031 (±0.0001)	0.0002 (±0.0001)	1 (±0)	13.1681 (±0.0019)	50.2445 (±0.0035)	0 (±0)
10&13	0.0057 (±0.0000)	0.0074 (±0.0001)	1 (±0)	12.0405 (±0.0006)	48.1449 (±0.0004)	0 (±0)

continued on next page

Table 4.54.: *continued*

Plane Intersection	a_x (±)	a_y (±)	a_z (±)	b_x (m±m)	b_y (m±m)	b_z (m±m)
10&14	0.0013 (±0.0000)	-0.0017 (±0.0000)	1 (±0)	15.6714 (±0.0008)	55.5432 (±0.0007)	0 (±0)
10&15	0.0005 (±0.0000)	-0.0032 (±0.0001)	1 (±0)	13.0902 (±0.0007)	50.2838 (±0.0006)	0 (±0)
10&16	0.0024 (±0.0001)	0.0006 (±0.0001)	1 (±0)	13.0898 (±0.0018)	50.2830 (±0.0036)	0 (±0)
11&13	0.0051 (±0.0000)	0.0077 (±0.0001)	1 (±0)	12.1025 (±0.0016)	48.1152 (±0.0008)	0 (±0)
11&14	0.0006 (±0.0000)	-0.0014 (±0.0000)	1 (±0)	15.7409 (±0.0019)	55.5093 (±0.0011)	0 (±0)
11&15	-0.0001 (±0.0000)	-0.0029 (±0.0001)	1 (±0)	13.1541 (±0.0017)	50.2525 (±0.0010)	0 (±0)
11&16	0.0017 (±0.0001)	0.0009 (±0.0001)	1 (±0)	13.1537 (±0.0024)	50.2516 (±0.0036)	0 (±0)
12&13	0.0065 (±0.0000)	0.0070 (±0.0001)	1 (±0)	12.0853 (±0.0008)	48.1234 (±0.0005)	0 (±0)
12&14	0.0020 (±0.0000)	-0.0021 (±0.0000)	1 (±0)	15.7239 (±0.0009)	55.5176 (±0.0008)	0 (±0)
12&15	0.0013 (±0.0000)	-0.0036 (±0.0001)	1 (±0)	13.1371 (±0.0008)	50.2608 (±0.0007)	0 (±0)
12&16	0.0032 (±0.0001)	0.0002 (±0.0001)	1 (±0)	13.1367 (±0.0019)	50.2600 (±0.0036)	0 (±0)

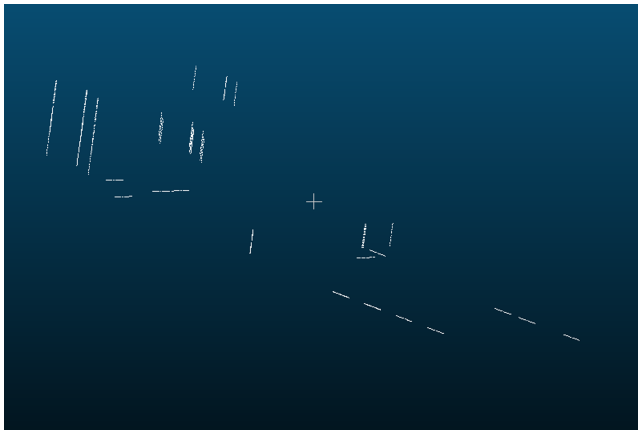

Fig. 4.25.: Simulated points along linear features in the overlapping area between scans 7 and 8

After the estimation of line parameters, the next step is to estimate transformation parameters using the three alternative registration approaches. The aim of the registration process is to estimate the 3D similarity transformation parameters, which include three translations (t_x, t_y, t_z) and three rotation parameters (ω, ϕ, κ). The observations and weight matrix P in the three alternative registration approaches are specified as follows. In the linear feature-based approach, the observations are estimated line parameters from a line fitting procedure, and the weight matrix P is defined by the inverse of the variance-covariance matrix of extracted line parameters, which is derived by using the law of error propagation.

In the pseudo-conjugate point-based method, the observations are coordinates of simulated points along lines in the source and reference scans. The weight matrix P depends on the noise added to the point clouds. The estimated line parameters in the reference scan are used to modify the weight matrix to eliminate the additional vector resulting from using non-corresponding points along linear features. In the 3D similarity transformation function, each 3D point pair contributes three equations towards the transformation parameters estimation. There are 1,300 points along linear features in each scan, so the total number of observation equations is $1,300 \times 3 = 3,900$. However, the discussion in the subsection 3.3.2 indicates that the effective

contribution is only two equations from each point pair. According to Equation (3.73) in the subsection 3.3.2, all the elements in the weight matrix pertaining to the U-axis along the linear features are assigned a zero weight. The modified weight matrix in the LSA procedure nullifies the error along the line direction while minimizing the errors in the two directions normal to the line. Therefore, the effective contribution of a 3D point pair towards redundancy is 2 equations instead of 3. In this case, the redundancy is given by the difference between the rank of the weight matrix and the number of the unknowns, thus resulting in a redundancy of $1,300 \times 2 - 6 = 2,594$.

In the closed-form solution, the rotation parameters and the translation parameters are estimated separately. The rotation matrix is derived first using a quaternion-based approach, which is a single-step solution. The observations are the direction vectors of linear features. A weight matrix is not used in this procedure. Also, there is no standard deviation to evaluate the estimated rotation parameters. Once the rotation matrix is derived, the next step is to estimate translation parameters using the pseudo-conjugate point-based method. In this step, the observations are coordinates of points along linear features, and the weight matrix P is obtained as the inverse of the variance-covariance matrix of the observations.

The estimated transformation parameters, standard deviations, a-posteriori variance factors, and execution times from the linear feature-based approach, pseudo-conjugate point-based method, and closed-form solution using the linear features in scans 7 and 8 are presented in Table 4.55. In the linear feature-based approach and pseudo-conjugate point-based method, the standard deviation overall was below 4 mm and 0.0032 degrees for the translation and the rotation parameters, respectively, which indicates reliable transformation parameters are estimated by using the two registration approaches. In the closed-form registration results, the standard deviation overall was below 1 mm for the translation parameters, which indicates the estimated translation parameters are reliable. Since the rotation parameters were estimated by quaternions, there is no standard deviation for the rotation parameters.

Table 4.55.: The estimated transformation parameters, standard deviations, a-posteriori variance factors, and execution times from the linear feature-based approach, pseudo-conjugate point-based method, and closed-form solution using the linear features in scans 7 and 8

	$t_x(m \pm m)$	$t_y(m \pm m)$	$t_z(m \pm m)$	$\omega(^\circ \pm ^\circ)$	$\phi(^\circ \pm ^\circ)$	$\kappa(^\circ \pm ^\circ)$	$\hat{\sigma}_0^2$	$\hat{\sigma}_0$	Execution time (seconds)
Linear feature-based approach	-14.7906 (±0.0005)	-31.2156 (±0.0004)	-0.4143 (±0.0039)	-0.0221 (±0.0023)	-0.0080 (±0.0031)	-31.5821 (±0.0013)	104.5179	10.2234	0.2
Pseudo-conjugate point-based method	-14.7942 (±0.0008)	-31.2208 (±0.0005)	-0.3909 (±0.0011)	-0.0030 (±0.0028)	-0.0772 (±0.0017)	-31.5791 (±0.0008)	4.82E-05 (m^2)	0.0069 (m)	7.4
Closed-form solution	-14.7854 (±0.0004)	-31.2176 (±0.0004)	-0.4335 (±0.0008)	-0.0079 (N/A)	-0.0142 (N/A)	-31.5818 (N/A)	1.03E-04 (m^2)	0.0102 (m)	14.4

Furthermore, the a-posteriori variance factor $\hat{\sigma}_0^2$ in Table 4.55 is used to evaluate the estimated transformation parameters. In the linear feature-based approach, the weight matrix P is derived by the inverse of variance-covariance matrix, so the $\hat{\sigma}_0^2$ should be close to 1. The a-posteriori variance factor $\hat{\sigma}_0^2$ was 104.5179, which indicates that the noise level in the observation is larger than previously assumed. In the pseudo-conjugate point-based method and closed-form solution, the $\hat{\sigma}_0^2$ is the variance of the observations since the weight matrix P is an identity matrix. The square roots of the a-posteriori variance factors ($\hat{\sigma}_0$) in Table 4.55 are not significantly different from the expected accuracy of around 2 mm according to the accuracy of the TLS, thus indicating the validity of the estimated transformation parameters using the pseudo-conjugate point-based method and closed-form solution based on linear features. Regarding the execution time, the linear feature-based approach had the shortest execution time, as listed in Table 4.55. The pseudo-conjugate point-based and closed-form approaches based on linear features led to longer execution times due to a large number of point cloud data.

The quality evaluation of the registration results was analyzed by calculating the point-to-patch normal distances between TLS scans. After applying the estimated registration parameters, the point clouds in the source scan were transformed to the reference scan. A point-patch pair is established by using the approach discussed in section 3.4. The normal distance between the transformed point and the patch must be within a certain threshold, which is 10 cm in this test. The mean, standard deviation, and RMSE of the point-to-patch normal distances between the TLS scans are presented in Table 4.56. The mean of the calculated point-to-patch normal distances of the linear feature-based approach was below 2.2 mm, while it was all below 6 mm for the pseudo-conjugate point-based method and closed-form solution, which indicates that the feature-based approach can produce better results than the pseudo-conjugate point-based method and closed-form solution using linear features. The mean, standard deviation, and RMSE of the calculated point-to-patch normal distances of the closed-form solution were all larger than the values of the pseudo-

conjugate point-based method, which indicates that the registration results using the closed-form solution were worse than the pseudo-conjugate point-based method.

Table 4.56.: Quantitative comparison between linear feature-based approach, pseudo-conjugate point-based method, and closed-form solution based on linear features through the mean, standard deviation, and RMSE of the point-to-patch normal distances between the TLS scans 7 and 8

	Mean (m)	Standard deviation (m)	RMSE (m)	Number of used points	Total number of points
Linear feature-based approach	0.0021	0.0053	0.0057	116,481	588,604
Pseudo-conjugate point-based method	0.0043	0.0056	0.0070	116,322	588,604
Closed-form solution	0.0059	0.0071	0.0093	115,167	588,604

Moreover, the comparison between registration approaches using linear and planar features is conducted based on point-to-patch normal distances between TLS scans. The quality evaluation of the registration results shows that these two features can produce equivalent registration results by using the feature-based approach since the normal distances calculated were all below 2.2 mm. However, the pseudo-conjugate point-based method and closed-form solution can produce better registration results when the planar features were the registration primitives. For example, when linear features are the registration primitives, the normal distances calculated using the registration results of the two approaches were below 6 mm, while it was below 2.2 mm when planar features are the registration primitives.

4.2.8 Registration Between Scans 1 and 8

The positions of TLS scans 1 and 8 are shown in Figure 4.26. Scan 8 is the source scan, and scan 1 is the reference scan.

Fig. 4.26.: Position of TLS scans 1 and 8

4.2.8.1 Registration Between Scans 1 and 8 Using Planar Features

The planar features in scans 1 and 8 are shown in Figure 4.27. I-LIVE is used to extract the planar features from the point cloud data. After a plane fitting procedure as stated in subsection 3.2.5, the estimated plane parameters, standard deviations, and square roots of the a-posteriori variance factors of 12 pairs of planar features in scans 1 and 8 are presented in Table 4.57. The standard deviation overall was below 3 mm for plane parameters in the source and reference scans. The small standard deviation values indicate the estimated plane parameters are reliable. Furthermore, the a-posteriori variance factor $\hat{\sigma}_0^2$ is used to check the quality of the estimated plane parameters. Since the weight matrix P is an identity matrix, the $\hat{\sigma}_0^2$ is the variance of the measurements. The square roots of the a-posteriori variance factors ($\hat{\sigma}_0$) after plane fitting are close to the expected accuracy of around 2 mm according to the accuracy of the TLS, thus indicating the validity of the estimated plane parameters.

Fig. 4.27.: Planar features in the overlapping area between scans 1 and 8 displayed in images (a, c, e), which are captured by an external camera, and point clouds (b, d, f) (continued on next page)

Table 4.57.: The estimated plane parameters, standard deviations, and square roots of the a-posteriori variance factors of 12 pairs of planar features in scans 1 and 8

	Plane ID	$a_x(m \pm m)$	$a_y(m \pm m)$	$a_z(m \pm m)$	$\hat{\sigma}_0(mm)$
Scan 8	1	5.6405 (±0.0002)	-2.7690 (±0.0000)	0.0062 (±0.0002)	1.7
	2	12.3164 (±0.0001)	-6.0397 (±0.0001)	0.0163 (±0.0001)	1.1
	3	12.3166 (±0.0000)	-6.0305 (±0.0000)	-0.0025 (±0.0000)	2.1
	4	-4.1391 (±0.0000)	-8.3738 (±0.0001)	-0.0048 (±0.0001)	1.3
	5	8.0842 (±0.0000)	-3.9262 (±0.0001)	-0.0034 (±0.0000)	1.5
	6	-0.0202 (±0.0002)	0.0023 (±0.0001)	-1.4498 (±0.0015)	2.1
	7	-9.3276 (±0.0000)	4.5792 (±0.0001)	0.0074 (±0.0000)	1.4
	8	-9.3240 (±0.0001)	4.5688 (±0.0002)	0.0056 (±0.0001)	1.3
	9	-9.3091 (±0.0003)	4.5443 (±0.0005)	0.0098 (±0.0001)	2.1
	10	-9.3351 (±0.0007)	4.5832 (±0.0008)	0.0116 (±0.0002)	1.5
	11	24.9912 (±0.0023)	50.9938 (±0.0006)	-0.0953 (±0.0018)	1.7
	12	19.1707 (±0.0008)	39.7861 (±0.0003)	0.3165 (±0.0016)	1.3
Scan 1	1	6.8078 (±0.0001)	-3.1106 (±0.0001)	0.0005 (±0.0001)	1.6
	2	13.5629 (±0.0002)	-6.1936 (±0.0002)	0.0185 (±0.0002)	1.0

continued on next page

Table 4.57.: *continued*

Plane ID	$a_x(m \pm m)$	$a_y(m \pm m)$	$a_z(m \pm m)$	$\hat{\sigma}_0(mm)$
3	13.5378 ($\pm$0.0001)	-6.1730 ($\pm$0.0001)	-0.0044 ($\pm$0.0001)	2.1
4	-21.0202 ($\pm$0.0013)	-45.6416 ($\pm$0.0010)	-0.0306 ($\pm$0.0015)	1.1
5	9.1447 ($\pm$0.0024)	-4.1373 ($\pm$0.0017)	-0.0030 ($\pm$0.0004)	1.9
6	-0.0130 ($\pm$0.0002)	-0.0024 ($\pm$0.0001)	-1.4724 ($\pm$0.0012)	1.2
7	-8.3623 ($\pm$0.0026)	3.8211 ($\pm$0.0005)	0.0095 ($\pm$0.0003)	1.4
8	-8.3767 ($\pm$0.0013)	3.8224 ($\pm$0.0002)	0.0055 ($\pm$0.0001)	1.3
9	-8.4033 ($\pm$0.0013)	3.8241 ($\pm$0.0001)	0.0085 ($\pm$0.0001)	2.3
10	-8.3522 ($\pm$0.0006)	3.8216 ($\pm$0.0000)	0.0045 ($\pm$0.0001)	1.6
11	6.6004 ($\pm$0.0005)	14.4625 ($\pm$0.0002)	0.0279 ($\pm$0.0004)	1.8
12	1.3352 ($\pm$0.0000)	2.9688 ($\pm$0.0000)	0.0290 ($\pm$0.0000)	2.0

The estimated transformation parameters, standard deviations, a-posteriori variance factors, and execution times from the planar feature-based approach, pseudo-conjugate point-based method, and closed-form solution using the planar features in scans 1 and 8 are presented in Table 4.58. Since the rotation parameters were estimated by quaternions in the closed-form solution, there is no standard deviation for the rotation parameters. The standard deviation values of the registration parameters indicate that reliable results were estimated using the three alternative registration approaches. The standard deviations of the estimated parameters were below 0.2 mm for the translation parameters and below 0.0003 degrees for the rotation angels by using the pseudo-conjugate point-based method, while it is below 7 mm and 0.02 degrees for the translation and the rotation parameters, respectively, by using the planar feature-based approach, which indicates that the pseudo-conjugate point-based method can produce better registration results than the planar feature-based approach. In the closed-form solution, the standard deviations of the estimated parameters were below 0.2 mm for the translation parameters, which indicates the estimated translation parameters are reliable.

Furthermore, the a-posteriori variance factor $\hat{\sigma}_0^2$ in Table 4.58 is used to evaluate the estimated transformation parameters. In the planar feature-based approach, the weight matrix P is derived by the inverse of the variance-covariance matrix, so the $\hat{\sigma}_0^2$ should be close to 1. The a-posteriori variance factor $\hat{\sigma}_0^2$ was 1,513.292, which indicates that the noise level in the observation is larger than previously assumed. In the pseudo-conjugate point-based method and closed-form solution, the $\hat{\sigma}_0^2$ is the variance of the observations since the weight matrix P is an identity matrix. The square roots of the a-posteriori variance factors ($\hat{\sigma}_0$) in Table 4.58 are not significantly different from the expected accuracy of around 2 mm according to the accuracy of the TLS, thus indicating the validity of the estimated transformation parameters using the pseudo-conjugate point-based method and closed-form solution based on planar features. Regarding the execution time, the planar feature-based approach had the shortest execution time, as listed in Table 4.58. The pseudo-conjugate point-based

and closed-form approaches based on planar features led to longer execution times due to a large number of point cloud data.

The quality evaluation of the registration results was analyzed by calculating the point-to-patch normal distances between TLS scans. After applying the estimated registration parameters, the point clouds in the source scan were transformed to the reference scan. A point-patch pair is established by using the approach discussed in section 3.4. The normal distance between the transformed point and the patch must be within a certain threshold, which is 10 cm in this test. The mean, standard deviation, and RMSE of the point-to-patch normal distances between the TLS scans are presented in Table 4.59. The mean, standard deviation, and RMSE of the calculated point-to-patch normal distances of each approach were all below 1.1 cm, which substantiates the quality of the registration results. In the planar feature-based approach and pseudo-conjugate point-based method, the average of the calculated point-to-patch normal distances were around 3 mm, and the values of standard deviation and RMSE are close between the two approaches, which indicates the equivalency between the two approaches. The average point-to-patch normal distances is 5.7 mm for the closed-form solution. The standard deviation and RMSE values are also larger than the other two approaches, which indicates that the registration results produced by the closed-form solution are worse than the registration results by using the other two approaches.

Table 4.58.: The estimated transformation parameters, standard deviations, a-posteriori variance factors, and execution times from the planar feature-based approach, pseudo-conjugate point-based method, and closed-form solution using the planar features in scans 1 and 8

	$t_x(m \pm m)$	$t_y(m \pm m)$	$t_z(m \pm m)$	$\omega(^\circ \pm ^\circ)$	$\phi(^\circ \pm ^\circ)$	$\kappa(^\circ \pm ^\circ)$	$\hat{\sigma}_0^2$	$\hat{\sigma}_0$	Execution time (seconds)
Planar feature-based approach	-15.9154 (±0.0009)	-37.7087 (±0.0009)	0.1683 (±0.0063)	-0.0073 (±0.0112)	-0.0143 (±0.0076)	-1.5724 (±0.0023)	1513.2919	38.9011	0.2
Pseudo-conjugate point-based method	-15.9143 (±0.0000)	-37.7100 (±0.0000)	0.1698 (±0.0001)	-0.0012 (±0.0002)	-0.0061 (±0.0001)	-1.5778 (±0.0000)	3.91E-06 (m^2)	2 (mm)	151.2
Closed-form solution	-15.9081 (±0.0000)	-37.7100 (±0.0000)	0.1423 (±0.0001)	-0.0481 (N/A)	0.0603 (N/A)	-1.5683 (N/A)	8.97E-06 (m^2)	3 (mm)	111.6

Table 4.59.: Quantitative comparison between planar feature-based approach, pseudo-conjugate point-based method, and closed-form solution based on planar features through the mean, standard deviation, and RMSE of the point-to-patch normal distances between the TLS scans 1 and 8

	Mean (m)	Standard deviation (m)	RMSE (m)	Number of used points	Total number of points
Planar feature-based approach	0.0031	0.0081	0.0087	296,544	2,165,111
Pseudo-conjugate point-based method	0.0031	0.0081	0.0086	296,708	2,165,111
Closed-form solution	0.0057	0.0085	0.0102	296,201	2,165,111

4.2.8.2 Registration Between Scans 1 and 8 Using Linear Features

After the planar features were used for the introduced registration approaches, the linear features were used as the registration primitives for the same experiment data to investigate the quality of the registration results with a different type of feature. Linear features are extracted indirectly using the segmented planar features from the TLS scans. The estimated line parameters and standard deviations of linear features which are derived by the intersection of neighboring planar features in scans 1 and 8 are presented in Table 4.60. Then, twenty points are simulated along the derived linear features in each scan. The simulated points along linear features are presented in Figure 4.28. The standard deviation overall was below 0.0003 and 5 mm for the direction vector (a_x, a_y, a_z) and position parameter (b_x, b_y, b_z), respectively, which indicates the estimated line parameters are reliable.

Table 4.60.: The estimated line parameters and standard deviations of linear features which are derived by the intersection of neighboring planar features in scans 1 and 8

	Plane Intersection	a_x (±)	a_y (±)	a_z (±)	b_x (m±m)	b_y (m±m)	b_z (m±m)
Scan 8	1&6	0.4909 (±0.0000)	1 (±0)	-0.0053 (±0.0001)	7.0015 (±0.0002)	0 (±0)	-1.5478 (±0.0014)
	2&6	0.4904 (±0.0000)	1 (±0)	-0.0053 (±0.0001)	15.2804 (±0.0001)	0 (±0)	-1.6633 (±0.0022)
	3&6	0.4896 (±0.0000)	1 (±0)	-0.0053 (±0.0001)	15.2689 (±0.0000)	0 (±0)	-1.6631 (±0.0022)
	4&6	1 (±0)	-0.4943 (±0.0000)	-0.0147 (±0.0002)	0 (±0)	-10.4189 (±0.0001)	-1.4663 (±0.0021)
	5&6	0.4857 (±0.0000)	1 (±0)	-0.0052 (±0.0001)	9.9904 (±0.0001)	0 (±0)	-1.5895 (±0.0016)
	7&6	0.4909 (±0.0000)	1 (±0)	-0.0053 (±0.0001)	-11.5767 (±0.0001)	0 (±0)	-1.2885 (±0.0030)
	8&6	0.4900 (±0.0000)	1 (±0)	-0.0053 (±0.0001)	-11.5635 (±0.0002)	0 (±0)	-1.2887 (±0.0030)
	9&6	0.4882 (±0.0000)	1 (±0)	-0.0053 (±0.0001)	-11.5288 (±0.0007)	0 (±0)	-1.2892 (±0.0030)
	10&6	0.4910 (±0.0001)	1 (±0)	-0.0053 (±0.0001)	-11.5869 (±0.0013)	0 (±0)	-1.2884 (±0.0030)
	11&6	1 (±0)	-0.4901 (±0.0001)	-0.0147 (±0.0002)	0 (±0)	63.2392 (±0.0018)	-1.3516 (±0.0043)

continued on next page

Table 4.60.: *continued*

Plane Intersection	a_x (±)	a_y (±)	a_z (±)	b_x (m±m)	b_y (m±m)	b_z (m±m)
12&6	1 (±0)	-0.4817 (±0.0000)	-0.0147 (±0.0002)	0 (±0)	49.0368 (±0.0006)	-1.3737 (±0.0033)
4&1	-0.0011 (±0.0000)	-0.0000 (±0.0000)	1 (±0)	1.5165 (±0.0002)	-11.1694 (±0.0001)	0 (±0)
11&1	-0.0001 (±0.0000)	0.0019 (±0.0000)	1 (±0)	30.6681 (±0.0003)	48.2118 (±0.0003)	0 (±0)
12&1	-0.0040 (±0.0000)	-0.0060 (±0.0000)	1 (±0)	25.1246 (±0.0002)	36.9198 (±0.0001)	0 (±0)
4&2	-0.0013 (±0.0000)	0.0001 (±0.0000)	1 (±0)	8.1846 (±0.0002)	-14.4654 (±0.0001)	0 (±0)
11&2	-0.0003 (±0.0000)	0.0020 (±0.0000)	1 (±0)	37.3215 (±0.0003)	44.9511 (±0.0002)	0 (±0)
12&2	-0.0042 (±0.0000)	-0.0059 (±0.0000)	1 (±0)	31.8046 (±0.0002)	33.7010 (±0.0002)	0 (±0)
4&3	-0.0001 (±0.0000)	-0.0005 (±0.0000)	1 (±0)	8.1862 (±0.0000)	-14.4662 (±0.0000)	0 (±0)
11&3	0.0009 (±0.0000)	0.0014 (±0.0000)	1 (±0)	37.2866 (±0.0001)	44.9682 (±0.0002)	0 (±0)
12&3	-0.0030 (±0.0000)	-0.0065 (±0.0000)	1 (±0)	31.7766 (±0.0001)	33.7145 (±0.0001)	0 (±0)
4&5	0.0001 (±0.0000)	-0.0006 (±0.0000)	1 (±0)	3.9760 (±0.0000)	-12.3851 (±0.0000)	0 (±0)

continued on next page

Table 4.60.: *continued*

	Plane Intersection	a_x (±)	a_y (±)	a_z (±)	b_x (m±m)	b_y (m±m)	b_z (m±m)
	11&5	0.0011 (±0.0000)	0.0013 (±0.0000)	1 (±0)	32.8797 (±0.0004)	47.1280 (±0.0003)	0 (±0)
	12&5	-0.0028 (±0.0000)	-0.0066 (±0.0000)	1 (±0)	27.3914 (±0.0003)	35.8275 (±0.0002)	0 (±0)
	4&7	0.0004 (±0.0000)	-0.0008 (±0.0000)	1 (±0)	-13.4317 (±0.0001)	-3.7805 (±0.0002)	0 (±0)
	11&7	0.0014 (±0.0000)	0.0012 (±0.0000)	1 (±0)	15.6954 (±0.0006)	55.5497 (±0.0009)	0 (±0)
	12&7	-0.0025 (±0.0000)	-0.0067 (±0.0000)	1 (±0)	10.1028 (±0.0004)	44.1579 (±0.0003)	0 (±0)
Scan 1	1&6	0.4569 (±0.0000)	1 (±0)	-0.0056 (±0.0001)	8.2292 (±0.0001)	0 (±0)	-1.5453 (±0.0018)
	2&6	0.4567 (±0.0000)	1 (±0)	-0.0056 (±0.0001)	16.3935 (±0.0003)	0 (±0)	-1.6175 (±0.0027)
	3&6	0.4560 (±0.0000)	1 (±0)	-0.0056 (±0.0001)	16.3521 (±0.0002)	0 (±0)	-1.6171 (±0.0027)
	4&6	1 (±0)	-0.4605 (±0.0000)	-0.0081 (±0.0002)	0 (±0)	-55.3215 (±0.0005)	-1.3842 (±0.0035)
	5&6	0.4524 (±0.0001)	1 (±0)	-0.0056 (±0.0001)	11.0160 (±0.0035)	0 (±0)	-1.5699 (±0.0021)
	7&6	0.4569 (±0.0001)	1 (±0)	-0.0056 (±0.0001)	-10.1100 (±0.0025)	0 (±0)	-1.3831 (±0.0016)

continued on next page

Table 4.60.: *continued*

Plane Intersection	a_x (±)	a_y (±)	a_z (±)	b_x (m±m)	b_y (m±m)	b_z (m±m)
8&6	0.4563 (±0.0001)	1 (±0)	-0.0056 (±0.0001)	-10.1218 (±0.0012)	0 (±0)	-1.3830 (±0.0016)
9&6	0.4551 (±0.0001)	1 (±0)	-0.0056 (±0.0001)	-10.1450 (±0.0011)	0 (±0)	-1.3828 (±0.0016)
10&6	0.4576 (±0.0000)	1 (±0)	-0.0056 (±0.0001)	-10.1016 (±0.0005)	0 (±0)	-1.3832 (±0.0016)
11&6	1 (±0)	-0.4564 (±0.0000)	-0.0081 (±0.0002)	0 (±0)	17.4778 (±0.0006)	-1.5004 (±0.0024)
12&6	1 (±0)	-0.4497 (±0.0000)	-0.0081 (±0.0002)	0 (±0)	3.5840 (±0.0000)	-1.4782 (±0.0014)
4&1	-0.0003 (±0.0000)	-0.0005 (±0.0000)	1 (±0)	-14.0849 (±0.0001)	-48.8356 (±0.0001)	0 (±0)
11&1	-0.0008 (±0.0000)	-0.0016 (±0.0000)	1 (±0)	13.4160 (±0.0002)	11.3521 (±0.0002)	0 (±0)
12&1	-0.0038 (±0.0000)	-0.0081 (±0.0000)	1 (±0)	8.1793 (±0.0001)	-0.1089 (±0.0000)	0 (±0)
4&2	-0.0014 (±0.0000)	-0.0000 (±0.0000)	1 (±0)	-7.3305 (±0.0002)	-51.9464 (±0.0002)	0 (±0)
11&2	-0.0019 (±0.0000)	-0.0011 (±0.0000)	1 (±0)	20.1681 (±0.0003)	8.2706 (±0.0002)	0 (±0)
12&2	-0.0048 (±0.0000)	-0.0076 (±0.0000)	1 (±0)	14.9508 (±0.0003)	-3.1543 (±0.0001)	0 (±0)

continued on next page

Table 4.60.: *continued*

Plane Intersection	a_x (±)	a_y (±)	a_z (±)	b_x (m±m)	b_y (m±m)	b_z (m±m)
4&3	0.0000 (±0.0000)	-0.0007 (±0.0000)	1 (±0)	-7.3334 (±0.0001)	-51.9450 (±0.0002)	0 (±0)
11&3	-0.0005 (±0.0000)	-0.0017 (±0.0000)	1 (±0)	20.1315 (±0.0002)	8.2873 (±0.0002)	0 (±0)
12&3	-0.0034 (±0.0000)	-0.0082 (±0.0000)	1 (±0)	14.9205 (±0.0002)	-3.1407 (±0.0001)	0 (±0)
4&5	0.0000 (±0.0000)	-0.0007 (±0.0000)	1 (±0)	-11.5968 (±0.0002)	-49.9815 (±0.0001)	0 (±0)
11&5	-0.0004 (±0.0000)	-0.0017 (±0.0000)	1 (±0)	15.6842 (±0.0035)	10.3169 (±0.0016)	0 (±0)
12&5	-0.0034 (±0.0000)	-0.0082 (±0.0000)	1 (±0)	10.4959 (±0.0029)	-1.1508 (±0.0013)	0 (±0)
4&7	0.0007 (±0.0000)	-0.0010 (±0.0000)	1 (±0)	-29.2353 (±0.0009)	-41.8581 (±0.0007)	0 (±0)
11&7	0.0002 (±0.0000)	-0.0020 (±0.0000)	1 (±0)	-1.7569 (±0.0033)	18.2767 (±0.0016)	0 (±0)
12&7	-0.0028 (±0.0000)	-0.0085 (±0.0000)	1 (±0)	-7.0322 (±0.0025)	6.7321 (±0.0011)	0 (±0)

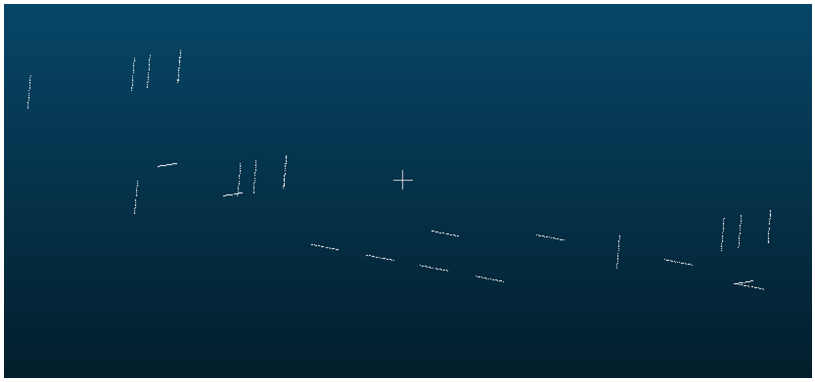

Fig. 4.28.: Simulated points along linear features in the overlapping area between scans 1 and 8

After the estimation of line parameters, the next step is to estimate transformation parameters using the three alternative registration approaches. The aim of the registration process is to estimate the 3D similarity transformation parameters, which include three translations (t_x, t_y, t_z) and three rotation parameters (ω, ϕ, κ). The observations and weight matrix P in the three alternative registration approaches are specified as follows. In the linear feature-based approach, the observations are estimated line parameters from a line fitting procedure, and the weight matrix P is defined by the inverse of the variance-covariance matrix of extracted line parameters, which is derived by using the law of error propagation.

In the pseudo-conjugate point-based method, the observations are coordinates of simulated points along lines in the source and reference scans. The weight matrix P depends on the noise added to the point clouds. The estimated line parameters in the reference scan are used to modify the weight matrix to eliminate the additional vector resulting from using non-corresponding points along linear features. In the 3D similarity transformation function, each 3D point pair contributes three equations towards the transformation parameters estimation. There are 520 points along linear features in each scan, so the total number of observation equations is $520 \times 3 = 1,560$. However, the discussion in the subsection 3.3.2 indicates that the effective contribution is only two equations from each point pair. According to Equation (3.73)

in the subsection 3.3.2, all the elements in the weight matrix pertaining to the U-axis along the linear features are assigned a zero weight. The modified weight matrix in the LSA procedure nullifies the error along the line direction while minimizing the errors in the two directions normal to the line. Therefore, the effective contribution of a 3D point pair towards redundancy is 2 equations instead of 3. In this case, the redundancy is given by the difference between the rank of the weight matrix and the number of the unknowns, thus resulting in a redundancy of $520 \times 2 - 6 = 1,034$.

In the closed-form solution, the rotation parameters and the translation parameters are estimated separately. The rotation matrix is derived first using a quaternion-based approach, which is a single-step solution. The observations are the direction vectors of linear features. A weight matrix is not used in this procedure, and there is no standard deviation to evaluate the estimated rotation parameters. Once the rotation matrix is derived, the next step is to estimate translation parameters using the pseudo-conjugate point-based method. In this step, the observations are coordinates of points along linear features, and the weight matrix P is obtained as the inverse of the variance-covariance matrix of the observations.

The estimated transformation parameters, standard deviations, a-posteriori variance factors, and execution times from the linear feature-based approach, pseudo-conjugate point-based method, and closed-form solution using the linear features in scans 1 and 8 are presented in Table 4.61. In the linear feature-based approach, the standard deviation for the translation along the x, y axes were below 0.1 cm, while it was below 1.27 cm along the z-axis, which indicates the translation along the x, y axes were more reliable. The standard deviation for the rotation was below 0.011 degrees, while it is below 0.06 degrees by using the pseudo-conjugate point-based method, which indicates that the rotation produced by the linear feature-based approach is more reliable. In the closed-form registration results, the standard deviation overall was below 0.9 cm for the translation parameters, which indicates the estimated rotation parameters are reliable. Since the rotation parameters were estimated by quaternions, there is no standard deviation for the rotation parameters.

Furthermore, the a-posteriori variance factor $\hat{\sigma}_0^2$ in Table 4.61 is used to evaluate the estimated transformation parameters. In the linear feature-based approach, the weight matrix P is derived by the inverse of variance-covariance matrix, so the $\hat{\sigma}_0^2$ should be close to 1. The a-posteriori variance factor $\hat{\sigma}_0^2$ was 1,120, which indicates that the noise level in the observation is larger than previously assumed. In the pseudo-conjugate point-based method and closed-form solution, the $\hat{\sigma}_0^2$ is the variance of the observations since the weight matrix P is an identity matrix. The square roots of the a-posteriori variance factors ($\hat{\sigma}_0$) in Table 4.61 are larger than the expected accuracy of around 2 mm according to the accuracy of the TLS. In the experiment with real data, linear features are extracted indirectly by the intersection of neighboring planar features. To get enough lines, planes that are far apart from each other have to be extrapolated to derive lines, which will result in large ($\hat{\sigma}_0$) values. Regarding the execution time, the linear feature-based approach had the shortest execution time, as listed in Table 4.61. The pseudo-conjugate point-based and closed-form approaches based on linear features led to longer execution times due to a large number of point cloud data.

Table 4.61.: The estimated transformation parameters, standard deviations, a-posteriori variance factors, and execution times from the linear feature-based approach, pseudo-conjugate point-based method, and closed-form solution using the linear features in scans 1 and 8

	$t_x(m \pm m)$	$t_y(m \pm m)$	$t_z(m \pm m)$	$\omega(^\circ \pm ^\circ)$	$\phi(^\circ \pm ^\circ)$	$\kappa(^\circ \pm ^\circ)$	$\hat{\sigma}_0^2$	$\hat{\sigma}_0$	Execution time (seconds)
Linear feature-based approach	-15.9141 (±0.0010)	-37.7104 (±0.0008)	0.2562 (±0.0127)	-0.0197 (±0.0104)	0.0049 (±0.0070)	-1.5785 (±0.0029)	1,119.9996	33.4664	0.1
Pseudo-conjugate point-based method	-15.9383 (±0.0081)	-37.7091 (±0.0074)	0.1777 (±0.0107)	-0.0878 (±0.0446)	0.0339 (±0.0503)	-1.6047 (±0.0127)	0.0082 (m^2)	0.0903 (m)	3.0
Closed-form solution	-15.9529 (±0.0061)	-37.7010 (±0.0066)	0.1700 (±0.0086)	-0.0325 (N/A)	0.0648 (N/A)	-1.5684 (N/A)	0.0082 (m^2)	0.0906 (m)	6.4

The quality evaluation of the registration results was analyzed by calculating the point-to-patch normal distances between TLS scans. After applying the estimated registration parameters, the point clouds in the source scan were transformed to the reference scan. A point-patch pair is established by using the approach discussed in section 3.4. The normal distance between the transformed point and the patch must be within a certain threshold, which is 10 cm in this test. The mean, standard deviation, and RMSE of the point-to-patch normal distances between the TLS scans are presented in Table 4.62. The mean of the calculated point-to-patch normal distances of the linear feature-based approach was below 5.3 mm, while it was all below 3.7 cm for the pseudo-conjugate point-based method and closed-form solution, which indicates that the feature-based approach can produce better results than the pseudo-conjugate point-based method and closed-form solution using linear features. The mean, standard deviation, and RMSE of the calculated point-to-patch normal distances of the closed-form solution were all larger than the values of the pseudo-conjugate point-based method, which indicates that the registration results using the closed-form solution were worse than the pseudo-conjugate point-based method.

Moreover, the comparison between registration approaches using linear and planar features is conducted based on point-to-patch normal distances between TLS scans. The quality evaluation of the registration results shows that these two features can produce equivalent registration results by using the linear feature-based approach since the normal distances calculated were all below 5.3 mm. However, the pseudo-conjugate point-based method and closed-form solution can produce better registration results when the planar features were the registration primitives. For example, when linear features are the registration primitives, the normal distances calculated using the registration results of the two approaches were below 3.7 cm, while it was below 6 mm when planar features are the registration primitives.

Table 4.62.: Quantitative comparison between linear feature-based approach, pseudo-conjugate point-based method, and closed-form solution based on linear features through the mean, standard deviation, and RMSE of the point-to-patch normal distances between the TLS scans 1 and 8

	Mean (m)	Standard deviation (m)	RMSE (m)	Number of used points	Total number of points
Linear feature-based approach	0.0052	0.0115	0.0126	295,744	216,5111
Pseudo-conjugate point-based method	0.0219	0.0099	0.0240	296,267	216,5111
Closed-form solution	0.0366	0.0157	0.0398	295,148	216,5111

4.2.9 Qualitative evaluation of the registration results

The overall quality of the registration results was checked by visually inspecting the degree of alignment between adjacent scans. All TLS scans were transformed to scan 1 with the estimated transformation parameters. Figure 4.29 provides the visualization of the registered scans. The quality of fit between overlapping scans is good, which demonstrates that the registration result was reliable.

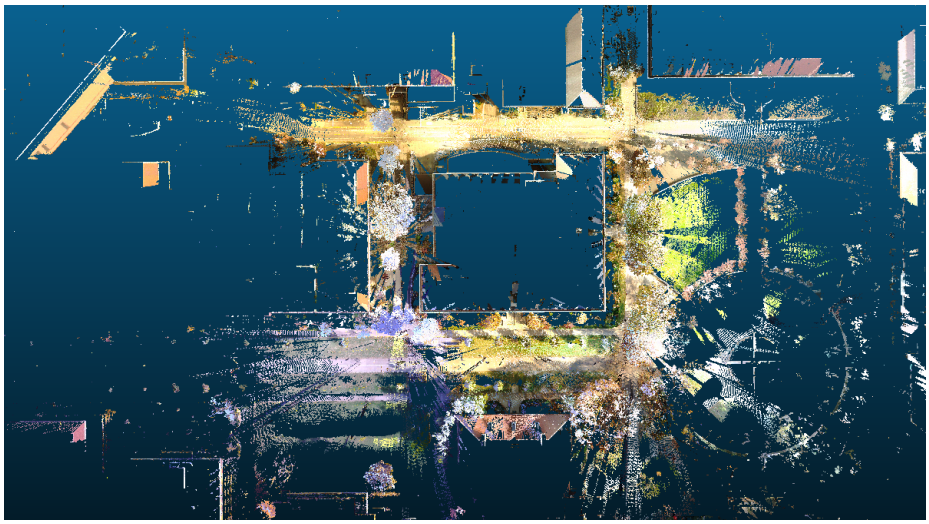

(a) Top view

(b) 3D view

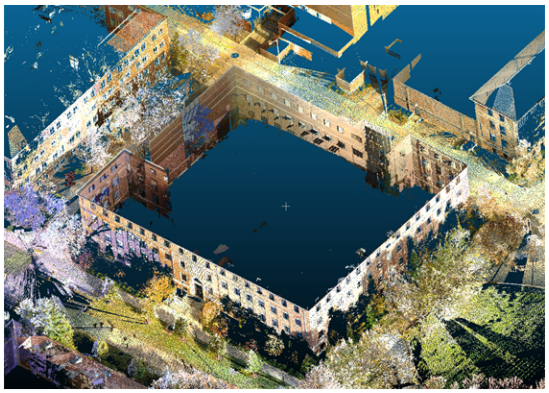

(c) 3D view

(d) 3D view

(e) 3D view

Fig. 4.29.: General view of the registered TLS scans of Forney Hall (continued on next page)

(f) 3D view

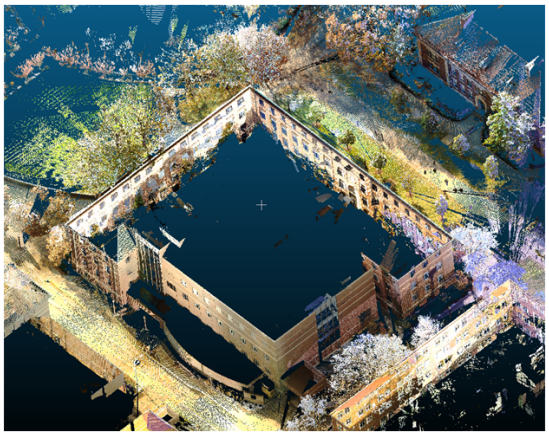

(g) 3D view

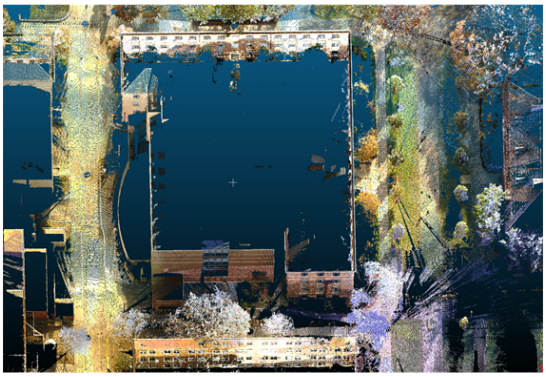

(h) 3D view

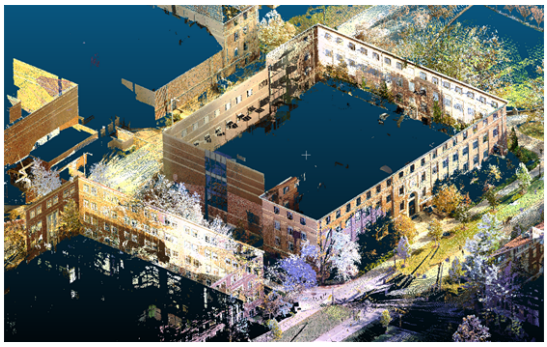

(i) 3D view

Fig. 4.29.: General view of the registered TLS scans of Forney Hall (continued from the previous page)

4.3 Summary

In this chapter, the three alternative registration approaches are tested with simulated and real datasets. First, the proposed line fitting approaches are verified using simulated datasets. The results indicate that the proposed two approaches of line fitting can produce identical line parameters and variance-covariance matrix. The line fitting approach by minimizing 2D distances of points from the line measured parallel to the coordinated planes is used in the remaining part of the experiment.

The correlation matrix of the estimated line parameters shows that there is a high correlation between the estimated parameters. In this research, the linear features are represented with minimal parameters. However, the minimal representation of the linear features will create an artificial correlation between the estimated line parameters. For a line segment that is mainly oriented along the z-axis and is very far from the xy-plane, the (b_x, b_y, b_z) is derived by extrapolating the line segment until it intersects the xy-plane. The problem is that the extrapolation of the line segment will create an artificial correlation between the line parameters if the line segment is too far from the xy-plane. This research shows that the correlation between the estimated line parameters can be reduced by shifting the origin of the coordinate system to the center of the line segment. In this case, the estimated (b_x, b_y, b_z) in the line fitting procedure is one point that is close to the center of the line segment, and the correlation between the (a_x, a_y, a_z) and (b_x, b_y, b_z) will be eliminated.

Then, this chapter compares three alternative approaches for the coarse registration of two partially overlapping point clouds using linear and planar features. In the tests using synthetic datasets, the registration results indicate that the introduced three alternative registration approaches using linear/planar features can produce equivalent transformation parameters. In addition, the comparison between the simulated linear and planar features shows that both features can produce equivalent registration results. After the experiment with simulated datasets, real datasets were collected to compare the registration results of the three alternative registration approaches. The results suggest that the three registration approaches can produce equivalent transformation parameters using planar features. Furthermore, the comparison between the planar and linear features shows that the three registration approaches produce better registration results when planar features are the registration primitives. When using the real datasets, linear features are not preferred since linear features are extracted indirectly by the intersection of neighboring planar features. To get enough lines, planes that are far apart from each other have to be extrapolated to derive lines. Regarding the execution time, the linear/planar feature-based

approach had the shortest execution time. The pseudo-conjugate point-based and closed-form approaches based on linear/planar features, on the other hand, led to longer execution times due to a large number of point cloud data.

5. CONCLUSIONS

TLS has become a dominant tool to acquire an accurate and dense representation of the surface of objects. Throughout the development of laser scanners, TLS has been widely used in many areas, such as building modeling, cultural heritage documentation, and forestry. Due to the line-of-sight measurement principle of laser scanners and occlusion of objects, it is necessary to collect data from multiple scan locations to provide complete coverage of the objects. Since the point clouds captured from different locations refer to separate coordinate systems centered at each scan location, a registration process is required to incorporate point clouds of different scans under a common coordinate system. Geometric features are used in this research because many man-made objects in the urban areas are comprised of linear and planar features, and a good estimation of the transformation parameters is not required in the registration approaches using linear and planar features.

Alternative approaches for fitting a line or plane to data with errors in 3D space are investigated. Two different approaches of line fitting are proposed in this research. In the first approach, line parameters are estimated by minimizing 2D distances of points from the line measured parallel to the coordinated planes. In the second approach, the line fitting is conducted by minimizing the 3D normal distance between points and a line. The proposed line fitting approaches are tested using simulated datasets. The results indicate that the proposed two approaches of line fitting can produce equivalent results. The correlation matrix of the estimated line parameters shows that there is a high correlation between the estimated parameters. In this research, the linear features are represented with minimal parameters. However, the minimal representation of the linear features will create an artificial correlation between the estimated line parameters. This research shows that the correlation between the

estimated line parameters can be reduced by shifting the origin of the coordinate system to the center of the line segment in the line fitting procedure.

This thesis compares three alternative approaches for the coarse registration of two partially overlapping point clouds using linear and planar features. Linear and planar features in the overlapping areas can provide a strong link between adjacent scans because the corresponding features will coincide after being transformed into a common coordinate system. Therefore, in the feature-based approach, the transformation parameters can be estimated by matching corresponding features in different scans. However, the partial derivatives are difficult to compute due to the complicated functions of the feature-based approach. The pseudo-conjugate point-based method utilizes the non-corresponding points along the common linear and planar features to estimate transformation parameters. The nonrandom component along corresponding linear and planar features, which is introduced by using non-corresponding points, is eliminated by modifying their weight matrices in the corresponding direction. The pseudo-conjugate point-based method is simpler than the feature-based approach since the partial derivatives are easier to implement. The mathematical models of feature-based and point-based approaches are nonlinear. Thus, an initial estimation of the transformation parameters is required in these approaches. In the closed-form solution, a linear mathematical model is presented, where the unit quaternion is used to represent the rotation angles. Hence, an initial approximation of the transformation parameters is not required in the closed-form solution.

In order to compare the three alternative registration approaches, experiments were conducted using simulated and real datasets. In the tests using synthetic datasets, the registration results indicate that the introduced three alternative registration approaches using linear/planar features can produce equivalent transformation parameters. In addition, the comparison between the simulated linear and planar features shows that both features can produce equivalent registration results. After the experiment with simulated datasets, real datasets were collected to compare the registration results of the three alternative registration approaches. The results suggest

that the three registration approaches can produce equivalent transformation parameters using planar features. Furthermore, the comparison between the planar and linear features shows that the three registration approaches produce better registration results when planar features are the registration primitives. When using the real datasets, linear features are not preferred since linear features are extracted indirectly by the intersection of neighboring planar features. To get enough lines, planes that are far apart from each other have to be extrapolated to derive lines.

The registration results with both simulated and real data indicate that any one of the three introduced approaches could be used for the coarse registration because they produced equivalent results. Nevertheless, the pseudo-conjugate point-based method and closed-form solution are the preferred approaches for coarse registration using linear or planar features. The pseudo-conjugate point-based method is much easier to implement since any existing code for the rigid body transformation using points can be adapted to use this approach. In addition, the pseudo-conjugate point-based method and feature-based approach are nonlinear and they require an initial guess for transformation parameters. In order to eliminate the requirement for the initial guess, the closed-form solution can be employed for the estimation of transformation parameters since this approach is linear.

5.1 Recommendations for Future Work

Future work will concentrate on the automatic identification of corresponding features. The manual identification of the corresponding features between adjacent scans need human interaction and is very time-consuming. An automatic feature matching strategy can establish correspondences automatically, hence speed up the registration process.

The global registration should be considered in future work for better overall results. Specifically, in the case where multiple point sets exist, instead of matching a pair of scans at a time, a global registration will be conducted to register multiple

scans that partially overlap each other simultaneously. The global registration approach utilizes information from all point clouds and can avoid the accumulation of errors.

Future work should also include the co-registration of the TLS data and digital image data. Currently, TLS is often combined with image sensors. The digital image data has higher resolution and can provide additional information about the scenes. Therefore, the integration of laser scanning and image data can achieve more reliable results.

REFERENCES

REFERENCES

[1] A. F. Habib and R. I. Alruzouq, "Line-based modified iterated hough transform for automatic registration of multi-source imagery," *The Photogrammetric Record*, vol. 19, no. 105, pp. 5–21, 2004.

[2] P. J. Besl and N. D. McKay, "Method for registration of 3-d shapes," in *Sensor fusion IV: control paradigms and data structures*, vol. 1611. International Society for Optics and Photonics, 1992, pp. 586–606.

[3] C. Yi, H. Xing, Q. Wu, Y. Zhang, M. Wei, B. Wang, and L. Zhou, "Automatic detection of cross-shaped targets for laser scan registration," *IEEE Access*, vol. 6, pp. 8483–8500, 2018.

[4] M. Scaioni, "Direct georeferencing of tls in surveying of complex sites," *Proceedings of the ISPRS Working Group*, vol. 4, pp. 22–24, 2005.

[5] A. Habib, A. P. Kersting, K. I. Bang, and D.-C. Lee, "Alternative methodologies for the internal quality control of parallel lidar strips," *IEEE Transactions on Geoscience and Remote Sensing*, vol. 48, no. 1, pp. 221–236, 2009.

[6] M. Al-Durgham, I. Detchev, and A. Habib, "Analysis of two triangle-based multi-surface registration algorithms of irregular point clouds," *ISPRS-International Archives of the Photogrammetry, Remote Sensing and Spatial Information Sciences*, vol. 3812, pp. 61–66, 2011.

[7] E. Renaudin, A. Habib, and A. P. Kersting, "Featured-based registration of terrestrial laser scans with minimum overlap using photogrammetric data," *Etri Journal*, vol. 33, no. 4, pp. 517–527, 2011.

[8] I. Stamos and M. Leordeanu, "Automated feature-based range registration of urban scenes of large scale," in *2003 IEEE Computer Society Conference on Computer Vision and Pattern Recognition, 2003. Proceedings.*, vol. 2. IEEE, 2003, pp. II–Ii.

[9] A. Habib, M. Ghanma, M. Morgan, and R. Al-Ruzouq, "Photogrammetric and lidar data registration using linear features," *Photogrammetric Engineering & Remote Sensing*, vol. 71, no. 6, pp. 699–707, 2005.

[10] M. Alshawa, "lcl: Iterative closest line a novel point cloud registration algorithm based on linear features," *Ekscentar*, no. 10, pp. 53–59, 2007.

[11] C. Dold and C. Brenner, "Registration of terrestrial laser scanning data using planar patches and image data," *International Archives of the Photogrammetry, Remote Sensing and Spatial Information Sciences-ISPRS Archives 36 (2006)*, vol. 36, pp. 78–83, 2006.

[12] W. Von Hansen, "Robust automatic marker-free registration of terrestrial scan data," *Proc. Photogramm. Comput. Vis*, vol. 36, pp. 105–110, 2006.

[13] M. A. Fischler and R. C. Bolles, "Random sample consensus: a paradigm for model fitting with applications to image analysis and automated cartography," *Communications of the ACM*, vol. 24, no. 6, pp. 381–395, 1981.

[14] J. Jaw, T. Chuang *et al.*, "Feature-based registration of terrestrial lidar point clouds," *The International Archives of the Photogrammetry, Remote Sensing and Spatial Information Sciences*, vol. 37, pp. 303–308, 2008.

[15] K. Al-Durgham, A. Habib, and E. Kwak, "Ransac approach for automated registration of terrestrial laser scans using linear features," *ISPRS Int. Arch. Photogramm. Remote Sens. Spat. Inf. Sci*, vol. 2, pp. 13–18, 2013.

[16] K. Al-Durgham and A. Habib, "Association-matrix-based sample consensus approach for automated registration of terrestrial laser scans using linear features," *Photogrammetric Engineering & Remote Sensing*, vol. 80, no. 11, pp. 1029–1039, 2014.

[17] B. K. Horn, "Closed-form solution of absolute orientation using unit quaternions," *Josa a*, vol. 4, no. 4, pp. 629–642, 1987.

[18] Y. Guan and H. Zhang, "Initial registration for point clouds based on linear features," in *2011 Fourth International Symposium on Knowledge Acquisition and Modeling*. IEEE, 2011, pp. 474–477.

[19] H. Fangning and H. Ayman, "A closed-form solution for coarse registration of point clouds using linear features," *Journal of Surveying Engineering*, vol. 142, no. 3, p. 04016006, 2016.

[20] D. C. Mulawa and E. M. Mikhail, "Photogrammetric treatment of linear features," *International Archives of Photogrammetry and Remote Sensing*, vol. 27, no. B3, pp. 383–393, 1988.

[21] K. S. Roberts, "A new representation for a line," in *Proceedings CVPR'88: The Computer Society Conference on Computer Vision and Pattern Recognition*. IEEE, 1988, pp. 635–640.

[22] N. Ayache and O. D. Faugeras, "Maintaining representations of the environment of a mobile robot," *IEEE transactions on Robotics and Automation*, vol. 5, no. 6, pp. 804–819, 1989.

[23] Wikipedia contributors, "Spherical coordinate system — Wikipedia, the free encyclopedia," 2020, [Online; accessed 18-September-2020]. [Online]. Available: https://en.wikipedia.org/w/index.php?title=Spherical_coordinate_system&oldid=978704166

[24] K. Al-Durgham, "Geometric features extraction and automated registration of static laser scans using linear features," Master's thesis, Graduate Studies, 2014.

[25] D. Girardeau-Montaut, "Cloudcompare-open source project," *OpenSource Project*, 2011.

[26] A. Habib, M. Ghanma, and M. Tait, "Integration of lidar and photogrammetry for close range applications," *International Archives of Photogrammetry, Remote Sensing and Spatial Information Sciences*, vol. 35, no. B5, pp. 1045–1050, 2004.

[27] F. T. Inc., "User manuals for the focus3d x 330," 2015, [Online; accessed 9-October-2020]. [Online]. Available: https://faro.app.box.com/s/4f908b59hcjjj8mezdr58z6n4qy5neli

[28] R. Ravi and A. Habib, "Image-lidar interactive visualization environment (i-live) for mobile mapping systems."